

Gamma-Ray Bursts

Contents

1	Topics	155
2	Participants	157
2.1	ICRANet participants	157
2.2	Past collaborators	157
2.3	Ongoing collaborations	159
2.4	Students	160
3	Selected publications before 2005	161
3.1	Refereed journals	161
3.2	Conference proceedings	168
4	Publications (2005–2019)	173
4.1	Refereed journals	173
4.2	Conference proceedings	213

1 Topics

- GRB classification in different families with different progenitor systems.
- “Genuine short” GRBs: Possible identifications and selection effects
- A modified spectral energy distribution for highly energetic GRBs
- The observed spectra of the P-GRBs
- GRB prompt emission spectra below 5 keV: challenges for future missions
- Interpretation of the ultra high energy emission from GRBs observed by Fermi, AGILE and MAGIC
- Analysis of different families of progenitors for GRBs with different energetics
- GRBs at redshift $z > 6$
- GRBs originating from a multiple collapse
- Prompt emission: the clumpiness of CBM
- Microphysical description of the interaction between the fireshell and the CBM
- Theoretical interpretation of the “plateau” phase in the X-ray afterglow
- Emission from newly born neutron stars, or “neo neutron stars”.
- Induced Gravitational Collapse process for GRBs associated with supernovae.
- Redshift estimators for GRBs with no measured redshift.

- Binary Driven Hypernovae (BdHNe) as progenitor of GRBs via Induced Gravitational Collapse.
- GRB light curves as composed of different episodes.
- Different kinds of binary systems as GRB progenitors.
- “Cosmic Matrix” for GRBs.
- GRB X-Ray Flares and Gamma-Ray Flares.
- GRB afterglow theory consistent with the mildly relativistic velocities inferred from the observations.
- Gravitational wave emission associated to GRBs of different families.
- Extended thermal emission components in GRBs.
- GRBs from merging white dwarfs.
- “Inner engine” of GRB emission.
- Quantized emission in GRBs.

2 Participants

2.1 ICRANet participants

- David Arnett
- Carlo Luciano Bianco
- Massimo Della Valle
- Li Liang
- Jorge Armando Rueda Hernandez
- Remo Ruffini
- Narek Sahakyan
- Gregory Vereshchagin
- Yu Wang
- She-Sheng Xue

2.2 Past collaborators

- Andrey Baranov
- Maria Grazia Bernardini (OAB, Italy)
- Joao Braga (INPE, Brazil)
- Sabrina Casanova (MPIK, Germany)
- Letizia Caito

2 Participants

- Pascal Chardonnet (Université de Savoie, France)
- Guido Chincarini (Università di Milano “Bicocca”, Italy)
- Demetrios Christodoulou (ETH Zurich, Switzerland)
- Alessandra Corsi (INAF-IASF Roma, Italy)
- Valeri Chechetkin
- Maria Giovanna Dainotti
- Thibault Damour (IHES, France)
- Maxime Enderli
- Walter Ferrara
- Federico Fraschetti (CEA Saclay, France)
- Roberto Guida
- Vahe Gurzadyan (Yerevan Physics Institute, Armenia)
- Wen-Biao Han
- Massimiliano Lattanzi (Oxford Astrophysics, UK)
- Vincenzo Liccardo
- Hendrik Ludwig
- Marco Muccino
- Nino Panagia
- Barbara Patricelli (Pisa University, Italy)
- Elena Pian
- Giovanni Battista Pisani
- Giuliano Preparata (Università di Milano, Italy)
- Jay D. Salmonson (Livermore Lab, USA)

- Vineeth Valsan
- Jim Wilson (Livermore Lab, USA)

2.3 Ongoing collaborations

- Alexey Aksenov (ITEP, Russia)
- Lorenzo Amati (INAF-IASF Bologna, Italy)
- Ulisses Barres de Almeida (CBPF, Brazil)
- Laura Marcela Becerra Bayona (Universidad Industrial de Santander, Colombia)
- Riccardo Belvedere (ICRANet-Rio, Brazil)
- Sandip Kumar Chakrabarti (S.N. Bose National Centre and Indian Centre for Space Physics, India)
- Christian Cherubini (Università Campus Biomedico, Italy)
- Alessandro Chieffi (INAF-IASF Roma, Italy)
- Stefano Covino (OAB, Italy)
- Gustavo de Barros (UFRJ, Brazil)
- Simonetta Filippi (Università Campus Biomedico, Italy)
- Filippo Frontera (Università di Ferrara, Italy)
- Chris Fryer (Los Alamos National Laboratories, USA).
- Dafne Guetta (OAR, Italy)
- Cristiano Guidorzi (OAB, Italy)
- Stanislav Kelner (MEPhI, Russia, and MPIK, Germany)
- Marco Limongi (OAR, Italy)
- Clovis Maia (University of Brasilia, Brazil)

- Vanessa Mangano (INAF-IASF Palermo, Italy)
- Grant Mathews (University of Notre Dame, USA)
- Ana Virginia Penacchioni (INPE, Brazil)
- Luis Juracy Rangel Lemos (Fundação Universidade Federal do Tocantins, Brazil)
- Soroush Shakeri (Isfahan University of Technology, Iran)
- Ivan Siutsou (ICRANet-Rio, Brazil)
- Susanna Vergani (Dunsink Observatory, Ireland)
- Francesco Vissani (INFN, Italy)
- Elena Zaninoni (ICRANet-Rio, Brazil)

2.4 Students

- Yerlan Aimuratov (IRAP PhD, Kazakhstan)
- Yen-Chen Chen (IRAP-PhD, China-Taiwan)
- Mile Karlika (IRAP PhD, Croatia)
- Milos Kovacevic (IRAP PhD, Serbia)
- Ronaldo V. Lobato (IRAP-PhD, Brazil)
- J. David Melon Fuksman (IRAP PhD, Argentina)
- Rahim Moradi (IRAP PhD, Iran)
- Daria Primorac (IRAP PhD, Croatia)
- Jose Fernando Rodriguez Ruiz (IRAP PhD, Colombia)

3 Selected publications before 2005

3.1 Refereed journals

1. D. Christodoulou, R. Ruffini; “Reversible Transformations of a Charged Black Hole”; *Physical Review D*, 4, 3552 (1971).

A formula is derived for the mass of a black hole as a function of its “irreducible mass”, its angular momentum, and its charge. It is shown that 50% of the mass of an extreme charged black hole can be converted into energy as contrasted with 29% for an extreme rotating black hole.

2. T. Damour, R. Ruffini; “Quantum electrodynamical effects in Kerr-Newman geometries”; *Physical Review Letters*, 35, 463 (1975).

Following the classical approach of Sauter, of Heisenberg and Euler and of Schwinger the process of vacuum polarization in the field of a “bare” Kerr-Newman geometry is studied. The value of the critical strength of the electromagnetic fields is given together with an analysis of the feedback of the discharge on the geometry. The relevance of this analysis for current astrophysical observations is mentioned.

3. G. Preparata, R. Ruffini, S.-S. Xue; “The dyadosphere of black holes and gamma-ray bursts”; *Astronomy & Astrophysics*, 338, L87 (1999).

The “dyadosphere” has been defined as the region outside the horizon of a black hole endowed with an electromagnetic field (abbreviated to EMBH for “electromagnetic black hole”) where the electromagnetic field exceeds the critical value, predicted by Heisenberg & Euler for e^\pm pair production. In a very short time ($\sim O(\hbar/mc^2)$) a very large number of pairs is created there. We here give limits on the EMBH parameters leading to a Dyadosphere for $10M_\odot$ and 10^5M_\odot EMBH’s, and give as well the pair densities as functions of the radial coordinate. We here assume that the pairs reach thermodynamic equilibrium

with a photon gas and estimate the average energy per pair as a function of the EMBH mass. These data give the initial conditions for the analysis of an enormous pair-electromagnetic-pulse or "P.E.M. pulse" which naturally leads to relativistic expansion. Basic energy requirements for gamma ray bursts (GRB), including GRB971214 recently observed at $z=3.4$, can be accounted for by processes occurring in the dyadosphere. In this letter we do not address the problem of forming either the EMBH or the dyadosphere: we establish some inequalities which must be satisfied during their formation process.

4. R. Ruffini, J.D. Salmonson, J.R. Wilson, S.-S. Xue; "On the pair electromagnetic pulse of a black hole with electromagnetic structure"; *Astronomy & Astrophysics*, 350, 334 (1999).

We study the relativistically expanding electron-positron pair plasma formed by the process of vacuum polarization around an electromagnetic black hole (EMBH). Such processes can occur for EMBH's with mass all the way up to $6 \times 10^5 M_{\odot}$. Beginning with a idealized model of a Reissner-Nordstrom EMBH with charge to mass ratio $\zeta = 0.1$, numerical hydrodynamic calculations are made to model the expansion of the pair-electromagnetic pulse (PEM pulse) to the point that the system is transparent to photons. Three idealized special relativistic models have been compared and contrasted with the results of the numerically integrated general relativistic hydrodynamic equations. One of the three models has been validated: a PEM pulse of constant thickness in the laboratory frame is shown to be in excellent agreement with results of the general relativistic hydrodynamic code. It is remarkable that this precise model, starting from the fundamental parameters of the EMBH, leads uniquely to the explicit evaluation of the parameters of the PEM pulse, including the energy spectrum and the astrophysically unprecedented large Lorentz factors (up to 6×10^3 for a $10^3 M_{\odot}$ EMBH). The observed photon energy at the peak of the photon spectrum at the moment of photon decoupling is shown to range from 0.1 MeV to 4 MeV as a function of the EMBH mass. Correspondingly the total energy in photons is in the range of 10^{52} to 10^{54} ergs, consistent with observed gamma-ray bursts. In these computations we neglect the presence of baryonic matter which will be the subject of forthcoming publications.

5. R. Ruffini, J.D. Salmonson, J.R. Wilson, S.-S. Xue; "On the pair-electromagnetic pulse from an electromagnetic black hole surrounded by a baryonic remnant"; *Astronomy & Astrophysics*, 359, 855 (2000).

The interaction of an expanding Pair-Electromagnetic pulse (PEM pulse) with

a shell of baryonic matter surrounding a Black Hole with electromagnetic structure (EMBH) is analyzed for selected values of the baryonic mass at selected distances well outside the dyadosphere of an EMBH. The dyadosphere, the region in which a super critical field exists for the creation of e^+e^- pairs, is here considered in the special case of a Reissner-Nordstrom geometry. The interaction of the PEM pulse with the baryonic matter is described using a simplified model of a slab of constant thickness in the laboratory frame (constant-thickness approximation) as well as performing the integration of the general relativistic hydrodynamical equations. The validation of the constant-thickness approximation, already presented in a previous paper Ruffini et al. (1999) for a PEM pulse in vacuum, is here generalized to the presence of baryonic matter. It is found that for a baryonic shell of mass-energy less than 1% of the total energy of the dyadosphere, the constant-thickness approximation is in excellent agreement with full general relativistic computations. The approximation breaks down for larger values of the baryonic shell mass, however such cases are of less interest for observed Gamma Ray Bursts (GRBs). On the basis of numerical computations of the slab model for PEM pulses, we describe (i) the properties of relativistic evolution of a PEM pulse colliding with a baryonic shell; (ii) the details of the expected emission energy and observed temperature of the associated GRBs for a given value of the EMBH mass; $10^3 M_\odot$, and for baryonic mass-energies in the range 10^{-8} to 10^{-2} the total energy of the dyadosphere.

6. C.L. Bianco, R. Ruffini, S.-S. Xue; "The elementary spike produced by a pure e^+e^- pair-electromagnetic pulse from a Black Hole: The PEM Pulse"; *Astronomy & Astrophysics*, 368, 377 (2001).

In the framework of the model that uses black holes endowed with electromagnetic structure (EMBH) as the energy source, we study how an elementary spike appears to the detectors. We consider the simplest possible case of a pulse produced by a pure e^+e^- pair-electro-magnetic plasma, the PEM pulse, in the absence of any baryonic matter. The resulting time profiles show a *Fast-Rise-Exponential-Decay* shape, followed by a power-law tail. This is obtained without any special fitting procedure, but only by fixing the energetics of the process taking place in a given EMBH of selected mass, varying in the range from 10 to $10^3 M_\odot$ and considering the relativistic effects to be expected in an electron-positron plasma gradually reaching transparency. Special attention is given to the contributions from all regimes with Lorentz γ factor varying from $\gamma = 1$ to $\gamma = 10^4$ in a few hundreds of the PEM pulse travel time. Although the

main goal of this paper is to obtain the elementary spike intensity as a function of the arrival time, and its observed duration, some qualitative considerations are also presented regarding the expected spectrum and on its departure from the thermal one. The results of this paper will be comparable, when data will become available, with a subfamily of particularly short GRBs not followed by any afterglow. They can also be propedeutical to the study of longer bursts in presence of baryonic matter currently observed in GRBs.

7. R. Ruffini, C.L. Bianco, P. Chardonnet, F. Fraschetti, S.-S. Xue; "Relative spacetime transformations in Gamma-Ray Bursts"; *The Astrophysical Journal*, 555, L107 (2001).

The GRB 991216 and its relevant data acquired from the BATSE experiment and RXTE and Chandra satellites are used as a prototypical case to test the theory linking the origin of gamma ray bursts (GRBs) to the process of vacuum polarization occurring during the formation phase of a black hole endowed with electromagnetic structure (EMBH). The relative space-time transformation paradigm (RSTT paradigm) is presented. It relates the observed signals of GRBs to their past light cones, defining the events on the worldline of the source essential for the interpretation of the data. Since GRBs present regimes with unprecedentedly large Lorentz γ factor, also sharply varying with time, particular attention is given to the constitutive equations relating the four time variables: the comoving time, the laboratory time, the arrival time at the detector, duly corrected by the cosmological effects. This paradigm is at the very foundation of any possible interpretation of the data of GRBs.

8. R. Ruffini, C.L. Bianco, P. Chardonnet, F. Fraschetti, S.-S. Xue; "On the interpretation of the burst structure of Gamma-Ray Bursts"; *The Astrophysical Journal*, 555, L113 (2001).

Given the very accurate data from the BATSE experiment and RXTE and Chandra satellites, we use the GRB 991216 as a prototypical case to test the EMBH theory linking the origin of the energy of GRBs to the electromagnetic energy of black holes. The fit of the afterglow fixes the only two free parameters of the model and leads to a new paradigm for the interpretation of the burst structure, the IBS paradigm. It leads as well to a reconsideration of the relative roles of the afterglow and burst in GRBs by defining two new phases in this complex phenomenon: a) the injector phase, giving rise to the proper-GRB (P-GRB), and b) the beam-target phase, giving rise to the extended afterglow peak emission (E-APE) and to the afterglow. Such differentiation leads to a

natural possible explanation of the bimodal distribution of GRBs observed by BATSE. The agreement with the observational data in regions extending from the horizon of the EMBH all the way out to the distant observer confirms the uniqueness of the model.

9. R. Ruffini, C.L. Bianco, P. Chardonnet, F. Frascchetti, S.-S. Xue; "On a possible Gamma-Ray Burst-Supernova time sequence"; *The Astrophysical Journal*, 555, L117 (2001).

The data from the Chandra satellite on the iron emission lines in the afterglow of GRB 991216 are used to give further support for the EMBH theory, which links the origin of the energy of GRBs to the extractable energy of electromagnetic black holes (EMBHs), leading to an interpretation of the GRB-supernova correlation. Following the relative space-time transformation (RSTT) paradigm and the interpretation of the burst structure (IBS) paradigm, we introduce a paradigm for the correlation between GRBs and supernovae. The following sequence of events is shown as kinematically possible and consistent with the available data: a) the GRB-progenitor star P_1 first collapses to an EMBH, b) the proper GRB (P-GRB) and the peak of the afterglow (E-APE) propagate in interstellar space until the impact on a supernova-progenitor star P_2 at a distance $\leq 2.69 \times 10^{17}$ cm, and they induce the supernova explosion, c) the accelerated baryonic matter (ABM) pulse, originating the afterglow, reaches the supernova remnants 18.5 hours after the supernova explosion and gives rise to the iron emission lines. Some considerations on the dynamical implementation of the paradigm are presented. The concept of induced supernova explosion introduced here specifically for the GRB-supernova correlation may have more general application in relativistic astrophysics.

10. R. Ruffini, C.L. Bianco, P. Chardonnet, F. Frascchetti, S.-S. Xue; "On the physical processes which lie at the bases of time variability of GRBs"; *Il Nuovo Cimento B*, 116, 99 (2001).

The relative-space-time-transformation (RSTT) paradigm and the interpretation of the burst-structure (IBS) paradigm are applied to probe the origin of the time variability of GRBs. Again GRB 991216 is used as a prototypical case, thanks to the precise data from the CGRO, RXTE and Chandra satellites. It is found that with the exception of the relatively inconspicuous but scientifically very important signal originating from the initial "proper gamma ray burst" (P-GRB), all the other spikes and time variabilities can be explained by the interaction of the accelerated-baryonic-matter pulse with inhomogeneities in the

interstellar matter. This can be demonstrated by using the RSTT paradigm as well as the IBS paradigm, to trace a typical spike observed in arrival time back to the corresponding one in the laboratory time. Using these paradigms, the identification of the physical nature of the time variability of the GRBs can be made most convincingly. It is made explicit the dependence of a) the intensities of the afterglow, b) the spikes amplitude and c) the actual time structure on the Lorentz gamma factor of the accelerated-baryonic-matter pulse. In principle it is possible to read off from the spike structure the detailed density contrast of the interstellar medium in the host galaxy, even at very high redshift.

11. R. Ruffini, C.L. Bianco, P. Chardonnet, F. Fraschetti, S.-S. Xue; "On the structures in the afterglow peak emission of gamma ray bursts"; *The Astrophysical Journal*, 581, L19 (2002).

Using GRB 991216 as a prototype, it is shown that the intensity substructures observed in what is generally called the "prompt emission" in gamma ray bursts (GRBs) do originate in the collision between the accelerated baryonic matter (ABM) pulse with inhomogeneities in the interstellar medium (ISM). The initial phase of such process occurs at a Lorentz factor $\gamma \sim 310$. The crossing of ISM inhomogeneities of sizes $\Delta R \sim 10^{15}$ cm occurs in a detector arrival time interval of ~ 0.4 s implying an apparent superluminal behavior of $\sim 10^5 c$. The long lasting debate between the validity of the external shock model vs. the internal shock model for GRBs is solved in favor of the first.

12. R. Ruffini, C.L. Bianco, P. Chardonnet, F. Fraschetti, S.-S. Xue; "On the structure of the burst and afterglow of Gamma-Ray Bursts I: the radial approximation"; *International Journal of Modern Physics D*, 12, 173 (2003).

We have recently proposed three paradigms for the theoretical interpretation of gamma-ray bursts (GRBs). (1) The relative space-time transformation (RSTT) paradigm emphasizes how the knowledge of the entire world-line of the source from the moment of gravitational collapse is a necessary condition in order to interpret GRB data. (2) The interpretation of the burst structure (IBS) paradigm differentiates in all GRBs between an injector phase and a beam-target phase. (3) The GRB-supernova time sequence (GSTS) paradigm introduces the concept of *induced supernova explosion* in the supernovae-GRB association. In the introduction the RSTT and IBS paradigms are enunciated and illustrated using our theory based on the vacuum polarization process occurring around an electromagnetic black hole (EMBH theory). The results are summarized

using figures, diagrams and a complete table with the space-time grid, the fundamental parameters and the corresponding values of the Lorentz gamma factor for GRB 991216 used as a prototype. In the following sections the detailed treatment of the EMBH theory needed to understand the results of the three above letters is presented. We start from the considerations on the dyadosphere formation. We then review the basic hydrodynamic and rate equations, the equations leading to the relative space-time transformations as well as the adopted numerical integration techniques. We then illustrate the five fundamental eras of the EMBH theory: the self acceleration of the e^+e^- pair-electromagnetic plasma (PEM pulse), its interaction with the baryonic remnant of the progenitor star, the further self acceleration of the e^+e^- pair-electromagnetic radiation and baryon plasma (PEMB pulse). We then study the approach of the PEMB pulse to transparency, the emission of the proper GRB (P-GRB) and its relation to the “short GRBs”. Particular attention is given to the free parameters of the theory and to the values of the thermodynamical quantities at transparency. Finally the three different regimes of the afterglow are described within the fully radiative and radial approximations: the ultrarelativistic, the relativistic and the nonrelativistic regimes. The best fit of the theory leads to an unequivocal identification of the “long GRBs” as extended emission occurring at the afterglow peak (E-APE). The relative intensities, the time separation and the hardness ratio of the P-GRB and the E-APE are used as distinctive observational test of the EMBH theory and the excellent agreement between our theoretical predictions and the observations are documented. The afterglow power-law indexes in the EMBH theory are compared and contrasted with the ones in the literature, and no beaming process is found for GRB 991216. Finally, some preliminary results relating the observed time variability of the E-APE to the inhomogeneities in the interstellar medium are presented, as well as some general considerations on the EMBH formation. The issue of the GSTS paradigm will be the object of a forthcoming publication and the relevance of the iron-lines observed in GRB 991216 is shortly reviewed. The general conclusions are then presented based on the three fundamental parameters of the EMBH theory: the dyadosphere energy, the baryonic mass of the remnant, the interstellar medium density. An in depth discussion and comparison of the EMBH theory with alternative theories is presented as well as indications of further developments beyond the radial approximation, which will be the subject of paper II in this series. Future needs for specific GRB observations are outlined.

13. R. Ruffini, C.L. Bianco, P. Chardonnet, F. Fraschetti, V. Gurzadyan, S.-S. Xue; "On the instantaneous spectrum of gamma ray bursts"; *International Journal of Modern Physics D*, 13, 843 (2004).

A theoretical attempt to identify the physical process responsible for the afterglow emission of Gamma-Ray Bursts (GRBs) is presented, leading to the occurrence of thermal emission in the comoving frame of the shock wave giving rise to the bursts. The determination of the luminosities and spectra involves integration over an infinite number of Planckian spectra, weighted by appropriate relativistic transformations, each one corresponding to a different viewing angle in the past light cone of the observer. The relativistic transformations have been computed using the equations of motion of GRBs within our theory, giving special attention to the determination of the equitemporal surfaces. The only free parameter of the present theory is the "effective emitting area" in the shock wave front. A self consistent model for the observed hard-to-soft transition in GRBs is also presented. When applied to GRB 991216 a precise fit ($\chi^2 \simeq 1.078$) of the observed luminosity in the 2–10 keV band is obtained. Similarly, detailed estimates of the observed luminosity in the 50–300 keV and in the 10–50 keV bands are obtained.

3.2 Conference proceedings

1. R. Ruffini; "Beyond the critical mass: The dyadosphere of black holes"; in "Black Holes and High Energy Astrophysics", H. sato, N. Sugiyama, Editors; p. 167; Universal Academy Press (Tokyo, Japan, 1998).

The "dyadosphere" (from the Greek word "duas-duados" for pairs) is here defined as the region outside the horizon of a black hole endowed with an electromagnetic field (abbreviated to EMBH for "electromagnetic black hole") where the electromagnetic field exceeds the critical value, predicted by Heisenberg and Euler for e^+e^- pair production. In a very short time ($\sim O(\hbar/mc^2)$), a very large number of pairs is created there. I give limits on the EMBH parameters leading to a Dyadosphere for $10M_\odot$ and 10^5M_\odot EMBH's, and give as well the pair densities as functions of the radial coordinate. These data give the initial conditions for the analysis of an enormous pair-electromagnetic-pulse or "PEM-pulse" which naturally leads to relativistic expansion. Basic energy requirements for gamma ray bursts (GRB), including GRB971214 recently observed at $z = 3.4$, can be accounted for by processes occurring in the dyado-

sphere.

2. R. Ruffini, C.L. Bianco, P. Chardonnet, F. Fraschetti, L. Vitagliano, S.-S. Xue; "New perspectives in physics and astrophysics from the theoretical understanding of Gamma-Ray Bursts"; in "COSMOLOGY AND GRAVITATION: Xth Brazilian School of Cosmology and Gravitation; 25th Anniversary (1977-2002)", Proceedings of the Xth Brazilian School on Cosmology and Gravitation, Mangaratiba, Rio de Janeiro (Brazil), July - August 2002, M. Novello, S.E. Perez Bergliaffa, Editors; AIP Conference Proceedings, 668, 16 (2003).

If due attention is given in formulating the basic equations for the Gamma-Ray Burst (GRB) phenomenon and in performing the corresponding quantitative analysis, GRBs open a main avenue of inquiring on totally new physical and astrophysical regimes. This program is very likely one of the greatest computational efforts in physics and astrophysics and cannot be actuated using shortcuts. A systematic approach is needed which has been highlighted in three basic new paradigms: the relative space-time transformation (RSTT) paradigm, the interpretation of the burst structure (IBS) paradigm, the GRB-supernova time sequence (GSTS) paradigm. From the point of view of fundamental physics new regimes are explored: (1) the process of energy extraction from black holes; (2) the quantum and general relativistic effects of matter-antimatter creation near the black hole horizon; (3) the physics of ultrarelativistic shock waves with Lorentz gamma factor $\gamma > 100$. From the point of view of astronomy and astrophysics also new regimes are explored: (i) the occurrence of gravitational collapse to a black hole from a critical mass core of mass $M \gtrsim 10M_{\odot}$, which clearly differs from the values of the critical mass encountered in the study of stars "catalyzed at the endpoint of thermonuclear evolution" (white dwarfs and neutron stars); (ii) the extremely high efficiency of the spherical collapse to a black hole, where almost 99.99% of the core mass collapses leaving negligible remnant; (iii) the necessity of developing a fine tuning in the final phases of thermonuclear evolution of the stars, both for the star collapsing to the black hole and the surrounding ones, in order to explain the possible occurrence of the "induced gravitational collapse". New regimes are as well encountered from the point of view of nature of GRBs: (I) the basic structure of GRBs is uniquely composed by a proper-GRB (P-GRB) and the afterglow; (II) the long bursts are then simply explained as the peak of the afterglow (the E-APE) and their observed time variability is explained in terms of inhomogeneities in the interstellar medium (ISM); (III) the short bursts are

identified with the P-GRBs and the crucial information on general relativistic and vacuum polarization effects are encoded in their spectra and intensity time variability. A new class of space missions to acquire information on such extreme new regimes are urgently needed.

3. R. Ruffini, C.L. Bianco, P. Chardonnet, F. Fraschetti, S.-S. Xue; "The EMBH Model in GRB 991216 and GRB 980425"; in Proceedings of "Third Rome Workshop on Gamma-Ray Burst in the Afterglow Era", 17-20 September 2002; M. Feroci, F. Frontera, N. Masetti, L. Piro, Editors; ASP Conference Series, 312, 349 (2004).

This is a summary of the two talks presented at the Rome GRB meeting by C.L. Bianco and R. Ruffini. It is shown that by respecting the Relative Space-Time Transformation (RSTT) paradigm and the Interpretation of the Burst Structure (IBS) paradigm, important inferences are possible: a) in the new physics occurring in the energy sources of GRBs, b) on the structure of the bursts and c) on the composition of the interstellar matter surrounding the source.

4. M.G. Bernardini, C.L. Bianco, P. Chardonnet, F. Fraschetti, R. Ruffini, S.-S. Xue; "A New Astrophysical 'Triptych': GRB030329/SN2003dh/URCA-2"; in "GAMMA-RAY BURSTS: 30 YEARS OF DISCOVERY", Proceedings of the Los Alamos "Gamma Ray Burst Symposium", Santa Fe, New Mexico, 8 – 12 September 2003, E.E. Fenimore, M. Galassi, Editors; AIP Conference Proceedings, 727, 312 (2004).

We analyze the data of the Gamma-Ray Burst/Supernova GRB030329/SN2003dh system obtained by HETE-2, R-XTE, XMM and VLT within our theory for GRB030329. By fitting the only three free parameters of the EMBH theory, we obtain the luminosity in fixed energy bands for the prompt emission and the afterglow. Since the Gamma-Ray Burst (GRB) analysis is consistent with a spherically symmetric expansion, the energy of GRB030329 is $E = 2.1 \times 10^{52}$ erg, namely $\sim 2 \times 10^3$ times larger than the Supernova energy. We conclude that either the GRB is triggering an induced-supernova event or both the GRB and the Supernova are triggered by the same relativistic process. In no way the GRB can be originated from the supernova. We also evidence that the XMM observations, much like in the system GRB980425/SN1998bw, are not part of the GRB afterglow, as interpreted in the literature, but are associated to the Supernova phenomenon. A dedicated campaign of observations is needed to confirm the nature of this XMM source as a newly born neutron star cooling by generalized URCA processes.

5. F. Frascchetti, M.G. Bernardini, C.L. Bianco, P. Chardonnet, R. Ruffini, S.-S. Xue; "The GRB980425-SN1998bw Association in the EMBH Model"; in "GAMMA-RAY BURSTS: 30 YEARS OF DISCOVERY", Proceedings of the Los Alamos "Gamma Ray Burst Symposium", Santa Fe, New Mexico, 8 – 12 September 2003, E.E. Fenimore, M. Galassi, Editors; AIP Conference Proceedings, 727, 424 (2004).

Our GRB theory, previously developed using GRB 991216 as a prototype, is here applied to GRB 980425. We fit the luminosity observed in the 40–700 keV, 2–26 keV and 2–10 keV bands by the BeppoSAX satellite. In addition the supernova SN1998bw is the outcome of an "induced gravitational collapse" triggered by GRB 980425, in agreement with the GRB-Supernova Time Sequence (GSTS) paradigm. A further outcome of this astrophysically exceptional sequence of events is the formation of a young neutron star generated by the SN1998bw event. A coordinated observational activity is recommended to further enlighten the underlying scenario of this most unique astrophysical system.

6. A. Corsi, M.G. Bernardini, C.L. Bianco, P. Chardonnet, F. Frascchetti, R. Ruffini, S.-S. Xue; "GRB 970228 Within the EMBH Model"; in "GAMMA-RAY BURSTS: 30 YEARS OF DISCOVERY", Proceedings of the Los Alamos "Gamma Ray Burst Symposium", Santa Fe, New Mexico, 8 – 12 September 2003, E.E. Fenimore, M. Galassi, Editors; AIP Conference Proceedings, 727, 428 (2004).

We consider the gamma-ray burst of 1997 February 28 (GRB 970228) within the ElectroMagnetic Black Hole (EMBH) model. We first determine the value of the two free parameters that characterize energetically the GRB phenomenon in the EMBH model, that is to say the dyadosphere energy, $E_{dya} = 5.1 \times 10^{52}$ ergs, and the baryonic remnant mass M_B in units of E_{dya} , $B = M_B c^2 / E_{dya} = 3.0 \times 10^{-3}$. Having in this way estimated the energy emitted during the beam-target phase, we evaluate the role of the InterStellar Medium (ISM) number density (n_{ISM}) and of the ratio \mathcal{R} between the effective emitting area and the total surface area of the GRB source, in reproducing the observed profiles of the GRB 970228 prompt emission and X-ray (2-10 keV energy band) afterglow. The importance of the ISM distribution three-dimensional treatment around the central black hole is also stressed in this analysis.

4 Publications (2005–2019)

4.1 Refereed journals

1. R. Ruffini, C.L. Bianco, P. Chardonnet, F. Fraschetti, V. Gurzadyan, S.-S. Xue; “Emergence of a filamentary structure in the fireball from GRB spectra”; *International Journal of Modern Physics D*, 14, 97 (2005).

It is shown that the concept of a fireball with a definite filamentary structure naturally emerges from the analysis of the spectra of Gamma-Ray Bursts (GRBs). These results, made possible by the recently obtained analytic expressions of the equitemporal surfaces in the GRB afterglow, depend crucially on the single parameter R describing the effective area of the fireball emitting the X-ray and gamma-ray radiation. The X-ray and gamma-ray components of the afterglow radiation are shown to have a thermal spectrum in the co-moving frame of the fireball and originate from a stable shock front described self-consistently by the Rankine-Hugoniot equations. Precise predictions are presented on a correlation between spectral changes and intensity variations in the prompt radiation verifiable, e.g., by the Swift and future missions. The highly variable optical and radio emission depends instead on the parameters of the surrounding medium. The GRB 991216 is used as a prototype for this model.

2. R. Ruffini, M.G. Bernardini, C.L. Bianco, P. Chardonnet, F. Fraschetti, V. Gurzadyan, M. Lattanzi, L. Vitagliano, S.-S. Xue; “Extracting energy from black holes: ‘long’ and ‘short’ GRBs and their astrophysical settings”; *Il Nuovo Cimento C*, 28, 589 (2005).

The introduction of the three interpretational paradigms for Gamma-Ray Bursts (GRBs) and recent progress in understanding the X- and gamma-ray luminosity in the afterglow allow us to make assessments about the astrophysical settings of GRBs. In particular, we evidence the distinct possibility that some GRBs occur in a binary system. This subclass of GRBs manifests itself in a “tryptich”: one component formed by the collapse of a massive star to a black

hole, which originates the GRB; a second component by a supernova and a third one by a young neutron star born in the supernova event. Similarly, the understanding of the physics of quantum relativistic processes during the gravitational collapse makes possible precise predictions about the structure of short GRBs.

3. M.G. Bernardini, C.L. Bianco, P. Chardonnet, F. Fraschetti, R. Ruffini, S.-S. Xue; "Theoretical interpretation of luminosity and spectral properties of GRB 031203"; *The Astrophysical Journal*, 634, L29 (2005).

The X-ray and gamma-ray observations of the source GRB 031203 by INTEGRAL are interpreted within our theoretical model. In addition to a complete spacetime parameterization of the GRB, we specifically assume that the afterglow emission originates from a thermal spectrum in the comoving frame of the expanding baryonic matter shell. By determining the two free parameters of the model and estimating the density and filamentary structure of the ISM, we reproduce the observed luminosity in the 20-200 keV energy band. As in previous sources, the prompt radiation is shown to coincide with the peak of the afterglow, and the luminosity substructure is shown to originate in the filamentary structure of the ISM. We predict a clear hard-to-soft behavior in the instantaneous spectra. The time-integrated spectrum over 20 s observed by INTEGRAL is well fitted. Despite the fact that this source has been considered "unusual", it appears to us to be a normal low-energy GRB.

4. R. Ruffini, M.G. Bernardini, C.L. Bianco, P. Chardonnet, F. Fraschetti, S.-S. Xue; Evidence for isotropic emission in GRB991216; *Advances in Space Research*, 38, 1291 (2006).

The issue of the possible presence or absence of jets in GRBs is here re-examined for GRB991216. We compare and contrast our theoretically predicted afterglow luminosity in the 2–10 keV band for spherically symmetric versus jetted emission. At these wavelengths the jetted emission can be excluded and data analysis confirms spherical symmetry. These theoretical fits are expected to be improved by the forthcoming data of the Swift mission.

5. R. Ruffini, M.G. Bernardini, C.L. Bianco, P. Chardonnet, F. Fraschetti, R. Guida, S.-S. Xue; "GRB 050315: A step toward understanding the uniqueness of the overall GRB structure"; *The Astrophysical Journal*, 645, L109 (2006).

Using the Swift data of GRB 050315, we are making progress toward understanding the uniqueness of our theoretically predicted gamma-ray burst (GRB) structure, which is composed of a proper GRB (P-GRB), emitted at the transparency of an electron-positron plasma with suitable baryon loading, and an afterglow comprising the so-called prompt emission due to external shocks. Thanks to the Swift observations, the P-GRB is identified, and for the first time we can theoretically fit detailed light curves for selected energy bands on a continuous timescale ranging over 10⁶ s. The theoretically predicted instantaneous spectral distribution over the entire afterglow is presented, confirming a clear hard-to-soft behavior encompassing, continuously, the “prompt emission” all the way to the latest phases of the afterglow.

6. C.L. Bianco, L. Caito, R. Ruffini; “Theoretical interpretation of GRB 011121”; *Il Nuovo Cimento B*, 121, 1441 (2006).

GRB011121 is analyzed as a prototype to understand the “flares” recently observed by Swift in the afterglow of many GRB sources. Detailed theoretical computation of the GRB011121 light curves in selected energy bands are presented and compared and contrasted with observational BeppoSAX data.

7. R. Ruffini, M.G. Bernardini, C.L. Bianco, P. Chardonnet, F. Frascchetti, R. Guida, S.-S. Xue; “GRB 050315: A step toward the uniqueness of the overall GRB structure”; *Il Nuovo Cimento B*, 121, 1367 (2006).

Using the *Swift* data of GRB 050315, we progress on the uniqueness of our theoretically predicted Gamma-Ray Burst (GRB) structure as composed by a proper-GRB (P-GRB), emitted at the transparency of an electron-positron plasma with suitable baryon loading, and an afterglow comprising the so called “prompt emission” as due to external shocks. Thanks to the *Swift* observations, we can theoretically fit detailed light curves for selected energy bands on a continuous time scale ranging over 10⁶ seconds. The theoretically predicted instantaneous spectral distribution over the entire afterglow confirms a clear hard-to-soft behavior encompassing, continuously, the “prompt emission” all the way to the latest phases of the afterglow. Consequences of the instrumental threshold on the definition of “short” and “long” GRBs are discussed.

8. M.G. Bernardini, C.L. Bianco, L. Caito, P. Chardonnet, A. Corsi, M.G. Dainotti, F. Frascchetti, R. Guida, R. Ruffini, S.-S. Xue; GRB970228 as a prototype for short GRBs with afterglow; *Il Nuovo Cimento B*, 121, 1439 (2006).

GRB970228 is analyzed as a prototype to understand the relative role of short GRBs and their associated afterglows, recently observed by Swift and HETE-II. Detailed theoretical computation of the GRB970228 light curves in selected energy bands are presented and compared with observational BeppoSAX data.

9. M.G. Dainotti, M.G. Bernardini, C.L. Bianco, L. Caito, R. Guida, R. Ruffini; “GRB060218 and GRBs associated with Supernovae Ib/c”; *Astronomy & Astrophysics*, 471, L29 (2007).

Context: The *Swift* satellite has given continuous data in the range 0.3–150 keV from 0 s to 10^6 s for GRB060218 associated with SN2006aj. This Gamma-Ray Burst (GRB) which has an unusually long duration ($T_{90} \sim 2100$ s) fulfills the Amati relation. These data offer the opportunity to probe theoretical models for GRBs connected with Supernovae (SNe).

Aims: We plan to fit the complete γ - and X-ray light curves of this long duration GRB, including the prompt emission, in order to clarify the nature of the progenitors and the astrophysical scenario of the class of GRBs associated with SNe Ib/c.

Methods: We apply our “fireshell” model based on the formation of a black hole, giving the relevant references. It is characterized by the precise equations of motion and equitemporal surfaces and by the role of thermal emission.

Results: The initial total energy of the electron-positron plasma $E_{e^\pm}^{tot} = 2.32 \times 10^{50}$ erg has a particularly low value, similar to the other GRBs associated with SNe. For the first time, we observe a baryon loading $B = 10^{-2}$ which coincides with the upper limit for the dynamical stability of the fireshell. The effective CircumBurst Medium (CBM) density shows a radial dependence $n_{cbm} \propto r^{-\alpha}$ with $1.0 \lesssim \alpha \lesssim 1.7$ and monotonically decreases from 1 to 10^{-6} particles/cm³. This behavior is interpreted as being due to a fragmentation in the fireshell. Analogies with the fragmented density and filling factor characterizing Novae are outlined. The fit presented is particularly significant in view of the complete data set available for GRB060218 and of the fact that it fulfills the Amati relation.

Conclusions: We fit GRB060218, usually considered as an X-Ray Flash (XRF), as a “canonical GRB” within our theoretical model. The smallest possible black hole, formed by the gravitational collapse of a neutron star in a binary system, is consistent with the especially low energetics of the class of GRBs associated with SNe Ib/c. We provide the first evidence for a fragmentation in the fireshell. This fragmentation is crucial in explaining both the unusually large T_{90} and the consequently inferred abnormally low value of the CBM effective

density.

10. M.G. Bernardini, C.L. Bianco, L. Caito, M.G. Dainotti, R. Guida, R. Ruffini; “GRB970228 and a class of GRBs with an initial spikelike emission”; *Astronomy & Astrophysics*, 474, L13 (2007).

Context: The discovery by *Swift* and HETE-2 of an afterglow emission associated possibly with short GRBs opened the new problematic of their nature and classification. This issue has been further enhanced by the observation of GRB060614 and by a new analysis of the BATSE catalog which led to the identification of a new class of GRBs with “an occasional softer extended emission lasting tenths of seconds after an initial spikelike emission”.

Aims: We plan a twofold task: a) to fit this new class of “hybrid” sources within our “canonical GRB” scenario, where all GRBs are generated by a “common engine” (i.e. the gravitational collapse to a black hole); b) to propose GRB970228 as the prototype of the above mentioned class, since it shares the same morphology and observational features.

Methods: We analyze *BeppoSAX* data on GRB970228 within the “fireshell” model and we determine the parameters describing the source and the CircumBurst Medium (CBM) needed to reproduce its light curves in the 40–700 keV and 2–26 keV energy bands.

Results: We find that GRB970228 is a “canonical GRB”, like e.g. GRB050315, with the main peculiarity of a particularly low average density of the CBM $\langle n_{cbm} \rangle \sim 10^{-3}$ particles/cm³. We also simulate the light curve corresponding to a rescaled CBM density profile with $\langle n_{cbm} \rangle = 1$ particle/cm³. From such a comparison it follows that the total time-integrated luminosity is a faithful indicator of the nature of GRBs, contrary to the peak luminosity which is merely a function of the CBM density.

Conclusions: We call attention on discriminating the short GRBs between the “genuine” and the “fake” ones. The “genuine” ones are intrinsically short, with baryon loading $B \lesssim 10^{-5}$, as stated in our original classification. The “fake” ones, characterized by an initial spikelike emission followed by an extended emission lasting tenths of seconds, have a baryon loading $10^{-4} \lesssim B \leq 10^{-2}$. They are observed as such only due to an underdense CBM consistent with a galactic halo environment which deflates the afterglow intensity.

11. R. Guida, M.G. Bernardini, C.L. Bianco, L. Caito, M.G. Dainotti, R. Ruffini; “The Amati relation in the “fireshell” model”; *Astronomy & Astrophysics*, 487, L37 (2008).

Context: The cosmological origin of gamma-ray bursts (GRBs) has been firmly established, with redshifts up to $z = 6.29$. They are possible candidates for use as “distance indicators” for testing cosmological models in a redshift range hardly achievable by other cosmological probes. Asserting the validity of the empirical relations among GRB observables is now crucial for their calibration.

Aims: Motivated by the relation proposed by Amati and collaborators, we look within the “fireshell” model for a relation between the peak energy E_p of the νF_ν total time-integrated spectrum of the afterglow and the total energy of the afterglow E_{aft} , which in our model encompasses and extends the prompt emission.

Methods: The fit within the fireshell model, as for the “canonical” GRB050315, uses the complete arrival time coverage given by the Swift satellite. It is performed simultaneously, self-consistently, and recursively in the four BAT energy bands (15–25 keV, 25–50 keV, 50–100 keV, and 100–150 keV), as well as in the XRT one (0.2–10 keV). It uniquely determines the two free parameters characterizing the GRB source, the total energy $E_{tot}^{e^\pm}$ of the e^\pm plasma and its baryon loading B , as well as the effective CircumBurst Medium (CBM) distribution. We can then build two sets of “gedanken” GRBs varying the total energy of the electron-positron plasma $E_{tot}^{e^\pm}$ and keeping the same baryon loading B of GRB050315. The first set assumes the one obtained in the fit of GRB050315 for the effective CBM density. The second set assumes instead a constant CBM density equal to the average value of the GRB050315 prompt phase.

Results: For the first set of “gedanken” GRBs we find a relation $E_p \propto (E_{aft})^a$, with $a = 0.45 \pm 0.01$, whose slope strictly agrees with the Amati one. Such a relation, in the limit $B \rightarrow 10^{-2}$, coincides with the Amati one. Instead, no correlation is found in the second set of “gedanken” GRBs.

Conclusions: Our analysis excludes the proper GRB (P-GRB) from the prompt emission, extends all the way to the latest afterglow phases, and is independent of the assumed cosmological model, since all “gedanken” GRBs are at the same redshift. The Amati relation, on the other hand, includes the P-GRB, focuses only on the prompt emission, being therefore influenced by the instrumental threshold that fixes the end of the prompt emission, and depends on the assumed cosmology. This might explain the intrinsic scatter observed in the Amati relation.

12. L. Caito, M.G. Bernardini, C.L. Bianco, M.G. Dainotti, R. Guida, R. Ruffini; “GRB060614: a “fake” short GRB from a merging binary system”; *Astronomy & Astrophysics*, 489, 501 (2009).

Context: GRB060614 observations by VLT and by Swift have infringed the traditionally accepted gamma-ray burst (GRB) collapsar scenario that purports the origin of all long duration GRBs from supernovae (SN). GRB060614 is the first nearby long duration GRB clearly not associated with a bright Ib/c SN. Moreover, its duration ($T_{90} \sim 100$ s) makes it hardly classifiable as a short GRB. It presents strong similarities with GRB970228, the prototype of a new class of “fake” short GRBs that appear to originate from the coalescence of binary neutron stars or white dwarfs spiraled out into the galactic halo. *Aims:* Within the “canonical” GRB scenario based on the “fireshell” model, we test if GRB060614 can be a “fake” or “disguised” short GRB. We model the traditionally termed “prompt emission” and discriminate the signal originating from the gravitational collapse leading to the GRB from the process occurring in the circumburst medium (CBM). *Methods:* We fit GRB060614 light curves in Swift’s BAT (15 – 150 keV) and XRT (0.2 – 10 keV) energy bands. Within the fireshell model, light curves are formed by two well defined and different components: the proper-GRB (P-GRB), emitted when the fireshell becomes transparent, and the extended afterglow, due to the interaction between the leftover accelerated baryonic and leptonic shell and the CBM. *Results:* We determine the two free parameters describing the GRB source within the fireshell model: the total e^\pm plasma energy ($E_{tot}^{e^\pm} = 2.94 \times 10^{51}$ erg) and baryon loading ($B = 2.8 \times 10^{-3}$). A small average CBM density $\sim 10^{-3}$ particles/cm³ is inferred, typical of galactic halos. The first spikelike emission is identified with the P-GRB and the following prolonged emission with the extended afterglow peak. We obtain very good agreement in the BAT (15 – 150 keV) energy band, in what is traditionally called “prompt emission”, and in the XRT (0.2 – 10 keV) one. *Conclusions:* The *anomalous* GRB060614 finds a natural interpretation within our canonical GRB scenario: it is a “disguised” short GRB. The total time-integrated extended afterglow luminosity is greater than the P-GRB one, but its peak luminosity is smaller since it is deflated by the peculiarly low average CBM density of galactic halos. This result points to an old binary system, likely formed by a white dwarf and a neutron star, as the progenitor of GRB060614 and well justifies the absence of an associated SN Ib/c. Particularly important for further studies of the final merging process are the temporal structures in the P-GRB down to 0.1 s.

13. M.G. Bernardini, C.L. Bianco, L. Caito, M.G. Dainotti, R. Guida, R. Ruffini; “GRB970228 in the “canonical GRB” scenario”; *Journal of the Korean Physical Society*, 56, 1575 (2010).

Within the “fireshell” model, we define a “canonical GRB” light curve with two sharply different components: the proper-GRB (P-GRB), emitted when the optically thick fireshell of an electron-positron plasma originating from the phenomenon reaches transparency, and the afterglow, emitted due to the collision between the remaining optically thin fireshell and the circumburst medium (CBM). On the basis of the recent understanding of GRB970228 as the prototype for a new class of GRBs with “an occasional softer extended emission lasting tenths of seconds after an initial spikelike emission”, we outline our “canonical GRB” scenario, originating from the gravitational collapse to a black hole, with special emphasis on the discrimination between “genuine” and “fake” short GRBs. Furthermore, we investigate how the GRB970228 analysis provides a theoretical explanation for the apparent absence of such a correlation for the GRBs belonging to this new class.

14. L. Caito, M.G. Bernardini, C.L. Bianco, M.G. Dainotti, R. Guida, R. Ruffini; “GRB060614: a preliminary result”; *Journal of the Korean Physical Society*, 56, 1579 (2010).

The explosion of GRB 060614 produced a deep break in the GRB scenario and opened new horizons of investigation because it can't be traced back to any traditional scheme of classification. In fact, it manifests peculiarities both of long bursts and of short bursts, and above all, it is the first case of a long-duration near GRB without any bright Ib/c associated Supernova. We will show that, in our canonical GRB scenario, this “anomalous” situation finds a natural interpretation and allows us to discuss a possible variation in the traditional classification scheme, introducing a distinction between “genuine” and “fake” short bursts.

15. M.G. Dainotti, M.G. Bernardini, C.L. Bianco, L. Caito, R. Guida, R. Ruffini; “The astrophysical tryptic: GRB, SN and URCA can be extended to GRB060218?”; *Journal of the Korean Physical Society*, 56, 1588 (2010).

The *Swift* satellite has given continuous data in the range 0.3–150 keV from 0 s to 10^6 s for GRB060218 associated with SN2006aj. This GRB is the fourth GRB spectroscopically associated with SNe after the cases of GRB980425-SN1998bw, GRB031203-SN2003lw, GRB 030329-SN2003dh. It has an unusually long duration ($T_{90} \sim 2100$ s). These data offer the opportunity to probe theoretical models for Gamma-Ray Bursts (GRBs) connected with Supernovae (SNe). We plan to fit the complete γ - and X-ray light curves of this long duration GRB,

including the prompt emission, in order to clarify the nature of the progenitors and the astrophysical scenario of the class of GRBs associated to SNe Ib/c. We apply our “fireshell” model based on the formation of a black hole, giving the relevant references. The initial total energy of the electron-positron plasma $E_{e^\pm}^{tot} = 2.32 \times 10^{50}$ erg has a particularly low value similarly to the other GRBs associated with SNe. For the first time we observe a baryon loading $B = 10^{-2}$ which coincides with the upper limit for the dynamical stability of the fireshell. The effective CircumBurst Medium (CBM) density shows a radial dependence $n_{cbm} \propto r^{-\alpha}$ with $1.0 \lesssim \alpha \lesssim 1.7$ and monotonically decreases from 1 to 10^{-6} particles/cm³. Such a behavior is interpreted as due to a fragmentation in the fireshell. Such a fragmentation is crucial in explaining both the unusually large T_{90} and the consequently inferred abnormal low value of the CBM effective density. We fit GRB060218, usually considered as an X-Ray Flash (XRF), as a “canonical GRB” within our theoretical model. The smallest possible black hole, formed by the gravitational collapse of a neutron star in a binary system, is consistent with the especially low energetics of the class of GRBs associated with SNe Ib/c. We present the URCA process and the connection between the GRBs associated with SNe extended also to the case of GRB060218.

16. L. Izzo, M.G. Bernardini, C.L. Bianco, L. Caito, B. Patricelli, R. Ruffini; “GRB 090423 at Redshift 8.1: a Theoretical Interpretation”; *Journal of the Korean Physical Society*, 57, 551 (2010).

GRB 090423 is the farthest gamma ray burst ever observed, with a redshift of about 8.1. We present within the fireshell scenario a complete analysis of this GRB. We model the prompt emission and the first rapid flux decay of the afterglow emission as being to the canonical emission of the interaction in the interval $0 \leq t \leq 440$ s by using accelerated baryonic matter with the circumburst medium. After the data reduction of the Swift data in the BAT (15 - 150 keV) and XRT (0.2 - 10 keV) energy bands, we interpret the light curves and the spectral distribution in the context of the fireshell scenario. We also confirm in this source the existence of a second component, a plateau phase, as being responsible for the late emission in the X-ray light curve. This extra component originates from the fact that the ejecta have a range of the bulk Lorentz Γ factor, which starts to interact each other ejecta at the start of the plateau phase.

17. L. Caito, L. Amati, M.G. Bernardini, C.L. Bianco, G. De Barros, L. Izzo, B. Patricelli, R. Ruffini; “GRB 071227: an additional case of a disguised

short burst”; *Astronomy & Astrophysics*, 521, A80 (2010).

Context: Observations of gamma-ray bursts (GRBs) have shown an hybridization between the two classes of long and short bursts. In the context of the fireshell model, the GRB light curves are formed by two different components: the *proper* GRB (P-GRB) and the extended afterglow. Their relative intensity is linked to the fireshell baryon loading B . The GRBs with P-GRB predominance are the short ones, the remainders are long. A new family of *disguised* short bursts has been identified: long bursts with a protracted low instantaneous luminosity due to a low density CircumBurst Medium (CBM). In the 15–150 keV energy band GRB 071227 exhibits a short duration (about 1.8s) spike-like emission followed by a very soft extended tail up to one hundred seconds after the trigger. It is a faint ($E_{iso} = 5.8 \times 10^{50}$) nearby GRB ($z = 0.383$) that does not have an associated type Ib/c bright supernova (SN). For these reasons, GRB 071227 has been classified as a short burst not fulfilling the Amati relation holding for long burst. *Aims:* We check the classification of GRB 071227 provided by the fireshell model. In particular, we test whether this burst is another example of a *disguised* short burst, after GRB 970228 and GRB 060614, and, for this reason, whether it fulfills the Amati relation. *Methods:* We simulate GRB 071227 light curves in the *Swift* BAT 15–50 keV bandpass and in the XRT (0.3–10 keV) energy band within the fireshell model. *Results:* We perform simulations of the tail in the 15–50 keV bandpass, as well as of the first part of the X-ray afterglow. This infers that: $E_{tot}^{e^{\pm}} = 5.04 \times 10^{51}$ erg, $B = 2.0 \times 10^{-4}$, $E_{P-GRB}/E_{aft} \sim 0.25$, and $\langle n_{cbm} \rangle = 3.33$ particles/cm³. These values are consistent with those of “long duration” GRBs. We interpret the observed energy of the first hard emission by identifying it with the P-GRB emission. The remaining long soft tail indeed fulfills the Amati relation. *Conclusions:* Previously classified as a short burst, GRB 071227 on the basis of our analysis performed in the context of the fireshell scenario represents another example of a *disguised* short burst, after GRB 970228 and GRB 060614. Further confirmation of this result is that the soft tail of GRB 071227 fulfills the Amati relation.

18. M.G. Bernardini, C.L. Bianco, L. Caito, L. Izzo, B. Patricelli, R. Ruffini; “Analysis of GRB060607A within the fireshell model: prompt emission, X-ray flares and late afterglow phase”; *Astronomy & Astrophysics*, submitted to.

Context: GRB060607A is a very distant ($z = 3.082$) and energetic event ($E_{iso} \sim 10^{53}$ erg). Its main peculiarity is that the peak of the near-infrared (NIR) af-

terglow has been observed with the REM robotic telescope. This NIR peak has been interpreted as the afterglow onset within the fireball forward shock model, and the initial Lorentz gamma factor of the emitting system has been inferred. *Aims:* We analyze GRB060607A within the fireshell model. We emphasize the central role of the prompt emission in determining the initial Lorentz gamma factor of the extended afterglow and we interpret the X-ray flares as produced by the interaction of the optically thin fireshell with overdense CircumBurst Medium (CBM) clumps. *Methods:* We deal only with the Swift BAT and XRT observations, that are the basic contribution to the GRB emission and that are neglected in the treatment adopted in the current literature. The numerical modeling of the fireshell dynamics allows to calculate all its characteristic quantities, in particular the exact value of the Lorentz gamma factor at the transparency. *Results:* We show that the theoretically computed prompt emission light curves are in good agreement with the observations in all the Swift BAT energy bands as well as the spectra integrated over different time intervals. The flares observed in the decaying phase of the X-ray afterglow are also reproduced by the same mechanism, but in a region in which the typical dimensions of the clumps are smaller than the visible area of the fireshell and most energy lies in the X-ray band due to the hard-to-soft evolution. *Conclusions:* We show that it is possible to obtain flares with $\Delta t/t$ compatible with the observations when the three-dimensional structure of the CBM clumps is duly taken into account. We stop our analysis at the beginning of the X-ray plateau phase, since we suppose this originates from the instabilities developed in the collision between different subshells within a structured fireshell.

19. G. de Barros, M. G. Bernardini, C.L. Bianco, L. Caito, L. Izzo, B. Patricelli, R. Ruffini; "On the nature of GRB 050509b: a disguised short GRB"; *Astronomy & Astrophysics*, 529, A130 (2011)

Context: GRB 050509b, detected by the Swift satellite, is the first case where an X-ray afterglow has been observed associated with a short gamma-ray burst (GRB). Within the fireshell model, the canonical GRB light curve presents two different components: the proper-GRB (P-GRB) and the extended afterglow. Their relative intensity is a function of the fireshell baryon loading parameter B and of the CircumBurst Medium (CBM) density (n_{CBM}). In particular, the traditionally called short GRBs can be either "genuine" short GRBs (with $B \lesssim 10^{-5}$, where the P-GRB is energetically predominant) or "disguised" short GRBs (with $B \gtrsim 3.0 \times 10^{-4}$ and $n_{CBM} \ll 1$, where the extended afterglow is energetically predominant). *Aims:* We verify whether GRB 050509b can be clas-

sified as a “genuine” short or a “disguised” short GRB, in the fireshell model. *Methods:* We investigate two alternative scenarios. In the first, we start from the assumption that this GRB is a “genuine” short burst. In the second attempt, we assume that this GRB is a “disguised” burst. *Results:* If GRB 050509b were a genuine short GRB, there should initially be very hard emission which is ruled out by the observations. The analysis that assumes that this is a disguised short GRB is compatible with the observations. The theoretical model predicts a value of the extended afterglow energy peak that is consistent with the Amati relation. *Conclusions:* GRB 050509b cannot be classified as a “genuine” short GRB. The observational data are consistent with a “disguised” short GRB classification, i.e., a long burst with a weak extended afterglow “deflated” by the low density of the CBM. We expect that all short GRBs with measured redshifts are disguised short GRBs because of a selection effect: if there is enough energy in the afterglow to measure the redshift, then the proper GRB must be less energetic than the afterglow. The Amati relation is found to be fulfilled only by the extended afterglow excluding the P-GRB.

20. L. Caito, M.G. Bernardini, C.L. Bianco, L. Izzo, B. Patricelli, R. Ruffini; “GRB 071227: another disguised short burst”; *International Journal of Modern Physics D*, 20, 1931 (2011).

Observations of Gamma-ray Bursts (GRBs) put forward in the recent years have revealed, with increasing evidence, that the historical classification between long and short bursts has to be revised. Within the Fireshell scenario, both short and long bursts are canonical bursts, consisting of two different phases. First, a Proper-GRB (P-GRB), that is the emission of photons at the transparency of the fireshell. Then, the Extended Afterglow, multiwavelength emission due to the interaction of the baryonic remnants of the fireshell with the CircumBurst Medium (CBM). We discriminate between long and short bursts by the amount of energy stored in the first phase with respect to the second one. Within the Fireshell scenario, we have introduced a third intermediate class: the disguised GRBs. They appear like short bursts, because their morphology is characterized by a first, short, hard episode and a following deflated tail, but this last part — coincident with the peak of the afterglow — is energetically predominant. The origin of this peculiar kind of sources is inferred to a very low average density of the environment (of the order of 10^{-3}). After GRB 970228 and GRB 060614, we find in GRB 071227 a third example of disguised burst.

21. L. Izzo, M.G. Bernardini, C.L. Bianco, L. Caito, B. Patricelli, L.J. Rangel Lemos, R. Ruffini; “GRB 080916C and the high-energy emission in the fireshell scenario”; *International Journal of Modern Physics D*, 20, 1949 (2011).

In this paper we discuss a possible explanation for the high energy emission (up to \sim GeV) seen in GRB 080916C. We propose that the GeV emission is originated by the collision between relativistic baryons in the fireshell after the transparency and the nucleons located in molecular clouds near the burst site. This collision should give rise pion production, whose immediate decay provides high energy photons, neutrinos and leptons. Using a public code (SYBILL) we simulate these relativistic collisions in their simple form, so that we can draw our preliminar results in this paper. We will present moreover our hypothesis that the delayed onset of this emission identifies in a complete way the P-GRB emission.

22. B. Patricelli, M.G. Bernardini, C.L. Bianco, L. Caito, L. Izzo, R. Ruffini, G. Vereshchagin; “A new spectral energy distribution of photons in the fireshell model of GRBs”; *International Journal of Modern Physics D*, 20, 1983 (2011).

The analysis of various Gamma-Ray Bursts (GRBs) having a low energetics (an isotropic energy $E_{iso} \lesssim 10^{53}$ ergs) within the fireshell model has shown how the $N(E)$ spectrum of their prompt emission can be reproduced in a satisfactory way by a convolution of thermal spectra. Nevertheless, from the study of very energetic bursts ($E_{iso} \lesssim 10^{54}$ ergs) such as, for example, GRB 080319B, some discrepancies between the numerical simulations and the observational data have been observed. We investigate a different spectrum of photons in the comoving frame of the fireshell in order to better reproduce the spectral properties of GRB prompt emission within the fireshell model. We introduce a phenomenologically modified thermal spectrum: a thermal spectrum characterized by a different asymptotic power-law index in the low energy region. Such an index depends on a free parameter α , so that the pure thermal spectrum corresponds to the case $\alpha = 0$. We test this spectrum by comparing the numerical simulations with the observed prompt emission spectra of various GRBs. From this analysis it has emerged that the observational data can be correctly reproduced by assuming a modified thermal spectrum with $\alpha = -1.8$.

23. A.V. Penacchioni, R. Ruffini, L. Izzo, M. Muccino, C.L. Bianco, L. Caito, B. Patricelli, L. Amati; “Evidence for a proto-black hole and a double

astrophysical component in GRB 101023"; *Astronomy & Astrophysics*, 538, A58 (2012).

Context: It has been recently shown that GRB 090618, observed by AGILE, Coronas Photon, Fermi, Konus, Suzaku and Swift, is composed of two very different components: episode 1, lasting 50 s, shows a thermal plus power-law spectrum with a characteristic temperature evolving in time as a power law; episode 2 (the remaining 100 s) is a canonical long GRB. We have associated episode 1 to the progenitor of a collapsing bare core leading to the formation of a black hole: what was defined as a "proto black hole". *Aims:* In precise analogy with GRB 090618 we aim to analyze the 89s of the emission of GRB 101023, observed by Fermi, Gemini, Konus and Swift, to see if there are two different episodes: the first one presenting a characteristic black-body temperature evolving in time as a broken power law, and the second one consistent with a canonical GRB. *Methods:* To obtain information on the spectra, we analyzed the data provided by the GBM detector onboard the Fermi satellite, and we used the heasoft package XSPEC and RMFIT to obtain their spectral distribution. We also used the numerical code GRBsim to simulate the emission in the context of the fireshell scenario for episode 2. *Results:* We confirm that the first episode can be well fit by a black body plus power-law spectral model. The temperature changes with time following a broken power law, and the photon index of the power-law component presents a soft-to-hard evolution. We estimate that the radius of this source increases with time with a velocity of $1.5 \times 10^4 km/s$. The second episode appears to be a canonical GRB. By using the Amati and the Atteia relations, we determined the cosmological redshift, $z \sim 0.9 \pm 0.084(stat.) \pm 0.2(sys.)$. The results of GRB 090618 are compared and contrasted with the results of GRB 101023. Particularly striking is the scaling law of the soft X-ray component of the afterglow. *Conclusions:* We identify GRB 090618 and GRB 101023 with a new family of GRBs related to a single core collapse and presenting two astrophysical components: a first one related to the proto-black hole prior to the process of gravitational collapse (episode 1), and a second one, which is the canonical GRB (episode 2) emitted during the formation of the black hole. For the first time we are witnessing the process of a black hole formation from the instants preceding the gravitational collapse up to the GRB emission. This analysis indicates progress towards developing a GRB distance indicator based on understanding the P-GRB and the prompt emission, as well as the soft X-ray behavior of the late afterglow.

24. R. Negreiros, R. Ruffini, C. L. Bianco, J. A. Rueda; "Cooling of young

neutron stars in GRB associated to supernovae"; *Astronomy & Astrophysics*, 540, A12 (2012).

Context: The traditional study of neutron star cooling has been generally applied to quite old objects such as the Crab Pulsar (957 years) or the central compact object in Cassiopeia A (330 years) with an observed surface temperature $\sim 10^6$ K. However, recent observations of the late ($t = 10^8$ – 10^9 s) emission of the supernovae (SNe) associated to GRBs (GRB-SN) show a distinctive emission in the X-ray regime consistent with temperatures $\sim 10^7$ – 10^8 K. Similar features have been also observed in two Type Ic SNe SN 2002ap and SN 1994I that are not associated to GRBs. *Aims:* We advance the possibility that the late X-ray emission observed in GRB-SN and in isolated SN is associated to a hot neutron star just formed in the SN event, here defined as a neo-neutron star. *Methods:* We discuss the thermal evolution of neo-neutron stars in the age regime that spans from ~ 1 minute (just after the proto-neutron star phase) all the way up to ages < 10 – 100 yr. We examine critically the key factor governing the neo-neutron star cooling with special emphasis on the neutrino emission. We introduce a phenomenological heating source, as well as new boundary conditions, in order to mimic the high temperature of the atmosphere for young neutron stars. In this way we match the neo-neutron star luminosity to the observed late X-ray emission of the GRB-SN events: URCA-1 in GRB980425-SN1998bw, URCA-2 in GRB030329-SN2003dh, and URCA-3 in GRB031203-SN2003lw. *Results:* We identify the major role played by the neutrino emissivity in the thermal evolution of neo-neutron stars. By calibrating our additional heating source at early times to $\sim 10^{12}$ – 10^{15} erg/g/s, we find a striking agreement of the luminosity obtained from the cooling of a neo-neutron stars with the prolonged ($t = 10^8$ – 10^9 s) X-ray emission observed in GRB associated with SN. It is therefore appropriate a revision of the boundary conditions usually used in the thermal cooling theory of neutron stars, to match the proper conditions of the atmosphere at young ages. The traditional thermal processes taking place in the crust might be enhanced by the extreme high-temperature conditions of a neo-neutron star. Additional heating processes that are still not studied within this context, such as e^+e^- pair creation by overcritical fields, nuclear fusion, and fission energy release, might also take place under such conditions and deserve further analysis. *Conclusions:* Observation of GRB-SN has shown the possibility of witnessing the thermal evolution of neo-neutron stars. A new campaign of dedicated observations is recommended both of GRB-SN and of isolated Type Ic SN.

25. L. Izzo, R. Ruffini, A.V. Penacchioni, C.L. Bianco, L. Caito, S.K. Chakrabarti, J.A. Rueda, A. Nandi, B. Patricelli; “A double component in GRB 090618: a proto-black hole and a genuinely long gamma-ray burst”; *Astronomy & Astrophysics*, 543, A10 (2012).

Context: The joint X-ray and gamma-ray observations of GRB 090618 by very many satellites offer an unprecedented possibility of testing crucial aspects of theoretical models. In particular, they allow us to test (a) in the process of gravitational collapse, the formation of an optically thick e^+e^- -baryon plasma self-accelerating to Lorentz factors in the range $200 < \Gamma < 3000$; (b) its transparency condition with the emission of a component of 10^{53-54} baryons in the TeV region and (c) the collision of these baryons with the circumburst medium (CBM) clouds, characterized by dimensions of 10^{15-16} cm. In addition, these observations offer the possibility of testing a new understanding of the thermal and power-law components in the early phase of this GRB. *Aims:* We test the fireshell model of GRBs in one of the closest ($z = 0.54$) and most energetic ($E_{iso} = 2.90 \times 10^{53}$ erg) GRBs, namely GRB 090618. It was observed at ideal conditions by several satellites, namely *Fermi*, *Swift*, Konus-WIND, AGILE, RT-2, and Suzaku, as well as from on-ground optical observatories. *Methods:* We analyzed the emission from GRB 090618 using several spectral models, with special attention to the thermal and power-law components. We determined the fundamental parameters of a canonical GRB within the context of the fireshell model, including the identification of the total energy of the e^+e^- plasma, $E_{tot}^{e^+e^-}$, the proper GRB (P-GRB), the baryon load, the density and structure of the CBM. *Results:* We find evidence of the existence of two different episodes in GRB 090618. The first episode lasts 50 s and is characterized by a spectrum consisting of a thermal component, which evolves between $kT = 54$ keV and $kT = 12$ keV, and a power law with an average index $\gamma = 1.75 \pm 0.04$. The second episode, which lasts for ~ 100 s, behaves as a canonical long GRB with a Lorentz gamma factor at transparency of $\Gamma = 495$, a temperature at transparency of 29.22 keV and with a characteristic size of the surrounding clouds of $R_{cl} \sim 10^{15-16}$ cm and masses of $\sim 10^{22-24}$ g. *Conclusions:* We support the recently proposed two-component nature of GRB 090618, namely, episode 1 and episode 2, with a specific theoretical analysis. We furthermore illustrate that episode 1 cannot be considered to be either a GRB or a part of a GRB event, but it appears to be related to the progenitor of the collapsing bare core, leading to the formation of the black hole, which we call a “proto-black hole”. Thus, for the first time, we are witnessing the process of formation of a black

hole from the phases just preceding the gravitational collapse all the way up to the GRB emission.

26. B. Patricelli, M.G. Bernardini, C.L. Bianco, L. Caito, G. De Barros, L. Izzo, R. Ruffini, G.V. Vereshchagin; “Analysis of GRB 080319B and GRB 050904 within the Fireshell Model: Evidence for a Broader Spectral Energy Distribution”; *The Astrophysical Journal*, 756, 16 (2012).

The observation of GRB 080319B, with an isotropic energy $E_{iso} = 1.32 \times 10^{54}$ erg, and GRB 050904, with $E_{iso} = 1.04 \times 10^{54}$ erg, offers the possibility of studying the spectral properties of the prompt radiation of two of the most energetic Gamma Ray Bursts (GRBs). This allows us to probe the validity of the fireshell model for GRBs beyond 10^{54} erg, well outside the energy range where it has been successfully tested up to now (10^{49} – 10^{53} erg). We find that in the low energy region, the prompt emission spectra observed by *Swift* BAT reveals more power than theoretically predicted. The opportunities offered by these observations to improve the fireshell model are outlined in this paper. One of the distinguishing features of the fireshell model is that it relates the observed GRB spectra to the spectrum in the comoving frame of the fireshell. Originally, a fully radiative condition and a comoving thermal spectrum were adopted. An additional power-law in the comoving thermal spectrum is required due to the discrepancy of the theoretical and observed light curves and spectra in the fireshell model for GRBs 080319B and 050904. A new phenomenological parameter α is correspondingly introduced in the model. We perform numerical simulations of the prompt emission in the *Swift* BAT bandpass by assuming different values of α within the fireshell model. We compare them with the GRB 080319B and GRB 050904 observed time-resolved spectra, as well as with their time-integrated spectra and light curves. Although GRB 080319B and GRB 050904 are at very different redshifts ($z=0.937$ and $z=6.29$ respectively), a value of $\alpha = -1.8$ leads for both of them to a good agreement between the numerical simulations and the observed BAT light curves, time-resolved and time-integrated spectra. Such a modified spectrum is also consistent with the observations of previously analyzed less energetic GRBs and reasons for this additional agreement are given. Perspectives for future low energy missions are outlined.

27. M. Muccino, R. Ruffini, C.L. Bianco, L. Izzo, A.V. Penacchioni; “GRB 090227B: The missing link between the genuine short and long GRBs”; *The Astrophysical Journal*, 763, 125 (2013).

The time-resolved spectral analysis of GRB 090227B, made possible by the *Fermi*-GBM data, allows to identify in this source the missing link between the genuine short and long GRBs. Within the Fireshell model of the Gamma-Ray Bursts (GRBs) we predict genuine short GRBs: bursts with the same inner engine of the long bursts but endowed with a severely low value of the Baryon load, $B \lesssim 5 \times 10^{-5}$. A first energetically predominant emission occurs at the transparency of the e^+e^- plasma, the Proper-GRB (P-GRB), followed by a softer emission, the extended afterglow. The typical separation between the two emissions is expected to be of the order of $10^{-3} - 10^{-2}$ s. We identify the P-GRB of GRB 090227B in the first 96 ms of emission, where a thermal component with the temperature $kT = (517 \pm 28)$ keV and a flux comparable with the non thermal part of the spectrum is observed. This non thermal component as well as the subsequent emission, where there is no evidence for a thermal spectrum, is identified with the extended afterglow. We deduce a theoretical cosmological redshift $z = 1.61 \pm 0.14$. We then derive the total energy $E_{e^+e^-}^{tot} = (2.83 \pm 0.15) \times 10^{53}$ ergs, the Baryon load $B = (4.13 \pm 0.05) \times 10^{-5}$, the Lorentz Γ factor at transparency $\Gamma_{tr} = (1.44 \pm 0.01) \times 10^4$, and the intrinsic duration $\Delta t' \sim 0.35$ s. We also determine the average density of the CircumBurst Medium (CBM), $\langle n_{CBM} \rangle = (1.90 \pm 0.20) \times 10^{-5}$ particles/cm³. There is no evidence of beaming in the system. In view of the energetics and of the Baryon load of the source, as well as of the low interstellar medium and of the intrinsic time scale of the signal, we identify the GRB progenitor as a binary neutron star. From the recent progress in the theory of neutron stars, we obtain masses of the stars $m_1 = m_2 = 1.34M_\odot$ and their corresponding radii $R_1 = R_2 = 12.24$ km and thickness of their crusts ~ 0.47 km, consistent with the above values of the Baryon load, of the energetics and of the time duration of the event.

28. A.V. Penacchioni, R. Ruffini, C.L. Bianco, L. Izzo, M. Muccino, G.B. Pisani, J.A. Rueda; “GRB 110709B in the induced gravitational collapse paradigm”; *Astronomy & Astrophysics*, 551, A133 (2013).

Context: GRB 110709B is the first source for which *Swift* BAT triggered twice, with a time separation of ~ 10 minutes. The first emission (called here Episode 1) goes from 40 s before the first trigger up to 60 s after it. The second emission (hereafter Episode 2) goes from 35 s before the second trigger to 100 s after it. These features reproduce the ones of GRB 090618, which has been recently interpreted within the Induced Gravitational Collapse paradigm (IGC). In line with this paradigm we assume the progenitor to be a close binary system composed of a core of an evolved star and a Neutron Star (NS). The evolved star

explodes as a Supernova (SN) and ejects material that is partially accreted by the NS. We identify this process with Episode 1. The accretion process brings the NS over its critical mass, thus gravitationally collapsing to a BH. This process leads to the GRB emission, Episode 2. The double trigger has given for the first time the possibility to have a coverage of the X-ray emission observed by XRT both prior to and during the prompt phase of GRB 110709B. *Aims:* We analyze the spectra and time variability of Episode 1 and 2 and compute the relevant parameters of the binary progenitor, as well as the astrophysical parameters both in the SN and the GRB phase in the IGC paradigm. *Methods:* We perform a time-resolved spectral analysis of Episode 1 by fitting the spectrum with a blackbody (BB) plus a power-law (PL) spectral model. From the BB fluxes and temperatures of Episode 1 and the luminosity distance d_L , we evaluate the evolution with time of the radius of the BB emitter, associated here to the evolution of the SN ejecta. We analyze Episode 2 within the Fireshell model, identifying the Proper-GRB (P-GRB) and simulating the light curve and spectrum. We establish the redshift to be $z = 0.75$, following the phenomenological methods by Amati, by Yonetoku and by Grupe, and our analysis of the late X-ray afterglow. It is most remarkable that the determination of the cosmological redshift on the ground of the scaling of the late X-ray afterglow, already verified in GRB 090618 and GRB 101023, is again verified by this analysis. *Results:* We find for Episode 1 a temperature of the BB component that evolves with time following a broken PL, with the slope of the PL at early times $\alpha = 0$ (constant function) and the slope of the PL at late times $\beta = -4 \pm 2$. The break occurs at $t = 41.21$ s. The total energy of Episode 1 is $E_{iso}^{(1)} = 1.42 \times 10^{53}$ erg. The total energy of Episode 2 is $E_{iso}^{(2)} = 2.43 \times 10^{52}$ erg. We find at transparency a Lorentz factor $\Gamma \sim 1.73 \times 10^2$, laboratory radius of 6.04×10^{13} cm, P-GRB observed temperature $kT_{P-GRB} = 12.36$ keV, baryon load $B = 5.7 \times 10^{-3}$ and P-GRB energy of $E_{P-GRB} = 3.44 \times 10^{50}$ erg. We find a remarkable coincidence of the cosmological redshift by the scaling of the XRT data and with three other phenomenological methods. *Conclusions:* We interpret GRB 110709B as a member of the IGC sources, together with GRB 970828, GRB 090618 and GRB 101023. The existence of the XRT data during the prompt phase of the emission of GRB 110709B (Episode 2) offers an unprecedented tool for improving the diagnostic of GRBs emission.

29. G.B. Pisani, L. Izzo, R. Ruffini, C.L. Bianco, M. Muccino, A.V. Penacchioni, J.A. Rueda, Y. Wang; “Novel distance indicator for gamma-ray bursts associated with supernovae”; *Astronomy & Astrophysics*, 552,

L5 (2013).

Context: In recent years it has been proposed that the temporal coincidence of a Gamma Ray Burst (GRB) and a type Ib/c supernova (SN) can be explained by the concept of Induced Gravitational Collapse (IGC) of a Neutron Star (NS) to a Black Hole (BH) by accretion of matter ejected by a SN Ib/c. This scenario reveals a possible common behavior in the late time X-ray emission of this subclass of GRBs. *Aims:* We want to test if such a common behavior can actually be present in the sources belonging to this GRB sub-class and if this may lead to a redshift estimator for these sources. *Methods:* We build a sample of GRBs belonging to this sub-class, and we rescale the X-ray light curves of all of them both in time and in flux to a common cosmological redshift. *Results:* We found that the X-ray light curves of all the GRBs of the sample with a measured redshift present a common late time behavior when rescaled to a common redshift $z = 1$. We then use this result to estimate the redshift of the GRBs of the sample with no measured redshift. *Conclusions:* The common behavior in the late decay of the X-ray light curves of the GRBs of the sample points to a common physical mechanism in this particular phase of the GRB emission, possibly related to the SN process. This scenario may represent an invaluable tool to estimate the redshift of GRBs belonging to this sub-class of events. More GRBs are therefore needed in order to enlarge the subclass and to make more stringent constraints on the redshift estimates performed with this method for GRBs pertaining to this class.

30. C.L. Bianco, M. G. Bernardini, L. Caito, G. De Barros, L. Izzo, M. Muccino, B. Patricelli, A.V. Penacchioni, G.B. Pisani, R. Ruffini; “The canonical GRB scenario”; *Il Nuovo Cimento C*, 36 s01, 21 (2013).

The canonical GRB scenario implied by the fireshell model is briefly summarized.

31. A.V. Penacchioni, R. Ruffini, L. Izzo, M. Muccino, C.L. Bianco, L. Caito, B. Patricelli; “Evidences for a double component in the emission of GRB 101023”; *Il Nuovo Cimento C*, 36 s01, 117 (2013).

In this work we present the results of the analysis of GRB 101023 in the fireshell scenario. Its redshift is not known, so we attempted to infer it from the Amati Relation, obtaining $z = 0.9$. Its light curve presents a double emission, which makes it very similar to the already studied GRB 090618. We called each part Episode 1 and Episode 2. We performed a time-resolved spectral

analysis with RMFIT using different spectral models, and fitted the light curve with a numerical code integrating the fireshell equations of motion. We used Fermi GBM data to build the light curve, in particular the second NaI detector, in the range (8.5–1000 keV). We considered different hypotheses regarding which part of the light curve could be the GRB and performed the analysis of all of them. We noticed a great variation of the temperature with time in the first episode, as well as almost no variation of the progenitor radius. We found that the first emission does not match the requirements for a GRB, while the second part perfectly agrees with being a canonical GRB, with a P-GRB lasting 4 s.

32. M. Muccino, R. Ruffini, C.L. Bianco, L. Izzo, A.V. Penacchioni, G.B. Pisani; “GRB 090510: A Disguised Short Gamma-Ray Burst with the Highest Lorentz Factor and Circumburst Medium”; *The Astrophysical Journal*, 772, 62 (2013).

GRB 090510, observed both by Fermi and AGILE satellites, is the first bright short-hard Gamma-Ray Burst (GRB) with an emission from the keV up to the GeV energy range. Within the Fireshell model, we interpret the faint precursor in the light curve as the emission at the transparency of the expanding e^+e^- plasma: the Proper-GRB (P-GRB). From the observed isotropic energy we assume a total plasma energy $E_{e^+e^-}^{tot} = (1.10 \pm 0.06) \times 10^{53}$ erg and derive a Baryon load $B = (1.45 \pm 0.28) \times 10^{-3}$ and a Lorentz factor at transparency $\Gamma_{tr} = (6.7 \pm 1.6) \times 10^2$. The main emission ~ 0.4 s after the initial spike is interpreted as the extended afterglow, due to the interaction of the ultrarelativistic baryons with the CircumBurst Medium (CBM). Using the condition of fully radiative regime, we infer a CBM average spherically symmetric density of $\langle n_{CBM} \rangle = (1.85 \pm 0.14) \times 10^3$ particles/cm³, one of the highest found in the Fireshell model. The value of the filling factor, $1.5 \times 10^{-10} \leq \mathcal{R} \leq 3.8 \times 10^{-8}$, leads to the estimate of filaments with densities $n_{fil} = n_{CBM}/\mathcal{R} \approx (10^6 - 10^{14})$ particles/cm³. The sub-MeV and the MeV emissions are well reproduced. When compared to the canonical GRBs with $\langle n_{CBM} \rangle \approx 1$ particles/cm³ and to the disguised short GRBs with $\langle n_{CBM} \rangle \approx 10^{-3}$ particles/cm³, the case of GRB 090510 leads to the existence of a new family of bursts exploding in an over-dense galactic region with $\langle n_{CBM} \rangle \approx 10^3$ particles/cm³. The joint effect of the high Γ_{tr} and the high density compresses in time and “inflates” in intensity the extended afterglow, making it appear as a short burst, which we here define as “disguised short GRB by excess”. The determination of the above parameters values may represent an important step towards the explanation

of the GeV emission.

33. R. Ruffini, M. Muccino, C.L. Bianco, M. Enderli, L. Izzo, M. Kovacevic, A.V. Penacchioni, G.B. Pisani, J.A. Rueda, Y. Wang; “On Binary Driven Hypernovae and their nested late X-ray emission”; *Astronomy & Astrophysics*, 565, L10 (2014).

Context: The induced gravitational collapse (IGC) paradigm addresses the very energetic (10^{52} – 10^{54} erg) long gamma-ray bursts (GRBs) associated to supernovae (SNe). Unlike the traditional “collapsar” model, an evolved FeCO core with a companion neutron star (NS) in a tight binary system is considered as the progenitor. This special class of sources, here named “binary driven hypernovae” (BdHNe), presents a composite sequence composed of four different episodes with precise spectral and luminosity features.

Aims: We first compare and contrast the steep decay, the plateau, and the power-law decay of the X-ray luminosities of three selected BdHNe (GRB 060729, GRB 061121, and GRB 130427A). Second, to explain the different sizes and Lorentz factors of the emitting regions of the four episodes, for definiteness, we use the most complete set of data of GRB 090618. Finally, we show the possible role of r-process, which originates in the binary system of the progenitor.

Methods: We compare and contrast the late X-ray luminosity of the above three BdHNe. We examine correlations between the time at the starting point of the constant late power-law decay t_a^* , the average prompt luminosity $\langle L_{iso} \rangle$, and the luminosity at the end of the plateau L_a . We analyze a thermal emission (~ 0.97 – 0.29 keV), observed during the X-ray steep decay phase of GRB 090618.

Results: The late X-ray luminosities of the three BdHNe, in the rest-frame energy band 0.3–10 keV, show a precisely constrained “nested” structure. In a space-time diagram, we illustrate the different sizes and Lorentz factors of the emitting regions of the three episodes. For GRB 090618, we infer an initial dimension of the thermal emitter of $\sim 7 \times 10^{12}$ cm, expanding at $\Gamma \approx 2$. We find tighter correlations than the Dainotti-Willingale ones.

Conclusions: We confirm a constant slope power-law behavior for the late X-ray luminosity in the source rest frame, which may lead to a new distance indicator for BdHNe. These results, as well as the emitter size and Lorentz factor, appear to be inconsistent with the traditional afterglow model based on synchrotron emission from an ultra-relativistic ($\Gamma \sim 10^2$ – 10^3) collimated jet outflow. We argue, instead, for the possible role of r-process, originating in the binary system, to power the mildly relativistic X-ray source.

34. R. Ruffini, L. Izzo, M. Muccino, G.B. Pisani, J.A. Rueda, Y. Wang, C. Barbarino, C.L. Bianco, M. Enderli, M. Kovacevic; “Induced gravitational collapse at extreme cosmological distances: the case of GRB 090423”; *Astronomy & Astrophysics*, 569, A39 (2014).

Context: The induced gravitational collapse (IGC) scenario has been introduced in order to explain the most energetic gamma ray bursts (GRBs), $E_{iso} = 10^{52} - 10^{54}$ erg, associated with type Ib/c supernovae (SNe). It has led to the concept of binary-driven hypernovae (BdHNe) originating in a tight binary system composed by a FeCO core on the verge of a SN explosion and a companion neutron star (NS). Their evolution is characterized by a rapid sequence of events: 1) The SN explodes, giving birth to a new NS (ν NS). The accretion of SN ejecta onto the companion NS increases its mass up to the critical value; 2) The consequent gravitational collapse is triggered, leading to the formation of a black hole (BH) with GRB emission; 3) A novel feature responsible for the emission in the GeV, X-ray, and optical energy range occurs and is characterized by specific power-law behavior in their luminosity evolution and total spectrum; 4) The optical observations of the SN then occurs.

Aims: We investigate whether GRB 090423, one of the farthest observed GRB at $z = 8.2$, is a member of the BdHN family.

Methods: We compare and contrast the spectra, the luminosity evolution, and the detectability in the observations by *Swift* of GRB 090423 with the corresponding ones of the best known BdHN case, GRB 090618.

Results: Identification of constant slope power-law behavior in the late X-ray emission of GRB 090423 and its overlapping with the corresponding one in GRB 090618, measured in a common rest frame, represents the main result of this article. This result represents a very significant step on the way to using the scaling law properties, proven in Episode 3 of this BdHN family, as a cosmological standard candle.

Conclusions: Having identified GRB 090423 as a member of the BdHN family, we can conclude that SN events, leading to NS formation, can already occur already at $z = 8.2$, namely at 650 Myr after the Big Bang. It is then possible that these BdHNe originate stem from 40-60 M_{\odot} binaries. They are probing the Population II stars after the completion and possible disappearance of Population III stars.

35. M. Muccino, C.L. Bianco, L. Izzo, Y. Wang, M. Enderli, M. Kovacevic, G.B. Pisani, A.V. Penacchioni, R. Ruffini; “The Genuine Short GRB 090227B and the Disguised by Excess GRB 090510”; *Gravitation and*

Cosmology, 20, 197 (2014).

GRB 090227B and GRB 090510, traditionally classified as short gamma-ray Bursts (GRBs), indeed originate from different systems. For GRB 090227B we inferred a total energy of the e^+e^- plasma $E_{e^+e^-}^{tot} = (2.83 \pm 0.15) \times 10^{53}$ erg, a baryon load of $B = (4.1 \pm 0.05) \times 10^{-5}$, and a CircumBurst Medium (CBM) average density $\langle n_{CBM} \rangle = (1.90 \pm 0.20) \times 10^{-5} \text{ cm}^{-3}$. From these results we have assumed the progenitor of this burst to be a symmetric neutron stars (NSs) merger with masses $m = 1.34M_{\odot}$, radii $R = 12.24$ km. GRB 090510, instead, has $E_{e^+e^-}^{tot} = (1.10 \pm 0.06) \times 10^{53}$ erg, $B = (1.45 \pm 0.28) \times 10^{-3}$, implying a Lorentz factor at transparency of $\Gamma = (6.7 \pm 1.7) \times 10^2$, which are characteristic of the long GRB class, and a very high CBM density, $\langle n_{CBM} \rangle = (1.85 \pm 0.14) \times 10^3 \text{ cm}^{-3}$. The joint effect of the high values of Γ and of $\langle n_{CBM} \rangle$ compresses in time and “inflates” in intensity in an extended afterglow, making appear GRB 090510 as a short burst, which we here define as “disguised short GRB by excess” occurring an overdense region with 10^3 cm^{-3} .

36. M. Muccino, C.L. Bianco, L. Izzo, Y. Wang, M. Enderli, G.B. Pisani, A.V. Penacchioni, R. Ruffini; “Two short bursts originating from different astrophysical systems: The genuine short GRB 090227B and the disguised short GRB 090510 by excess”; Journal of the Korean Physical Society, 65, 865 (2014).

GRB 090227B and GRB 090510 are two gamma-ray bursts (GRBs) traditionally classified as short bursts. The major outcome of our analysis is that they indeed originate from different systems. In the case of GRB 090227B, from the inferred values of the total energy of the e^+e^- plasma, $E_{e^+e^-}^{tot} = (2.83 \pm 0.15) \times 10^{53}$ erg, the engulfed baryonic mass M_B , expressed as $B = M_B c^2 / E_{e^+e^-}^{tot} = (4.1 \pm 0.05) \times 10^{-5}$, and the circumburst medium (CBM) average density, $\langle n_{CBM} \rangle = (1.90 \pm 0.20) \times 10^{-5} \text{ cm}^{-3}$, we have assumed the progenitor of this burst to be a symmetric neutron star (NS) merger with masses $m = 1.34M_{\odot}$, radii $R = 12.24$ km, and crustal thicknesses of ~ 0.47 km. In the case of GRB 090510, we have derived the total plasma energy, $E_{e^+e^-}^{tot} = (1.10 \pm 0.06) \times 10^{53}$ erg, the Baryon load, $B = (1.45 \pm 0.28) \times 10^{-3}$, and the Lorentz factor at transparency, $\Gamma = (6.7 \pm 1.7) \times 10^2$, which are characteristic of the long GRB class, as well as a very high CBM density, $\langle n_{CBM} \rangle = (1.85 \pm 0.14) \times 10^3 \text{ cm}^{-3}$. The joint effect of the high values of Γ and $\langle n_{CBM} \rangle$ compresses in time and “inflates” in intensity the extended afterglow, making GRB 090510 appear to be a short burst, which we here define as a “disguised short GRB by excess”, occurring

in an overdense region with 10^3 cm^{-3} .

37. R. Ruffini, Y. Wang, M. Kovacevic, C.L. Bianco, M. Enderli, M. Muccino, A.V. Penacchioni, G.B. Pisani, J. Rueda; “GRB 130427A and SN 2013cq: A Multi-wavelength Analysis of An Induced Gravitational Collapse Event”; *The Astrophysical Journal*, 798, 10 (2015).

We have performed our data analysis of the observations by *Swift*, *NuStar* and *Fermi* satellites in order to probe the induced gravitational collapse (IGC) paradigm for GRBs associated with supernovae (SNe), in the “terra incognita” of GRB 130427A. We compare and contrast our data analysis with those in the literature. We have verified that the GRB 130427A conforms to the IGC paradigm by examining the power law behavior of the luminosity in the early 10^4 s of the XRT observations. This has led to the identification of the four different episodes of the “binary driven hypernovae” (BdHNe) and to the prediction, on May 2, 2013, of the occurrence of SN 2013cq, duly observed in the optical band on May 13, 2013. The exceptional quality of the data has allowed the identification of novel features in *Episode 3* including: a) the confirmation and the extension of the existence of the recently discovered “nested structure” in the late X-ray luminosity in GRB 130427A, as well as the identification of a spiky structure at 10^2 s in the cosmological rest-frame of the source; b) a power law emission of the GeV luminosity light curve and its onset at the end of *Episode 2*; c) different Lorentz Γ factors for the emitting regions of the X-ray and GeV emissions in this *Episode 3*. These results make it possible to test the details of the physical and astrophysical regimes at work in the BdHNe: 1) a newly born neutron star and the supernova ejecta, originating in *Episode 1, 2*) a newly formed black hole originating in *Episode 2*, and 3) the possible interaction among these components, observable in the standard features of *Episode 3*.

38. M. Muccino, R. Ruffini, C.L. Bianco, M. Enderli, M. Kovacevic, L. Izzo, A.V. Penacchioni, G.B. Pisani, J.A. Rueda, Y. Wang; “On binary driven hypernovae and their nested late X-ray emission”; *Astronomy Reports*, 59, 581 (2015).

The induced gravitational collapse (IGC) paradigm addresses energetic (10^{52} – 10^{54} erg), long gamma-ray bursts (GRBs) associated to supernovae (SNe) and proposes as their progenitors tight binary systems composed of an evolved FeCO core and a companion neutron star (NS). Their emission is characterized by four specific episodes: *Episode 1*, corresponding to the on-set of the FeCO

SN explosion and the accretion of the ejecta onto the companion NS; Episode 2, related the collapse of the companion NS to a black hole (BH) and to the emission of a long GRB; Episode 3, observed in X-rays and characterized by a steep decay, a plateau phase and a late power-law decay; Episode 4, corresponding to the optical SN emission due to the ^{56}Ni decay. We focus on Episode 3 and we show that, from the thermal component observed during the steep decay of the prototype GRB 090618, the emission region has a typical dimension of $\sim 10^{13}$ cm, which is inconsistent with the typical size of the emitting region of GRBs, e.g., $\sim 10^{16}$ cm. We propose, therefore, that the X-ray afterglow emission originates from a spherically symmetric SN ejecta expanding at $\Gamma \sim 2$ or, possibly, from the accretion onto the newly formed black hole, and we name these systems “binary driven hypernovae” (BdHNe). This interpretation is alternative to the traditional afterglow model based on the GRB synchrotron emission from a collimated jet outflow, expanding at ultra-relativistic Lorentz factor of $\Gamma \sim 10^2 - 10^3$ and originating from the collapse of a single object. We show then that the rest-frame energy band 0.3–10 keV X-ray luminosities of three selected BdHNe, GRB 060729, GRB 061121, and GRB 130427A, evidence a precisely constrained “nested” structure and satisfy precise scaling laws between the average prompt luminosity, $\langle L_{iso} \rangle$, and the luminosity at the end of the plateau, L_a , as functions of the time at the end of the plateau. All these features extend the applicability of the “cosmic candle” nature of Episode 3. The relevance of r-process in fulfilling the demanding scaling laws and the nested structure are indicated.

39. R. Ruffini, J.A. Rueda, C. Barbarino, C. L. Bianco, H. Dereli, M. Enderli, L. Izzo, M. Muccino, A.V. Penacchioni, G.B. Pisani, Y. Wang; “Induced Gravitational Collapse in the BATSE era: the case of GRB 970828”; *Astronomy Reports*, 59, 626 (2015).

Following the recently established “Binary-driven HyperNova” (BdHN) paradigm, we here interpret GRB 970828 in terms of the four episodes typical of such a model. The “Episode 1”, up to 40 s after the trigger time t_0 , with a time varying thermal emission and a total energy of $E_{iso,1st} = 2.60 \times 10^{53}$ erg, is interpreted as due to the onset of an hyper-critical accretion process onto a companion neutron star, triggered by the companion star, an FeCO core approaching a SN explosion. The “Episode 2”, observed up t_0+90 s, is interpreted as a canonical gamma ray burst, with an energy of $E_{tot}^{e^+e^-} = 1.60 \times 10^{53}$ erg, a baryon load of $B = 7 \times 10^{-3}$ and a bulk Lorentz factor at transparency of $\Gamma = 142.5$. From this Episode 2, we infer that the GRB exploded in an environment with a large av-

erage particle density $\langle n \rangle \approx 10^3$ particles/cm³ and dense clouds characterized by typical dimensions of $(4 \div 8) \times 10^{14}$ cm and $\delta n/n \sim 10$. The “Episode 3” is identified from t_0+90 s all the way up to 10^{5-6} s: despite the paucity of the early X-ray data, typical in the BATSE, pre-Swift era, we find extremely significant data points in the late X-ray afterglow emission of GRB 970828, which corresponds to the ones observed in all BdHNe sources. The “Episode 4”, related to the Supernova emission, does not appear to be observable in this source, due to the presence of darkening from the large density of the GRB environment, also inferred from the analysis of the Episode 2.

40. Y. Wang, R. Ruffini, M. Kovacevic, C.L. Bianco, M. Enderli, M. Muccino, A.V. Penacchioni, G.B. Pisani, J.A. Rueda; “Predicting supernova associated to gamma-ray burst 130427a”; *Astronomy Reports*, 59, 667 (2015).

Binary systems constituted by a neutron star and a massive star are not rare in the universe. The Induced Gravitational Gamma-ray Burst (IGC) paradigm interprets Gamma-ray bursts as the outcome of a neutron star that collapses into a black hole due to the accretion of the ejecta coming from its companion massive star that underwent a supernova event. GRB 130427A is one of the most luminous GRBs ever observed, of which isotropic energy exceeds 10^{54} erg. And it is within one of the few GRBs obtained optical, X-ray and GeV spectra simultaneously for hundreds of seconds, which provides an unique opportunity so far to understand the multi-wavelength observation within the IGC paradigm, our data analysis found low Lorentz factor blackbody emission in the Episode 3 and its X-ray light curve overlaps typical IGC Golden Sample, which comply to the IGC mechanisms. We consider these findings as clues of GRB 130427A belonging to the IGC GRBs. We predicted on GCN the emergence of a supernova on May 2, 2013, which was later successfully detected on May 13, 2013.

41. R. Ruffini, M. Muccino, M. Kovacevic, F.G. Oliveira, J.A. Rueda, C.L. Bianco, M. Enderli, A.V. Penacchioni, G.B. Pisani, Y. Wang, E. Zaninoni; “GRB 140619B: a short GRB from a binary neutron star merger leading to black hole formation”; *The Astrophysical Journal*, 808, 190 (2015).

We show the existence of two families of short GRBs, both originating from the merger of binary neutron stars (NSs): family-1 with $E_{iso} < 10^{52}$ erg, leading to a massive NS as the merged core, and family-2 with $E_{iso} > 10^{52}$ erg, leading to a black hole (BH). Following the identification of the prototype

GRB 090227B, we present the details of a new example of family-2 short burst: GRB 140619B. From the spectral analysis of the early ~ 0.2 s, we infer an observed temperature $kT = (324 \pm 33)$ keV of the e^+e^- -plasma at transparency (P-GRB), a theoretically derived redshift $z = 2.67 \pm 0.37$, a total burst energy $E_{e^+e^-}^{tot} = (6.03 \pm 0.79) \times 10^{52}$ erg, a rest-frame peak energy $E_{p,i} = 4.7$ MeV, and a baryon load $B = (5.52 \pm 0.73) \times 10^{-5}$. We also estimate the corresponding emission of gravitational waves. Two additional examples of family-2 short bursts are identified: GRB 081024B and GRB 090510, remarkable for its well determined cosmological distance. We show that marked differences exist in the nature of the afterglows of these two families of short bursts: family-2 bursts, leading to BH formation, consistently exhibit high energy emission following the P-GRB emission; family-1 bursts, leading to the formation of a massive NS, should never exhibit high energy emission. We also show that both the families fulfill an $E_{p,i}-E_{iso}$ relation with slope $\gamma = 0.59 \pm 0.07$ and a normalization constant incompatible with the one for long GRBs. The observed rate of such family-2 events is $\rho_0 = (2.1_{-1.4}^{+2.8}) \times 10^{-4} \text{Gpc}^{-3} \text{yr}^{-1}$.

42. R. Ruffini, Y. Aimuratov, C.L. Bianco, M. Enderli, M. Kovacevic, R. Moradi, M. Muccino, A.V. Penacchioni, G.B. Pisani, J.A. Rueda, Y. Wang; “Induced gravitational collapse in FeCO Core-Neutron star binaries and Neutron star-Neutron star binary mergers”; *International Journal of Modern Physics A*, 30, 1545023 (2015).

We review the recent progress in understanding the nature of gamma-ray bursts (GRBs). The occurrence of GRB is explained by the Induced Gravitational Collapse (IGC) in FeCO Core-Neutron star binaries and Neutron star-Neutron star binary mergers, both processes occur within binary system progenitors. Making use of this most unexpected new paradigm, with the fundamental implications by the neutron star (NS) critical mass, we find that different initial configurations of binary systems lead to different GRB families with specific new physical predictions confirmed by observations.

43. R. Ruffini, M. Muccino, Y. Aimuratov, C.L. Bianco, C. Cherubini, M. Enderli, M. Kovacevic, R. Moradi, A.V. Penacchioni, G.B. Pisani, J.A. Rueda, Y. Wang; “GRB 090510: A genuine short-GRB from a binary neutron star coalescing into a Kerr-Newman black hole”; *The Astrophysical Journal*, 831, 178 (2016).

In a new classification of merging binary neutron stars (NSs) we separate short gamma-ray bursts (GRBs) in two sub-classes. The ones with $E_{iso} \lesssim 10^{52}$ erg

coalesce to form a massive NS and are indicated as short gamma-ray flashes (S-GRFs). The hardest, with $E_{\text{iso}} \gtrsim 10^{52}$ erg, coalesce to form a black hole (BH) and are indicated as genuine short-GRBs (S-GRBs). Within the fireshell model, S-GRBs exhibit three different components: the P-GRB emission, observed at the transparency of a self-accelerating baryon- e^+e^- plasma; the prompt emission, originating from the interaction of the accelerated baryons with the circumburst medium; the high-energy (GeV) emission, observed after the P-GRB and indicating the formation of a BH. GRB 090510 gives the first evidence for the formation of a Kerr BH or, possibly, a Kerr-Newman BH. Its P-GRB spectrum can be fitted by a convolution of thermal spectra whose origin can be traced back to an axially symmetric dyadotorus. A large value of the angular momentum of the newborn BH is consistent with the large energetics of this S-GRB, which reach in the 1–10000 keV range $E_{\text{iso}} = (3.95 \pm 0.21) \times 10^{52}$ erg and in the 0.1–100 GeV range $E_{\text{LAT}} = (5.78 \pm 0.60) \times 10^{52}$ erg, the most energetic GeV emission ever observed in S-GRBs. The theoretical redshift $z_{\text{th}} = 0.75 \pm 0.17$ that we derive from the fireshell theory is consistent with the spectroscopic measurement $z = 0.903 \pm 0.003$, showing the self-consistency of the theoretical approach. All S-GRBs exhibit GeV emission, when inside the *Fermi*-LAT field of view, unlike S-GRFs, which never evidence it. The GeV emission appears to be the discriminant for the formation of a BH in GRBs, confirmed by their observed overall energetics.

44. Ruffini, R.; Rueda, J. A.; Muccino, M.; Aimuratov, Y.; Becerra, L. M.; Bianco, C. L.; Kovacevic, M.; Moradi, R.; Oliveira, F. G.; Pisani, G. B.; Wang, Y.; On the classification of GRBs and their occurrence rates; *The Astrophysical Journal*, 832, 136 (2016).

There is mounting evidence for the binary nature of the progenitors of gamma-ray bursts (GRBs). For a long GRB, the induced gravitational collapse (IGC) paradigm proposes as progenitor, or “in-state”, a tight binary system composed of a carbon-oxygen core (CO_{core}) undergoing a supernova (SN) explosion which triggers hypercritical accretion onto a neutron star (NS) companion. For a short GRB, a NS-NS merger is traditionally adopted as the progenitor. We divide long and short GRBs into two sub-classes, depending on whether or not a black hole (BH) is formed in the merger or in the hypercritical accretion process exceeding the NS critical mass. For long bursts, when no BH is formed we have the sub-class of X-ray flashes (XRFs), with isotropic energy $E_{\text{iso}} \lesssim 10^{52}$ erg and rest-frame spectral peak energy $E_{p,i} \lesssim 200$ keV. When a BH is formed we have the sub-class of binary-driven hypernovae (BdHNe),

with $E_{iso} \gtrsim 10^{52}$ erg and $E_{p,i} \gtrsim 200$ keV. In analogy, short bursts are similarly divided into two sub-classes. When no BH is formed, short gamma-ray flashes (S-GRFs) occur, with $E_{iso} \lesssim 10^{52}$ erg and $E_{p,i} \lesssim 2$ MeV. When a BH is formed, the authentic short GRBs (S-GRBs) occur, with $E_{iso} \gtrsim 10^{52}$ erg and $E_{p,i} \gtrsim 2$ MeV. We give examples and observational signatures of these four sub-classes and their rate of occurrence. From their respective rates it is possible that “in-states” of S-GRFs and S-GRBs originate from the “out-states” of XRFs. We indicate two additional progenitor systems: white dwarf-NS and BH-NS. These systems have hybrid features between long and short bursts. In the case of S-GRBs and BdHNe evidence is given of the coincidence of the onset of the high energy GeV emission with the birth of a Kerr BH.

45. Becerra, L.; Bianco, C. L.; Fryer, C. L.; Rueda, J. A.; Ruffini, R.; On the induced gravitational collapse scenario of gamma-ray bursts associated with supernovae; *The Astrophysical Journal*, 833, 107 (2016).

Following the induced gravitational collapse (IGC) paradigm of gamma-ray bursts (GRBs) associated with type Ib/c supernovae, we present numerical simulations of the explosion of a carbon-oxygen (CO) core in a binary system with a neutron-star (NS) companion. The supernova ejecta trigger a *hypercritical* accretion process onto the NS thanks to a copious neutrino emission and the trapping of photons within the accretion flow. We show that temperatures 1–10 MeV develop near the NS surface, hence electron-positron annihilation into neutrinos becomes the main cooling channel leading to accretion rates 10^{-9} – $10^{-1} M_{\odot} \text{ s}^{-1}$ and neutrino luminosities 10^{43} – $10^{52} \text{ erg s}^{-1}$ (the shorter the orbital period the higher the accretion rate). We estimate the maximum orbital period, P_{max} , as a function of the NS initial mass, up to which the NS companion can reach by hypercritical accretion the critical mass for gravitational collapse leading to black-hole (BH) formation. We then estimate the effects of the accreting and orbiting NS companion onto a novel geometry of the supernova ejecta density profile. We present the results of a 1.4×10^7 particle simulation which show that the NS induces accentuated asymmetries in the ejecta density around the orbital plane. We elaborate on the observables associated with the above features of the IGC process. We apply this framework to specific GRBs: we find that X-ray flashes (XRFs) and binary-driven hypernovae (BdHNe) are produced in binaries with $P > P_{\text{max}}$ and $P < P_{\text{max}}$, respectively. We analyze in detail the case of XRF 060218.

46. Pisani, G. B.; Ruffini, R.; Aimuratov, Y.; Bianco, C. L.; Kovacevic, M.;

Moradi, R.; Muccino, M.; Penacchioni, A. V.; Rueda, J. A.; Shakeri, S.; Wang, Y.; On the universal late X-ray emission of binary-driven hypernovae and its possible collimation; *The Astrophysical Journal*, 833, 159 (2016).

It has been previously discovered a universal power-law behaviour of the late X-ray emission (LXRE) of a “golden sample” (GS) of six long energetic GRBs, when observed in the rest-frame of the source. This remarkable feature, independent on the different isotropic energy (E_{iso}) of each GRB, has been used to estimate the cosmological redshift of some long GRBs. This analysis is here extended to a new class of 161 long GRBs, all with $E_{iso} > 10^{52}$ erg. These GRBs are indicated as binary-driven hypernovae (BdHNe) in view of their progenitors: a tight binary systems composed of a carbon-oxygen core (CO_{core}) and a neutron star (NS) undergoing an induced gravitational collapse (IGC) to a black hole (BH) triggered by the CO_{core} explosion as a supernova (SN). We confirm the universal behaviour of the LXRE for the “enlarged sample” (ES) of 161 BdHNe observed up to the end of 2015, assuming a double-cone emitting region. We obtain a distribution of half-opening angles peaking at $\theta = 17.62^\circ$, with mean value 30.05° , and a standard deviation 19.65° . This, in turn, leads to the possible establishment of a new cosmological candle. Within the IGC model, such universal LXRE behaviour is only indirectly related to the GRB and originates from the SN ejecta, of a standard constant mass, being shocked by the GRB emission. The fulfillment of the universal relation in the LXRE and its independence of the prompt emission, further confirmed in this article, establishes a crucial test for any viable GRB model.

47. Y. Aimuratov, R. Ruffini, M. Muccino, C.L. Bianco, A.V. Penacchioni, G.B. Pisani, D. Primorac, J.A. Rueda, Y. Wang; GRB 081024B and GRB 140402A: Two Additional Short GRBs from Binary Neutron Star Mergers; *The Astrophysical Journal*, 844, 83 (2017).

Theoretical and observational evidences have been recently gained for a two-fold classification of short bursts: 1) short gamma-ray flashes (S-GRFs), with isotropic energy $E_{iso} < 10^{52}$ erg and no BH formation, and 2) the authentic short gamma-ray bursts (S-GRBs), with isotropic energy $E_{iso} > 10^{52}$ erg evidencing a BH formation in the binary neutron star merging process. The signature for the BH formation consists in the on-set of the high energy (0.1–100 GeV) emission, coeval to the prompt emission, in all S-GRBs. No GeV emission is expected nor observed in the S-GRFs. In this paper we present

two additional S-GRBs, GRB 081024B and GRB 140402A, following the already identified S-GRBs, i.e., GRB 090227B, GRB 090510 and GRB 140619B. We also return on the absence of the GeV emission of the S-GRB 090227B, at an angle of 71° from the *Fermi*-LAT boresight. All the correctly identified S-GRBs correlate to the high energy emission, implying no significant presence of beaming in the GeV emission. The existence of a common power-law behavior in the GeV luminosities, following the BH formation, when measured in the source rest-frame, points to a commonality in the mass and spin of the newly-formed BH in all S-GRBs.

48. J.A. Rueda, Y. Aimuratov, U. Barres de Almeida, L.M. Becerra, C.L. Bianco, C. Cherubini, S. Filippi, M. Karlica, M. Kovacevic, J.D. Melon Fuksman, R. Moradi, M. Muccino, A.V. Penacchioni, G.B. Pisani, D. Primorac, R. Ruffini, N. Sahakyan, S. Shakeri, Y. Wang; The binary systems associated with short and long gamma-ray bursts and their detectability; *International Journal of Modern Physics D*, 26, 1730016 (2017).

Short and long-duration gamma-ray bursts (GRBs) have been recently subclassified into seven families according to the binary nature of their progenitors. For short GRBs, mergers of neutron star binaries (NS-NS) or neutron star-black hole binaries (NS-BH) are proposed. For long GRBs, the induced gravitational collapse (IGC) paradigm proposes a tight binary system composed of a carbon-oxygen core (COcore) and a NS companion. The explosion of the COcore as supernova (SN) triggers a hypercritical accretion process onto the NS companion which might reach the critical mass for the gravitational collapse to a BH. Thus, this process can lead either to a NS-BH or to NS-NS depending on whether or not the accretion is sufficient to induce the collapse of the NS into a BH. We shall discuss for the above compact object binaries: (1) the role of the NS structure and the equation-of-state on their final fate; (2) their occurrence rates as inferred from the X and gamma-ray observations; (3) the expected number of detections of their gravitational wave (GW) emission by the Advanced LIGO interferometer.

49. R. Ruffini, Y. Aimuratov, L.M. Becerra, C.L. Bianco, M. Karlica, M. Kovacevic, J.D. Melon Fuksman, R. Moradi, M. Muccino, A.V. Penacchioni, G.B. Pisani, D. Primorac, J.A. Rueda, S. Shakeri, G.V. Vereshchagin, Y. Wang, S.-S. Xue; The cosmic matrix in the 50th anniversary of relativistic astrophysics; *International Journal of Modern Physics D*, 26, 1730019 (2017).

Our concept of induced gravitational collapse (IGC paradigm) starting from a supernova occurring with a companion neutron star, has unlocked the understanding of seven different families of gamma ray bursts (GRBs), indicating a path for the formation of black holes in the universe. An authentic laboratory of relativistic astrophysics has been unveiled in which new paradigms have been introduced in order to advance knowledge of the most energetic, distant and complex systems in our universe. A novel cosmic matrix paradigm has been introduced at a relativistic cosmic level, which parallels the concept of an S-matrix introduced by Feynmann, Wheeler and Heisenberg in the quantum world of microphysics. Here the “in” states are represented by a neutron star and a supernova, while the “out” states, generated within less than a second, are a new neutron star and a black hole. This novel field of research needs very powerful technological observations in all wavelengths ranging from radio through optical, X-ray and gamma ray radiation all the way up to ultra-high-energy cosmic rays.

50. R. Ruffini, Y. Wang, Y. Aimuratov, U. Barres de Almeida, L.M. Becerra, C.L. Bianco, Y.C. Chen, M. Karlica, M. Kovacevic, L. Li, J.D. Melon Fuksman, R. Moradi, M. Muccino, A.V. Penacchioni, G.B. Pisani, D. Primorac, J.A. Rueda, S. Shakeri, G.V. Vereshchagin, S.-S. Xue; Early X-Ray Flares in GRBs; *The Astrophysical Journal*, 852, 53 (2018).

We analyze the early X-ray flares in the GRB “flare-plateau-afterglow” (FPA) phase observed by Swift-XRT. The FPA occurs only in one of the seven GRB subclasses: the binary-driven hypernovae (BdHNe). This subclass consists of long GRBs with a carbon-oxygen core and a neutron star (NS) binary companion as progenitors. The hypercritical accretion of the supernova (SN) ejecta onto the NS can lead to the gravitational collapse of the NS into a black hole. Consequently, one can observe a GRB emission with isotropic energy $E_{iso} \gtrsim 10^{52}$ erg, as well as the associated GeV emission and the FPA phase. Previous work had shown that gamma-ray spikes in the prompt emission occur at $\sim 10^{15}$ – 10^{17} cm with Lorentz gamma factor $\Gamma \sim 10^2$ – 10^3 . Using a novel data analysis we show that the time of occurrence, duration, luminosity and total energy of the X-ray flares correlate with E_{iso} . A crucial feature is the observation of thermal emission in the X-ray flares that we show occurs at radii $\sim 10^{12}$ cm with $\Gamma \lesssim 4$. These model independent observations cannot be explained by the “fireball” model, which postulates synchrotron and inverse Compton radiation from a single ultra relativistic jetted emission extending from the prompt to the late afterglow and GeV emission phases. We show that

in BdHNe a collision between the GRB and the SN ejecta occurs at $\simeq 10^{10}$ cm reaching transparency at $\sim 10^{12}$ cm with $\Gamma \lesssim 4$. The agreement between the thermal emission observations and these theoretically derived values validates our model and opens the possibility of testing each BdHN episode with the corresponding Lorentz gamma factor.

51. R. Ruffini, J. Rodriguez, M. Muccino, J.A. Rueda, Y. Aimuratov, U. Barres de Almeida, L.M. Becerra, C.L. Bianco, C. Cherubini, S. Filippi, D. Gizzi, M. Kovacevic, R. Moradi, F.G. Oliveira, G.B. Pisani, Y. Wang; On the Rate and on the Gravitational Wave Emission of Short and Long GRBs; *The Astrophysical Journal*, 859, 30 (2018).

On the ground of the large number of gamma-ray bursts (GRBs) detected with cosmological redshift, we classified GRBs in seven subclasses, all with binary progenitors which emit gravitational waves (GWs). Each binary is composed of combinations of carbon-oxygen cores (COcore), neutron stars (NSs), black holes (BHs), and white dwarfs (WDs). The long bursts, traditionally assumed to originate from a BH with an ultrarelativistic jetted emission, not emitting GWs, have been subclassified as (I) X-ray flashes (XRFs), (II) binary-driven hypernovae (BdHNe), and (III) BH-supernovae (BH-SNe). They are framed within the induced gravitational collapse paradigm with a progenitor COcore-NS/BH binary. The SN explosion of the COcore triggers an accretion process onto the NS/BH. If the accretion does not lead the NS to its critical mass, an XRF occurs, while when the BH is present or formed by accretion, a BdHN occurs. When the binaries are not disrupted, XRFs lead to NS-NS and BdHNe lead to NS-BH. The short bursts, originating in NS-NS, are subclassified as (IV) short gamma-ray flashes (S-GRFs) and (V) short GRBs (S-GRBs), the latter when a BH is formed. There are (VI) ultrashort GRBs (U-GRBs) and (VII) gamma-ray flashes (GRFs) formed in NS-BH and NS-WD, respectively. We use the occurrence rate and GW emission of these subclasses to assess their detectability by Advanced LIGO-Virgo, eLISA, and resonant bars. We discuss the consequences of our results in view of the announcement of the LIGO/Virgo Collaboration of the source GW 170817 as being originated by an NS-NS.

52. J.A. Rueda, R. Ruffini, Y. Wang, Y. Aimuratov, U. Barres de Almeida, C.L. Bianco, Y.-C. Chen, R.V. Lobato, C. Maia, D. Primorac, R. Moradi, J. Rodriguez; GRB 170817A-GW170817-AT 2017gfo and the observations of NS-NS, NS-WD and WD-WD mergers; *Journal of Cosmology and Astroparticle Physics*, 10, 006 (2018).

The LIGO-Virgo Collaboration has announced the detection of GW170817 and has associated it with GRB 170817A. These signals have been followed after 11 hours by the optical and infrared emission of AT 2017gfo. The origin of this complex phenomenon has been attributed to a neutron star-neutron star (NS-NS) merger. In order to probe this association we confront our current understanding of the gravitational waves and associated electromagnetic radiation with four observed GRBs originating in binaries composed of different combinations NSs and white dwarfs (WDs). We consider 1) GRB 090510 the prototype of NS-NS merger leading to a black hole (BH); 2) GRB 130603B the prototype of a NS-NS merger leading to massive NS (MNS) with an associated kilonova; 3) GRB 060614 the prototype of a NS-WD merger leading to a MNS with an associated kilonova candidate; 4) GRB 170817A the prototype of a WD-WD merger leading to massive WD with an associated AT 2017gfo-like emission. None of these systems support the above mentioned association. The clear association between GRB 170817A and AT 2017gfo has led to introduce a new model based on a new subfamily of GRBs originating from WD-WD mergers. We show how this novel model is in agreement with the exceptional observations in the optical, infrared, X- and gamma-rays of GRB 170817A-AT 2017gfo.

53. R. Ruffini, M. Karlica, N. Sahakyan, J.A. Rueda, Y. Wang, G.W. Mathews, C.L. Bianco, M. Muccino; A GRB Afterglow Model Consistent with Hypernova Observations; *The Astrophysical Journal*, 869, 101 (2018).

We describe the afterglows of the long gamma-ray-burst (GRB) 130427A within the context of a binary-driven hypernova. The afterglows originate from the interaction between a newly born neutron star (ν NS), created by an Ic supernova (SN), and a mildly relativistic ejecta of a hypernova (HN). Such an HN in turn results from the impact of the GRB on the original SN Ic. The mildly relativistic expansion velocity of the afterglow ($\Gamma \sim 3$) is determined, using our model-independent approach, from the thermal emission between 196 and 461 s. The power law in the optical and X-ray bands of the afterglow is shown to arise from the synchrotron emission of relativistic electrons in the expanding magnetized HN ejecta. Two components contribute to the injected energy: the kinetic energy of the mildly relativistic expanding HN and the rotational energy of the fast-rotating highly magnetized ν NS. We reproduce the afterglow in all wavelengths from the optical (10^{14} Hz) to the X-ray band (10^{19} Hz) over times from 604 s to 5.18×10^6 s relative to the Fermi-GBM trigger. Initially, the emission is dominated by the loss of kinetic energy of the HN component.

After 10^5 s the emission is dominated by the loss of rotational energy of the ν NS, for which we adopt an initial rotation period of 2 ms and a dipole plus quadrupole magnetic field of $\lesssim 7 \times 10^{12}$ G or $\sim 10^{14}$ G. This scenario with a progenitor composed of a COcore and an NS companion differs from the traditional ultra-relativistic-jetted treatments of the afterglows originating from a single black hole.

54. R. Ruffini, L.M. Becerra, C.L. Bianco, Y.-C. Chen, M. Karlica, M. Kovacevic, J.D. Melon Fuksman, R. Moradi, M. Muccino, G.B. Pisani, D. Primorac, J.A. Rueda, G.V. Vereshchagin, Y. Wang, S.-S. Xue; On the ultra-relativistic Prompt Emission (UPE), the Hard and Soft X-ray Flares, and the extended thermal emission (ETE) in GRB 151027A; *The Astrophysical Journal*, 869, 151 (2018).

We analyze GRB 151027A within the binary-driven hypernova approach, with a progenitor of a carbon–oxygen core on the verge of a supernova (SN) explosion and a binary companion neutron star (NS). The hypercritical accretion of the SN ejecta onto the NS leads to its gravitational collapse into a black hole (BH), to the emission of the gamma-ray burst (GRB), and to a copious $e+e-$ plasma. The impact of this $e+e-$ plasma on the SN ejecta explains the early soft X-ray flare observed in long GRBs. Here, we apply this approach to the ultra-relativistic prompt emission (UPE) and to the hard X-ray flares. We use GRB 151027A as a prototype. From the time-integrated and the time-resolved analysis, we identify a double component in the UPE and confirm its ultra-relativistic nature. We confirm the mildly relativistic nature of the soft X-ray flare, of the hard X-ray flare, and of the extended thermal emission (ETE). We show that the ETE identifies the transition from an SN to a hypernova (HN). We then address the theoretical justification of these observations by integrating the hydrodynamical propagation equations of the $e+e-$ into the SN ejecta, with the latter independently obtained from 3D smoothed particle hydrodynamics simulations. We conclude that the UPE, the hard X-ray flare, and the soft X-ray flare do not form a causally connected sequence. Within our model, they are the manifestation of the same physical process of the BH formation as seen through different viewing angles, implied by the morphology and the ~ 300 s rotation period of the HN ejecta.

55. R. Moradi, R. Ruffini, C.L. Bianco, Y.-C. Chen, M. Karlica, J.D. Melon Fuksman, D. Primorac, J.A. Rueda, S. Shakeri, Y. Wang, S.-S. Xue; Relativistic Behavior and Equitemporal Surfaces in Ultra-Relativistic Prompt

Emission Phase of Gamma-Ray Bursts; *Astronomy Reports*, 62, 905 (2018).

In this work we study a role of baryon load and interstellar medium density to explain the nature of peaks in the ultra-relativistic prompt emission (UPE) phase of Gamma-ray Bursts (GRBs). We study the behavior of their Γ Lorenz factor from the moment of transparency all the way up to interstellar medium. We finally study the characteristic of equitemporal surfaces in the UPE phase.

56. D. Primorac, M. Muccino, R. Moradi, Y. Wang, J.D. Melon Fuksman, R. Ruffini, C.L. Bianco, J.A. Rueda; Structure of the Prompt Emission of GRB 151027A Within the Fireshell Model; *Astronomy Reports*, 62, 933 (2018).

Long gamma-ray burst GRB 151027A was observed by all three detectors on-board the Swift spacecraft, and many more, including MAXI, Konus-Wind and Fermi GBM/LAT instruments. This revealed a complex structure of the prompt and afterglow emission, consisting of a double-peak gamma-ray prompt with a quiescent period and a HRF/SXF within the X-ray afterglow, together with multiple BB components seen within the time-resolved spectral analysis. These features, within the fireshell model, are interpreted as the manifestation of the same physical process viewed at different angles with respect to the HN ejecta. Here we present the time-resolved and time-integrated spectral analysis used to determine the energy of the e-e+ plasma E_{tot} and the baryon load B . These quantities describe the dynamics of the fireshell up to the transparency point. We proceed with the light-curve simulation from which CBM density values and its inhomogeneities are deduced. We also investigate the properties of GRB 140206A, whose prompt emission exhibits a similar structure.

57. Y. Wang, J.A. Rueda, R. Ruffini, C.L. Bianco, L.M. Becerra, L. Li, M. Karlica; Two Predictions of Supernova: GRB 130427A/SN 2013cq and GRB 180728A/SN 2018fip; *The Astrophysical Journal*, 874, 39 (2019).

On 2018 July 28, GRB 180728A triggered *Swift* satellites and, soon after the determination of the redshift, we identified this source as a type II binary-driven hypernova (BdHN II) in our model. Consequently, we predicted the appearance time of its associated supernova (SN), which was later confirmed as SN 2018fip. A BdHN II originates in a binary composed of a carbon-oxygen core (CO_{core}) undergoing SN, and the SN ejecta hypercritically accrete onto a companion neutron star (NS). From the time of the SN shock breakout to the time when the hypercritical accretion starts, we infer the binary separation

$\simeq 3 \times 10^{10}$ cm. The accretion explains the prompt emission of isotropic energy $\simeq 3 \times 10^{51}$ erg, lasting ~ 10 s, and the accompanying observed blackbody emission from a thermal convective instability bubble. The new neutron star (ν NS) originating from the SN powers the late afterglow from which a ν NS initial spin of 2.5 ms is inferred. We compare GRB 180728A with GRB 130427A, a type I binary-driven hypernova (BdHN I) with isotropic energy $> 10^{54}$ erg. For GRB 130427A we have inferred an initially closer binary separation of $\simeq 10^{10}$ cm, implying a higher accretion rate leading to the collapse of the NS companion with consequent black hole formation, and a faster, 1 ms spinning ν NS. In both cases, the optical spectra of the SNe are similar, and not correlated to the energy of the gamma-ray burst. We present three-dimensional smoothed-particle-hydrodynamic simulations and visualisations of the BdHNe I and II.

58. J.A. Rueda, R. Ruffini, Y. Wang, C.L. Bianco, J.M. Blanco-Iglesias, M. Karlica, P. Lorén-Aguilar, R. Moradi, N. Sahakyan; Electromagnetic emission of white dwarf binary mergers; *Journal of Cosmology and Astroparticle Physics*, 03, 044 (2019).

It has been recently proposed that the ejected matter from white dwarf (WD) binary mergers can produce transient, optical and infrared emission similar to the “kilonovae” of neutron star (NS) binary mergers. To confirm this we calculate the electromagnetic emission from WD-WD mergers and compare with kilonova observations. We simulate WD-WD mergers leading to a massive, fast rotating, highly magnetized WD with an adapted version of the smoothed-particle-hydrodynamics (SPH) code Phantom. We thus obtain initial conditions for the ejecta such as escape velocity, mass and initial position and distribution. The subsequent thermal and dynamical evolution of the ejecta is obtained by integrating the energy-conservation equation accounting for expansion cooling and a heating source given by the fallback accretion onto the newly-formed WD and its magneto-dipole radiation. We show that magneto-spheric processes in the merger can lead to a prompt, short gamma-ray emission of up to $\approx 10^{46}$ erg in a timescale of 0.1–1 s. The bulk of the ejecta initially expands non-relativistically with velocity $0.01 c$ and then it accelerates to $0.1 c$ due to the injection of fallback accretion energy. The ejecta become transparent at optical wavelengths around ~ 7 days post-merger with a luminosity 10^{41} – 10^{42} erg s^{-1} . The X-ray emission from the fallback accretion becomes visible around ~ 150 – 200 day post-merger with a luminosity of 10^{39} erg s^{-1} . We also predict the post-merger time at which the central WD should appear as a pulsar depending on the value of the magnetic field and rotation period.

59. J.A. Rueda, R. Ruffini, Y. Wang; Induced Gravitational Collapse, Binary-Driven Hypernovae, Long Gamma-ray Bursts and Their Connection with Short Gamma-ray Bursts; *Universe*, 5, 110 (2019).

There is increasing observational evidence that short and long Gamma-ray bursts (GRBs) originate in different subclasses, each one with specific energy release, spectra, duration, etc, and all of them with binary progenitors. The binary components involve carbon-oxygen cores (CO_{core}), neutron stars (NSs), black holes (BHs), and white dwarfs (WDs). We review here the salient features of the specific class of binary-driven hypernovae (BdHNe) within the induced gravitational collapse (IGC) scenario for the explanation of the long GRBs. The progenitor is a CO_{core} -NS binary. The supernova (SN) explosion of the CO_{core} , producing at its center a new NS (νNS), triggers onto the NS companion a hypercritical, i.e., highly super-Eddington accretion process, accompanied by a copious emission of neutrinos. By accretion the NS can become either a more massive NS or reach the critical mass for gravitational collapse with consequent formation of a BH. We summarize the results on this topic from the first analytic estimates in 2012 all the way up to the most recent three-dimensional (3D) smoothed-particle-hydrodynamics (SPH) numerical simulations in 2018. Thanks to these results it is by now clear that long GRBs are richer and more complex systems than thought before. The SN explosion and its hypercritical accretion onto the NS explain the X-ray precursor. The feedback of the NS accretion, the NS collapse and the BH formation produce asymmetries in the SN ejecta, implying the necessity of a 3D analysis for GRBs. The newborn BH, the surrounding matter and the magnetic field inherited from the NS, comprises the *inner engine* from which the GRB electron-positron (e^+e^-) plasma and the high-energy emission are initiated. The impact of the e^+e^- on the asymmetric ejecta transforms the SN into a hypernova (HN). The dynamics of the plasma in the asymmetric ejecta leads to signatures depending on the viewing angle. This explains the ultrarelativistic prompt emission in the MeV domain and the mildly-relativistic flares in the early afterglow in the X-ray domain. The feedback of the νNS pulsar-like emission on the HN explains the X-ray late afterglow and its power-law regime. All of the above is in contrast with a simple GRB model attempting to explain the entire GRB with the kinetic energy of an ultrarelativistic jet extending through all of the above GRB phases, as traditionally proposed in the “collapsar-fireball” model. In addition, BdHNe in their different flavors lead to νNS -NS or νNS -BH binaries. The gravitational wave emission drives these binaries to merge

producing short GRBs. It is thus established a previously unthought interconnection between long and short GRBs and their occurrence rates. This needs to be accounted for in the cosmological evolution of binaries within population synthesis models for the formation of compact-object binaries.

60. R. Ruffini, J.D. Melon Fuksman, G.V. Vereshchagin; On the role of a cavity in the hypernova ejecta of GRB 190114C; *The Astrophysical Journal*, 883, 191 (2019).

Within the binary-driven hypernova I (BdHN I) scenario, the gamma-ray burst GRB190114C originates in a binary system composed of a massive carbon-oxygen core (CO_{core}), and a binary neutron star (NS) companion. As the CO_{core} undergoes a supernova explosion with the creation of a new neutron star (νNS), hypercritical accretion occurs onto the companion binary neutron star until it exceeds the critical mass for gravitational collapse. The formation of a black hole (BH) captures 10^{57} baryons by enclosing them within its horizon, and thus a cavity of approximately 10^{11} cm is formed around it with initial density 10^{-7} g/cm³. A further depletion of baryons in the cavity originates from the expansion of the electron-positron-photon ($e^+e^-\gamma$) plasma formed at the collapse, reaching a density of 10^{-14} g/cm³ by the end of the interaction. It is demonstrated here using an analytical model complemented by a hydrodynamical numerical simulation that part of the $e^+e^-\gamma$ plasma is reflected off the walls of the cavity. The consequent outflow and its observed properties are shown to coincide with the featureless emission occurring in a time interval of duration t_{rf} , measured in the rest frame of the source, between 11 and 20 s of the GBM observation. Moreover, similar features of the GRB light curve were previously observed in GRB 090926A and GRB 130427A, all belonging to the BdHN I class. This interpretation supports the general conceptual framework presented in R. Ruffini et al. and guarantees that a low baryon density is reached in the cavity, a necessary condition for the operation of the “*inner engine*” of the GRB presented in an accompanying article.

61. R. Ruffini, R. Moradi, J.A. Rueda, L.M. Becerra, C.L. Bianco, C. Cherubini, S. Filippi, Y.C. Chen, M. Karlica, N. Sahakyan, Y. Wang, S.-S. Xue; On the GeV Emission of the Type I BdHN GRB 130427A; *The Astrophysical Journal*, 886, 82 (2019).

We propose that the *inner engine* of a type I binary-driven hypernova (BdHN) is composed of a Kerr black hole (BH) in a non-stationary state, embedded in a uniform magnetic field B_0 aligned with the BH rotation axis, and surrounded

by an ionized plasma of extremely low density of 10^{-14} g cm $^{-3}$. Using GRB 130427A as a prototype we show that this *inner engine* acts in a sequence of *elementary impulses*. Electrons are accelerated to ultra-relativistic energy near the BH horizon and, propagating along the polar axis, $\theta = 0$, they can reach energies of $\sim 10^{18}$ eV, and partially contribute to ultra-high energy cosmic rays (UHECRs). When propagating with $\theta \neq 0$ through the magnetic field B_0 they give origin by synchrotron emission to GeV and TeV radiation. The mass of BH, $M = 2.3M_{\odot}$, its spin, $\alpha = 0.47$, and the value of magnetic field $B_0 = 3.48 \times 10^{10}$ G, are determined self-consistently in order to fulfill the energetic and the transparency requirement. The repetition time of each elementary impulse of energy $\mathcal{E} \sim 10^{37}$ erg, is $\sim 10^{-14}$ s at the beginning of the process, then slowly increasing with time evolution. In principle, this “*inner engine*” can operate in a GRB for thousands of years. By scaling the BH mass and the magnetic field the same “*inner engine*” can describe active galactic nuclei (AGN).

4.2 Conference proceedings

1. R. Ruffini, M.G. Bernardini, C.L. Bianco, P. Chardonnet, F. Fraschetti, V. Gurzadyan, L. Vitagliano, S.-S. Xue; “The Blackholic energy: long and short Gamma-Ray Bursts (New perspectives in physics and astrophysics from the theoretical understanding of Gamma-Ray Bursts, II)”; in Proceedings of the XIth Brazilian School on Cosmology and Gravitation, Mangaratiba, Rio de Janeiro (Brazil), July – August 2004, M. Novello, S.E. Perez Bergliaffa, Editors; AIP Conference Proceedings, 782, 42 (2005).

We outline the confluence of three novel theoretical fields in our modeling of Gamma-Ray Bursts (GRBs): 1) the ultrarelativistic regime of a shock front expanding with a Lorentz gamma factor ~ 300 ; 2) the quantum vacuum polarization process leading to an electron-positron plasma originating the shock front; and 3) the general relativistic process of energy extraction from a black hole originating the vacuum polarization process. There are two different classes of GRBs: the long GRBs and the short GRBs. We here address the issue of the long GRBs. The theoretical understanding of the long GRBs has led to the detailed description of their luminosities in fixed energy bands, of their spectral features and made also possible to probe the astrophysical scenario in which they originate. We are specially interested, in this report, to a subclass of long GRBs which appear to be accompanied by a supernova explo-

sion. We are considering two specific examples: GRB980425/SN1998bw and GRB030329/SN2003dh. While these supernovae appear to have a standard energetics of 10^{49} ergs, the GRBs are highly variable and can have energetics $10^4 - 10^5$ times larger than the ones of the supernovae. Moreover, many long GRBs occurs without the presence of a supernova. It is concluded that in no way a GRB can originate from a supernova. The precise theoretical understanding of the GRB luminosity we present evidence, in both these systems, the existence of an independent component in the X-ray emission, usually interpreted in the current literature as part of the GRB afterglow. This component has been observed by Chandra and XMM to have a strong decay on scale of months. We have named here these two sources respectively URCA-1 and URCA-2, in honor of the work that George Gamow and Mario Shoenberg did in 1939 in this town of Urca identifying the basic mechanism, the Urca processes, leading to the process of gravitational collapse and the formation of a neutron star and a supernova. The further hypothesis is considered to relate this X-ray source to a neutron star, newly born in the Supernova. This hypothesis should be submitted to further theoretical and observational investigation. Some theoretical developments to clarify the astrophysical origin of this new scenario are outlined. We turn then to the theoretical developments in the short GRBs: we first report some progress in the understanding the dynamical phase of collapse, the mass-energy formula and the extraction of blackholic energy which have been motivated by the analysis of the short GRBs. In this context progress has also been accomplished on establishing an absolute lower limit to the irreducible mass of the black hole as well as on some critical considerations about the relations of general relativity and the second law of thermodynamics. We recall how this last issue has been one of the most debated in theoretical physics in the past thirty years due to the work of Bekenstein and Hawking. Following these conceptual progresses we analyze the vacuum polarization process around an overcritical collapsing shell. We evidence the existence of a separatrix and a dyadosphere trapping surface in the dynamics of the electron-positron plasma generated during the process of gravitational collapse. We then analyze, using recent progress in the solution of the Vlasov-Boltzmann-Maxwell system, the oscillation regime in the created electron-positron plasma and their rapid convergence to a thermalized spectrum. We conclude by making precise predictions for the spectra, the energy fluxes and characteristic time-scales of the radiation for short-bursts. If the precise luminosity variation and spectral hardening of the radiation we have predicted will be confirmed by observations of short-bursts, these systems will

play a major role as standard candles in cosmology. These considerations will also be relevant for the analysis of the long-bursts when the baryonic matter contribution will be taken into account.

2. R. Ruffini, M.G. Bernardini, C.L. Bianco, P. Chardonnet, F. Frascchetti, V. Gurzadyan, L. Vitagliano, S.-S. Xue; "Black hole physics and astrophysics: The GRB-Supernova connection and URCA-1 – URCA-2"; in Proceedings of the Tenth Marcel Grossmann Meeting on General Relativity, Rio de Janeiro, Brazil, July 2003, M. Novello, S.E. Perez-Bergliaffa, Editors; p. 369; World Scientific, (Singapore, 2006).

We outline the confluence of three novel theoretical fields in our modeling of Gamma-Ray Bursts (GRBs): 1) the ultrarelativistic regime of a shock front expanding with a Lorentz gamma factor ~ 300 ; 2) the quantum vacuum polarization process leading to an electron-positron plasma originating the shock front; and 3) the general relativistic process of energy extraction from a black hole originating the vacuum polarization process. There are two different classes of GRBs: the long GRBs and the short GRBs. We here address the issue of the long GRBs. The theoretical understanding of the long GRBs has led to the detailed description of their luminosities in fixed energy bands, of their spectral features and made also possible to probe the astrophysical scenario in which they originate. We are specially interested, in this report, to a subclass of long GRBs which appear to be accompanied by a supernova explosion. We are considering two specific examples: GRB980425/SN1998bw and GRB030329/SN2003dh. While these supernovae appear to have a standard energetics of 10^{49} ergs, the GRBs are highly variable and can have energetics $10^4 - 10^5$ times larger than the ones of the supernovae. Moreover, many long GRBs occurs without the presence of a supernova. It is concluded that in no way a GRB can originate from a supernova. The precise theoretical understanding of the GRB luminosity we present evidence, in both these systems, the existence of an independent component in the X-ray emission, usually interpreted in the current literature as part of the GRB afterglow. This component has been observed by Chandra and XMM to have a strong decay on scale of months. We have named here these two sources respectively URCA-1 and URCA-2, in honor of the work that George Gamow and Mario Shoenberg did in 1939 in this town of Urca identifying the basic mechanism, the Urca processes, leading to the process of gravitational collapse and the formation of a neutron star and a supernova. The further hypothesis is considered to relate this X-ray source to a neutron star, newly born in the Supernova. This hypothesis should

be submitted to further theoretical and observational investigation. Some theoretical developments to clarify the astrophysical origin of this new scenario are outlined.

3. M.G. Bernardini, C.L. Bianco, P. Chardonnet, F. Frascchetti, R. Ruffini, S.-S. Xue; “General features of GRB 030329 in the EMBH model”; in Proceedings of the Tenth Marcel Grossmann Meeting on General Relativity, Rio de Janeiro, Brazil, July 2003, M. Novello, S.E. Perez-Bergliaffa, Editors; p. 2459; World Scientific, (Singapore, 2006).

GRB 030329 is considered within the EMBH model. We determine the three free parameters and deduce its luminosity in given energy bands comparing it with the observations. The observed substructures are compared with the predictions of the model: by applying the result that substructures observed in the extended afterglow peak emission (E-APE) do indeed originate in the collision of the accelerated baryonic matter (ABM) pulse with the inhomogeneities in the interstellar medium around the black-hole, masks of density inhomogeneities are considered in order to reproduce the observed temporal substructures. The induced supernova concept is applied to this system and the general consequences that we are witnessing are the formation of a cosmological thriptych of a black hole originating the GRB 030329, the supernova SN2003dh and a young neutron star. Analogies to the system GRB 980425–SN1998bw are outlined.

4. R. Ruffini, M.G. Bernardini, C.L. Bianco, P. Chardonnet, A. Corsi, F. Frascchetti, S.-S. Xue; “GRB 970228 and its associated Supernova in the EMBH model”; in Proceedings of the Tenth Marcel Grossmann Meeting on General Relativity, Rio de Janeiro, Brazil, July 2003, M. Novello, S.E. Perez-Bergliaffa, Editors; p. 2465; World Scientific, (Singapore, 2006).

The γ -ray burst of 1997 February 28 is analyzed within the Electromagnetic Black Hole model. We first estimate the value of the total energy deposited in the dyadosphere, E_{dya} , and the amount of baryonic matter left over by the EMBH progenitor star, $B = M_B c^2 / E_{dya}$. We then consider the role of the interstellar medium number density n_{ISM} and of the ratio R between the effective emitting area and the total surface area of the γ -ray burst source, in reproducing the prompt emission and the X-ray afterglow of this burst. Some considerations are also done concerning the possibility of explaining, within the theory, the observed evidence for a supernova in the optical afterglow.

5. F. Fraschetti, M.G. Bernardini, C.L. Bianco, P. Chardonnet, R. Ruffini, S.-S. Xue; "Inferences on the ISM structure around GRB980425 and GRB980425-SN1998bw association in the EMBH Model"; in Proceedings of the Tenth Marcel Grossmann Meeting on General Relativity, Rio de Janeiro, Brazil, July 2003, M. Novello, S.E. Perez-Bergliaffa, Editors; p. 2451; World Scientific, (Singapore, 2006).

We determine the four free parameters within the EMBH model for GRB 980425 and deduce its luminosity in given energy bands, its spectra and its time variability in the prompt radiation. We compute the basic kinematical parameters of GRB 980425. In the extended afterglow peak emission the Lorentz γ factor is lower than the critical value 150 which has been found in Ruffini et al. (2002) to be necessary in order to perform the tomography of the ISM surrounding the GRB as suggested by Dermer & Mitman (1999). The detailed structure of the density inhomogeneities as well as the effects of radial apparent superluminal effects are evaluated within the EMBH model. Under the assumption that the energy distribution of emitted radiation is thermal in the comoving frame, time integrated spectra of EMBH model for prompt emission are computed. The induced supernova concept is applied to this system and general consequences on the astrophysical and cosmological scenario are derived.

6. R. Ruffini, M.G. Bernardini, C.L. Bianco, P. Chardonnet, F. Fraschetti, R. Guida, S.-S. Xue; "GRB 050315: A step in the proof of the uniqueness of the overall GRB structure"; in "GAMMA-RAY BURSTS IN THE SWIFT ERA: Sixteenth Maryland Astrophysics Conference", Washington, DC, USA, November 29th – December 2nd 2005, Stephen S. Holt, Neil Gehrels, John A. Nousek, Editors; AIP Conference Proceedings, 836, 103 (2006).

Using the Swift data of GRB 050315, we progress in proving the uniqueness of our theoretically predicted Gamma-Ray Burst (GRB) structure as composed by a proper-GRB, emitted at the transparency of an electron-positron plasma with suitable baryon loading, and an afterglow comprising the "prompt radiation" as due to external shocks. Detailed light curves for selected energy bands are theoretically fitted in the entire temporal region of the Swift observations ranging over 10^6 seconds.

7. R. Ruffini, M.G. Bernardini, C.L. Bianco, P. Chardonnet, F. Fraschetti, S.-S. Xue; "Theoretical Interpretation of GRB 031203 and URCA-3"; in

“Relativistic Astrophysics and Cosmology - Einstein’s Legacy”, B. Aschenbach, V. Burwitz, G. Hasinger, B. Leibundgut, Editors; Springer-Verlag (2007).

8. R. Ruffini, M.G. Bernardini, C.L. Bianco, L. Caito, P. Chardonnet, M.G. Dainotti, F. Fraschetti, R. Guida, M. Rotondo, G. Vereshchagin, L. Vitagliano, S.-S. Xue; “The Blackholic energy and the canonical Gamma-Ray Burst”; in Proceedings of the XIIth Brazilian School on Cosmology and Gravitation, Mangaratiba, Rio de Janeiro (Brazil), September 2006, M. Novello, S.E. Perez Bergliaffa, Editors; AIP Conference Proceedings, 910, 55 (2007).

Gamma-Ray Bursts (GRBs) represent very likely “the” most extensive computational, theoretical and observational effort ever carried out successfully in physics and astrophysics. The extensive campaign of observation from space based X-ray and γ -ray observatory, such as the *Vela*, CGRO, BeppoSAX, HETE-II, INTEGRAL, *Swift*, R-XTE, *Chandra*, XMM satellites, have been matched by complementary observations in the radio wavelength (e.g. by the VLA) and in the optical band (e.g. by VLT, Keck, ROSAT). The net result is unprecedented accuracy in the received data allowing the determination of the energetics, the time variability and the spectral properties of these GRB sources. The very fortunate situation occurs that these data can be confronted with a mature theoretical development. Theoretical interpretation of the above data allows progress in three different frontiers of knowledge: **a)** the ultrarelativistic regimes of a macroscopic source moving at Lorentz gamma factors up to ~ 400 ; **b)** the occurrence of vacuum polarization process verifying some of the yet untested regimes of ultrarelativistic quantum field theories; and **c)** the first evidence for extracting, during the process of gravitational collapse leading to the formation of a black hole, amounts of energies up to 10^{55} ergs of blackholic energy — a new form of energy in physics and astrophysics. We outline how this progress leads to the confirmation of three interpretation paradigms for GRBs proposed in July 2001. Thanks mainly to the observations by *Swift* and the optical observations by VLT, the outcome of this analysis points to the existence of a “canonical” GRB, originating from a variety of different initial astrophysical scenarios. The communality of these GRBs appears to be that they all are emitted in the process of formation of a black hole with a negligible value of its angular momentum. The following sequence of events appears to be canonical: the vacuum polarization process in the dyadosphere with the creation of the optically thick self accelerating electron-positron plasma; the

engulfment of baryonic mass during the plasma expansion; adiabatic expansion of the optically thick “fireshell” of electron-positron-baryon plasma up to the transparency; the interaction of the accelerated baryonic matter with the interstellar medium (ISM). This leads to the canonical GRB composed of a proper GRB (P-GRB), emitted at the moment of transparency, followed by an extended afterglow. The sole parameters in this scenario are the total energy of the dyadosphere E_{dya} , the fireshell baryon loading M_B defined by the dimensionless parameter $B \equiv M_B c^2 / E_{dya}$, and the ISM filamentary distribution around the source. In the limit $B \rightarrow 0$ the total energy is radiated in the P-GRB with a vanishing contribution in the afterglow. In this limit, the canonical GRBs explain as well the short GRBs. In these lecture notes we systematically outline the main results of our model comparing and contrasting them with the ones in the current literature. In both cases, we have limited ourselves to review already published results in refereed publications. We emphasize as well the role of GRBs in testing yet unexplored grounds in the foundations of general relativity and relativistic field theories.

9. R. Ruffini, M.G. Bernardini, C.L. Bianco, L. Caito, P. Chardonnet, M.G. Dainotti, F. Fraschetti, R. Guida, G. Vereshchagin, S.-S. Xue; “The role of GRB 031203 in clarifying the astrophysical GRB scenario”; in Proceedings of the 6th Integral Workshop - The Obscured Universe, Moscow, (Russia), July 2006, S. Grebenev, R. Sunyaev, C. Winkler, A. Parmar, L. Ouweland, Editors; ESA Special Publication, SP-622, 561 (2007).

The luminosity and the spectral distribution of the afterglow of GRB 031203 have been presented within our theoretical framework, which envisages the GRB structure as composed by a proper-GRB, emitted at the transparency of an electron-positron plasma with suitable baryon loading, and an afterglow comprising the “prompt emission” as due to external shocks. In addition to the GRB emission, there appears to be a prolonged soft X-Ray emission lasting for 10^6 – 10^7 seconds followed by an exponential decay. This additional source has been called by us URCA-3. It is urgent to establish if this component is related to the GRB or to the Supernova (SN). In this second case, there are two possibilities: either the interaction of the SN ejecta with the interstellar medium or, possibly, the cooling of a young neutron star formed in the SN 2003lw process. The analogies and the differences between this triptych GRB 031203 / SN 2003lw / URCA-3 and the corresponding ones GRB 980425 / SN 1998bw / URCA-1 and GRB 030329 / SN 2003dh / URCA-2, as well as GRB 060218 / SN 2006aj are discussed.

10. M.G. Bernardini, C.L. Bianco, L. Caito, M.G. Dainotti, R. Guida, R. Ruffini; “GRB970228 and the class of GRBs with an initial spikelike emission: do they follow the Amati relation?”; in *Relativistic Astrophysics – Proceedings of the 4th Italian-Sino Workshop, Pescara (Italy), July 2007*, C.L. Bianco, S.-S. Xue, Editors; AIP Conference Proceedings, 966, 7 (2008).

On the basis of the recent understanding of GRB050315 and GRB060218, we return to GRB970228, the first Gamma-Ray Burst (GRB) with detected afterglow. We proposed it as the prototype for a new class of GRBs with “an occasional softer extended emission lasting tenths of seconds after an initial spikelike emission”. Detailed theoretical computation of the GRB970228 light curves in selected energy bands for the prompt emission are presented and compared with observational *BeppoSAX* data. From our analysis we conclude that GRB970228 and likely the ones of the above mentioned new class of GRBs are “canonical GRBs” have only one peculiarity: they exploded in a galactic environment, possibly the halo, with a very low value of CBM density. Here we investigate how GRB970228 unveils another peculiarity of this class of GRBs: they do not fulfill the “Amati relation”. We provide a theoretical explanation within the fireshell model for the apparent absence of such correlation for the GRBs belonging to this new class.

11. C.L. Bianco, M.G. Bernardini, L. Caito, M.G. Dainotti, R. Guida, R. Ruffini; “The “Fireshell” Model and the “Canonical” GRB Scenario; in *Relativistic Astrophysics – Proceedings of the 4th Italian-Sino Workshop, Pescara (Italy), July 2007*, C.L. Bianco, S.-S. Xue, Editors; AIP Conference Proceedings, 966, 12 (2008).

In the “fireshell” model we define a “canonical GRB” light curve with two sharply different components: the Proper-GRB (P-GRB), emitted when the optically thick fireshell of electron-positron plasma originating the phenomenon reaches transparency, and the afterglow, emitted due to the collision between the remaining optically thin fireshell and the CircumBurst Medium (CBM). We outline our “canonical GRB” scenario, originating from the gravitational collapse to a black hole, with a special emphasis on the discrimination between “genuine” and “fake” short GRBs.

12. L. Caito, M.G. Bernardini, C.L. Bianco, M.G. Dainotti, R. Guida, R. Ruffini; “GRB 060614: A Progress Report”; in *Relativistic Astrophysics – Proceedings of the 4th Italian-Sino Workshop, Pescara (Italy), July 2007*, C.L. Bianco, S.-S. Xue, Editors; AIP Conference Proceedings, 966, 16 (2008).

The explosion of GRB 060614, detected by the Swift satellite, produced a deep break in the GRB scenario opening new horizons of investigation, because it can't be traced back to any traditional scheme of classification. In fact, it manifests peculiarities both of long bursts and of short bursts. Above all, it is the first case of long duration near GRB without any bright Ib/c associated Supernova. We will show that, in our canonical GRB scenario, this "anomalous" situation finds a natural interpretation and allows us to discuss a possible variation to the traditional classification scheme, introducing the distinction between "genuine" and "fake" short bursts.

13. M.G. Dainotti, M.G. Bernardini, C.L. Bianco, L. Caito, R. Guida, R. Ruffini; "GRB 060218 and the Binaries as Progenitors of GRB-SN Systems"; in *Relativistic Astrophysics – Proceedings of the 4th Italian-Sino Workshop, Pescara (Italy), July 2007*, C.L. Bianco, S.-S. Xue, Editors; AIP Conference Proceedings, 966, 25 (2008).

We study the Gamma-Ray Burst (GRB) 060218: a particularly close source at $z = 0.033$ with an extremely long duration, namely $T_{90} \sim 2000$ s, related to SN 2006aj. This source appears to be a very soft burst, with a peak in the spectrum at 4.9 keV, therefore interpreted as an X-Ray Flash (XRF). It fulfills the Amati relation. I present the fitting procedure, which is time consuming. In order to show its sensitivity I also present two examples of fits with the same value of B and different value of $E_{e^\pm}^{tot}$. We fit the X- and γ -ray observations by *Swift* of GRB 060218 in the 0.1–150 keV energy band during the entire time of observations from 0 all the way to 10^6 s within a unified theoretical model. The free parameters of our theory are only three, namely the total energy $E_{e^\pm}^{tot}$ of the e^\pm plasma, its baryon loading $B \equiv M_B c^2 / E_{e^\pm}^{tot}$, as well as the CircumBurst Medium (CBM) distribution. We justify the extremely long duration of this GRB by a total energy $E_{e^\pm}^{tot} = 2.32 \times 10^{50}$ erg, a very high value of the baryon loading $B = 1.0 \times 10^{-2}$ and the effective CircumBurst Medium (CBM) density which shows a radial dependence $n_{cbm} \propto r^{-\alpha}$ with $1.0 \leq \alpha \leq 1.7$ and monotonically decreases from 1 to 10^{-6} particles/cm³. We recall that this value of the B parameter is the highest among the sources we have analyzed and it is very close to its absolute upper limit expected. By our fit we show that there is no basic differences between XRFs and more general GRBs. They all originate from the collapse process to a black hole and their difference is due to the variability of the three basic parameters within the range of full applicability of the theory. We also think that the smallest possible black hole, formed by the gravitational collapse of a neutron star in a binary system, is consistent with

the especially low energetics of the class of GRBs associated with SNe Ib/c.

14. R. Guida, M.G. Bernardini, C.L. Bianco, L. Caito, M.G. Dainotti, R. Ruffini; “The Amati Relation within the Fireshell Model”; in *Relativistic Astrophysics – Proceedings of the 4th Italian-Sino Workshop, Pescara (Italy), July 2007*, C.L. Bianco, S.-S. Xue, Editors; AIP Conference Proceedings, 966, 46 (2008).

In this work we show the existence of a spectral-energy correlation within our “fireshell” model for GRBs. The free parameters of the model are the total energy $E_{tot}^{e^\pm}$ of the e^\pm plasma and its baryon loading $B \equiv M_B c^2 / E_{tot}^{e^\pm}$, characterizing the source, and the parameters describing the effective CircumBurst medium (CBM) distribution, namely its particle number density ρ and its effective emitting area R . We build a sample of pseudo-GRBs, i.e. a set of theoretically simulated light curves, varying the total energy of the electron-positron plasma $E_{tot}^{e^\pm}$ and keeping the same baryon loading; the parametrization used to describe the distribution of the CircumBurst medium is the same as well for all the pseudo-GRBs. The values of these parameters (B , ρ and R) used in this work are equal to the ones assumed to fit GRB050315, a *Swift* burst representing a good example of what in the literature has been addressed as “canonical light curve”. For each GRB of the sample we calculate the νF_ν spectrum integrating the theoretically computed light curve over the total time, namely from our T_0 , the end of the Proper-GRB (P-GRB), up to the end of our afterglow phase, when the fireshell Lorentz gamma factor is close to unity; we exclude the P-GRB from this spectral computation because, following our “canonical” GRB scenario, this component of the GRB emission is physically different from the other component, that is our afterglow component, so one should take care in no mixing them. We find that the maximum of this spectrum, that is the observed peak energy $E_{p,tot}$, correlates with the initial electron-positron plasma energy $E_{tot}^{e^\pm}$ in a way very similar to the Amati one: $E_{p,tot} \propto (E_{tot}^{e^\pm})^{0.5}$.

15. R. Guida, M.G. Bernardini, C.L. Bianco, L. Caito, M.G. Dainotti, R. Ruffini; “Theoretical interpretation of the Amati relation within the fireshell model”; in *GAMMA-RAY BURSTS 2007: Proceedings of the Santa Fe Conference, Santa Fe (NM, USA), November 2007*, M. Galassi, D. Palmer, E. Fenimore, Editors; AIP Conference Proceedings, 1000, 60 (2008).

We discuss within our theoretical “fireshell” model for Gamma-Ray Bursts (GRBs) the theoretical interpretation of the phenomenological correlation between the isotropic-equivalent radiated energy of the prompt emission E_{iso} and

the cosmological rest-frame νF_ν spectrum peak energy E_p observed by Amati and collaborators. Possible reasons for some of the outliers of this relation are given.

16. L. Caito, M.G. Bernardini, C.L. Bianco, M.G. Dainotti, R. Guida, R. Ruffini; "GRB 060614: a Fake Short Gamma-Ray Burst"; in GAMMA-RAY BURSTS 2007: Proceedings of the Santa Fe Conference, Santa Fe (NM, USA), November 2007, M. Galassi, D. Palmer, E. Fenimore, Editors; AIP Conference Proceedings, 1000, 301 (2008).

The explosion of GRB 060614 produced a deep break in the GRB scenario and opened new horizons of investigation because it can't be traced back to any traditional scheme of classification. In fact, it manifests peculiarities both of long bursts and of short bursts and, above all, it is the first case of long duration near GRB without any bright Ib/c associated Supernova. We will show that, in our canonical GRB scenario, this "anomalous" situation finds a natural interpretation and allows us to discuss a possible variation to the traditional classification scheme, introducing the distinction between "genuine" and "fake" short bursts.

17. C.L. Bianco, M.G. Bernardini, L. Caito, M.G. Dainotti, R. Guida, R. Ruffini; "Short and canonical GRBs"; in GAMMA-RAY BURSTS 2007: Proceedings of the Santa Fe Conference, Santa Fe (NM, USA), November 2007, M. Galassi, D. Palmer, E. Fenimore, Editors; AIP Conference Proceedings, 1000, 305 (2008).

Within the "fireshell" model for the Gamma-Ray Bursts (GRBs) we define a "canonical GRB" light curve with two sharply different components: the Proper-GRB (P-GRB), emitted when the optically thick fireshell of electron-positron plasma originating the phenomenon reaches transparency, and the afterglow, emitted due to the collision between the remaining optically thin fireshell and the CircumBurst Medium (CBM). We outline our "canonical GRB" scenario, with a special emphasis on the discrimination between "genuine" and "fake" short GRBs.

18. C.L. Bianco, M.G. Bernardini, L. Caito, M.G. Dainotti, R. Guida, R. Ruffini, G. Vereshchagin, S.-S. Xue; "The Equations of motion of the "fireshell""; in OBSERVATIONAL EVIDENCE FOR BLACK HOLES IN THE UNIVERSE: Proceedings of the 2nd Kolkata Conference, Kolkata (India),

February 2008, S.K. Chakrabarti, A.S. Majumdar, Editors; AIP Conference Proceedings, 1053, 259 (2008).

The Fireshell originating a Gamma-Ray Burst (GRB) encompasses an optically thick regime followed by an optically thin one. In the first one the fireshell self-accelerates from a Lorentz gamma factor equal to 1 all the way to 200-300. The physics of this system is based on the continuous annihilation of electron-positron pairs in an optically thick e^+e^- plasma with a small baryon loading. In the following regime, the optically thin fireshell, composed by the baryons left over after the transparency point, ballistically expands into the Circum-Burst Medium (CBM). The dynamics of the fireshell during both regimes will be analyzed. In particular we will re-examine the validity of the constant-index power-law relation between the fireshell Lorentz gamma factor and its radial coordinate, usually adopted in the current literature on the grounds of an “ultrarelativistic” approximation. Such expressions are found to be mathematically correct but only approximately valid in a very limited range of the physical and astrophysical parameters and in an asymptotic regime which is reached only for a very short time, if any.

19. M.G. Bernardini, C.L. Bianco, L. Caito, M.G. Dainotti, R. Guida, R. Ruffini; “The “Canonical” GRBs within the fireshell model”; in OBSERVATIONAL EVIDENCE FOR BLACK HOLES IN THE UNIVERSE: Proceedings of the 2nd Kolkata Conference, Kolkata (India), February 2008, S.K. Chakrabarti, A.S. Majumdar, Editors; AIP Conference Proceedings, 1053, 267 (2008).

Within the fireshell model we define a “canonical” GRB light curve with two sharply different components: the Proper-GRB (P-GRB), emitted when the optically thick fireshell of electron-positron plasma originating the phenomenon reaches transparency, and the afterglow, emitted due to the collision between the remaining optically thin fireshell and the CircumBurst Medium (CBM). On the basis of the recent understanding of GRB970228 as the prototype for a new class of GRBs with “an occasional softer extended emission lasting tenths of seconds after an initial spikelike emission” we outline our “canonical” GRB scenario, originating from the gravitational collapse to a black hole, with a special emphasis on the discrimination between short GRBs and the ones appearing as such due to their peculiar astrophysical setting.

20. M.G. Dainotti, M.G. Bernardini, C.L. Bianco, L. Caito, R. Guida, R. Ruffini; “GRB 060218: the density mask and its peculiarity compared to the other sources”; in OBSERVATIONAL EVIDENCE FOR BLACK HOLES

IN THE UNIVERSE: Proceedings of the 2nd Kolkata Conference, Kolkata (India), February 2008, S.K. Chakrabarti, A.S. Majumdar, Editors; AIP Conference Proceedings, 1053, 283 (2008).

The Swift satellite has given continuous data in the range 0.3–150 keV from 0 s to 106 s for GRB060218 associated with SN2006aj. It has an unusually long duration ($T_{90} \sim 2100$ s). We plan to fit the complete γ - and X-ray light curves of this long duration GRB, including the prompt emission and we give peculiar attention to the afterglow lightcurve in order to better constrain the density mask. We apply our “fireshell” model based on the formation of a black hole, giving the relevant references. The initial total energy of the electron-positron plasma $E_{e^\pm}^{tot} = 2.32 \times 10^{50}$ erg has a particularly low value similarly to the other GRBs associated with SNe. For the first time we observe a baryon loading $B = 10^{-2}$ which coincides with the upper limit for the dynamical stability of the fireshell. The effective CircumBurst Medium (CBM) density shows a radial dependence $n_{cbm} \propto r^{-a}$ with $1.0 \leq a \leq 1.7$ and monotonically decreases from 1 to 10^{-6} particles/cm³. Such a behavior is interpreted as due to a fragmentation in the fireshell. Such a fragmentation is crucial in explaining both the unusually large T_{90} and the consequently inferred abnormal low value of the CBM effective density. We present the comparison between the density mask of this source and the ones of a normal GRB 050315 and a fake short, GRB 970228, making some assumptions on the CBM behaviour in the surrounding of the Black hole.

21. L. Caito, M.G. Bernardini, C.L. Bianco, M.G. Dainotti, R. Guida, R. Ruffini; “GRB 060614 in the canonical fireshell model”; in OBSERVATIONAL EVIDENCE FOR BLACK HOLES IN THE UNIVERSE: Proceedings of the 2nd Kolkata Conference, Kolkata (India), February 2008, S.K. Chakrabarti, A.S. Majumdar, Editors; AIP Conference Proceedings, 1053, 291 (2008).

Gamma-Ray Burst (GRB) 060614 is the first nearby long duration GRB clearly not associated to any bright Ib/c Supernova. The explosion of this burst undermines one of the fundamental assumptions of the standard scenario and opens new horizons and hints of investigation. GRB 060614, hardly classifiable as a short GRB, is not either a “typical” long GRB since it occurs in a low star forming region. Moreover, it presents deep similarities with GRB 970228, which is the prototype of the “fake” short bursts, or better canonical GRBs disguised as short ones. Within the “fireshell” model, we test if this “anomalous” source can be a disguised short GRB.

22. L.J. Rangel Lemos, S. Casanova, R. Ruffini, S.S. Xue; “Fermi’s approach to the study of pp interactions”; in OBSERVATIONAL EVIDENCE FOR BLACK HOLES IN THE UNIVERSE: Proceedings of the 2nd Kolkata Conference, Kolkata (India), February 2008, S.K. Chakrabarti, A.S. Majumdar, Editors; AIP Conference Proceedings, 1053, 275 (2008).

The physics of hadronic interactions found much difficulties for explain the experimental data. In this work we study the approach of Fermi (1950) about the multiplicity of pions emitted in pp interactions and in follow we compare with the modern approach

23. R. Ruffini, A.G. Aksenov, M.G. Bernardini, C.L. Bianco, L. Caito, M.G. Dainotti, G. De Barros, R. Guida, G.V. Vereshchagin, S.-S. Xue; “The canonical Gamma-Ray Bursts and their ‘precursors’”; in 2008 NANJING GAMMA-RAY BURST CONFERENCE, Proceedings of the 2008 Nanjing Gamma-Ray Burst Conference, Nanjing (China), June 2008, Y.-F. Huang, Z.-G. Dai, B. Zhang, Editors; AIP Conference Proceedings, 1065, 219 (2008).

The fireshell model for Gamma-Ray Bursts (GRBs) naturally leads to a canonical GRB composed of a proper-GRB (P-GRB) and an afterglow. P-GRBs, introduced by us in 2001, are sometimes considered “precursors” of the main GRB event in the current literature. We show in this paper how the fireshell model leads to the understanding of the structure of GRBs, with precise estimates of the time sequence and intensities of the P-GRB and the of the afterglow. It leads as well to a natural classification of the canonical GRBs which overcomes the traditional one in short and long GRBs.

24. M.G. Bernardini, C.L. Bianco, L. Caito, M.G. Dainotti, R. Guida, R. Ruffini; “Preliminary analysis of GRB060607A within the fireshell model”; in 2008 NANJING GAMMA-RAY BURST CONFERENCE; Proceedings of the 2008 Nanjing Gamma-Ray Burst Conference, Nanjing (China), June 2008, Y.-F. Huang, Z.-G. Dai, B. Zhang, Editors; AIP Conference Proceedings, 1065, 227 (2008).

GRB060607A is a very distant ($z = 3.082$) and energetic event ($E_{iso} \sim 10^{53}$ erg). Its main peculiarity is that the peak of the near-infrared afterglow has been observed with the REM robotic telescope, allowing to infer the initial Lorentz gamma factor of the emitting system. We present a preliminary analysis of the spectra and light curves of GRB060607A prompt emission within

the fireshell model. We show that the $N(E)$ spectrum of the prompt emission, whose behavior is usually described as “simple power-law”, can also be fitted in a satisfactory way by a convolution of thermal spectra as predicted by the model we applied. The theoretical time-integrated spectrum of the prompt emission as well as the light curves in the BAT and XRT energy band are in good agreement with the observations, enforcing the plausibility of our approach. Furthermore, the initial value of Lorentz gamma factor we predict is compatible with the one deduced from the REM observations.

25. C.L. Bianco, M.G. Bernardini, L. Caito, M.G. Dainotti, R. Guida, R. Ruffini; “The “fireshell” model and the “canonical GRB” scenario”; in 2008 NANJING GAMMA-RAY BURST CONFERENCE; Proceedings of the 2008 Nanjing Gamma-Ray Burst Conference, Nanjing (China), June 2008, Y.-F. Huang, Z.-G. Dai, B. Zhang, Editors; AIP Conference Proceedings, 1065, 223 (2008).

The Swift observation of GRB 060614, as well as the catalog analysis by Norris & Bonnell (2006), opened the door “on a new Gamma-Ray Bursts (GRBs) classification scheme that straddles both long and short bursts” (Gehrels et al. 2006). Within the “fireshell” model for the Gamma-Ray Bursts (GRBs) we define a “canonical GRB” light curve with two sharply different components: the Proper-GRB (P-GRB), emitted when the optically thick fireshell of electron-positron plasma originating the phenomenon reaches transparency, and the afterglow, emitted due to the collision between the remaining optically thin fireshell and the CircumBurst Medium (CBM). We here outline our “canonical GRB” scenario, which implies three different GRB classes: the “genuine” short GRBs, the “fake” or “disguised” short GRBs and the other (so-called “long”) GRBs. We also outline some implications for the theoretical interpretation of the Amati relation.

26. G. De Barros, M.G. Bernardini, C.L. Bianco, L. Caito, M.G. Dainotti, R. Guida, R. Ruffini; “Is GRB 050509b a “genuine” short GRB?”; in 2008 NANJING GAMMA-RAY BURST CONFERENCE; Proceedings of the 2008 Nanjing Gamma-Ray Burst Conference, Nanjing (China), June 2008, Y.-F. Huang, Z.-G. Dai, B. Zhang, Editors; AIP Conference Proceedings, 1065, 231 (2008).

Within our “fireshell” model we introduced a “canonical” GRB scenario which differentiates physically the “proper GRB” (P-GRB) emission when photons decouple, and the afterglow emission due to interaction of the accelerated

baryons with the CircumBurst Medium (CBM). The ratio between energetics of the two components is ruled by the baryon loading of the fireshell. We here analyse the possibility that GRB050509b is the first case of a “genuine” short GRB the ones with smaller baryon loading. In such a case, the GRB050509b “prompt emission” would be dominated by the “proper GRB” and, moreover, the P-GRB total energy would be greater than the afterglow one. Our fit of the afterglow data and of the P-GRB energetics indicates that this source present the smallest baryon loading we ever encountered so far, being on the order of 10^{-4} .

27. G. De Barros, A.G. Aksenov, C.L. Bianco, R. Ruffini, G.V. Vereshchagin; “Fireshell versus Fireball scenarios”; in 2008 NANJING GAMMA-RAY BURST CONFERENCE; Proceedings of the 2008 Nanjing Gamma-Ray Burst Conference, Nanjing (China), June 2008, Y.-F. Huang, Z.-G. Dai, B. Zhang, Editors; AIP Conference Proceedings, 1065, 234 (2008).

We revisit Cavallo and Rees classification based on the analysis of initial conditions in electron-positron-photon plasma which appears suddenly around compact astrophysical objects and gives origin to GRBs. These initial conditions were recently studied in [1,2] by numerical integration of relativistic Boltzmann equations with collision integrals, including binary and triple interactions between particles. The main conclusion is that the pair plasma in GRB sources quickly reaches thermal equilibrium well before its expansion starts. In light of this work we comment on each of the four scenarios proposed by Cavallo and Rees and discuss their applicability to describe evolution of GRB sources.

28. M.G. Bernardini, C.L. Bianco, L. Caito, M.G. Dainotti, R. Guida, R. Ruffini; “GRB970228 as a prototype for the class of GRBs with an initial spike-like emission”; in Proceedings of the Eleventh Marcel Grossmann Meeting on General Relativity, Berlin, Germany, July 2006, H. Kleinert, R.T. Jantzen, Editors; World Scientific, (Singapore, 2008).

We interpret GRB970228 prompt emission within our “canonical” GRB scenario, identifying the initial spikelike emission with the Proper-GRB (P-GRB) and the following bumps with the afterglow peak emission. Furthermore, we emphasize the necessity to consider the “canonical” GRB as a whole due to the highly non-linear nature of the model we applied.

29. M.G. Bernardini, C.L. Bianco, L. Caito, M.G. Dainotti, R. Guida, R. Ruffini;

“GRB980425 and the puzzling URCA1 emission”; in Proceedings of the Eleventh Marcel Grossmann Meeting on General Relativity, Berlin, Germany, July 2006, H. Kleinert, R.T. Jantzen, Editors; World Scientific, (Singapore, 2008).

We applied our “fireshell” model to GRB980425 observational data, reproducing very satisfactorily its prompt emission. We use the results of our analysis to provide a possible interpretation for the X-ray emission of the source S1. The effect on the GRB analysis of the lack of data in the pre-Swift observations is also outlined.

30. C.L. Bianco, M.G. Bernardini, L. Caito, P. Chardonnet, M.G. Dainotti, F. Fraschetti, R. Guida, R. Ruffini, S.-S. Xue; “Theoretical interpretation of ‘long’ and ‘short’ GRBs”; in Proceedings of the Eleventh Marcel Grossmann Meeting on General Relativity, Berlin, Germany, July 2006, H. Kleinert, R.T. Jantzen, Editors; World Scientific, (Singapore, 2008).

Within the “fireshell” model we define a “canonical GRB” light curve with two sharply different components: the Proper-GRB (P-GRB), emitted when the optically thick fireshell of electron-positron plasma originating the phenomenon reaches transparency, and the afterglow, emitted due to the collision between the remaining optically thin fireshell and the CircumBurst Medium (CBM). We here present the consequences of such a scenario on the theoretical interpretation of the nature of “long” and “short” GRBs.

31. C.L. Bianco, M.G. Bernardini, P. Chardonnet, F. Fraschetti, R. Ruffini, S.-S. Xue; “Theoretical interpretation of luminosity and spectral properties of GRB 031203”; in Proceedings of the Eleventh Marcel Grossmann Meeting on General Relativity, Berlin, Germany, July 2006, H. Kleinert, R.T. Jantzen, Editors; World Scientific, (Singapore, 2008).

We show how an emission endowed with an instantaneous thermal spectrum in the co-moving frame of the expanding fireshell can reproduce the time-integrated GRB observed non-thermal spectrum. An explicit example in the case of GRB 031203 is presented.

32. C.L. Bianco, R. Ruffini; “The ‘Fireshell’ model in the Swift era”; in Proceedings of the Eleventh Marcel Grossmann Meeting on General Relativity, Berlin, Germany, July 2006, H. Kleinert, R.T. Jantzen, Editors; World Scientific, (Singapore, 2008).

We here re-examine the validity of the constant-index power-law relation between the fireshell Lorentz gamma factor and its radial coordinate, usually adopted in the current Gamma-Ray Burst (GRB) literature on the grounds of an “ultrarelativistic” approximation. Such expressions are found to be mathematically correct but only approximately valid in a very limited range of the physical and astrophysical parameters and in an asymptotic regime which is reached only for a very short time, if any.

33. L. Caito, M.G. Bernardini, C.L. Bianco, M.G. Dainotti, R. Guida, R. Ruffini; “Theoretical interpretation of GRB011121”; in Proceedings of the Eleventh Marcel Grossmann Meeting on General Relativity, Berlin, Germany, July 2006, H. Kleinert, R.T. Jantzen, Editors; World Scientific, (Singapore, 2008).

GRB 011121, detected by the BeppoSAX satellite, is studied as a prototype to understand the presence of flares observed by Swift in the afterglow of many GRB sources. Detailed theoretical analysis of the GRB 011121 light curves in selected energy bands are presented and compared with observational data. An interpretation of the flare of this source is provided by the introduction of the three-dimensional structure of the CircumBurst Medium(CBM).

34. M.G. Dainotti, M.G. Bernardini, C.L. Bianco, L. Caito, R. Guida, R. Ruffini; “On GRB 060218 and the GRBs related to Supernovae Ib/c”; in Proceedings of the Eleventh Marcel Grossmann Meeting on General Relativity, Berlin, Germany, July 2006, H. Kleinert, R.T. Jantzen, Editors; World Scientific, (Singapore, 2008).

We study the Gamma-Ray Burst (GRB) 060218: a particularly close source at $z = 0.033$ with an extremely long duration, namely $T_{90} \sim 2000$ s, related to SN 2006aj. This source appears to be a very soft burst, with a peak in the spectrum at 4.9 keV, therefore interpreted as an X-Ray Flash (XRF) and it obeys to the Amati relation. We fit the X- and γ -ray observations by Swift of GRB 060218 in the 0.1–150 keV energy band during the entire time of observations from 0 all the way to 106 s within a unified theoretical model. The details of our theoretical analysis have been recently published in a series of articles. The free parameters of the theory are only three, namely the total energy $E_{e^\pm}^{tot}$ of the e^\pm plasma, its baryon loading $B = M_B c^2 / E_{e^\pm}^{tot}$, as well as the CircumBurst Medium (CBM) distribution. We fit the entire light curve, including the prompt emission as an essential part of the afterglow. We recall that this value of the B parameter is

the highest among the sources we have analyzed and it is very close to its absolute upper limit expected. We successfully make definite predictions about the spectral distribution in the early part of the light curve, exactly we derive the instantaneous photon number spectrum $N(E)$ and we show that although the spectrum in the co-moving frame of the expanding pulse is thermal, the shape of the final spectrum in the laboratory frame is clearly non thermal. In fact each single instantaneous spectrum is the result of an integration of thousands of thermal spectra over the corresponding EQuiTemporal Surfaces (EQTS). By our fit we show that there is no basic differences between XRFs and more general GRBs. They all originate from the collapse process to a black hole and their difference is due to the variability of the three basic parameters within the range of full applicability of the theory.

35. R. Guida, M.G. Bernardini, C.L. Bianco, L. Caito, M.G. Dainotti, R. Ruffini; "Theoretical interpretation of GRB060124"; in Proceedings of the Eleventh Marcel Grossmann Meeting on General Relativity, Berlin, Germany, July 2006, H. Kleinert, R.T. Jantzen, Editors; World Scientific, (Singapore, 2008).

We show the preliminary results of the application of our "fireshell" model to GRB060124. This source is very peculiar because it is the first event for which both the prompt and the afterglow emission were observed simultaneously by the three Swift instruments: BAT (15 - 350 keV), XRT (0,2 - 10 keV) and UVOT (170 - 650 nm), due to the presence of a precursor ~ 570 s before the main burst. We analyze GRB060124 within our "canonical" GRB scenario, identifying the precursor with the P-GRB and the prompt emission with the afterglow peak emission. In this way we reproduce correctly the energetics of both these two components. We reproduce also the observed time delay between the precursor (P-GRB) and the main burst. The effect of such a time delay in our model will be discussed.

36. R. Ruffini, M.G. Bernardini, C.L. Bianco, L. Caito, P. Chardonnet, C. Cherubini, M.G. Dainotti, F. Frascetti, A. Geralico, R. Guida, B. Patricelli, M. Rotondo, J. Rueda Hernandez, G. Vereshchagin, S.-S. Xue; "Gamma-Ray Bursts"; in Proceedings of the Eleventh Marcel Grossmann Meeting on General Relativity, Berlin, Germany, July 2006, H. Kleinert, R.T. Jantzen, Editors; World Scientific, (Singapore, 2008).

We show by example how the uncoding of Gamma-Ray Bursts (GRBs) offers unprecedented possibilities to foster new knowledge in fundamental physics

and in astrophysics. After recalling some of the classic work on vacuum polarization in uniform electric fields by Klein, Sauter, Heisenberg, Euler and Schwinger, we summarize some of the efforts to observe these effects in heavy ions and high energy ion collisions. We then turn to the theory of vacuum polarization around a Kerr-Newman black hole, leading to the extraction of the blackholic energy, to the concept of dyadosphere and dyadotorus, and to the creation of an electron-positron-photon plasma. We then present a new theoretical approach encompassing the physics of neutron stars and heavy nuclei. It is shown that configurations of nuclear matter in bulk with global charge neutrality can exist on macroscopic scales and with electric fields close to the critical value near their surfaces. These configurations may represent an initial condition for the process of gravitational collapse, leading to the creation of an electron-positron-photon plasma: the basic self-accelerating system explaining both the energetics and the high energy Lorentz factor observed in GRBs. We then turn to recall the two basic interpretational paradigms of our GRB model: 1) the Relative Space-Time Transformation (RSTT) paradigm and 2) the Interpretation of the Burst Structure (IBS) paradigm. These paradigms lead to a “canonical” GRB light curve formed from two different components: a Proper-GRB (P-GRB) and an extended afterglow comprising a raising part, a peak, and a decaying tail. When the P-GRB is energetically predominant we have a “genuine” short GRB, while when the afterglow is energetically predominant we have a so-called long GRB or a “fake” short GRB. We compare and contrast the description of the relativistic expansion of the electron-positron plasma within our approach and within the other ones in the current literature. We then turn to the special role of the baryon loading in discriminating between “genuine” short and long or “fake” short GRBs and to the special role of GRB 991216 to illustrate for the first time the “canonical” GRB bolometric light curve. We then propose a spectral analysis of GRBs, and proceed to some applications: GRB 031203, the first spectral analysis, GRB 050315, the first complete light curve fitting, GRB 060218, the first evidence for a critical value of the baryon loading, GRB 970228, the appearance of “fake” short GRBs. We finally turn to the GRB-Supernova Time Sequence (GSTS) paradigm: the concept of induced gravitational collapse. We illustrate this paradigm by the systems GRB 980425 / SN 1998bw, GRB 030329 / SN 2003dh, GRB 031203 / SN 2003lw, GRB 060218 / SN 2006aj, and we present the enigma of the URCA sources. We then present some general conclusions.

37. R. Ruffini, A.G. Aksenov, M.G. Bernardini, C.L. Bianco, L. Caito, M.G.

Dainotti, G. De Barros, R. Guida, G. Vereshchagin, S.-S. Xue; "The canonical Gamma-Ray Bursts: long, 'fake'-'disguised' and 'genuine' short bursts; in PROBING STELLAR POPULATIONS OUT TO THE DISTANT UNIVERSE: CEFALU 2008, Proceedings of the International Conference; Cefalù (Italy), September 2008, G. Giobbi, A. Tornambe, G. Raimondo, M. Limongi, L. A. Antonelli, N. Menci, E. Brocato, Editors; AIP Conference Proceedings, 1111, 325 (2009).

The Gamma-Ray Bursts (GRBs) offer the unprecedented opportunity to observe for the first time the blackholic energy extracted by the vacuum polarization during the process of gravitational collapse to a black hole leading to the formation of an electron-positron plasma. The uniqueness of the Kerr-Newman black hole implies that very different processes originating from the gravitational collapse a) of a single star in a binary system induced by the companion, or b) of two neutron stars, or c) of a neutron star and a white dwarf, do lead to the same structure for the observed GRB. The recent progress of the numerical integration of the relativistic Boltzmann equations with collision integrals including 2-body and 3-body interactions between the particles offer a powerful conceptual tool in order to differentiate the traditional "fireball" picture, an expanding hot cavity considered by Cavallo and Rees, as opposed to the "fireshell" model, composed of an internally cold shell of relativistically expanding electron-positron-baryon plasma. The analysis of the fireshell naturally leads to a canonical GRB composed of a proper-GRB and an extended afterglow. By recalling the three interpretational paradigms for GRBs we show how the fireshell model leads to an understanding of the GRB structure and to an alternative classification of short and long GRBs.

38. M.G. Bernardini, M.G. Dainotti, C.L. Bianco, L. Caito, R. Guida, R. Ruffini; "Prompt emission and X-ray flares: the case of GRB 060607 A"; in PROBING STELLAR POPULATIONS OUT TO THE DISTANT UNIVERSE: CEFALU 2008, Proceedings of the International Conference; Cefalù (Italy), September 2008, G. Giobbi, A. Tornambe, G. Raimondo, M. Limongi, L. A. Antonelli, N. Menci, E. Brocato, Editors; AIP Conference Proceedings, 1111, 383 (2009).

GRB 060607A is a very distant and energetic event. Its main peculiarity is that the peak of the near-infrared (NIR) afterglow has been observed with the REM robotic telescope, allowing to estimate the initial Lorentz gamma factor within the fireball forward shock model. We analyze GRB 060607A within the

fireshell model. The initial Lorentz gamma factor of the fireshell can be obtained adopting the exact solutions of its equations of motion, dealing only with the BAT and XRT observations, that are the basic contribution to the afterglow emission, up to a distance from the progenitor $r \sim 10^{18}$ cm. According to the “canonical GRB” scenario we interpret the whole prompt emission as the peak of the afterglow emission, and we show that the observed temporal variability of the prompt emission can be produced by the interaction of the fireshell with overdense CircumBurst Medium (CBM) clumps. This is indeed the case also of the X-ray flares which are present in the early phases of the afterglow light curve.

39. C.L. Bianco, M.G. Bernardini, L. Caito, M.G. Dainotti, R. Guida, R. Ruffini; “The ‘fireshell’ model and the ‘canonical GRB’ scenario. Implications for the Amati relation”; in PROBING STELLAR POPULATIONS OUT TO THE DISTANT UNIVERSE: CEFALU 2008, Proceedings of the International Conference; Cefalù (Italy), September 2008, G. Giobbi, A. Tornambe, G. Raimondo, M. Limongi, L. A. Antonelli, N. Menci, E. Brocato, Editors; AIP Conference Proceedings, 1111, 587 (2009).

Within the “fireshell” model for GRBs we define a “canonical GRB” light curve with two sharply different components: the Proper-GRB (P-GRB), emitted when the optically thick fireshell reaches transparency, and the extended afterglow, emitted due to the collision between the remaining optically thin fireshell and the CircumBurst Medium (CBM). We here outline our “canonical GRB” scenario, which implies three different GRB classes: the “genuine” short GRBs, the “fake” or “disguised” short GRBs and the other (so-called “long”) GRBs. We will also outline the corresponding implications for the Amati relation, which are opening its use for cosmology.

40. R. Ruffini, A.G. Aksenov, M.G. Bernardini, C.L. Bianco, L. Caito, P. Chardonnet, M.G. Dainotti, G. De Barros, R. Guida, L. Izzo, B. Patricelli, L.J. Rangel Lemos, M. Rotondo, J.A. Rueda Hernandez, G. Vereshchagin, S.-S. Xue; “The Blackholic energy and the canonical Gamma-Ray Burst IV: the ‘long’, ‘genuine short’ and ‘fake – disguised short’ GRBs”; in Proceedings of the XIIIth Brazilian School on Cosmology and Gravitation, Mangaratiba, Rio de Janeiro (Brazil), July-August 2008, M. Novello, S.E. Perez Bergliaffa, Editors; AIP Conference Proceedings, 1132, 199 (2009).

We report some recent developments in the understanding of GRBs based on

the theoretical framework of the “fireshell” model, already presented in the last three editions of the “Brazilian School of Cosmology and Gravitation”. After recalling the basic features of the “fireshell model”, we emphasize the following novel results: 1) the interpretation of the X-ray flares in GRB afterglows as due to the interaction of the optically thin fireshell with isolated clouds in the CircumBurst Medium (CBM); 2) an interpretation as “fake - disguised” short GRBs of the GRBs belonging to the class identified by Norris & Bonnell; we present two prototypes, GRB 970228 and GRB 060614; both these cases are consistent with an origin from the final coalescence of a binary system in the halo of their host galaxies with particularly low CBM density $n_{cbm} \sim 10^{-3}$ particles/cm³; 3) the first attempt to study a genuine short GRB with the analysis of GRB 050509B, that reveals indeed still an open question; 4) the interpretation of the GRB-SN association in the case of GRB 060218 via the “induced gravitational collapse” process; 5) a first attempt to understand the nature of the “Amati relation”, a phenomenological correlation between the isotropic-equivalent radiated energy of the prompt emission E_{iso} with the cosmological rest-frame νF_{ν} spectrum peak energy $E_{p,i}$. In addition, recent progress on the thermalization of the electron-positron plasma close to their formation phase, as well as the structure of the electrodynamics of Kerr-Newman Black Holes are presented. An outlook for possible explanation of high-energy phenomena in GRBs to be expected from the AGILE and the Fermi satellites are discussed. As an example of high energy process, the work by Enrico Fermi dealing with ultrarelativistic collisions is examined. It is clear that all the GRB physics points to the existence of overcritical electro-dynamical fields. In this sense we present some progresses on a unified approach to heavy nuclei and neutron stars cores, which leads to the existence of overcritical fields under the neutron star crust.

41. A.G. Aksenov, M.G. Bernardini, C.L. Bianco, L. Caito, C. Cherubini, G. De Barros, A. Gericco, L. Izzo, F.A. Massucci, B. Patricelli, M. Rotonondo, J.A. Rueda Hernandez, R. Ruffini, G. Vereshchagin, S.-S. Xue; “The fireshell model for Gamma-Ray Bursts”; in *The Shocking Universe, Proceedings of the conference held in Venice (Italy), September 2009*, G. Chincarini, P. D’Avanzo, R. Margutti, R. Salvaterra, Editors; SIF Conference Proceedings, 102, 451 (2010).

The fireshell model for GRBs is briefly outlined, and the currently ongoing developments are summarized.

42. M.G. Bernardini, C.L. Bianco, L. Caito, L. Izzo, B. Patricelli, R. Ruffini; “The end of the prompt emission within the fireshell model”; in *The Shocking Universe*, Proceedings of the conference held in Venice (Italy), September 2009, G. Chincarini, P. D’Avanzo, R. Margutti, R. Salvaterra, Editors; SIF Conference Proceedings, 102, 489 (2010)

The shallow decay emission, revealed by the Swift satellite in the X-ray afterglow of a good sample of bursts, is a puzzle. Within the fireshell model it has been recently proposed an alternative explanation: if we assume that after the prompt phase the system has a range of Lorentz factors, the plateau phase is simply the product of the injection of slower material into the fireshell. This injection produces a modification both in the dynamics of the fireshell and in the spectrum of the emitted radiation. We postulate that this spread in the fireshell Lorentz factor occurs when the fireshell becomes transparent and do not depend on a prolonged activity of the central engine. The aim of this paper is to characterize dynamically the system in order to understand the nature of that material.

43. L. Izzo, M.G. Bernardini, C.L. Bianco, L. Caito, B. Patricelli, R. Ruffini; “GRB 090423 in the fireshell scenario”; in *The Shocking Universe*, Proceedings of the conference held in Venice (Italy), September 2009, G. Chincarini, P. D’Avanzo, R. Margutti, R. Salvaterra, Editors; SIF Conference Proceedings, 102, 537 (2010).

44. B. Patricelli, M.G. Bernardini, C.L. Bianco, L. Caito, L. Izzo, R. Ruffini, G. Vereshchagin; “A new spectral energy distribution of photons in the fireshell model of GRBs”; in *The Shocking Universe*, Proceedings of the conference held in Venice (Italy), September 2009, G. Chincarini, P. D’Avanzo, R. Margutti, R. Salvaterra, Editors; SIF Conference Proceedings, 102, 559 (2010).

The fireshell model of Gamma Ray Bursts (GRBs) postulates that the emission process is thermal in the comoving frame of the fireshell, but this is just a first approximation. We investigate a different spectrum of photons in the comoving frame in order to better reproduce the observed spectral properties of GRB prompt emission. We introduce a modified thermal spectrum whose low energy slope depends on an index α , left as a free parameter. We test it by comparing the numerical simulations with observed BAT spectra integrated over different intervals of time. We find that the observational data can be correctly reproduced by assuming $\alpha = -1.8$.

45. C.L. Bianco, M.G. Bernardini, L. Caito, G. De Barros, L. Izzo, B. Patricelli, R. Ruffini; "Disguised Short Bursts and the Amati Relation"; in Deciphering the ancient universe with Gamma-Ray Bursts, Proceedings of the conference held in Kyoto (Japan), April 2010, N. Kawai, S. Nagataki, Editors; AIP Conference Proceedings, 1279, 299 (2010).

The class of "Disguised short" GRBs implied by the fireshell scenario is presented, with special emphasis on the implications for the Amati relation.

46. L. Izzo, M.G. Bernardini, C.L. Bianco, L. Caito, B. Patricelli, L.J. Rangel Lemos, R. Ruffini; "On GRB 080916C and GRB 090902B observed by the Fermi satellite"; in Deciphering the ancient universe with Gamma-Ray Bursts, Proceedings of the conference held in Kyoto (Japan), April 2010, N. Kawai, S. Nagataki, Editors; AIP Conference Proceedings, 1279, 343 (2010).

We propose a possible explanation, in the context of the Fireshell scenario, for the high-energy emission observed in GRB 080916C and GRB 090902B. The physical process underlying this emission consists mainly in the interaction of the baryon in the Fireshell with some high-density region around the burst site. Moreover we associate the observed delay of the onset of the high-energy emission as due to the P-GRB emission.

47. B. Patricelli, M.G. Bernardini, C.L. Bianco, L. Caito, G. De Barros, L. Izzo, R. Ruffini; "Black Holes in Gamma Ray Bursts"; in Deciphering the ancient universe with Gamma-Ray Bursts, Proceedings of the conference held in Kyoto (Japan), April 2010, N. Kawai, S. Nagataki, Editors; AIP Conference Proceedings, 1279, 406 (2010).

Within the fireshell model, Gamma Ray Bursts (GRBs) originate from an optically thick e^\pm plasma created by vacuum polarization process during the formation of a Black Hole (BH). Here we briefly recall the basic features of this model, then we show how it is possible to interpret GRB observational properties within it. In particular we present, as a specific example, the analysis of GRB 050904 observations of the prompt emission light curve and spectrum in the Swift BAT energy band (15-150 keV).

48. M.G. Bernardini, C.L. Bianco, L. Caito, M.G. Dainotti, R. Guida, R. Ruffini; "The GRB classification within the "fireshell" model: short, long and "fake" short GRBs"; in Proceedings of the 3rd Stueckelberg Workshop on Relativistic Field Theories, Pescara, Italy, July 2008, N. Carlevaro,

- R. Ruffini, G.V. Vereshchagin, Editors; Cambridge Scientific Publishers, (UK, 2011).
49. C.L. Bianco, M.G. Bernardini, L. Caito, M.G. Dainotti, R. Guida, R. Ruffini, G.V. Vereshchagin, S.-S. Xue; “Equations of motion of the “fireshell””; in Proceedings of the 3rd Stueckelberg Workshop on Relativistic Field Theories, Pescara, Italy, July 2008, N. Carlevaro, R. Ruffini, G.V. Vereshchagin, Editors; Cambridge Scientific Publishers, (UK, 2011).
50. L. Caito, M.G. Bernardini, C.L. Bianco, M.G. Dainotti, R. Guida, R. Ruffini; “GRB 060614: another example of “fake” short burst from a merging binary system”; in Proceedings of the 3rd Stueckelberg Workshop on Relativistic Field Theories, Pescara, Italy, July 2008, N. Carlevaro, R. Ruffini, G.V. Vereshchagin, Editors; Cambridge Scientific Publishers, (UK, 2011).
51. G. De Barros, M.G. Bernardini, C.L. Bianco, L. Caito, R. Guida, R. Ruffini; “Analysis of GRB 050509b”; in Proceedings of the 3rd Stueckelberg Workshop on Relativistic Field Theories, Pescara, Italy, July 2008, N. Carlevaro, R. Ruffini, G.V. Vereshchagin, Editors; Cambridge Scientific Publishers, (UK, 2011).
52. R. Ruffini, L. Izzo, A.V. Penacchioni, C.L. Bianco, L. Caito, S.K. Chakrabarti, A. Nandi; “GRB 090618: a possible case of multiple GRB?”; in Proceedings of the 25th Texas Symposium on Relativistic Astrophysics, held in Heidelberg (Germany), December 2010, F.M. Rieger, C. van Eldik, W. Hofmann, Editors; PoS(Texas2010), 101.
53. L.J. Rangel Lemos, C.L. Bianco, H.J. Mosquera Cuesta, J.A. Rueda, R. Ruffini; “Luminosity function of BATSE GRBs dominated by extended afterglow”; in Proceedings of the 25th Texas Symposium on Relativistic Astrophysics, held in Heidelberg (Germany), December 2010, F.M. Rieger, C. van Eldik, W. Hofmann, Editors; PoS(Texas2010), 204.
54. R. Ruffini, A.G. Aksenov, M.G. Bernardini, C.L. Bianco, L. Caito, P. Chardonnet, M.G. Dainotti, G. De Barros, R. Guida, L. Izzo, B. Patricelli, L.J. Rangel Lemos, M. Rotondo, J.A. Rueda Hernandez, G. Vereshchagin, She-Sheng Xue; “Black Holes Energetics and GRBs”; in *The Sun, the Stars, the Universe and General Relativity: Proceedings of Sobral*

- 2009; S.E. Perez Bergliaffa, M. Novello , R. Ruffini, Editors; Cambridge Scientific Publishers (UK, 2011).
55. C.L. Bianco, L. Amati, M.G. Bernardini, L. Caito, G. De Barros, L. Izzo, B. Patricelli, R. Ruffini; "The class of 'disguised' short GRBs and its implications for the Amati relation"; in GRBs as probes - from the progenitors environment to the high redshift Universe, Proceedings of the conference held in Como (Italy), May 2011, S. Campana, P. D'Avanzo, A. Melandri, Editors; Mem. S.A.It. Suppl., 21, 139 (2012).
56. A.V. Penacchioni, R. Ruffini, L. Izzo, M. Muccino, C.L. Bianco, L. Caito, B. Patricelli; "Evidences for a double component in the emission of GRB 101023"; in GRBs as probes - from the progenitors environment to the high redshift Universe, Proceedings of the conference held in Como (Italy), May 2011, S. Campana, P. D'Avanzo, A. Melandri, Editors; Mem. S.A.It. Suppl., 21, 230 (2012).
57. M.G. Bernardini, C.L. Bianco, L. Caito, L. Izzo, B. Patricelli, R. Ruffini; "The X-Ray Flares of GRB 060607A within the Fireshell Model"; in Proceedings of the Twelfth Marcel Grossmann Meeting on General Relativity, Paris, France, July 2009, T. Damour, R.T. Jantzen, R. Ruffini, Editors; World Scientific, (Singapore, 2012).
58. L. Izzo, M.G. Bernardini, C.L. Bianco, L. Caito, B. Patricelli, R. Ruffini; "GRB 090423 in the Fireshell Scenario: A Canonical GRB at Redshift 8.2"; in Proceedings of the Twelfth Marcel Grossmann Meeting on General Relativity, Paris, France, July 2009, T. Damour, R.T. Jantzen, R. Ruffini, Editors; World Scientific, (Singapore, 2012).
59. B. Patricelli, M.G. Bernardini, C.L. Bianco, L. Caito, L. Izzo, R. Ruffini, G.V. Vereshchagin; "A New Spectral Energy Distribution of Photons in the Fireshell Model of GRBs"; in Proceedings of the Twelfth Marcel Grossmann Meeting on General Relativity, Paris, France, July 2009, T. Damour, R.T. Jantzen, R. Ruffini, Editors; World Scientific, (Singapore, 2012).
60. C.L. Bianco, M.G. Bernardini, L. Caito, G. De Barros, L. Izzo, M. Muccino, B. Patricelli, A.V. Penacchioni, G.B. Pisani, R. Ruffini; "Needs for a new GRB classification following the fireshell model: "genuine short", "disguised short" and "long" GRBs"; in Proceedings of the Gamma-Ray

Bursts 2012 Conference, held in Munich (Germany), May 2012, A. Rau, J. Greiner, Editors; PoS(GRB 2012), 043.

61. A.V. Penacchioni, G.B. Pisani, R. Ruffini, C.L. Bianco, L. Izzo, M. Muccino; “The proto-black hole concept in GRB 101023 and its possible extension to GRB 110709B”; in Proceedings of the Gamma-Ray Bursts 2012 Conference, held in Munich (Germany), May 2012, A. Rau, J. Greiner, Editors; PoS(GRB 2012), 042.
62. B. Patricelli, M.G. Bernardini, C.L. Bianco, L. Caito, L. Izzo, R. Ruffini; “GRB 050904: The study of a high redshift GRB within the Fireshell Model”; in Proceedings of the Twelfth Marcel Grossmann Meeting on General Relativity, Paris, France, July 2009, T. Damour, R.T. Jantzen, R. Ruffini, Editors; World Scientific, (Singapore, 2012).
63. L. Izzo, G.B. Pisani, M. Muccino, J.A. Rueda, Y.Wang, C.L. Bianco, A.V. Penacchioni, R. Ruffini; “A common behavior in the late X-ray afterglow of energetic GRB-SN systems”; EAS Publications Series, Volume 61, 595-597 (2013).
64. R. Ruffini; “Black Holes, Supernovae and Gamma Ray Bursts”; in Proceedings of the Thirteenth Marcel Grossmann Meeting on General Relativity, Stockholm, Sweden, July 2012, R.T. Jantzen, K. Rosquist, R. Ruffini, Editors; World Scientific, (Singapore, 2015).
65. M. Muccino, R. Ruffini, C.L. Bianco, L. Izzo, A.V. Penacchioni, G.B. Pisani; “GRB 090227B: The missing link between the genuine short and long GRBs”; in Proceedings of the Thirteenth Marcel Grossmann Meeting on General Relativity, Stockholm, Sweden, July 2012, R.T. Jantzen, K. Rosquist, R. Ruffini, Editors; World Scientific, (Singapore, 2015).
66. A.V. Penacchioni, R. Ruffini, C.L. Bianco, L. Izzo, M. Muccino, G.B. Pisani, J.A. Rueda; “The family of the Induced Gravitational Collapse scenario: The case of GRB 110709B”; in Proceedings of the Thirteenth Marcel Grossmann Meeting on General Relativity, Stockholm, Sweden, July 2012, R.T. Jantzen, K. Rosquist, R. Ruffini, Editors; World Scientific, (Singapore, 2015).
67. A.V. Penacchioni, R. Ruffini, C.L. Bianco, L. Izzo, M. Muccino, G.B. Pisani; “GRB 111228, analysis within the Induced Gravitational Collapse scenario and association with a supernova”; in Proceedings of

- the Thirteenth Marcel Grossmann Meeting on General Relativity, Stockholm, Sweden, July 2012, R.T. Jantzen, K. Rosquist, R. Ruffini, Editors; World Scientific, (Singapore, 2015).
68. G.B. Pisani, L. Izzo, R. Ruffini, C.L. Bianco, M. Muccino, A.V. Penacchioni, J.A. Rueda, Y. Wang; "On a novel distance indicator for Gamma-Ray Bursts associated with supernovae"; in Proceedings of the Thirteenth Marcel Grossmann Meeting on General Relativity, Stockholm, Sweden, July 2012, R.T. Jantzen, K. Rosquist, R. Ruffini, Editors; World Scientific, (Singapore, 2015).
69. M. Muccino, R. Ruffini, C.L. Bianco, L. Izzo, A.V. Penacchioni, G.B. Pisani; "GRB 090510, explosion of a GRB in the highest circumburst medium even inferred: a disguised short GRB"; in Proceedings of the Thirteenth Marcel Grossmann Meeting on General Relativity, Stockholm, Sweden, July 2012, R.T. Jantzen, K. Rosquist, R. Ruffini, Editors; World Scientific, (Singapore, 2015).
70. L. Izzo, G.B. Pisani, M. Muccino, R. Ruffini, C.L. Bianco, M. Enderli, Y. Wang; "Hints for a physically based GRB distance indicator"; in Proceedings of the Thirteenth Marcel Grossmann Meeting on General Relativity, Stockholm, Sweden, July 2012, R.T. Jantzen, K. Rosquist, R. Ruffini, Editors; World Scientific, (Singapore, 2015).
71. R. Ruffini, Y. Aimuratov, V. Belinski, C.L. Bianco, M. Enderli, L. Izzo, M. Kovacevic, G.J. Mathews, R. Moradi, M. Muccino, A.V. Penacchioni, G.B. Pisani, J.A. Rueda, G.V. Vereshchagin, Y. Wang, S.-S. Xue; Cosmic matrix in the jubilee of relativistic astrophysics; in THE SECOND ICRANET CÉSAR LATTES MEETING: Supernovae, Neutron Stars and Black Holes, Proceedings of the conference held in Rio de Janeiro – Niterói – João Pessoa – Recife – Fortaleza (Brazil), 13-22 April 2015, U. Barres de Almeida, P. Chardonnet, R. Picanco Negreiros, J. Rueda, R. Ruffini, G. Vereshchagin, C. Zen Vasconcellos, Editors; AIP Conference Proceedings, 1693, 020001 (2015).
72. L. Becerra, C.L. Bianco, F. Cipolletta, M. Enderli, C.L. Fryer, L. Izzo, M. Kovacevic, R. Camargo Rodrigues de Lima, M. Muccino, F.G. de Oliveira, A.V. Penacchioni, G.B. Pisani, J.A. Rueda, R. Ruffini, Y. Wang, E. Zaninoni; Black holes, neutron stars and supernovae within the induced gravitational collapse paradigm for GRBs; in THE SECOND ICRANET

- CÉSAR LATTES MEETING: Supernovae, Neutron Stars and Black Holes, Proceedings of the conference held in Rio de Janeiro – Niterói – João Pessoa – Recife – Fortaleza (Brazil), 13-22 April 2015, U. Barres de Almeida, P. Chardonnet, R. Picanco Negreiros, J. Rueda, R. Ruffini, G. Vereshchagin, C. Zen Vasconcellos, Editors; AIP Conference Proceedings, 1693, 020002 (2015).
73. L.J. Rangel Lemos, C.L. Bianco, R. Ruffini; Applying the luminosity function statistics in the fireshell model; in THE SECOND ICRANET CÉSAR LATTES MEETING: Supernovae, Neutron Stars and Black Holes, Proceedings of the conference held in Rio de Janeiro – Niterói – João Pessoa – Recife – Fortaleza (Brazil), 13-22 April 2015, U. Barres de Almeida, P. Chardonnet, R. Picanco Negreiros, J. Rueda, R. Ruffini, G. Vereshchagin, C. Zen Vasconcellos, Editors; AIP Conference Proceedings, 1693, 070004 (2015).
74. J.A. Rueda, R. Ruffini, J.F. Rodriguez, M. Muccino, Y. Aimuratov, U. Barres de Almeida, L.M. Becerra, C.L. Bianco, C. Cherubini, S. Filippi, M. Kovacevic, R. Moradi, G.B. Pisani, Y. Wang; The binary progenitors of short and long GRBs and their gravitational-wave emission; EPJ Web of Conferences, 168, 01006 (2018).
75. M. Muccino, R. Ruffini, Y. Aimuratov, L.M. Becerra, C.L. Bianco, M. Karlika, M. Kovacevic, J.D. Melon Fuksman, R. Moradi, A.V. Penacchioni, G.B. Pisani, D. Primorac, J.A. Rueda, S. Shakeri, G.V. Vereshchagin, S.-S. Xue, Y. Wang; What can we learn from GRBs?; EPJ Web of Conferences, 168, 01015 (2018).
76. L.M. Becerra, C.L. Bianco, C. Fryer, J.A. Rueda, R. Ruffini; On the Induced Gravitational Collapse; EPJ Web of Conferences, 168, 02005 (2018).
77. G.B. Pisani, R. Ruffini, Y. Aimuratov, C.L. Bianco, M. Karlika, M. Kovacevic, R. Moradi, M. Muccino, A.V. Penacchioni, D. Primorac, J.A. Rueda, Y. Wang; The first ICRANet catalog of Binary-Driven Hypernovae; EPJ Web of Conferences, 168, 04002 (2018).
78. D. Primorac, R. Ruffini, G.B. Pisani, Y. Aimuratov, C.L. Bianco, M. Karlika, J.D. Melon Fuksman, R. Moradi, M. Muccino, A.V. Penacchioni, J.A. Rueda, Y. Wang; GRB 110731A within the IGC paradigm; EPJ Web of Conferences, 168, 04008 (2018).

79. J.D. Melon Fuksman, L.M. Becerra, C.L. Bianco, M. Karlika, M. Kovacevic, R. Moradi, M. Muccino, G.B. Pisani, D. Primorac, J.A. Rueda, R. Ruffini, G.V. Vereshchagin, Y. Wang; Evolution of an electron-positron plasma produced by induced gravitational collapse in binary-driven hypernovae; EPJ Web of Conferences, 168, 04009 (2018).



Two Predictions of Supernova: GRB 130427A/SN 2013cq and GRB 180728A/SN 2018fip

Y. Wang^{1,2} , J. A. Rueda^{1,2,3}, R. Ruffini^{1,2,3,4}, L. Becerra⁵, C. Bianco^{1,2} , L. Becerra⁵, L. Li², and M. Karlica^{1,2,4}

¹ ICRA and Dipartimento di Fisica, Sapienza Università di Roma, P.le Aldo Moro 5, I-00185 Rome, Italy; ruffini@icra.it

² ICRA/Net, P.zza della Repubblica 10, I-65122 Pescara, Italy

³ ICRA/Net-Rio, Centro Brasileiro de Pesquisas Físicas, Rua Dr. Xavier Sigaud 150, 22290-180 Rio de Janeiro, Brazil

⁴ Université de Nice Sophia Antipolis, CEDEX 2, Grand Château Parc Valrose, Nice, France

⁵ Escuela de Física, Universidad Industrial de Santander, A.A.678, Bucaramanga, 680002, Colombia

Received 2018 November 13; revised 2019 February 1; accepted 2019 February 5; published 2019 March 19

Abstract

On 2018 July 28, GRB 180728A triggered *Swift* satellites and, soon after the determination of the redshift, we identified this source as a type II binary-driven hypernova (BdHN II) in our model. Consequently, we predicted the appearance time of its associated supernova (SN), which was later confirmed as SN 2018fip. A BdHN II originates in a binary composed of a carbon–oxygen core (CO_{core}) undergoing SN, and the SN ejecta hypercritically accrete onto a companion neutron star (NS). From the time of the SN shock breakout to the time when the hypercritical accretion starts, we infer the binary separation $\simeq 3 \times 10^{10}$ cm. The accretion explains the prompt emission of isotropic energy $\simeq 3 \times 10^{51}$ erg, lasting ~ 10 s, and the accompanying observed blackbody emission from a thermal convective instability bubble. The new neutron star (νNS) originating from the SN powers the late afterglow from which a νNS initial spin of 2.5 ms is inferred. We compare GRB 180728A with GRB 130427A, a type I binary-driven hypernova (BdHN I) with isotropic energy $> 10^{54}$ erg. For GRB 130427A we have inferred an initially closer binary separation of $\simeq 10^{10}$ cm, implying a higher accretion rate leading to the collapse of the NS companion with consequent black hole formation, and a faster, 1 ms spinning νNS . In both cases, the optical spectra of the SNe are similar, and not correlated to the energy of the gamma-ray burst. We present three-dimensional smoothed-particle-hydrodynamic simulations and visualizations of the BdHN I and II.

Key words: binaries: general – black hole physics – gamma-ray burst: general – hydrodynamics – stars: neutron – supernovae: general

1. Introduction

By the first minutes of data retrieved from *Konus-Wind*, *Swift*, *Fermi*, *AGILE* or other gamma-ray telescopes (Aptekar et al. 1995; Barthelmy et al. 2005; Atwood et al. 2009; Tavani et al. 2009), and the determination of redshift by VLT/X-shooter, Gemini, NOT, or other optical telescopes (Vernin & Munoz-Tunon 1992; Hook et al. 2004; Vernet et al. 2011), it is possible to promptly and uniquely identify to which of the nine (9) subclasses of gamma-ray bursts (GRBs) a source belongs (see Table 1 and the references therein). Consequently, it is possible to predict its further evolution, including the possible appearance time of an associated supernova (SN) expected in some of the GRB subclasses. This is what we have done in the case of GRB 130427A (Ruffini et al. 2015, 2018d), and in the present case of GRB 180728A.

GRB 130427A is a BdHN I in our model; see details in Section 2 and in Fryer et al. (2014, 2015) and Becerra et al. (2015, 2016, 2018). The progenitor is a tight binary system, of orbital period ~ 5 minutes, composed of a carbon–oxygen core (CO_{core}), undergoing an SN event, and a neutron star (NS) companion accreting the SN ejecta and finally collapsing to a black hole (BH). The involvement of an SN in BdHN I and the low redshift of $z = 0.34$ (Flores et al. 2013; Levan et al. 2013; Xu et al. 2013b) enable us to predict that the optical signal of the SN will peak and be observed ~ 2 weeks after the GRB occurrence at the same position of the GRB (Ruffini et al. 2013). Indeed the SN was observed (de Ugarte Postigo et al. 2013; Xu et al. 2013a). Details of GRB 130427A are given in Section 3.

The current GRB 180728A is a BdHN II in our model; it has the same progenitor as BdHN I, a binary composed of a CO_{core}

and an NS companion, but with longer orbital period ($\gtrsim 10$ minutes), which is here determined for the first time. The CO_{core} undergoes SN explosion, the SN ejecta hypercritically accrete onto the companion NS. In view of the longer separation, the accretion rate is lower, it is not sufficient for the companion NS to reach the critical mass of BH. Since an SN is also involved in BdHN II and this source is located at low redshift $z = 0.117$ (Rossi 2018), its successful prediction and observation were also possible and it is summarized in Section 4. From a time-resolved analysis of the data in Section 5, we trace the physical evolution of the binary system. For the first time we observed a 2 s signal evidencing the SN shockwave, namely the emergence of the SN shockwave from the outermost layers of the CO_{core} (see, e.g., Arnett 1996). The SN ejecta expand and, after 10 s, reach the companion NS inducing onto it a high accretion rate of about $10^{-3} M_{\odot} \text{ s}^{-1}$. Such a process lasts about 10 s producing the prompt phenomena and an accompanying thermal component. The entire physical picture is described in Section 6, giving special attention to the new neutron star (νNS) originating from the SN. We explicitly show that the fast spinning νNS powers the afterglow emission by converting its rotational energy to synchrotron emission (see also Ruffini et al. 2018d), which has been never well considered in previous GRB models. We compare the initial properties of the νNS in GRB 130427A and in GRB 180728A, and derive that a 1 ms νNS is formed in GRB 130427A, while a 2.5 ms νNS is formed in GRB 180728A. In Section 7 we relate the very different energetic of the prompt emission to the orbital separation of the progenitors, which in turn determines the spin of the νNS , and the rest-frame luminosity afterglows. We simulate the accretion of

Table 1
Summary of the GRB Subclasses

Class	Type	Previous Alias	Number	In-state	Out-state	$E_{p,i}$ (MeV)	E_{iso} (erg)	$E_{iso,GeV}$ (erg)
Binary Driven	I	BdHN	329	CO _{core} -NS	ν NS-BH	$\sim 0.2-2$	$\sim 10^{52}-10^{54}$	$\gtrsim 10^{52}$
Hypernova	II	XRF	(30)	CO _{core} -NS	ν NS-NS	$\sim 0.01-0.2$	$\sim 10^{50}-10^{52}$...
(BdHN)	III	HN	(19)	CO _{core} -NS	ν NS-NS	~ 0.01	$\sim 10^{48}-10^{50}$...
	IV	BH-SN	5	CO _{core} -BH	ν NS-BH	$\gtrsim 2$	$> 10^{54}$	$\gtrsim 10^{53}$
Binary	I	S-GRF	18	NS-NS	MNS	$\sim 0.2-2$	$\sim 10^{49}-10^{52}$...
Merger	II	S-GRB	6	NS-NS	BH	$\sim 2-8$	$\sim 10^{52}-10^{53}$	$\gtrsim 10^{52}$
(BM)	III	GRF	(1)	NS-WD	MNS	$\sim 0.2-2$	$\sim 10^{49}-10^{52}$...
	IV	FB-KN ^a	(1)	WD-WD	NS/MWD	< 0.2	$< 10^{51}$...
	V	U-GRB	(0)	NS-BH	BH	$\gtrsim 2$	$> 10^{52}$...

Notes. This table is an updated version of the one presented in Ruffini et al. (2016, 2018e). We unify here all the GRB subclasses under two general names, BdHNe and BMs. Two new GRB subclasses are introduced; BdHN Type III and BM Type IV. In addition to the subclass name in the ‘‘Class’’ column and the ‘‘Type’’ column, as well as the previous names in the ‘‘Previous Alias’’ column, we report the number of GRBs with known redshift identified in each subclass updated by the end of 2016 in the ‘‘number’’ column (the value in brackets indicates the lower limit). We recall as well the ‘‘in-state’’ representing the progenitors and the ‘‘out-state’’ representing the outcomes, as well as the peak energy of the prompt emission, $E_{p,i}$, the isotropic gamma-ray energy, E_{iso} defined in the 1 keV–10 MeV energy range, and the isotropic emission of ultra-high-energy photons, $E_{iso,GeV}$, defined in the 0.1–100 GeV energy range. We can see from this last column that this GeV emission, for the long GRBs is only for the BdHN Type I and Type IV, and in the case of short bursts is only for BM Type II and, in all of them, the GeV emission has energy more than 10^{52} erg.

^a We here adopt a broad definition of kilonova as its name, a phenomenon that is 1000 times more luminous than a nova. A kilonova can be an infrared-optical counterpart of an NS–NS merger. In that case the transient is powered by the energy release from the decay of r -process heavy nuclei processed in the merger ejecta (e.g., Li & Paczyński 1998; Metzger et al. 2010; Berger et al. 2013; Tanvir et al. 2013). FB-KN stands for fallback-powered kilonova. We have shown that a WD–WD merger produces an infrared-optical transient from the merger ejecta, a kilonova, peaking at ~ 5 days post-merger but powered in this case by accretion of fallback matter onto the merged remnant (Rueda et al. 2018a, 2018b).

the SN matter onto the NS companion in the tight binaries via three-dimensional (3D) smoothed-particle-hydrodynamic (SPH) simulations (Becerra et al. 2019) that also provide a visualization of the BdHNe. The conclusions are given in Section 8.

2. Binary-driven Hypernova

Since the *Beppo-SAX* discovery of the spatial and temporal coincidence of a GRB and an SN (Galama et al. 1999), largely supported by many additional following events (Woosley & Bloom 2006; Cano et al. 2017), a theoretical paradigm has been advanced for long GRBs based on a binary system (Rueda & Ruffini 2012). This differs from the traditional theoretical interpretation of GRB, which implicitly assumes that all GRBs originate from a BH with an ultrarelativistic jet emission (see, e.g., Piran 1999, 2004; Mészáros 2002, 2006; Berger 2014; Kumar & Zhang 2015).

Specifically, the binary system is composed of a CO_{core} and an NS companion in tight orbit. Following the onset of the SN, a hypercritical accretion process of the SN ejecta onto the NS occurs, which markedly depends on the binary period of the progenitor (Fryer et al. 2014, 2015; Becerra et al. 2015, 2016). For short binary periods of the order of 5 minutes the NS reaches the critical mass for gravitational collapse and forms a BH (see, e.g., Ruffini et al. 2014b, 2018b, 2018f). For longer binary periods, the hypercritical accretion onto the NS is not sufficient to bring it to the critical mass and a more massive NS (MNS) is formed. These sources have been called BdHNe because the feedback of the GRB transforms the SN into a hypernova (HN; Ruffini et al. 2018b). The former scenario of short orbital period is classified as BdHN type I (BdHN I), which leads to a binary system composed by the BH, generated by the collapse of the NS companion, and the ν NS generated by the SN event. The latter scenario of longer orbital period is classified as BdHN type II (BdHN II), which leads to a binary NS system composed of the MNS and the ν NS.

Having developed the theoretical treatment of such a hypercritical process, and considering as well other binary systems with progenitors composed alternatively of CO_{core} and BH, to NS and white dwarf (WD), a general classification of GRBs has been developed; see Ruffini et al. (2016) and Table 1 for details. We report in the table estimates of the energetic, spectrum, and different component of the prompt radiation, of the plateau, and all the intermediate phases, all the way to the final afterglow phase. The GRBs are divided into two main classes, the BdHNe, which cover the traditional long duration GRBs (Woosley 1993; Paczyński 1998), and the binary mergers, which are short-duration GRBs (Goodman 1986; Paczyński 1986; Eichler et al. 1989). There are currently nine subclasses in our model, the classification depends on the different compositions of the binary progenitors and outcomes, which are CO_{core} and compact objects as BH, NS, and WD. The same progenitors can possibly produce different outcomes, due to the different masses and binary separations.

3. GRB 130427A as BdHN I

GRB 130427A, as a BdHN I in our model, has been studied in our previous articles (Ruffini et al. 2015, 2018d). This long GRB is nearby ($z = 0.314$) and energetic ($E_{iso} \sim 10^{54}$ erg; Flores et al. 2013; Levan et al. 2013; Xu et al. 2013b; Maselli et al. 2014). It has overall the most comprehensive data to date, including the well observed γ -ray prompt emission (Golenetskii 2013; von Kienlin 2013), the full coverage of X-ray, optical, and radio afterglow (Kouveliotou et al. 2013; Anderson et al. 2014; Levan et al. 2014; Perley et al. 2014; van der Horst et al. 2014; Vestrand et al. 2014; Becerra et al. 2017), and the long observation of the ultra-high-energy emission (UHE; Tam et al. 2013; Ackermann et al. 2014; Abeysekara et al. 2015). Also it has been theoretically well-studied, involving many interpretations, including a BH or a magnetar as the central engine (Bernardini et al. 2014); unaccountable temporal spectral

Table 2
Parameters of the Blackbody Evolution in Two Time Intervals

Time (s)	Total Flux (erg s ⁻¹ cm ⁻²)	Thermal Flux (erg s ⁻¹ cm ⁻²)	Percentage	Temperature (keV)
8.72–10.80	$5.6_{-0.9}^{+1.1} \times 10^{-6}$	$4.1_{-1.9}^{+3.2} \times 10^{-7}$	7.3 $_{-3.7}^{+5.8}\%$	7.9 $_{-0.7}^{+0.7}$
10.80–12.30	$2.0_{-0.1}^{+0.1} \times 10^{-5}$	$7.1_{-3.3}^{+6.0} \times 10^{-7}$	3.6 $_{-1.6}^{+3.3}\%$	5.6 $_{-0.5}^{+0.5}$

Note. Parameters include the total flux, the thermal flux, the percentage of thermal flux, and the temperature. One example of data fitting by Monte-Carlo iteration is shown in Appendix B. The time bin of 12.30–22.54 s does not show a convincing thermal component from the model comparison, still we report the fitting value, as a reference, from the cutoff power law plus blackbody model, that the temperature is found as $2.1_{-0.9}^{+0.5}$ keV, the thermal flux is $1.2_{-1.1}^{+9.0} \times 10^{-8}$ erg s⁻¹ cm⁻², and the total flux is $3.1_{-0.2}^{+0.22} \times 10^{-6}$ erg s⁻¹ cm⁻².

behaviors of the first 2.5 s pulse by the traditional models (Preece et al. 2014); the reverse-forward shock synchrotron model and its challenges in explaining the afterglow (Laskar et al. 2013; De Pasquale et al. 2016, 2017; Fraija et al. 2016); the synchrotron or the inverse Compton origins for the ultra-high-energy photons (Fan et al. 2013; Liu et al. 2013; Panaitescu et al. 2013; Tam 2014; Vurm et al. 2014); and the missing of the neutrino detection and its interpretation (Gao et al. 2013; Joshi et al. 2016). Our interpretation is alternative to the above traditional approach: (1) Long GRBs are traditionally described as single systems while we assume a very specific binary systems as their progenitors. (2) The roles of the SN and of the ν NS are there neglected, while they are essential in our approach as evidenced also in this article. (3) A central role in the energetics is traditionally attributed to the kinetic energy of ultrarelativistic blast waves extending from the prompt phase all the way to the late phase of the afterglow, in contrast to model-independent constraints observed in the mildly relativistic plateau and afterglow phases (Ruffini et al. 2015, 2018c, 2018d). In our approach the physics of the e^+e^- plasma and its interaction with the SN ejecta as well as the pulsar-like behavior of the ν NS are central to the description from the prompt radiation to the late afterglow phases (Ruffini et al. 2018f). One of the crucial aspects in our approach is the structure of the SN ejecta which, under the action of the hypercritical accretion process onto the NS companion and the binary interaction, becomes highly asymmetric. Such a new morphology of the SN ejecta has been made possible to visualized thanks to a set of three-dimensional numerical simulations of BdHNe (Fryer et al. 2014; Becerra et al. 2016, 2019).

On this ground, soon after the observational determination of the redshift (Levan et al. 2013), by examining the detailed observations in the early days, we identified the BdHN origin of this source. On 2013 May 2, we made the prediction of the occurrence of SN 2013cq on GCN (Ruffini et al. 2013, quoted in Appendix A), which was duly observed in the optical band on 2013 May 13 (de Ugarte Postigo et al. 2013; Xu et al. 2013a).

To summarize our work on this GRB: in Ruffini et al. (2015) we presented the multiwavelength light-curve evolution and interpreted them by a tight binary system with orbital separation $\sim 10^{10}$ cm. GRB 130427A has a very bright prompt γ -ray spike in the first 10 s, then it decays, coinciding with the rising of the UHE (100 MeV–100 GeV) emission. The UHE peaks at ~ 20 s, then gradually dims for some thousand seconds. Soft X-ray observations start from 195 s, and a steep decay then follows a normal power-law decay $\sim t^{-1.3}$. We evidenced the presence of a blackbody component in the soft

X-ray data in the time-interval from 196 to 461 s; within which the temperature decreases from 0.5 to 0.1 keV. The thermal component indicates an emitter expanding from $\sim 10^{12}$ to $\sim 10^{13}$ cm with velocity $\sim 0.8c$. This mildly relativistic expansion from our model-independent inference contrasts with the traditional ultrarelativistic external shockwave interpretation (see, e.g., Sari et al. 1998). We attributed this thermal emission to the transparency of the SN ejecta outermost layer after being heated and accelerated by the energetic e^+e^- plasma outflow of the GRB. The numerical simulations of this hydrodynamics process were presented in Ruffini et al. (2018f). As is shown there, the resulting distance, velocity, and occurring time of this emission are all in agreement with the observations. Later in Ruffini et al. (2018d), we showed that the mildly relativistic ejecta can also account for the nonthermal component, in the early thousands of seconds powered by its kinetic energy, and afterward powered by the release of rotational energy of the millisecond-period ν NS via a pulsar-like mechanism. The synchrotron emission well reproduces the observed optical and X-ray afterglow. A similar application of the ν NS on GRB 180728A will be presented in Section 6.2, as well as the comparison to GRB 130427A.

4. Observation and Prediction

On 2018 July 28, we had the opportunity to make a prediction of the SN appearance in a BdHN II.

At 17:29:00 UT, On 2018 July 28, GRB 180728A triggered the *Swift*-BAT. The BAT light curve shows a small precursor and ~ 10 s later it was followed by a bright pulse of ~ 20 s duration (Starling 2018). *Swift*-XRT did not slew to the position immediately due to the Earth limb; it began observing 1730.8 s after the BAT trigger (Perri 2018). The *Fermi*-GBM triggered and located GRB 180728A at 17:29:02.28 UT. The initial *Fermi*-LAT bore-sight angle at the GBM trigger time is 35° , within the threshold of detecting GeV photons, but no GeV photon was found. The GBM light curve is similar to that of *Swift*-BAT, consisting of a precursor and a bright pulse, the duration (T_{90}) is about 6.4 s (50–300 keV; Veres 2018). A red continuum was detected by VLT/X-shooter and the absorption features of Mg II (3124, 3132), Mg I (3187), and Ca II (4395, 4434) were consistent with a redshift of $z = 0.117$ (Rossi 2018).

After the detection of the redshift, On 2018 July 31, we classify this GRB as an BdHN II in our model, based on its duration, peak energy, isotropic energy, and the existence of photons with energy > 100 MeV, criteria in Table 1. BdHN II involves the Type Ib/c SN phenomenon; therefore, we

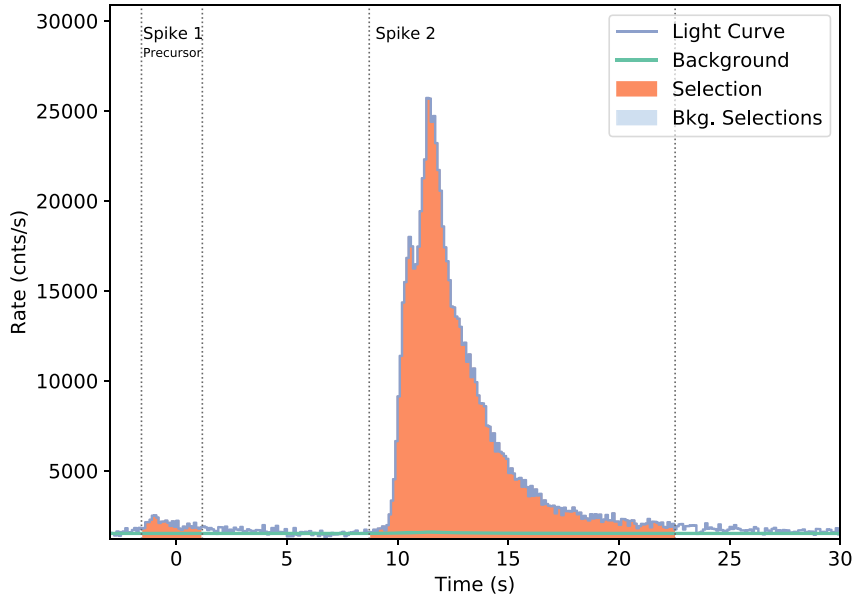


Figure 1. Count rate light curve of the prompt emission: data are retrieved from the NaI7 detector onboard *Fermi*-GBM. The prompt emission of GRB 180728A contains two spikes. The first spike, the precursor, ranges from -1.57 to 1.18 s. The second spike, which contains the majority of energy, rises at 8.72 s, peaks at 11.50 s, and fades at 22.54 s.

predicted that an SN would appear at 14.7 ± 2.9 days (Ruffini 2018) and be observed due to its low redshift. On 2018 August 18, Izzo (2018) on behalf of the VLT/X-shooter team reported the discovery of the SN appearance, which was confirmed in Selsing (2018). The texts of these GCNs are reported in the Appendix A. The SN associated with GRB 180728A was named SN 2018fip. Our prediction was confirmed.

We also predicted the SN appearance in GRB 140206A (Ruffini et al. 2014a) and GRB 180720A (Ruffini et al. 2018a), but unfortunately the optical observation does not cover the expected time (~ 13 days after the GRB trigger time) of the SN appearance.

5. Data Analysis

GRB 180728A contains two spikes in the prompt emission observed by *Swift*-BAT, *Fermi*-GBM, and *Konus-Wind* (Rossi 2018; Starling 2018; Veres 2018). In the following we defined our t_0 based on the trigger time of *Fermi*-GBM. The first spike, we name it as precursor, ranges from -1.57 to 1.18 s. And the second spike, which contains the majority of energy, rises at 8.72 s, peaks at 11.50 s, and fades at 22.54 s, see Figure 1. These time definitions are based on the count rate light curve observed by *Fermi*-GBM, and determined by applying the Bayesian block method (Scargle 1998). *Swift*-XRT started to observe 1730.8 s after the BAT trigger, the luminosity of the X-ray afterglow follows a shallow decay with a power-law index -0.56 until ~ 5000 s, then a normal decay with a power-law index -1.2 , which is a typical value (Li et al. 2015, 2018a).

5.1. Prompt Emission: Two Spikes

The first spike, the precursor, shows a power-law spectrum with a power-law index -2.31 ± 0.08 in its 2.75 s duration, shown in Figure 2 and in the Appendix C. The averaged luminosity is $3.24_{-0.55}^{+0.78} \times 10^{49}$ erg s^{-1} , and the integrated

energy gives $7.98_{-1.34}^{+1.92} \times 10^{49}$ erg in the energy range from 1 keV to 10 MeV, the Friedmann–Lemaître–Robertson–Walker metric with the cosmological parameters from the *Planck* mission (Planck Collaboration et al. 2018)⁶ are applied on computing the cosmological distance throughout the whole paper.

The second spike rises 10.29 s after the starting time of the first spike (8.72 s since the trigger time), lasts 13.82 s, and emits $2.73_{-0.10}^{+0.11} \times 10^{51}$ erg in the 1 keV– 10 MeV energy band, i.e., 84 times more energetic than the first spike. The best fit of the spectrum is a Band function or a cutoff power law, with an additional blackbody; see Table 3 in Appendix C for the model comparison of the time-resolved analysis and Figure 2 for the spectrum. We notice that the thermal component confidently exists in the second spike when the emission is luminous while, at times later than 12.30 s, the confidence of the thermal component drops and a single cutoff power law is enough to fit the spectrum. There could be many reasons for the missing thermal component at later times; for instance, the thermal component becomes less prominent and is covered by the nonthermal emission, or the thermal temperature cools to a value outside of the satellite energy band, or the thermal emission really disappears. In the present case the thermal blackbody component of temperature ~ 7 keV contributes $\sim 5\%$ to the total energy.

From the evolution of the thermal spectrum and the parameters presented in Table 2, it is possible to determine the velocity and the radius of the system in a model-independent way. Following Ruffini et al. (2018f), we obtain that the radius in each of the two time intervals is $1.4_{-0.4}^{+0.6} \times 10^{10}$ cm and $4.3_{-0.6}^{+0.9} \times 10^{10}$ cm, respectively, and the expanding velocity is $0.53_{-0.15}^{+0.18} c$.

⁶ Hubble constant $H_0 = (67.4 \pm 0.5)$ km s^{-1} Mpc $^{-1}$, matter density parameter $\Omega_M = 0.315 \pm 0.007$.

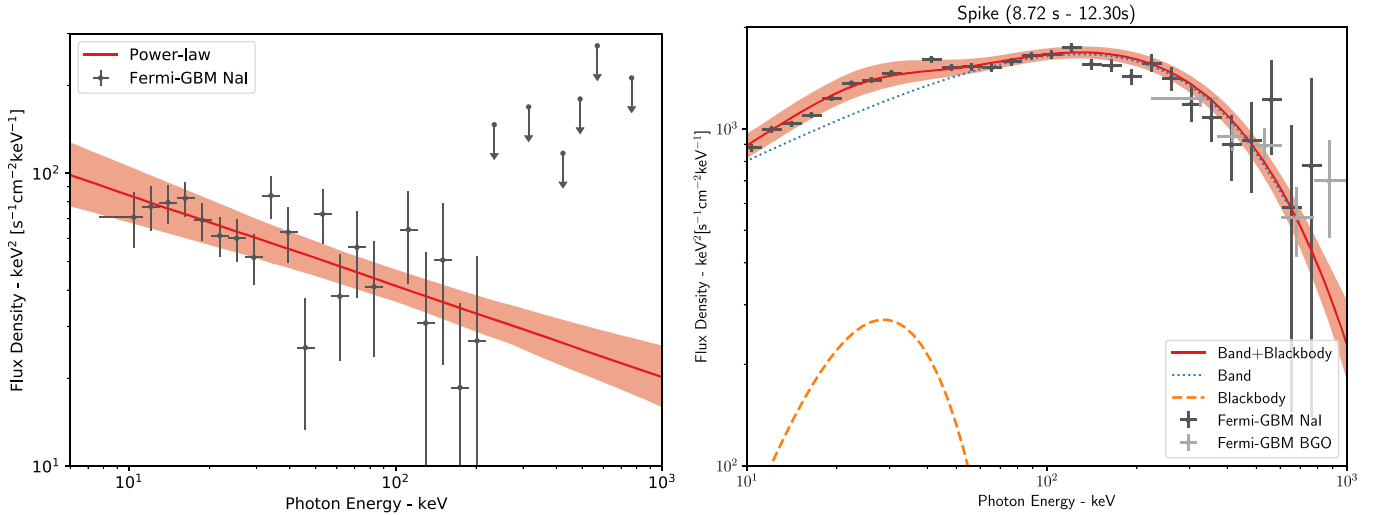


Figure 2. Left: spectrum of the precursor as observed by *Fermi*-GBM in the energy range of 8–900 keV. The red line indicates the power-law fitting with power-law index -2.31 , the red shadow is the 1σ region. Right: spectrum of the main prompt emission, from 8.72 to 12.30 s. The dotted curve represents a band function with low-energy index $\alpha = -1.55$ and high-energy index $\beta = -3.48$; the peak energy is $E_p = 129$ keV. The additional blackbody component is represented by the orange dashed curve, with temperature $kT = 7.3$ keV. The composite fit with 1σ confidence area is represented by the red line and red shadow.

5.2. Supernova

The optical signal of SN 2018fp associated with GRB 180728A was confirmed by the observations of the VLT telescope (Izzo 2018; Selsing 2018). The SN 2018fp is identified as a Type Ic SN, its spectrum at ~ 8 days after the peak of the optical light-curve matches with the Type Ic SN 2002ap (Mazzali et al. 2002), reported in Selsing et al. (2018). In Izzo (2018), there is the comparison of SN 2018fp with SN 1998bw and SN 2010bh, and in Xu et al. (2013a), there is the comparison of the SN associated with GRB 130427A, SN 2013cq, with SN 1998bw and SN 2010bh, associated with GRB 980425 (Galama et al. 1999) and GRB 100316D (Mazzali et al. 2003), respectively. We show in Figure 3 the spectral comparison of SN 1998bw, SN 2010bh, and SN 2013cq. We may conclude that the SNe are similar, regardless of the differences, e.g., in energetics ($\sim 10^{54}$ erg versus $\sim 10^{51}$ erg), of their associated GRBs (BdHN I versus BdHN II).

6. Physical Interpretation

All the observations in Section 5 can be well interpreted within the picture of a binary system initially composing a massive CO_{core} and an NS.

6.1. Prompt Emission from a Binary Accretion System

At a given time, the CO_{core} collapses forming a νNS at its center and producing an SN explosion. A strong shockwave is generated and emerges from the SN ejecta. A typical SN shockwave carries $\sim 10^{51}$ erg of kinetic energy (Arnett 1996), which is partially converted into electromagnetic emission by sweeping the circumburst medium (CBM) with an efficiency of $\sim 10\%$ (see, e.g., Bykov et al. 2012). Therefore, the energy of $\sim 10^{50}$ erg is consistent with the total energy in the first spike. The electrons from the CBM are accelerated by the shockwave via the Fermi mechanism and emit synchrotron emission, which explains the nonthermal emission with a power-law index -2.31 in the first spike.

The second spike with a thermal component is a result of the SN ejecta accreting onto the companion NS. The distance of

the binary separation can be estimated by the delay time between the two spikes, ~ 10 s. Since the outer shell of the SN ejecta moves at velocity $\sim 0.1c$ (Cano et al. 2017), we estimate a binary separation $\approx 3 \times 10^{10}$ cm. Following Becerra et al. (2016), the total mass accreted by the companion NS gives $\sim 10^{-2} M_{\odot}$, which produces an emission of total energy $\sim 10^{51}$ erg, considering the accretion efficiency as $\sim 10\%$ (Frank et al. 1992). The majority of the mass is accreted in ~ 10 s, with an accretion rate $\sim 10^{-3} M_{\odot} \text{ s}^{-1}$; therefore, a spike with luminosity $\sim 10^{50}$ erg s^{-1} and duration ~ 10 s is produced; this estimation fits the second spike observed well.

The time-resolved analysis of the blackbody components in the second spike indicate a mildly relativistic expanding source emitting thermal radiation. This emission is explained by the adiabatic expanding thermal outflow from the accretion region (Fryer et al. 2006; Fryer 2009). The Rayleigh–Taylor convective instability acts during the initial accretion phase driving material away from the NS with a final velocity of the order of the speed of light. This material expands and cools, assuming the spherically symmetric expansion, to a temperature (Fryer et al. 1996; Becerra et al. 2016)

$$T = 6.84 \left(\frac{S}{2.85} \right)^{-1} \left(\frac{r}{10^{10} \text{ cm}} \right)^{-1} \text{ keV}, \quad (1)$$

where S is the the entropy

$$S \approx 2.85 \left(\frac{M_{\text{NS}}}{1.4 M_{\odot}} \right)^{7/8} \left(\frac{\dot{M}_B}{10^{-3} M_{\odot} \text{ s}^{-1}} \right)^{-1/4} \times \left(\frac{r}{10^{10} \text{ cm}} \right)^{-3/8}, \quad (2)$$

in units of k_B per nucleon. The system parameters in the above equations have been normalized to self-consistent values that fit the observational data, namely, the thermal emitter has a temperature ~ 6 keV, radius $\sim 10^{10}$ cm, and expands with velocity $\sim 0.5c$.

To have more details of the time-resolved evolution: for the two time bins in Table 2, an expanding speed of $0.53c$ gives the

Table 3
Model Comparison of Time-resolved Analysis of *Fermi*-GBM Data

Segment	Time (s)	Model	Log(Likelihood)	AIC	BIC
Spike 1 Precursor (NaI7)	−1.57–1.18	<u>PL</u>	430.03	864.17	869.59
		CPL	430.03	866.27	874.35
		Band	429.72	867.80	878.49
		PL+BB	429.77	867.90	878.59
		CPL+BB	429.77	870.08	883.36
		Band+BB	429.61	871.98	887.79
Spike 2 (NaI7+BGO1)	8.72–10.80	PL	947.20	1898.46	1905.33
		CPL	838.91	1685.93	1696.22
		Band	831.02	1670.21	1683.90
		PL+BB	947.21	1902.59	1916.27
		CPL+BB	827.67	1665.60	1682.66
		<u>Band+BB</u>	823.90	1660.17	1680.59
	10.80–12.30	PL	1334.10	2672.25	2679.13
		CPL	809.83	1625.76	1636.05
		Band	821.25	1650.68	1664.37
		PL+BB	1334.10	2676.38	2690.06
		<u>CPL+BB</u>	794.79	1599.85	1616.91
		<u>Band+BB</u>	794.80	1599.86	1616.92
12.30–22.54	PL	1366.08	2736.23	2742.79	
	CPL	1216.52	2439.16	2448.97	
	Band	1366.43	2741.06	2754.09	
	PL+BB	1366.08	2740.37	2753.40	
	CPL+BB	1215.52	2443.35	2459.58	
	Band+BB	1366.63	2745.69	2765.11	

Note. In the segment column, the name and the instruments are presented. The time column gives the time interval. In the model column, the model with an underline is the preferred one. We have used the following abbreviations: PL (Power-law), CPL (cutoff power-law), and BB (blackbody).

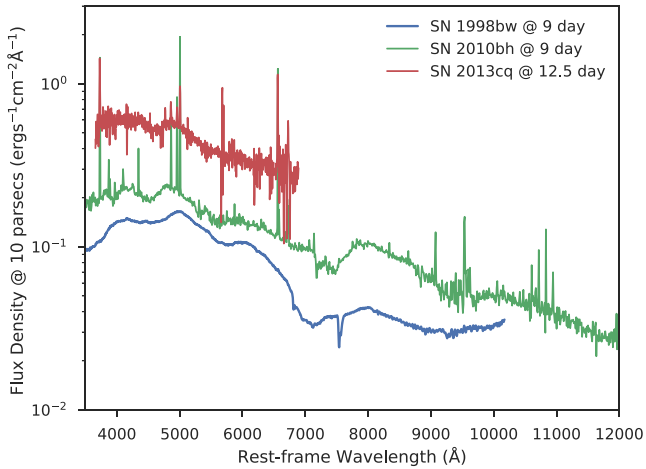


Figure 3. Spectra comparison of three SNe: 1998bw, 2010bh, 2013cq, flux density is normalized at 10 parsec, data are retrieved from the Wiserep website (<https://wiserep.weizmann.ac.il>).

radius 1.4×10^{10} cm and 4.3×10^{10} cm, respectively, as we fitted from the data. The luminosities are 2.11×10^{50} erg s $^{-1}$ and 7.56×10^{50} erg s $^{-1}$ respectively. If assuming the accretion efficiency is 10%, from the luminosity we obtain the accretion rate as $1.18 \times 10^{-3} M_{\odot}$ s $^{-1}$ and $4.32 \times 10^{-3} M_{\odot}$ s $^{-1}$. By applying the above two equations, the theoretical temperature is obtained to be 5.83 ± 1.25 keV and 3.93 ± 0.39 keV, the thermal flux are $1.22 \pm 0.97 \times 10^{-7}$ erg s $^{-1}$ cm $^{-2}$ and $2.37 \pm 0.85 \times 10^{-7}$ erg s $^{-1}$ cm $^{-2}$ respectively. If we assume the accretion efficiency is 7%, following the same procedure, the theoretical temperature shall be 8.32 ± 1.78 keV and 5.61 ± 0.56 keV, the

thermal flux shall be $5.78 \pm 3.89 \times 10^{-7}$ erg s $^{-1}$ cm $^{-2}$ and $7.17 \pm 2.51 \times 10^{-7}$ erg s $^{-1}$ cm $^{-2}$ respectively. The observed values in Table 2 are more consistent with the accretion efficiency of 7%.

The loss of rotational energy of the ν NS, born after the SN explosion, powers the afterglow. This will be discussed in the next session.

6.2. Afterglow from the Newly Born Pulsar

We have applied the synchrotron model of mildly relativistic outflow powered by the rotational energy of the ν NS to GRB 130427A (Ruffini et al. 2018d). From it we have inferred a 1 ms ν NS pulsar emitting dipole and quadrupole radiation. Here we summarize this procedure and apply it to GRB 180827A.

The late X-ray afterglow of GRB 180728A also shows a power-law decay of index ~ -1.3 which, as we show below, if powered by the pulsar implies the presence of a quadrupole magnetic field in addition to the traditional dipole one. The “magnetar” scenario with only a strong dipole field ($B_{\text{dip}} > 10^{14}$ G) is not capable of fitting the late time afterglow (Dai & Lu 1998; Zhang & Mészáros 2001; Metzger et al. 2011; Li et al. 2018b). The dipole and quadrupole magnetic fields are adopted from Pétri (2015), where the magnetic field is cast into an expansion of vector spherical harmonics, each harmonic mode is defined by a set of the multipole order number l and the azimuthal mode number m . The luminosity from a pure dipole ($l = 1$) is

$$L_{\text{dip}} = \frac{2}{3c^3} \Omega^4 B_{\text{dip}}^2 R_{\text{NS}}^6 \sin^2 \chi_1, \quad (3)$$

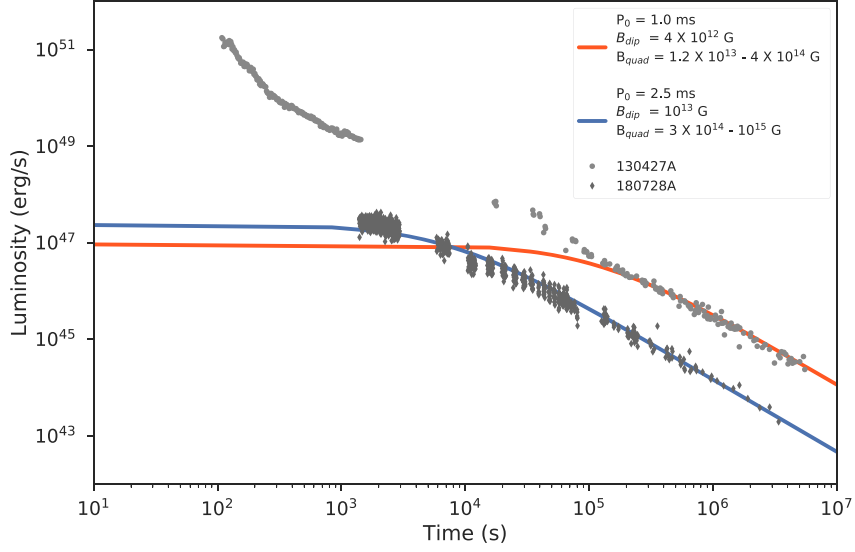


Figure 4. Afterglow powered by the ν NS pulsar: the gray and dark points correspond to the bolometric afterglow light curves of GRB 130427A and 180728A, respectively. The red and blue lines are the fitting of the energy injection from the rotational energy of the pulsar. The fitted parameters are shown in the legend, the quadruple fields are given in a range, and the upper value is 3.16 times the lower value, this is due to the oscillation angle χ_2 , which is a free parameter.

and a pure quadrupole ($l = 2$) is

$$L_{\text{quad}} = \frac{32}{135c^5} \Omega^6 B_{\text{quad}}^2 R_{\text{NS}}^8 \times \sin^2 \chi_1 (\cos^2 \chi_2 + 10 \sin^2 \chi_2), \quad (4)$$

where χ_1 and χ_2 are the inclination angles of the magnetic moment, the different modes are easily separated by taking $\chi_1 = 0$ and any value of χ_2 for $m = 0$, $(\chi_1, \chi_2) = (90, 0)$ degrees for $m = 1$ and $(\chi_1, \chi_2) = (90, 90)$ degrees for $m = 2$.

The observed luminosity is assumed to be equal to the spindown luminosity as

$$\begin{aligned} \frac{dE}{dt} &= -I\Omega\dot{\Omega} = -(L_{\text{dip}} + L_{\text{quad}}) \\ &= -\frac{2}{3c^3} \Omega^4 B_{\text{dip}}^2 R_{\text{NS}}^6 \sin^2 \chi_1 \left(1 + \eta^2 \frac{16 R_{\text{NS}}^2 \Omega^2}{45 c^2} \right), \end{aligned}$$

and

$$\eta^2 = (\cos^2 \chi_2 + 10 \sin^2 \chi_2) \frac{B_{\text{quad}}^2}{B_{\text{dip}}^2}, \quad (5)$$

where I is the moment of inertia. The parameter η relates to the ratio of quadrupole and dipole strength, $\eta = B_{\text{quad}}/B_{\text{dip}}$ for the $m = 1$ mode, and $\eta = 3.16 \times B_{\text{quad}}/B_{\text{dip}}$ for the $m = 2$ mode.

The bolometric luminosity is obtained by integrating the entire spectrum generated by the synchrotron model that fits the soft X-ray (0.3–10 keV) and the optical (see Ruffini et al. 2018d, and Figure 4 for an example). The bolometric luminosity has a factor ~ 5 times more luminous than the soft X-ray emission. In Figure 4, we show the bolometric luminosity light curve, the shape of the light curve is taken from the soft X-ray data because it offers the most complete time coverage.

We assume that the bolometric luminosity required from the synchrotron model is equal to the energy loss of the pulsar. The numerical fitting result shows that the BdHN II of GRB 180728A forms a pulsar with initial spin $P_0 = 2.5$ ms, which is

slower than the $P_0 = 1$ ms pulsar from the BdHN I of GRB 130427A. Both sources have similar dipole magnetic fields 10^{12} – 10^{13} G and a quadrupole components ~ 30 – 100 stronger ($\eta = 100$) than the dipole one. The strong quadrupole field dominates the emission in the early years, while the dipole radiation starts to be prominent later when the spin decays. This is because the quadrupole emission is more sensitive to the spin period, as $\propto \Omega^6$, while the dipole is $\propto \Omega^4$. Therefore, the ν NS shows a dipole behavior when observed today, because the quadrupole dominates a very small fraction ($\lesssim 10^{-5}$) of the pulsar lifetime.

7. A Consistent Picture and Visualization

In the previous sections, we have inferred the binary separation from the prompt emission, and the spin of the ν NS from the afterglow data. In the following, we confirm the consistency of these findings by numerical simulations of these systems, and compare the commonalities and diversities of GRB 130427A and GRB 180728A as examples of BdHN I and BdHN II systems in our model, respectively.

From an observational point of view, GRB 130427A and GRB 180728A are both long GRBs, but they are very different in the energetic: GRB 130427A is one of the most energetic GRBs with isotropic energy more than 10^{54} erg, while GRB 180728A is on the order of 10^{51} erg, a thousand times difference. GRB 130427A has observed the most significant ultra-high-energy photons (100 MeV–100 GeV, hereafter we call GeV photons), it has the longest duration (>1000 s) of GeV emission, and it has the highest energy of a photon ever observed from a GRB. In contrast, GRB 180728A has no GeV emission detected. As for the afterglow, the X-ray afterglow of GRB 130427A is more luminous than GRB 180728A, but they both share a power-law decaying index ~ -1.3 after 10^4 s. After more than 10 days, in both GRB sites emerges the coincident optical signal of a type Ic SN, and the SNe spectra are almost identical as shown in Section 5.2.

BdHN I and II have the same kind of binary progenitor, a binary composed of a CO_{core} and a companion NS, but the

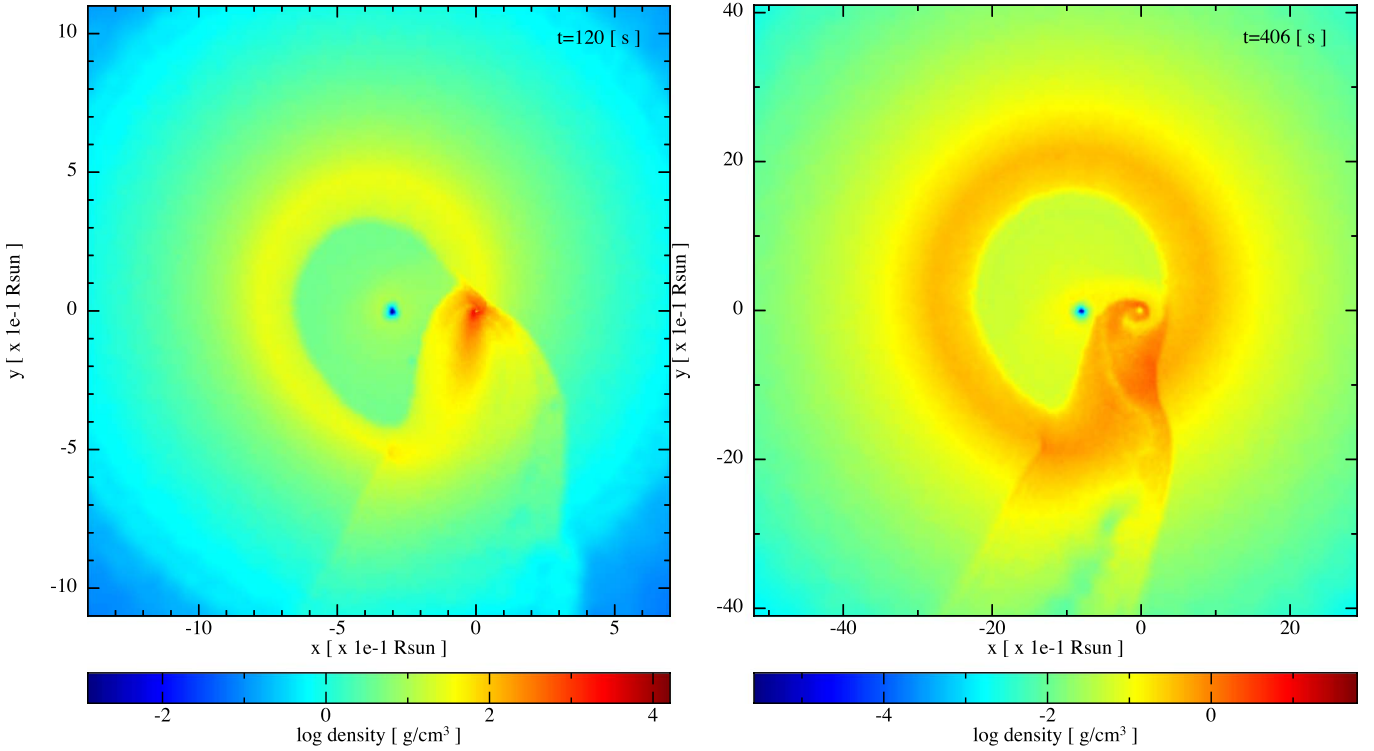


Figure 5. Two selected SPH simulations from Becerra et al. (2019) of the exploding CO_{core} as an SN in the presence of a companion NS: Model “25m1p08e” with $P_{\text{orb}} = 4.8$ minutes (left panel) and Model “25m3p1e” with $P_{\text{orb}} = 11.8$ minutes (right panel). The CO_{core} is taken from the $25 M_{\odot}$ ZAMS progenitor, so it has a mass $M_{\text{CO}} = 6.85 M_{\odot}$. The mass of the NS companion is $M_{\text{NS}} = 2 M_{\odot}$. The plots show the density profile on the equatorial orbital plane; the coordinate system has been rotated and translated in such a way that the NS companion is at the origin and the νNS is along the $-x$ axis. The system in the left panel leads to a BdHN I and the snapshot is at the time of the gravitational collapse of the NS companion to a BH, $t = 120$ s from the SN shock breakout ($t = 0$ of our simulation). The system forms a new binary system composed of the νNS (at the center of the deep-blue region) and the BH formed by the collapsing NS companion (at the center of the red vortices). The system in the right panel leads to a BdHN II because the NS in this case does not reach the critical mass. This snapshot corresponds to $t = 406$ s post SN shock breakout. In this simulation, the new system composed of the νNS and the NS companion becomes unbound after the explosion.

binary separation/period is different, being larger/longer for BdHN II.

The angular momentum conservation during the gravitational collapse of the pre-SN core that forms the νNS , i.e., $J_{\text{CO}} = J_{\nu\text{NS}}$, implies that the latter should be fast rotating, i.e.,

$$\Omega_{\nu\text{NS}} = \left(\frac{R_{\text{CO}}}{R_{\nu\text{NS}}} \right)^2 \Omega_{\text{Fe}} = \left(\frac{R_{\text{CO}}}{R_{\nu\text{NS}}} \right)^2 \Omega_{\text{orb}}, \quad (6)$$

where $\Omega_{\text{orb}} = 2\pi/P_{\text{orb}} = \sqrt{GM_{\text{tot}}/a_{\text{orb}}^3}$ from the Kepler law, being $M_{\text{tot}} = M_{\text{CO}} + M_{\text{NS}}$ the total mass of the binary before the SN explosion, and $M_{\text{CO}} = M_{\nu\text{NS}} + M_{\text{ej}}$. We have assumed that the mass of the νNS is set by the mass of the iron core of the pre-SN CO_{core} and that it has a rotation period equal to the orbital period owing to tidal synchronization.

From the above we can see that the νNS rotation period, $P_{\nu\text{NS}}$, has a linear dependence on the orbital period, P_{orb} . Therefore, the solution we have obtained for the rotation period of the νNS born in GRB 130427A ($P_{\nu\text{NS}} \approx 1$ ms) and in the GRB 180728A ($P_{\nu\text{NS}} \approx 2.5$ ms), see Figure 4, implies that the orbital period of the BdHN I would be a factor of ≈ 2.5 shorter than that of the BdHN II. Based on this information, we seek two systems in our simulations presented in Becerra et al. (2019) with the following properties: the same (or nearly) SN explosion energy, pre-SN CO_{core} , and initial NS companion mass, but different orbital periods, i.e., $P_{\text{II}}/P_{\text{I}} \approx 2.5$. The more compact binary leads to the BdHN I and the less compact one

to the BdHN II and, by angular momentum conservation, they lead to the abovementioned νNS s.

We examine the results of the simulations for the pre-SN core of a $25 M_{\odot}$ zero-age main-sequence progenitor and the initial mass of the NS companion $M_{\text{NS}} = 2 M_{\odot}$. A close look at Tables 2 and 7 in Becerra et al. (2019) shows that, indeed, Model “25m1p08e” with $P_{\text{orb}} = 4.81$ minutes ($a_{\text{orb}} \approx 1.35 \times 10^{10}$ cm) and Model “25m3p1e” with $P_{\text{orb}} = 11.8$ minutes ($a_{\text{orb}} \approx 2.61 \times 10^{10}$ cm) give a consistent solution. In Model “25m1p08e,” the NS companion reaches the critical mass (secular axisymmetric instability) and collapses to a BH; this model produces a BdHN I. In the Model “25m3p1e” the NS companion does not reach the critical mass; this system produces a BdHN II. The system leading to BdHN I remains bound after the explosion while, the one leading to the BdHN II, is disrupted. Concerning the νNS rotation period, adopting $R_{\text{CO}} \sim 2.141 \times 10^8$ cm (see Table 1 in Becerra et al. 2019), $P_{\text{orb}} \sim 4.81$ minutes, and $P_{\text{orb}} \sim 11.8$ minutes leads to $P_{\nu\text{NS}} \sim 1$ ms and 2.45 ms, respectively. We show in Figure 5 snapshots of the two simulations.

8. Conclusion

The classification of GRBs in nine different subclasses allows us to identify the origin of a new GRB with known redshift from the observation of its evolution in the first hundred seconds. Then, we are able to predict the presence of an associated SN in the BdHN and its occurring time. We

reviewed our previous successful prediction of a BdHN I in our model: GRB 130427A/SN 2013cq, and in this article, we presented our recent successful prediction of a BdHN II in our model: GRB 180728A/SN 2018fip.

The detailed observational data of GRB 180728A, for the first time, allowed us to follow the evolution of a BdHN II. The collapse of CO_{core} leads to an SN. We determine that the corresponding shockwave with energy $\sim 10^{51}$ erg emerges and produces the first 2 s spike in the prompt emission. The SN ejecta expands and reaches $\sim 3 \times 10^{10}$ cm away from the NS companion. The accretion process starts with a rate $\sim 10^{-3} M_{\odot} \text{ s}^{-1}$, the second powerful spike lasting 10 s with luminosity $\sim 10^{50}$ erg s^{-1} , and a thermal component at temperature ~ 7 keV.

A νNS is formed from the SN. The role of νNS powering the afterglow has been evidenced in our study of GRB 130427A (Ruffini et al. 2018d). This article emphasizes its application on GRB 180728A. The νNS pulsar loses its rotational energy by dipole and quadrupole emission. In order to fit the observed afterglow data using a synchrotron model (Ruffini et al. 2018d), we require an initial 1 ms spin pulsar for GRB 130427A, and a slower spin of 2.5 ms for GRB 180728A. For close binary systems, the binary components are synchronized with the orbital period, from which we are able to obtain the orbital separation by inferring the CO_{core} period from the νNS one via angular momentum conservation. This second independent method leads to a value of the binary separation in remarkable agreement with the one inferred from the prompt emission, which shows the self-consistency of this picture. The SNe spectra observed in BdNH I and in BdHN II are similar, although the associated two GRBs markedly differ in energy. The SN acts as a catalyst; it triggers the GRB process. After losing a part of the ejecta mass by hypercritical accretion, the remaining SN ejecta are heated by the GRB emission, but the nuclear composition, which relates to the observed optical emission owing to the nuclear decay of nickel and cobalt (Arnett 1996), is not influenced by such a GRB-SN interaction.

Besides providing the theoretical support of the BdHN I and II realization, we have presented 3D SPH simulations that help in visualizing the systems (see Figure 5).

In short, we made a successful prediction of SN 2018fip associated with GRB 180728A based on our GRB classification that GRB 180728A belongs to BdHN II. The observations of the prompt emission and the afterglow portray, for the first time, a complete transitional stage of two binary stars. We emphasize the νNS from SN playing a dominant role in the later afterglow, the comparison to GRB 130427A, a typical BdHN I in our model, is demonstrated and visualized.

The confirmation of the SN appearance, as well as the majority of this work were performed during R.R. and Y.W.'s visit to the *Yau Mathematical Sciences Center* in Tsinghua University, Beijing. We greatly appreciate the kind hospitality of and the helpful discussion with Prof. Shing-Tung Yau. We also acknowledge Dr. Luca Izzo for discussions on the SNe treated in this work. We thank the referee for constructive comments that helped clarify many concepts and strengthen the time-resolved analysis.

Appendix A GCNs

GCN 14526–GRB 130427A: Prediction of SN appearance

The late X-ray observations of GRB 130427A by *Swift*-XRT clearly evidence a pattern typical of a family of GRBs associated with the SN following the Induce Gravitational Collapse (IGC) paradigm (Rueda & Ruffini 2012; Pisani et al. 2013). We assume that the luminosity of the possible SN associated with GRB 130427A would be that of 1998bw, as found in the IGC sample described in Pisani et al. (2013). Assuming the intergalactic absorption in the *I*-band (which corresponds to the *R*-band rest-frame) and the intrinsic one, assuming a Milky Way type for the host galaxy, we obtain a magnitude expected for the peak of the SN of $I = 22\text{--}23$ occurring 13–15 days after the GRB trigger, namely between 2013 May 10th and 12th. Further optical and radio observations are encouraged.

GCN 23066–GRB 180728A: A long GRB of the X-ray flash (XRF) subclass, expecting SN appearance

GRB 180728A has $T_{90} = 6.4$ s (Rossi 2018), peak energy 142 (–15, +20) keV, and isotropic energy $E_{\text{iso}} = (2.33 \pm 0.10) \times 10^{51}$ erg (Frederiks 2018). It presents the typical characteristic of a subclass of long GRBs called XRFs⁷ (see Ruffini et al. 2016), originating from a tight binary of a CO_{core} undergoing an SN explosion in the presence of a companion NS that hypercritically accretes part of the SN matter. The outcome is a new binary composed by a more MNS and a newly born NS (νNS). Using the averaged observed value of the optical peak time of SN (Cano et al. 2017), and considering the redshift $z = 0.117$ (Rossi 2018), a bright optical signal will peak at 14.7 ± 2.9 days after the trigger (2018 August 12, uncertainty from August 9th to 15th) at the location of R. A. = 253.56472 and decl. = –54.04451, with an uncertainty 0.43 arcsec (LaPorte 2018). The follow-up observations, especially the optical bands for the SN, as well as attention to binary NS pulsar behaviors in the X-ray afterglow emission, are recommended.

GCN 23142–GRB 180728A: discovery of the associated SN

Up to now, we have observed at three epochs, specifically at 6.27, 9.32 and 12.28 days after the GRB trigger. The optical counterpart is visible in all epochs using the X-shooter acquisition camera in the *g*, *r*, and *z* filters. We report a rebrightening of 0.5 ± 0.1 mag in the *r* band between 6.27 and 12.28 days. This is consistent with what is observed in many other lo 170827w-redshift GRBs, which in those cases is indicative of an emerging type Ic SN.

Appendix B Data Fitting

Data are fitted by applying the Monte Carlo Bayesian iterations using a Python package: The Multi-Mission Maximum Likelihood framework (3ML).⁸ An example is shown in Figure 6.

Appendix C Model Comparison

Spectra are fitted by Bayesian iterations. The AIC is preferred for comparing nonnested models, and BIC is preferred for nested models (Kass & Raftery 1995). Log (likelihood) is adopted by the method of the maximum likelihood ratio test, which is treated as a reference of the

⁷ The previous name of BdHN I.

⁸ <https://github.com/giacomov/3ML>

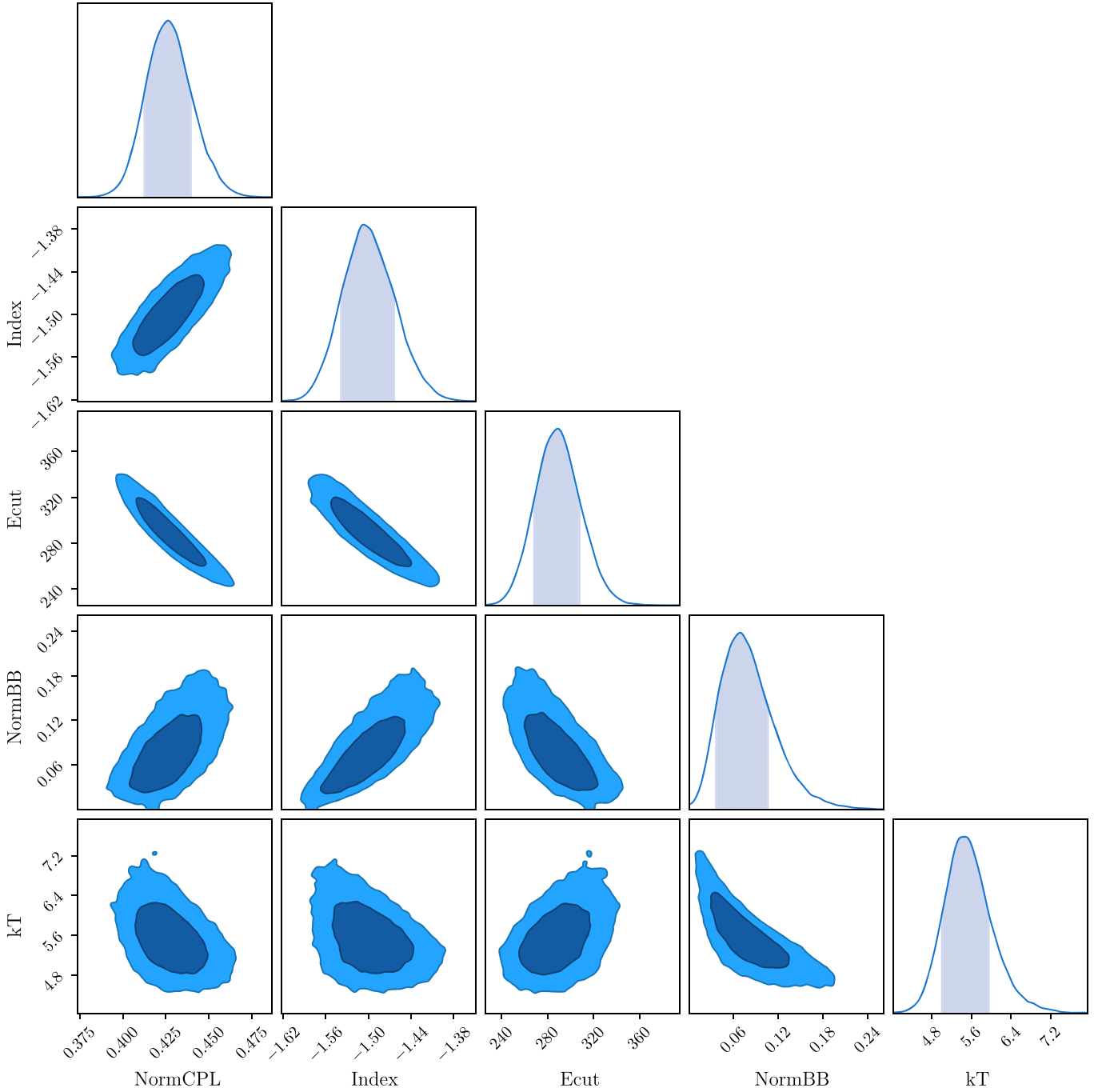


Figure 6. Example of fitting the *Fermi*-GBM data from 10.80 to 12.30 s. We apply 20 chains, each chain iterates 10^4 times and burns the first 10^3 times. The parameters are normalization (NormCPL), cutoff energy (ECut), and power-law index (Index) of the cutoff power-law model, as well as normalization (NormBB) and temperature (kT) of the blackbody model.

model comparison (Vuong 1989). Parameters are shown in Table 3.

ORCID iDs

Y. Wang  <https://orcid.org/0000-0001-7959-3387>
 C. Bianco  <https://orcid.org/0000-0001-7749-4078>

References

Abeysekara, A. U., Alfaro, R., Alvarez, C., et al. 2015, *ApJ*, 800, 78
 Ackermann, M., Ajello, M., Asano, K., et al. 2014, *Sci*, 343, 42

Anderson, G. E., van der Horst, A. J., Staley, T. D., et al. 2014, *MNRAS*, 440, 2059
 Aptekar, R. L., Frederiks, D. D., Golenetskii, S. V., et al. 1995, *SSRv*, 71, 265
 Arnett, D. 1996, *Supernovae and Nucleosynthesis: An Investigation of the History of Matter from the Big Bang to the Present* (Cambridge: Cambridge Univ. Press)
 Atwood, W. B., Abdo, A. A., Ackermann, M., et al. 2009, *ApJ*, 697, 1071
 Barthelmy, S. D., Barbier, L. M., Cummings, J. R., et al. 2005, *SSRv*, 120, 143
 Becerra, L., Bianco, C. L., Fryer, C. L., Rueda, J. A., & Ruffini, R. 2016, *ApJ*, 833, 107
 Becerra, L., Cipolletta, F., Fryer, C. L., Rueda, J. A., & Ruffini, R. 2015, *ApJ*, 812, 100
 Becerra, L., Ellinger, C. L., Fryer, C. L., Rueda, J. A., & Ruffini, R. 2019, *ApJ*, 871, 14

- Becerra, L., Guzzo, M. M., Rossi-Torres, F., et al. 2018, *ApJ*, **852**, 120
- Becerra, R. L., Watson, A. M., Lee, W. H., et al. 2017, *ApJ*, **837**, 116
- Berger, E. 2014, *ARA&A*, **52**, 43
- Berger, E., Fong, W., & Chornock, R. 2013, *ApJL*, **774**, L23
- Bernardini, M. G., Campana, S., Ghisellini, G., et al. 2014, *MNRAS*, **439**, L80
- Bykov, A., Gehrels, N., Krawczynski, H., et al. 2012, *SSRv*, **173**, 309
- Cano, Z., Wang, S.-Q., Dai, Z.-G., & Wu, X.-F. 2017, *AdAst*, 2017, 8929054
- Dai, Z. G., & Lu, T. 1998, *A&A*, **333**, L87
- De Pasquale, M., Page, M., Kann, D., et al. 2017, *Galax*, **5**, 6
- De Pasquale, M., Page, M. J., Kann, D. A., et al. 2016, *MNRAS*, **462**, 1111
- de Ugarte Postigo, A., Xu, D., Leloudas, G., et al. 2013, *GCN*, 14646, 1
- Eichler, D., Livio, M., Piran, T., & Schramm, D. N. 1989, *Natur*, **340**, 126
- Fan, Y.-Z., Tam, P. H. T., Zhang, F.-W., et al. 2013, *ApJ*, **776**, 95
- Flores, H., Covino, S., Xu, D., et al. 2013, *GCN*, 14491, 1
- Fraija, N., Lee, W., & Veres, P. 2016, *ApJ*, **818**, 190
- Frank, J., King, A., & Raine, D. 1992, *Accretion Power in Astrophysics* (Cambridge: Cambridge Univ. Press)
- Frederiks, D. 2018, *GCN*, 23061, 1
- Fryer, C. L. 2009, *ApJ*, **699**, 409
- Fryer, C. L., Benz, W., & Herant, M. 1996, *ApJ*, **460**, 801
- Fryer, C. L., Herwig, F., Hungerford, A., & Timmes, F. X. 2006, *ApJL*, **646**, L131
- Fryer, C. L., Oliveira, F. G., Rueda, J. A., & Ruffini, R. 2015, *PhRvL*, **115**, 231102
- Fryer, C. L., Rueda, J. A., & Ruffini, R. 2014, *ApJL*, **793**, L36
- Galama, T. J., Vreeswijk, P. M., van Paradijs, J., et al. 1999, *A&AS*, **138**, 465
- Gao, S., Kashiyama, K., & Mészáros, P. 2013, *ApJL*, **772**, L4
- Golenetskii, S. 2013, *GCN*, 14487, 1
- Goodman, J. 1986, *ApJL*, **308**, L47
- Hook, I. M., Jørgensen, I., Allington-Smith, J. R., et al. 2004, *PASP*, **116**, 425
- Izzo, L. 2018, *GCN*, 23142, 1
- Joshi, J. C., Razaque, S., & Moharana, R. 2016, *MNRAS*, **458**, L79
- Kass, R. E., & Raftery, A. E. 1995, *J. Am. Stat. Assoc.*, **90**, 773
- Kouveliotou, C., Granot, J., Racusin, J. L., et al. 2013, *ApJL*, **779**, L1
- Kumar, P., & Zhang, B. 2015, *PhR*, **561**, 1
- LaPorte, S. J. 2018, *GCN*, 23064, 1
- Laskar, T., Berger, E., Zauderer, B. A., et al. 2013, *ApJ*, **776**, 119
- Levan, A. J., Cenko, S. B., Perley, D. A., & Tanvir, N. R. 2013, *GCN*, 14455, 1
- Levan, A. J., Tanvir, N. R., Fruchter, A. S., et al. 2014, *ApJ*, **792**, 115
- Li, L., Wang, Y., Shao, L., et al. 2018a, *ApJS*, **234**, 26
- Li, L., Wu, X.-F., Huang, Y.-F., et al. 2015, *ApJ*, **805**, 13
- Li, L., Wu, X.-F., Lei, W.-H., et al. 2018b, *ApJS*, **236**, 26
- Li, L.-X., & Paczyński, B. 1998, *ApJL*, **507**, L59
- Liu, R.-Y., Wang, X.-Y., & Wu, X.-F. 2013, *ApJL*, **773**, L20
- Maselli, A., Melandri, A., Nava, L., et al. 2014, *Sci*, **343**, 48
- Mazzali, P. A., Deng, J., Maeda, K., et al. 2002, *ApJL*, **572**, L61
- Mazzali, P. A., Deng, J., Tominaga, N., et al. 2003, *ApJL*, **599**, L95
- Mészáros, P. 2002, *ARA&A*, **40**, 137
- Mészáros, P. 2006, *RPPH*, **69**, 2259
- Metzger, B. D., Giannios, D., Thompson, T. A., Bucciantini, N., & Quataert, E. 2011, *MNRAS*, **413**, 2031
- Metzger, B. D., Martínez-Pinedo, G., Darbha, S., et al. 2010, *MNRAS*, **406**, 2650
- Paczynski, B. 1986, *ApJL*, **308**, L43
- Paczyński, B. 1998, *ApJL*, **494**, L45
- Panaitescu, A., Vestrand, W. T., & Woźniak, P. 2013, *MNRAS*, **436**, 3106
- Perley, D. A., Cenko, S. B., Corsi, A., et al. 2014, *ApJ*, **781**, 37
- Perri, M. 2018, *GCN*, 23049, 1
- Pétri, J. 2015, *MNRAS*, **450**, 714
- Piran, T. 1999, *PhR*, **314**, 575
- Piran, T. 2004, *RvMP*, **76**, 1143
- Pisani, G. B., Izzo, L., Ruffini, R., et al. 2013, *A&A*, **552**, L5
- Planck Collaboration, Aghanim, N., Akrami, Y., et al. 2018, arXiv:1807.06209
- Preece, R., Burgess, J. M., von Kienlin, A., et al. 2014, *Sci*, **343**, 51
- Rossi, R. 2018, *GCN*, 23055, 1
- Rueda, J. A., & Ruffini, R. 2012, *ApJL*, **758**, L7
- Rueda, J. A., Ruffini, R., Wang, Y., et al. 2018a, *JCAP*, **10**, 006
- Rueda, J. A., Ruffini, R., Wang, Y., et al. 2018b, arXiv:1807.07905
- Ruffini, R. 2018, *GCN*, 23066, 1
- Ruffini, R., Aimuratov, Y., Bianco, C. L., et al. 2018a, *GCN*, 23019, 1
- Ruffini, R., Becerra, L., Bianco, C. L., et al. 2018b, *ApJ*, **869**, 151
- Ruffini, R., Becerra, L., Bianco, C. L., et al. 2018c, *ApJ*, **869**, 151
- Ruffini, R., Bianco, C. L., Enderli, M., et al. 2013, *GCN*, 14526, 1
- Ruffini, R., Bianco, C. L., Enderli, M., et al. 2014a, *GCN*, 15794, 1
- Ruffini, R., Karlica, M., Sahakyan, N., et al. 2018d, *ApJ*, **869**, 101
- Ruffini, R., Muccino, M., Bianco, C. L., et al. 2014b, *A&A*, **565**, L10
- Ruffini, R., Rodríguez, J., Muccino, M., et al. 2018e, *ApJ*, **859**, 30
- Ruffini, R., Rueda, J. A., Muccino, M., et al. 2016, *ApJ*, **832**, 136
- Ruffini, R., Wang, Y., Aimuratov, Y., et al. 2018f, *ApJ*, **852**, 53
- Ruffini, R., Wang, Y., Enderli, M., et al. 2015, *ApJ*, **798**, 10
- Sari, R., Piran, T., & Narayan, R. 1998, *ApJL*, **497**, L17
- Scargle, J. D. 1998, *ApJ*, **504**, 405
- Selsing, J. 2018, *GCN*, 23181, 1
- Selsing, J., Izzo, L., Rossi, A., & Malesani, D. B. 2018, *Transient Name Server Classification Report*, 1249, 2609
- Starling, R. L. C. 2018, *GCN*, 23046, 1
- Tam, P.-H. T. 2014, *IJMPS*, **28**, 1460174
- Tam, P.-H. T., Tang, Q.-W., Hou, S.-J., Liu, R.-Y., & Wang, X.-Y. 2013, *ApJL*, **771**, L13
- Tanvir, N. R., Levan, A. J., Fruchter, A. S., et al. 2013, *Natur*, **500**, 547
- Tavani, M., Barbiellini, G., Argan, A., et al. 2009, *A&A*, **502**, 995
- van der Horst, A. J., Paragi, Z., de Bruyn, A. G., et al. 2014, *MNRAS*, **444**, 3151
- Veres, P. 2018, *GCN*, 23053, 1
- Vernet, J., Dekker, H., D'Odorico, S., et al. 2011, *A&A*, **536**, A105
- Vernin, J., & Munoz-Tunon, C. 1992, *A&A*, **257**, 811
- Vestrand, W. T., Wren, J. A., Panaitescu, A., et al. 2014, *Sci*, **343**, 38
- von Kienlin, A. 2013, *GCN*, 14473, 1
- Vuong, Q. H. 1989, *Econometrica*, **57**, 307
- Vurm, I., Hascoët, R., & Beloborodov, A. M. 2014, *ApJL*, **789**, L37
- Woosley, S. E. 1993, *ApJ*, **405**, 273
- Woosley, S. E., & Bloom, J. S. 2006, *ARA&A*, **44**, 507
- Xu, D., de Ugarte Postigo, A., Leloudas, G., et al. 2013a, *ApJ*, **776**, 98
- Xu, D., de Ugarte Postigo, A., Schulze, S., et al. 2013b, *GCN*, 14478, 1
- Zhang, B., & Mészáros, P. 2001, *ApJL*, **552**, L35

Electromagnetic emission of white dwarf binary mergers

To cite this article: J.A. Rueda *et al* JCAP03(2019)044

View the [article online](#) for updates and enhancements.



AAS | **IOP Astronomy** ebooks

Part of your publishing universe and your first choice for astronomy, astrophysics, solar physics and planetary science ebooks.

iopscience.org/books/aas

Electromagnetic emission of white dwarf binary mergers

J.A. Rueda,^{*a,b,c*} **R. Ruffini**,^{*a,b,c,d*} **Y. Wang**,^{*a,b*} **C.L. Bianco**,^{*a,b*}
J.M. Blanco-Iglesias,^{*e,f*} **M. Karlica**,^{*a,b,d*} **P. Lorén-Aguilar**,^{*e,f*}
R. Moradi^{*a,b*} and **N. Sahakyan**^{*g*}

^{*a*}ICRA, Dipartimento di Fisica, Sapienza Università di Roma,
P.le Aldo Moro 5, I-00185 Rome, Italy

^{*b*}ICRANet,
P.zza della Repubblica 10, I-65122 Pescara, Italy

^{*c*}ICRANet-Rio, Centro Brasileiro de Pesquisas Físicas,
Rua Dr. Xavier Sigaud 150, 22290-180 Rio de Janeiro, Brazil

^{*d*}Université de Nice Sophia Antipolis,
CEDEX 2, Grand Château Parc Valrose, Nice, France

^{*e*}Departament de Física, Universitat Politècnica de Catalunya,
c/Esteve Terrades, 5, 08860 Castelldefels, Spain

^{*f*}School of Physics, University of Exeter,
Stocker Road, Exeter EX4 4QL, U.K.

^{*g*}ICRANet-Armenia,
Marshall Baghramian Avenue 24a, 0019 Yerevan, Armenia

E-mail: jorge.rueda@icra.it, ruffini@icra.it, yu.wang@icranet.org, bianco@icra.it,
josemiguelblancoiglesias@gmail.com, mikarlic@gmail.com,
p.loren-aguilar@exeter.ac.uk, rahim.moradi@icranet.org, narek@icra.it

Received September 25, 2018

Revised February 25, 2019

Accepted March 19, 2019

Published March 29, 2019

Abstract. It has been recently proposed that the ejected matter from white dwarf (WD) binary mergers can produce transient, optical and infrared emission similar to the “kilonovae” of neutron star (NS) binary mergers. To confirm this we calculate the electromagnetic emission from WD-WD mergers and compare with kilonova observations. We simulate WD-WD mergers leading to a massive, fast rotating, highly magnetized WD with an adapted version of the smoothed-particle-hydrodynamics (SPH) code Phantom. We thus obtain initial conditions for the ejecta such as escape velocity, mass and initial position and distribution. The subsequent thermal and dynamical evolution of the ejecta is obtained by integrating the energy-conservation equation accounting for expansion cooling and a heating source given by the fallback accretion onto the newly-formed WD and its magneto-dipole radiation. We show that magnetospheric processes in the merger can lead to a prompt, short gamma-ray emission of up to $\approx 10^{46}$ erg in a timescale of 0.1–1 s. The bulk of the ejecta initially expands non-relativistically with velocity $0.01c$ and then it accelerates to $0.1c$ due to the injection of fallback accretion energy. The ejecta become transparent at optical wavelengths around ~ 7 days post-merger with a luminosity 10^{41} – 10^{42} erg s $^{-1}$. The X-ray emission from the fallback accretion becomes visible around ~ 150 – 200 day post-merger with a luminosity of 10^{39} erg s $^{-1}$. We also predict the post-merger time at which the central WD should appear as a pulsar depending on the value of the magnetic field and rotation period.

Keywords: gamma ray bursts theory, white and brown dwarfs, accretion

ArXiv ePrint: [1807.07905](https://arxiv.org/abs/1807.07905)

Contents

1	Introduction	1
2	WD-WD mergers	2
2.1	Post-merger configuration	2
2.2	WD-WD merger rate	2
2.3	Magnetic field of the central WD	2
3	Optical and infrared emission	4
4	X-ray emission	7
4.1	Is the magnetic field buried?	8
4.2	Expected X-ray emission	8
4.3	WD-pulsar appearance	9
5	Gamma-ray emission	9
6	Summary and conclusions	10

1 Introduction

It was recently shown in Rueda et al. [29] that WD-WD mergers can produce optical and infrared emission that resemble the one emitted from the “kilonovae” produced by NS-NS mergers. This novel, previously not addressed possibility of WD-WD mergers emission was there applied to the analysis of the optical and infrared observations of the “kilonova” AT 2017gfo [2, 6, 22, 23], associated with GRB 170817A [1, 10].

The emission in the optical and infrared wavelengths is of thermal character being due to the adiabatic cooling of WD-WD merger ejecta, which is also powered by the fallback accretion onto the newly-formed WD. The ejecta mass is about $10^{-3} M_{\odot}$ [8, 15] and the fallback may inject 10^{47} – 10^{49} ergs $^{-1}$ at early times and then fall-off following a power-law behavior [15].

The thermal ejecta start to become transparent in the optical wavelengths at $t \sim 7$ days with a peak bolometric luminosity $L_{\text{bol}} \sim 10^{42}$ ergs $^{-1}$. These ejecta are therefore powered by a different mechanism with respect to the one in the kilonova from NS-NS which are powered by the radioactive decay of r-process heavy material synthesized in the merger.

Since the observational features of WD-WD mergers are an important topic by their own, the aim of this article is to give details on their expected electromagnetic emission, not only in the optical and infrared but also in the X- and gamma-rays.

The article is organized as follows. In section 2 we recall the properties of the WD-WD mergers obtained from numerical simulations, section 3 is devoted to the analysis of the optical and infrared emission from the cooling of the merger ejecta. We show in section 4 the X-ray emission from fallback accretion and spindown of the newly-formed central WD, in section 5 we present a brief discussion on the possible prompt emission in gamma-rays, and in section 6 we present the summary and the conclusions of the article.

2 WD-WD mergers

2.1 Post-merger configuration

Numerical simulations of WD-WD mergers indicate that, when the merger does not lead to a prompt type Ia supernova (SN) explosion, the merged configuration has in general three distinct regions [4, 7, 11, 14, 15, 26, 32]: a rigidly rotating, central WD, on top of which there is a hot, differentially-rotating, convective corona, surrounded by a rapidly rotating Keplerian disk. The corona is composed of about half of the mass of the secondary star which is totally disrupted and roughly the other half of the secondary mass is in the disk. Little mass ($\sim 10^{-3} M_{\odot}$) is ejected during the merger.

Depending on the merging component masses, the central remnant can be a massive ($1.0\text{--}1.5 M_{\odot}$), highly magnetized ($10^9\text{--}10^{10}$ G) and fast rotating ($P = 1\text{--}10$ s) WD [3, 28].

Figure 1 shows a series of snapshots of the time evolution of a $0.8 + 0.6 M_{\odot}$ WD-WD merger obtained by an adapted version of the smoothed-particle-hydrodynamics (SPH) code Phantom [24, 25]. This simulation was run with 7×10^4 SPH particles. The newly-formed central WD has approximately $1.1 M_{\odot}$. The ejected mass has been estimated to be $1.2 \times 10^{-3} M_{\odot}$. The average velocity of the ejected particles is $\approx 10^8$ cm s $^{-1}$.

It is worth to mention that the above ejecta mass is also consistent with other independent merger simulations, e.g. Dan et al. [7], who showed that the amount of mass expelled in the merger can be obtained by the following fitting rational polynomial

$$m_{\text{ej}} = M \frac{0.0001807}{-0.01672 + 0.2463q - 0.6982q^2 + q^3}, \quad (2.1)$$

where $M = m_1 + m_2$ is the total binary mass and $q \equiv m_2/m_1 \leq 1$ is the binary mass-ratio. Indeed, for the present case with $M = 1.4 M_{\odot}$ and $q = 0.6/0.8$, the above formula gives $m_{\text{ej}} = 0.00128 M_{\odot}$.

Figure 2 shows the distribution of the SPH particles in the xy and xz planes of the system as well as a density plot, just after the merger. It can be appreciated a still dissipating spiral arm, the disk and the ejected particles. We show the unbound particles in red and the bound particles in blue. It can be seen that the outer part of the spiral arm is gravitationally unbound while the inner region is bound and will fallback onto the newly-formed WD. With a mass of $1.1 M_{\odot}$ the central WD has a radius of $R_{\text{WD}} \approx 5 \times 10^8$ cm $\lesssim 0.01 R_{\odot}$ (see e.g. [5]), while the disk is shown here up to $\approx 0.05 R_{\odot}$.

2.2 WD-WD merger rate

The WD-WD merger rate has been recently estimated to be $(1\text{--}80) \times 10^{-13}$ yr $^{-1} M_{\odot}^{-1}$ (at 2σ) and $(5\text{--}9) \times 10^{-13}$ yr $^{-1} M_{\odot}^{-1}$ (at 1σ) [17, 18]. For a Milky Way stellar mass $6.4 \times 10^{10} M_{\odot}$ and using an extrapolating factor of Milky Way equivalent galaxies, 0.016 Mpc $^{-3}$ [13], it leads to a local cosmic rate $(0.74\text{--}5.94) \times 10^6$ Gpc $^{-3}$ yr $^{-1}$ (2σ) and $(3.7\text{--}6.7) \times 10^5$ Gpc $^{-3}$ yr $^{-1}$ (1σ).

The above rate implies that (12–22)% of WD-WD mergers may end as type Ia SN. This is consistent with previously estimated rates of WD-WD mergers leading to SNe Ia (see e.g. [30]). We are here interested in the rest of the merger population not leading to Ia SNe.

2.3 Magnetic field of the central WD

The hot, rapidly rotating, convective corona can produce, via an efficient $\alpha\omega$ dynamo, magnetic fields of up to $B \approx 10^{10}$ G (see e.g. [9]). Recent two-dimensional magneto-hydrodynamic

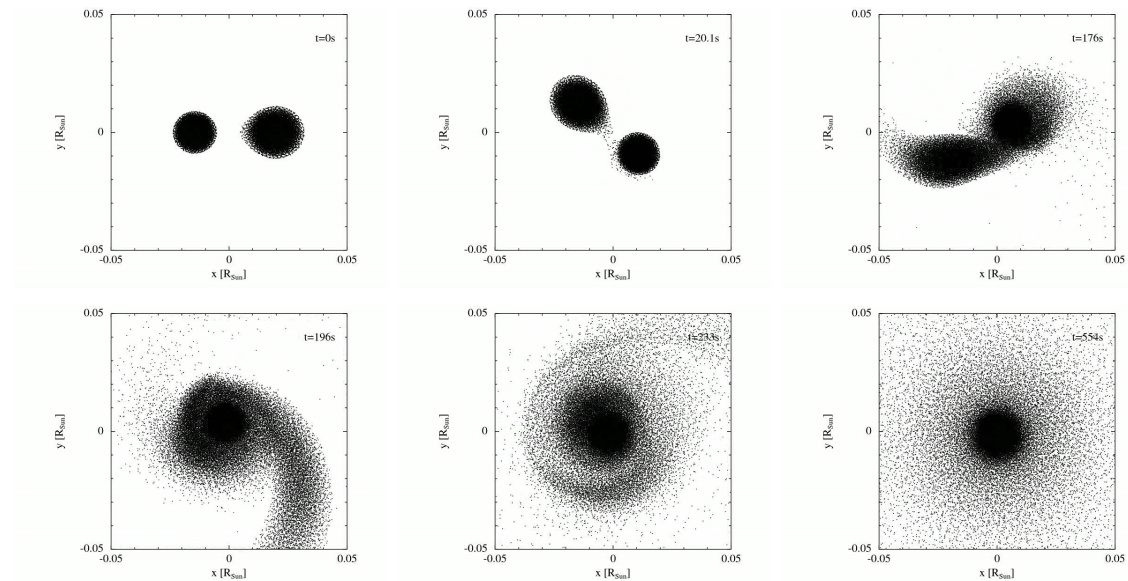


Figure 1. Snapshots of the time evolution of $0.8+0.6 M_{\odot}$ WD-WD merger from the SPH simulation with 7×10^4 particles. The newly-formed central WD has approximately $1.1 M_{\odot}$. In the sequence it can be seen how the secondary star is disrupted by Roche lobe overflow. Nearly half of the mass of the secondary star is transferred to the primary and the rest remains bound to the newly-formed central WD in form of a Keplerian disk. Little mass is ejected, in the present simulation nearly $1.2 \times 10^{-3} M_{\odot}$. These figures have been done using the visualization tool SPLASH [34].

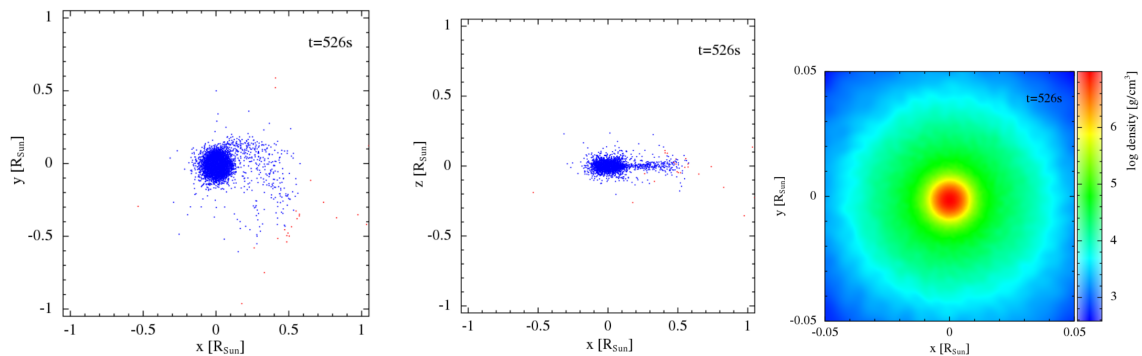


Figure 2. Left panel: distribution of the SPH particles in the xy plane just after the merger. We can see a still dissipating spiral arm, the disk and the ejected particles. Bound particles are shown in blue and unbound particles are shown in red. Center panel: same as in the left panel but for the xz plane. Right panel: density (in g cm^{-3}) plot in the xy plane. The central WD has a radius of $\approx 0.01 R_{\odot}$ while the disk is shown here up to $\approx 0.05 R_{\odot}$. These figures have been done using the visualization tool SPLASH [34].

simulations of post-merger systems confirm the growth of the WD magnetic field after the merger owing to the magneto-rotational instability [12, 33]. For a summary of the magnetic field configuration and its genesis in WD-WD mergers, as well as its role along with rotation in the aftermath of the dynamical mergers, see Becerra et al. [3].

3 Optical and infrared emission

The ejected matter m_{ej} moves with an initial velocity $v_{\text{ej},0}$ and we adopt for simplicity an evolving, uniform density profile

$$\rho_{\text{ej}} = \frac{3m_{\text{ej}}}{4\pi r_{\text{ej}}^3(t)}, \quad (3.1)$$

where $r_{\text{ej}}(t)$ is the ejecta radius.

The energy conservation equation is

$$\frac{dE}{dt} = -P \frac{dV}{dt} - L_{\text{rad}} + H, \quad (3.2)$$

where E is the energy, P the pressure, $V = (4\pi/3)r_{\text{ej}}^3$ is the volume, L_{rad} is the radiated energy and H is the heating source, namely the power injected into the ejecta. For the ejecta we adopt a radiation dominated equation of state, namely $E = 3PV$. The injected power H is represented by the rotational energy coming from the spindown of the WD and the fallback accretion onto the WD:

$$H = L_{\text{sd}} + L_{\text{fb}}. \quad (3.3)$$

We adopt the spindown power by a dipole magnetic field

$$L_{\text{sd}} = \frac{2}{3} \frac{B_d^2 R^6}{c^3} \omega^4, \quad (3.4)$$

where $\omega = 2\pi/P$ is the rotation angular velocity of the WD, P is the rotation period, B_d is the dipole field at the WD surface and R is the WD radius.

Our assumption of the pulsar-like emission as part of the injection power into the ejecta is supported by the analysis of section 4.1 where we show that the magnetic field values of interest are larger than the minimum magnetic field needed for it not to be buried by the accreted matter. This indeed agrees with the recent results of Becerra et al. [3] on the thermal and rotational evolution of the central, massive WD produced by a WD-WD merger accounting for the torque by accretion, propeller, magnetic field-disk interaction and magneto-dipole emission. There, the timescale on which each of these regimes dominates the evolution has been obtained and it is shown the emergence of the magneto-dipole emission already at very early times post-merger even for the highest possible accretion rates which are higher than the ones considered in the present work.

The fallback power can be parametrized by

$$L_{\text{fb}} = L_{\text{fb},0} \left(1 + \frac{t}{t_{\text{fb}}}\right)^{-n}, \quad (3.5)$$

where $L_{\text{fb},0}$ is the initial fallback luminosity, t_{fb} is the timescale on which the fallback power starts to follow a power-law behavior. This function fits the numerical results by Lorén-Aguilar et al. [15] of the luminosity produced by the fallback of material of the disrupted secondary which remained bound in highly eccentric orbits. The derivation of this luminosity follows the treatment of Rosswog [27]. The material interacts with the disk in a timescale set by the distribution of eccentricities and not by viscous dissipation. The energy released is calculated as the difference in the kinetic plus potential energy of the particles between the initial position and the debris disk (dissipation) radius (obtained from the SPH simulation).

Clearly, not all this energy can be released in form e.g. of photons to energize the ejecta so it has to be considered as an upper limit to the energy input from matter fallback.

Using eq. (3.5) we can also estimate the fallback accretion rate onto the WD as

$$\dot{m}_{\text{fb}} \approx \frac{L_{\text{fb}}}{GM_{\text{WD}}/R_{\text{WD}}}. \quad (3.6)$$

Since little energy is radiated (see below) by the system, namely it is highly adiabatic, we can assume the radius to evolve according to [21]

$$\frac{1}{2}m_{\text{ej}}v_{\text{ej}}^2 \approx \frac{1}{2}m_{\text{ej}}v_{\text{ej},0}^2 + \int_0^t H dt, \quad (3.7)$$

where $v_{\text{ej}} \equiv dr_{\text{ej}}/dt$ is the ejecta velocity. It is clear that in this most simple uniform density model under consideration this can be considered as a bulk average velocity. The density profile can have initially a radial dependence and in that case there would exist also a velocity profile with both faster and slower layers with respect to the unique one of our model.

Since the radiation travels on a photon diffusion timescale $t_{\text{ph}} = r_{\text{ej}}(1 + \tau_{\text{opt}})/c$, the radiated luminosity can be written as

$$L_{\text{rad}} = \frac{cE}{r_{\text{ej}}(1 + \tau_{\text{opt}})}, \quad (3.8)$$

where

$$\tau_{\text{opt}} = \kappa\rho_{\text{ej}}r_{\text{ej}}, \quad (3.9)$$

is the optical depth with κ the opacity. For the optical wavelengths and the composition of the merger ejecta we expect $\kappa \approx 0.1\text{--}0.2 \text{ cm}^2 \text{ g}^{-1}$. This is different from the higher opacity expected for r-process material composing the kilonova produced in NS-NS mergers.

The effective temperature of the observed blackbody radiation, T_{eff} , can be obtained as usual from the bolometric luminosity equation

$$L_{\text{rad}} = 4\pi r_{\text{ej}}^2 \sigma T_{\text{eff}}^4, \quad (3.10)$$

where σ is the Stefan-Boltzmann constant. Being thermal, the density flux at the Earth from a source located at a distance D is therefore

$$B_{\nu} = \frac{2\pi h\nu^3}{c^2} \frac{1}{\exp[h\nu/(kT_{\text{eff}})] - 1} \left(\frac{r_{\text{ej}}}{D}\right)^2, \quad (3.11)$$

where ν is the frequency.

The ejecta radius r_{ej} and effective temperature T_{eff} obtained from the cooling of the merger ejecta are shown in figure 3. Figure 4 shows the expected bolometric luminosity (left panel) as well as the corresponding expected density flux at Earth (right panel) in the optical and infrared, for a source at 10 kpc.

We have chosen fallback power parameters according to numerical simulations of WD-WD mergers (see e.g. section 5.3 and figure 8 in [15]): $L_{\text{fb},0} = 8.0 \times 10^{47} \text{ erg s}^{-1}$ and $t_{\text{fb}} = 10 \text{ s}$, and $n = 1.45$. For these parameters, it can be easily checked that the injection power from the WD spindown is negligible: even for a high field $B_d = 10^{10} \text{ G}$ and an initial (at $t = 0$) fast rotation period $P_0 = 5 \text{ s}$, we have $L_{\text{fb}} = 8.0 \times 10^{47} \text{ erg s}^{-1}$ and $L_{\text{sd}} = 9.6 \times 10^{40} \text{ erg s}^{-1}$, and for instance at $t = 1 \text{ day}$, $L_{\text{fb}} = 1.6 \times 10^{42} \text{ erg s}^{-1}$ and $L_{\text{sd}} = 9.6 \times 10^{40} \text{ erg s}^{-1}$ (the

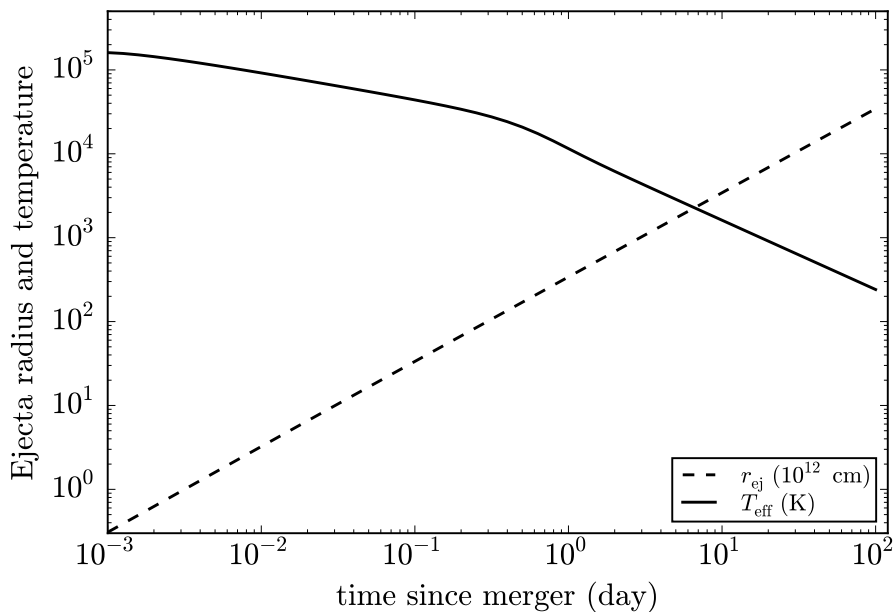


Figure 3. Expected evolution of the ejecta radius and effective temperature from the cooling of $1.3 \times 10^{-3} M_{\odot}$ ejecta heated by fallback accretion onto the newly-formed central WD.

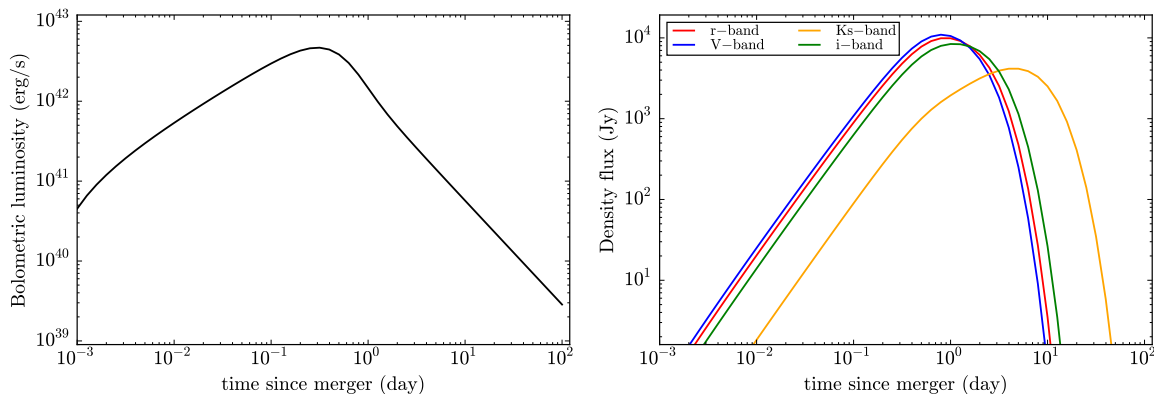


Figure 4. Left panel: expected bolometric luminosity from the cooling of $1.3 \times 10^{-3} M_{\odot}$ ejecta heated by fallback accretion onto the newly-formed central WD. Right panel: corresponding expected flux density at Earth in the optical and in the infrared for a source located at 10 kpc.

spindown timescale for these WD parameters is much longer than one day). Thus, the ejecta is essentially only fallback-powered, namely $H \approx L_{\text{fb}}$.

Again, it is important to check the consistency of our fallback parameters with independent simulations. Dan et al. [7] showed that the fallback mass is well fitted by

$$m_{\text{fb}} = M(0.07064 - 0.0648q), \quad (3.12)$$

which for our binary mass-ratio and total mass leads to $m_{\text{fb}} = 0.031 M_{\odot}$. The fallback accretion leads to an energy injection

$$E_{\text{fb}} = \int L_{\text{fb}} dt \approx \int \frac{GM_{\text{WD}}}{R_{\text{WD}}} \dot{m}_{\text{fb}} c^2 dt \approx \frac{GM_{\text{WD}}}{R_{\text{WD}}} m_{\text{fb}} c^2, \quad (3.13)$$

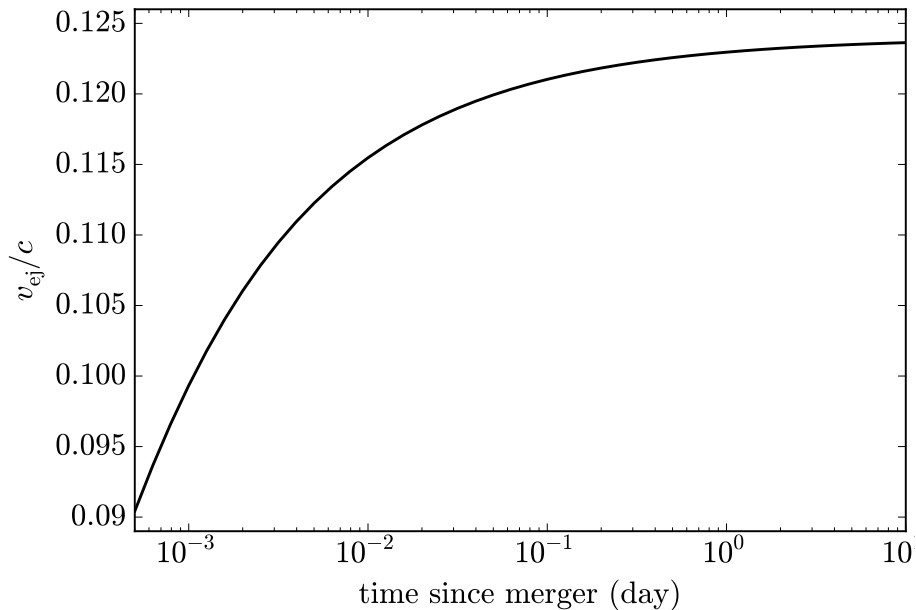


Figure 5. Time-evolution of the ejecta velocity obtained from the integration of eq. (3.7) accounting for the acceleration due to the presence of the heating source $H \approx L_{fb}$.

where m_{fb} is the fallback mass given by eq. (3.12). For our present case, $M_{WD} \approx 1.1 M_{\odot}$ and $R_{WD} \approx 5 \times 10^8$ cm, it leads to 1.79×10^{49} erg. This value has to be compared with the full integral $E_{fb} = \int L_{fb} dt \approx 1.78 \times 10^{49}$ erg, where L_{fb} is given by eq. (3.5). The above estimate not only cross-checks the amount of fallback mass as given independently by eqs. (3.6) and (3.12) but, at the same time, the mass and radius of the WD, as obtained from different simulations.

Since the ejecta are highly opaque at early times the fallback accretion and the spindown power are transformed into kinetic energy thereby increasing the expansion velocity of the ejecta; see eq. (3.7). The matter is ejected a few orbits (2–3) before the merger and start to move outward with an initial non-relativistic velocity $0.01 c$ typical of the WD escape velocity. In the present example, such ejecta is then accelerated to mildly relativistic velocities $0.1 c$ (see figure 5).

4 X-ray emission

The X-ray luminosity account for the absorption from the ejecta can be calculated as

$$L_X \approx \frac{1 - e^{-\tau_X}}{\tau_X} (L_{fb} + L_{sd}) \approx \frac{L_{fb} + L_{sd}}{1 + \tau_X}, \quad (4.1)$$

where τ_X is the optical depth of the X-rays through the ejecta (see e.g. [19]):

$$\tau_X = \kappa_X \rho_{ej} r_{ej}, \quad (4.2)$$

with κ_X the opacity to the X-rays which we assume to be dominated by bound-free electrons. For 1–10 keV photons it can be in the range 10^2 – 10^4 $\text{cm}^2 \text{g}^{-1}$ (see e.g. figure 4 in [20] and [31] for details), therefore for simplicity we here adopt a single value of $\kappa_X \approx 10^3$ $\text{cm}^2 \text{g}^{-1}$.

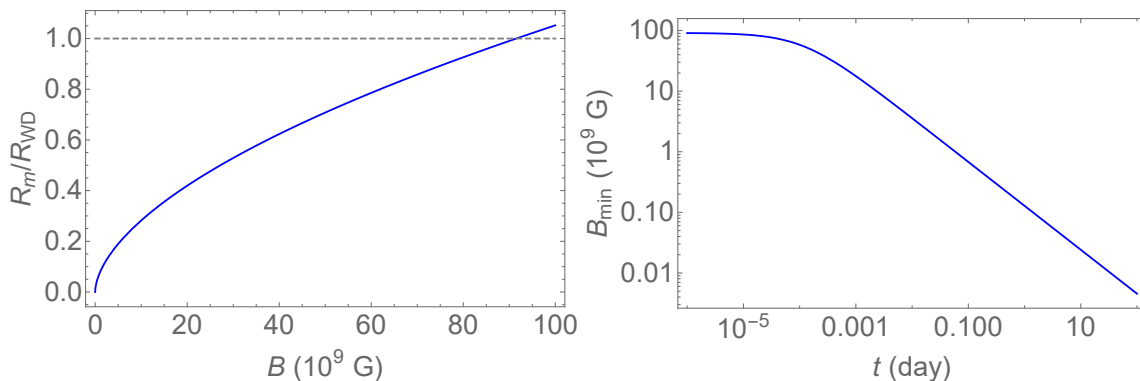


Figure 6. Left panel: magnetospheric to WD radii ratio as a function of the WD surface magnetic field for an accretion rate set to the fallback value at time $t = 0$ post-merger. Right panel: minimum magnetic field B_{min} needed to have $R_m > R_{WD}$, as a function of time, for the fallback accretion rate obtained from eq. (3.6). The mass and radius of the WD are $M_{WD} = 1.1M_{\odot}$ and $R_{WD} = 5 \times 10^8$ cm.

In the above general discussion we have assumed that the WD can behave as a pulsar due to its dipole magnetic field and injects energy into the ejecta at a rate given by the radiation power given by eq. (3.4). However, we have first to check whether the magnetic field of the WD can be buried by the fallback accretion.

4.1 Is the magnetic field buried?

The magnetic field is buried inside the star if the magnetospheric radius,

$$R_m = \left(\frac{B^2 R_{WD}^6}{\dot{m}_{fb} \sqrt{2GM_{WD}}} \right)^{2/7}, \quad (4.3)$$

is smaller than the WD radius, R_{WD} . Thus, using the value of \dot{m}_{fb} from eq. (3.6) we can compute the ratio R_m/R_{WD} and check if it is smaller or larger than unity.

The left panel of figure 6 shows this ratio for an accretion rate set to the fallback value at time $t = 0$ post-merger, while the right panel shows the value of the magnetic field for which $R_m = R_{WD}$, say B_{min} , as a function of time, for the fallback accretion rate given by eq. (3.6). B_{min} is the minimum value of the magnetic field that is not buried inside the star by the matter fallback. Therefore, for fields $B > B_{min}$ the WD can behave as a pulsar and it can inject energy into the ejecta at the expenses of the WD rotational energy.

4.2 Expected X-ray emission

Figure 7 shows the X-ray luminosity (4.1) in comparison with the late-time X-ray emission data of GRB170817A. The comparison is made for selected values of the magnetic field, B , and the initial rotation period of the WD, P_0 .

It can be seen that a good agreement with the X-ray data can be obtained. Although the fallback power dominates over the pulsar one, the agreement is improved by adding the presence of the WD-pulsar (spindown) component. It is clear from our plots that the current X-ray data is not yet sufficient to unambiguously identify the WD parameters since an agreement is obtained for different combinations of B and P_0 . This is to be expected due to the magnetic dipole power dependence on the ratio B^2/P^4 .

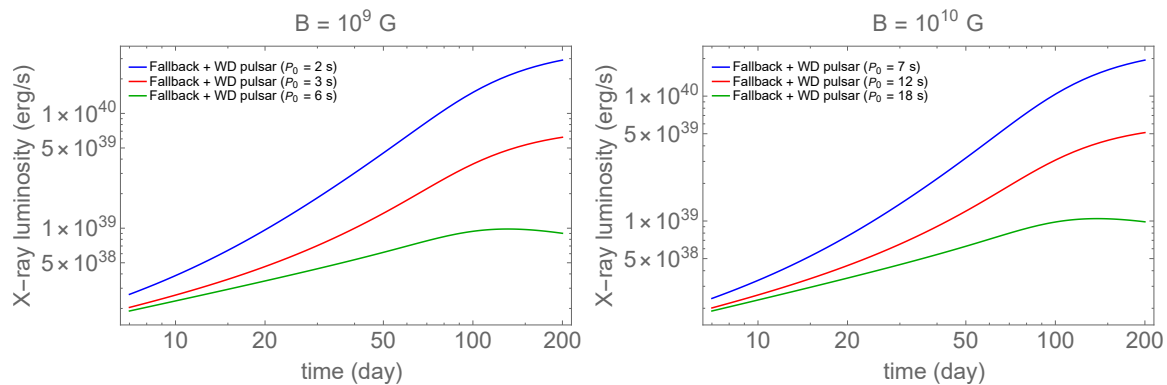


Figure 7. Expected X-ray luminosity calculated via eq. (4.1) for magnetic field values 10^9 G (left panel) and 10^{10} G (right panel).

4.3 WD-pulsar appearance

From the above analysis we can see that additional data from other wavelengths, or X-ray data at later times, are needed to have an unambiguous identification of the WD parameters. Thus, it is interesting to compute when the newly-formed WD is expected to appear as a pulsar-like object in the sky.

At the time of X-ray transparency, $t \sim 100$ – 150 day, the fallback power is still two orders of magnitude higher than the spindown one. However, at these post-merger timescales the fallback is fading continuously while the spindown power remains constant since, for the parameters in agreement with the current X-ray data (see figure 7), the spindown timescale is much longer. This implies that the WD can show up as a pulsar at a relatively early life of the post-merger system. To verify this we show in figure 8 the two components as a function of time after the X-ray transparency. At these times we can compare the unobserved luminosities given by eq. (3.5) and eq. (3.4) for the fallback and spindown power, respectively. It can be seen that in the two cases a deviation from the fallback power-law behavior to a less steep lightcurve decay appears at $t \gtrsim 500$ day. This is a predicted signature of the WD-pulsar presence. The precise crossing between the fallback power and the spindown component appears, in the case of $(B, P_0) = (10^9 \text{ G}, 6 \text{ s})$ and $(10^{10} \text{ G}, 18 \text{ s})$, at $t = 2318.3$ day (6.3 yr) and 2023.4 day (5.5 yr), respectively.

5 Gamma-ray emission

The energy observed in gamma-rays in GRB 170817A, $E_{\text{iso}} \approx 3 \times 10^{46}$ erg, can originate from flares owing to the twist and stress of the magnetic field lines during the merger process: a magnetic energy of 2×10^{46} erg is stored in a region of radius 10^9 cm and magnetic field of 10^{10} G [16]. Such a radius would imply a photon travel time of the order of $r/c \sim 0.1$ s, so a peak luminosity of few 10^{47} erg s $^{-1}$.

We are also currently exploring the temperature properties of the ejecta at the beginning of the expansion. The ejected matter might have temperatures of the order of 10^8 K at radii of 10^9 cm which could clearly give a luminosity of the order of $4\pi r^2 \sigma T^4 \approx 7 \times 10^{46}$ erg s $^{-1}$ with an energy peak of $\approx 3k_B T \approx 30$ keV, so observable as a hard X-ray (soft gamma-ray) emission. If the matter expands adiabatically and isotropically then the temperature would decrease as $T \propto R^{-1}$ (adopting radiation-dominated matter) and therefore it can rapidly

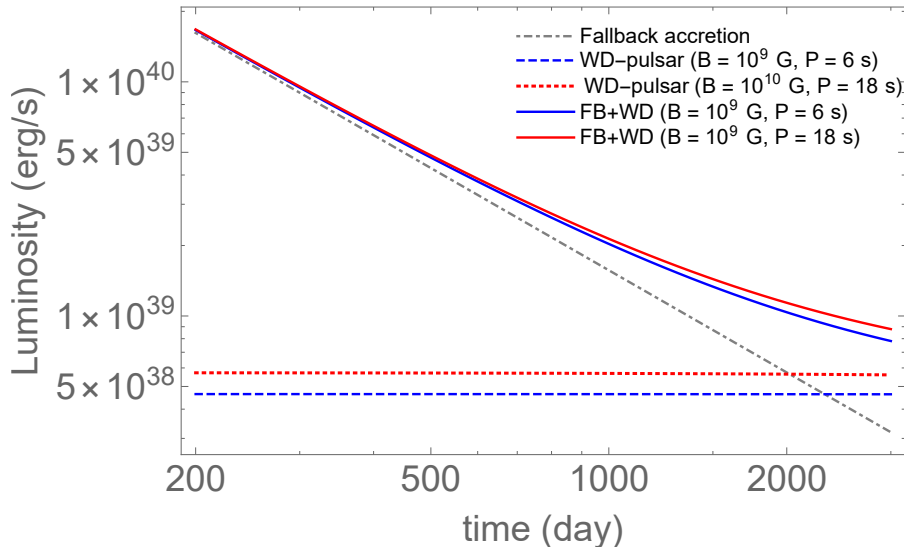


Figure 8. Fallback versus spindown emission at times after the X-ray transparency.

(in seconds timescale) fade to the soft X-rays to then become undetectable for the current X-ray satellites. The above makes the detection of this emission particularly difficult at early times post-merger. These issues are important by their own and deserve further analysis in dedicated forthcoming works.

6 Summary and conclusions

We have investigated the infrared, optical, X and gamma-ray emission associated with a WD-WD merger, the ejected matter and the post-merger signal from the newborn WD.

In view of the high magnetic fields involved in the merger, a prompt emission in the gamma-rays might occur as the result of magnetospheric flaring activity owing to the twist and magnetic stresses. For instance, the release of magnetic energy associated with a field of 10^{10} G in a region of radius 10^9 cm can lead to a total energy release of few 10^{46} erg in a burst of short (~ 0.1 – 1 s) duration with a peak luminosity of few 10^{47} erg s $^{-1}$.

We have modeled the time evolution of the ejecta as the expansion of a uniform density profile. We show our results for a fiducial case of a $0.6 + 0.8 M_{\odot}$ WD-WD merger leading to a central WD of $1.1 M_{\odot}$ and ejecta mass $\sim 10^{-3} M_{\odot}$. The latter start to move outward with initial bulk velocity $0.01 c$ and from a distance $\sim 10^9$ cm, typical of the escape velocity and radius from a WD-WD binary when the matter is ejected, i.e. 2–3 orbits before merger [15].

The cooling of the expanding ejecta, heated by the fallback accretion onto the WD (see section 3), results in a thermal emission observable in the infrared and in the optical. The bolometric luminosity associated with this thermal emission peaks with a value of 10^{41} – 10^{42} erg s $^{-1}$ about 0.5–1 day post-merger (see figure 4). We have shown that the ejecta initially expand at low, non-relativistic velocities $0.01 c$, to then being rapidly accelerated by the fallback energy injection to mildly-relativistic velocities of the order of $0.1 c$ (see figure 5).

The X-ray emission from the fallback accretion process (see section 4) emerges and peaks with a value of 10^{38} – 10^{39} erg s $^{-1}$ at 100–150 day post-merger (see figure 7). X-rays from the spindown power of the central WD become observable later at a time that depends on the WD parameters (see figure 8).

Once we have established for these systems their observable signatures across the electromagnetic spectrum and their nature, we can discuss some possibilities for their experimental identification. We have shown that the mass, rotation period and magnetic field of the newly-formed central WD are similar to the ones proposed in the WD model of soft gamma-repeaters (SGRs) and anomalous X-ray pulsars (AXPs) [16]. The merger rate is indeed enough to explain the Galactic population of SGRs/AXPs. Thus, if a WD-WD merger produced GRB 170817A-AT 2017gfo, an SGR/AXP (a WD-pulsar) may become observable in this sky position. As we have shown in section 5 (see figure 8), the identification of first instants of the appearance of the WD-pulsar will allow to establish the WD parameters.

In addition, it is remarkable that, as pointed out in [29] and here further scrutinized, a WD-WD merger and the evolution of the ejecta powered by fallback accretion onto the newborn WD, is able to produce observational features in the X and in the gamma-rays similar to the ones of GRB 170817A and in the infrared and in the optical similar to the ones of AT 2017gfo. The ejecta from a WD-WD merger are, nevertheless, different from the ejecta from a NS-NS merger in that: 1) they have a lighter nuclear composition and 2) they are powered by fallback accretion instead of the radioactive decay of r-process heavy nuclei. It is then clear that the spectroscopic identification of atomic species can discriminate between the two scenarios. However, such an identification has not been possible in any observed kilonovae since it needs accurate models of atomic spectra, nuclear reaction network, density profile, as well as radiative transport (opacity) which are not available at the moment.

Acknowledgments

JMBL thanks support from the FPU fellowship by Ministerio de Educación Cultura y Deporte from Spain. JAR is grateful to Elena Pian for the interesting discussions on kilonovae.

References

- [1] LIGO SCIENTIFIC, VIRGO, FERMI-GBM and INTEGRAL collaborations, *Gravitational Waves and Gamma-rays from a Binary Neutron Star Merger: GW170817 and GRB 170817A*, *Astrophys. J.* **848** (2017) L13 [[arXiv:1710.05834](#)] [[INSPIRE](#)].
- [2] I. Arcavi et al., *Optical emission from a kilonova following a gravitational-wave-detected neutron-star merger*, *Nature* **551** (2017) 64 [[arXiv:1710.05843](#)] [[INSPIRE](#)].
- [3] L. Becerra, J.A. Rueda, P. Loren-Aguilar and E. Garcia-Berro, *The Spin Evolution of Fast-Rotating, Magnetized Super-Chandrasekhar White Dwarfs in the Aftermath of White Dwarf Mergers*, *Astrophys. J.* **857** (2018) 134 [[arXiv:1804.01275](#)] [[INSPIRE](#)].
- [4] W. Benz, A.G.W. Cameron, W.H. Press and R.L. Bowers, *Dynamic mass exchange in doubly degenerate binaries. I — 0.9 and 1.2 solar mass stars*, *Astrophys. J.* **348** (1990) 647.
- [5] K. Boshkayev, J.A. Rueda, R. Ruffini and I. Siutsou, *On general relativistic uniformly rotating white dwarfs*, *Astrophys. J.* **762** (2013) 117 [[arXiv:1204.2070](#)] [[INSPIRE](#)].
- [6] P.S. Cowperthwaite et al., *The Electromagnetic Counterpart of the Binary Neutron Star Merger LIGO/Virgo GW170817. II. UV, Optical and Near-infrared Light Curves and Comparison to Kilonova Models*, *Astrophys. J.* **848** (2017) L17 [[arXiv:1710.05840](#)] [[INSPIRE](#)].
- [7] M. Dan, S. Rosswog, M. Brüggen and P. Podsiadlowski, *The structure and fate of white dwarf merger remnants*, *Mon. Not. Roy. Astron. Soc.* **438** (2014) 14 [[arXiv:1308.1667](#)] [[INSPIRE](#)].

- [8] M. Dan, S. Rosswog, J. Guillochon and E. Ramirez-Ruiz, *Prelude to a double degenerate merger: the onset of mass transfer and its impact on gravitational waves and surface detonations*, *Astrophys. J.* **737** (2011) 89 [[arXiv:1101.5132](#)] [[INSPIRE](#)].
- [9] E. Garcia-Berro et al., *Double degenerate mergers as progenitors of high-field magnetic white dwarfs*, *Astrophys. J.* **749** (2012) 25 [[arXiv:1202.0461](#)] [[INSPIRE](#)].
- [10] A. Goldstein et al., *An Ordinary Short Gamma-Ray Burst with Extraordinary Implications: Fermi-GBM Detection of GRB 170817A*, *Astrophys. J.* **848** (2017) L14 [[arXiv:1710.05446](#)] [[INSPIRE](#)].
- [11] J. Guerrero, E. García-Berro and J. Isern, *Smoothed Particle Hydrodynamics simulations of merging white dwarfs*, *Astron. Astrophys.* **413** (2004) 257.
- [12] S. Ji et al., *The Post-Merger Magnetized Evolution of White Dwarf Binaries: The Double-Degenerate Channel of Sub-Chandrasekhar Type Ia Supernovae and the Formation of Magnetized White Dwarfs*, *Astrophys. J.* **773** (2013) 136 [[arXiv:1302.5700](#)] [[INSPIRE](#)].
- [13] V. Kalogera, R. Narayan, D.N. Spergel and J.H. Taylor, *The Coalescence rate of double neutron star systems*, *Astrophys. J.* **556** (2001) 340 [[astro-ph/0012038](#)] [[INSPIRE](#)].
- [14] R. Longland, P. Lorén-Aguilar, J. José, E. García-Berro and L.G. Althaus, *Lithium production in the merging of white dwarf stars*, *Astron. Astrophys.* **542** (2012) A117 [[arXiv:1205.2538](#)] [[INSPIRE](#)].
- [15] P. Lorén-Aguilar, J. Isern and E. García-Berro, *High-resolution smoothed particle hydrodynamics simulations of the merger of binary white dwarfs*, *Astron. Astrophys.* **500** (2009) 1193.
- [16] M. Malheiro, J.A. Rueda and R. Ruffini, *SGRs and AXPs as Rotation-Powered Massive White Dwarfs*, *Publ. Astron. Soc. Jpn.* **64** (2012) 56.
- [17] D. Maoz and N. Hallakoun, *The binary fraction, separation distribution and merger rate of white dwarfs from SPY*, *Mon. Not. Roy. Astron. Soc.* **467** (2017) 1414 [[arXiv:1609.02156](#)] [[INSPIRE](#)].
- [18] D. Maoz, N. Hallakoun and C. Badenes, *The separation distribution and merger rate of double white dwarfs: improved constraints*, *Mon. Not. Roy. Astron. Soc.* **476** (2018) 2584 [[arXiv:1801.04275](#)] [[INSPIRE](#)].
- [19] R. Margutti et al., *The Binary Neutron Star Event LIGO/Virgo GW170817 160 Days after Merger: Synchrotron Emission across the Electromagnetic Spectrum*, *Astrophys. J.* **856** (2018) L18 [[arXiv:1801.03531](#)] [[INSPIRE](#)].
- [20] B.D. Metzger, *Kilonovae*, *Living Rev. Rel.* **20** (2017) 3 [[arXiv:1610.09381](#)] [[INSPIRE](#)].
- [21] B.D. Metzger and A.L. Piro, *Optical and X-ray emission from stable millisecond magnetars formed from the merger of binary neutron stars*, *Mon. Not. Roy. Astron. Soc.* **439** (2014) 3916 [[arXiv:1311.1519](#)] [[INSPIRE](#)].
- [22] M. Nicholl et al., *The Electromagnetic Counterpart of the Binary Neutron Star Merger LIGO/VIRGO GW170817. III. Optical and UV Spectra of a Blue Kilonova From Fast Polar Ejecta*, *Astrophys. J.* **848** (2017) L18 [[arXiv:1710.05456](#)] [[INSPIRE](#)].
- [23] E. Pian et al., *Spectroscopic identification of r-process nucleosynthesis in a double neutron star merger*, *Nature* **551** (2017) 67 [[arXiv:1710.05858](#)] [[INSPIRE](#)].
- [24] D.J. Price et al., *PHANTOM: Smoothed particle hydrodynamics and magnetohydrodynamics code*, Astrophysics Source Code Library (2017).
- [25] D.J. Price et al., *PHANTOM: A Smoothed Particle Hydrodynamics and Magnetohydrodynamics Code for Astrophysics*, *Publ. Astron. Soc. Austral.* **35** (2018) 31 [[arXiv:1702.03930](#)] [[INSPIRE](#)].

- [26] C. Raskin, E. Scannapieco, C. Fryer, G. Rockefeller and F.X. Timmes, *Remnants of Binary White Dwarf Mergers*, *Astrophys. J.* **746** (2012) 62 [[arXiv:1112.1420](#)].
- [27] S. Rosswog, *Fallback accretion in the aftermath of a compact binary merger*, *Mon. Not. Roy. Astron. Soc.* **376** (2007) L48 [[astro-ph/0611440](#)] [[INSPIRE](#)].
- [28] J.A. Rueda et al., *A white dwarf merger as progenitor of the anomalous X-ray pulsar 4U 0142+61?*, [arXiv:1306.5936](#) [[INSPIRE](#)].
- [29] J.A. Rueda et al., *GRB 170817A-GW170817-AT 2017gfo and the observations of NS-NS, NS-WD and WD-WD mergers*, *JCAP* **10** (2018) 006 [[arXiv:1802.10027](#)] [[INSPIRE](#)].
- [30] A.J. Ruiter, K. Belczynski and C.L. Fryer, *Rates and Delay Times of Type Ia Supernovae*, *Astrophys. J.* **699** (2009) 2026 [[arXiv:0904.3108](#)] [[INSPIRE](#)].
- [31] D.A. Verner, G.J. Ferland, K.T. Korista and D.G. Yakovlev, *Atomic data for astrophysics. 2. New analytic FITS for photoionization cross-sections of atoms and ions*, *Astrophys. J.* **465** (1996) 487 [[astro-ph/9601009](#)] [[INSPIRE](#)].
- [32] C. Zhu, P. Chang, M. van Kerkwijk and J. Wadsley, *A Parameter-Space Study of Carbon-Oxygen White Dwarf Mergers*, *Astrophys. J.* **767** (2013) 164 [[arXiv:1210.3616](#)] [[INSPIRE](#)].
- [33] C. Zhu, R. Pakmor, M.H. van Kerkwijk and P. Chang, *Magnetized moving mesh merger of a carbon-oxygen white dwarf binary*, *Astrophys. J. Lett.* **806** (2015) L1.
- [34] D.J. Price, *SPLASH: An Interactive Visualisation Tool for Smoothed Particle Hydrodynamics Simulations*, *Publ. Astron. Soc. Austral.* **24** (2007) 159 [[arXiv:0709.0832](#)].

Review

Induced Gravitational Collapse, Binary-Driven Hypernovae, Long Gamma-ray Bursts and Their Connection with Short Gamma-ray Bursts

J. A. Rueda ^{1,2,3,*}, R. Ruffini ^{1,2,4} and Y. Wang ^{1,2}¹ ICRA, Piazza della Repubblica 10, 65122 Pescara, Italy; ruffini@icra.it (R.R.); wangyu@me.com (Y.W.)² ICRA, Dipartimento di Fisica, Università di Roma Sapienza, Piazzale Aldo Moro 5, 00185 Rome, Italy³ INAF, Istituto de Astrofisica e Planetologia Spaziali, Via Fosso del Cavaliere 100, 00133 Rome, Italy⁴ INAF, Viale del Parco Mellini 84, 00136 Rome, Italy

* Correspondence: jorge.rueda@icra.it

Received: 25 February 2019; Accepted: 5 May 2019; Published: 9 May 2019



Abstract: There is increasing observational evidence that short and long Gamma-ray bursts (GRBs) originate in different subclasses, each one with specific energy release, spectra, duration, etc, and all of them with binary progenitors. The binary components involve carbon-oxygen cores (CO_{core}), neutron stars (NSs), black holes (BHs), and white dwarfs (WDs). We review here the salient features of the specific class of binary-driven hypernovae (BdHNe) within the induced gravitational collapse (IGC) scenario for the explanation of the long GRBs. The progenitor is a CO_{core} -NS binary. The supernova (SN) explosion of the CO_{core} , producing at its center a new NS (νNS), triggers onto the NS companion a hypercritical, i.e., highly super-Eddington accretion process, accompanied by a copious emission of neutrinos. By accretion the NS can become either a more massive NS or reach the critical mass for gravitational collapse with consequent formation of a BH. We summarize the results on this topic from the first analytic estimates in 2012 all the way up to the most recent three-dimensional (3D) smoothed-particle-hydrodynamics (SPH) numerical simulations in 2018. Thanks to these results it is by now clear that long GRBs are richer and more complex systems than thought before. The SN explosion and its hypercritical accretion onto the NS explain the X-ray precursor. The feedback of the NS accretion, the NS collapse and the BH formation produce asymmetries in the SN ejecta, implying the necessity of a 3D analysis for GRBs. The newborn BH, the surrounding matter and the magnetic field inherited from the NS, comprises the *inner engine* from which the GRB electron-positron (e^+e^-) plasma and the high-energy emission are initiated. The impact of the e^+e^- on the asymmetric ejecta transforms the SN into a hypernova (HN). The dynamics of the plasma in the asymmetric ejecta leads to signatures depending on the viewing angle. This explains the ultrarelativistic prompt emission in the MeV domain and the mildly-relativistic flares in the early afterglow in the X-ray domain. The feedback of the νNS pulsar-like emission on the HN explains the X-ray late afterglow and its power-law regime. All of the above is in contrast with a simple GRB model attempting to explain the entire GRB with the kinetic energy of an ultrarelativistic jet extending through all of the above GRB phases, as traditionally proposed in the “collapsar-fireball” model. In addition, BdHNe in their different flavors lead to νNS -NS or νNS -BH binaries. The gravitational wave emission drives these binaries to merge producing short GRBs. It is thus established a previously unthought interconnection between long and short GRBs and their occurrence rates. This needs to be accounted for in the cosmological evolution of binaries within population synthesis models for the formation of compact-object binaries.

Keywords: Gamma-ray Bursts; supernovae; accretion; Neutron Stars; Black Holes; binary systems

1. Introduction

1.1. The Quest for the Binary Nature of GRB Progenitors

We first recall that GRBs have been traditionally classified by a phenomenological division based on the duration of the time-interval in which the 90% of the total isotropic energy in Gamma-rays is emitted, the T_{90} . Long GRBs are those with $T_{90} > 2$ s and short GRBs the sources with $T_{90} < 2$ s [1–5].

In the case of short bursts, rapid consensus was reached in the scientific community that they could be the product of mergers of NS-NS and/or NS-BH binaries (see e.g., the pioneering works [6–9]). We shall return on this issue below by entering into the description of their properties and also to introduce additional mergers of compact-star object binaries leading to short bursts.

For long bursts, possibly the most compelling evidence of the necessity of a binary progenitor comes from the systematic and spectroscopic analysis of the GRBs associated with SNe, the so-called GRB-SNe, started with the pioneering discovery of the spatial and temporal concomitance of GRB 980425 [10] and SN 1998bw [11]. Soon after, many associations of other nearby GRBs with type Ib/c SNe were evidenced (see e.g., [12,13]).

There are models in the literature attempting an explanation of both the SN and the GRB within the same astrophysical system. For instance, GRBs have been assumed to originate from a violent SN from the collapse of a massive and fast rotating star, a “collapsar” [14]. A very high rotating rate of the star is needed to produce a collimated, jet emission. This traditional picture adopts for the GRB dynamics the “fireball” model based on the existence of a single ultrarelativistic collimated jet [15–19]. There is a vast literature devoted to this “traditional” approach and we refer the reader to it for additional details (see, e.g., [20–25], and references therein).

Nevertheless, it is worth to mention here some of the most important drawbacks of the aforementioned “traditional” approach and which has motivated the introduction of an alternative model, based on a binary progenitor, for the explanation of long GRBs:

- SNe Ic as the ones associated with GRBs lack hydrogen and helium in their spectra. It has been recognized that they most likely originate in helium stars, CO_{core} , or Wolf-Rayet stars, that have lost their outermost layers (see e.g., [26], and references therein). The pre-SN star, very likely, does not follow a single-star evolution but it belongs to a tight binary with a compact star companion (e.g., a NS). The compact star strips off the pre-SN star outermost layers via binary interactions such as mass-transfer and tidal effects (see e.g., [26–30]).
- Denoting the beaming angle by θ_j , to an observed isotropic energy E_{iso} it would correspond to a reduced intrinsic source energy released $E_s = f_b E_{\text{iso}} < E_{\text{iso}}$, where $f_b = (1 - \cos \theta_j) \sim \theta_j^2/2 < 1$. Extremely small beaming factors $f_b \sim 1/500$ (i.e., $\theta_j \sim 1^\circ$) are inferred to reduce the observed energetics of $E_{\text{iso}} \sim 10^{54}$ erg to the expected energy release by such a scenario $\sim 10^{51}$ erg [31]. However, the existence of such extremely narrow beaming angles have never been observationally corroborated [32–34].
- An additional drawback of this scenario is that it implies a dense and strong wind-like circumburst medium (CBM) in contrast with the one observed in most GRBs (see e.g., [35]). Indeed, the average CBM density inferred from GRB afterglows is of the order of 1 baryon per cubic centimeter [36]. The baryonic matter component in the GRB process is represented by the so-called baryon load [37]. The GRB e^+e^- plasma should engulf a limited amount of baryons in order to be able to expand at ultrarelativistic velocities with Lorentz factors $\Gamma \gtrsim 100$ as requested by the observed non-thermal component in the prompt Gamma-ray emission spectrum [16–18]. The amount of baryonic mass M_B is thus limited by the prompt emission to a maximum value of the baryon-load parameter, $B = M_B c^2 / E_{e^+e^-} \lesssim 10^{-2}$, where $E_{e^+e^-}$ is the total energy of the e^+e^- plasma [37].
- GRBs and SNe have markedly different energetics. SNe emit energies in the range 10^{49} – 10^{51} erg, while GRBs emit in the range 10^{49} – 10^{54} erg. Thus, the origin of GRB energetics point to the gravitational collapse to a stellar-mass BH. The SN origin points to evolutionary stages of a massive

star leading to a NS or to a complete disrupting explosion, but not to a BH. The direct formation of a BH in a core-collapse SN is currently ruled out by the observed masses of pre-SN progenitors, $\lesssim 18 M_{\odot}$ [38]. It is theoretically known that massive stars with such a relatively low mass do not lead to a direct collapse to a BH (see [38,39] for details).

- It was recently shown in [40] that the observed thermal emission in the X-ray flares present in the early (rest-frame time $t \sim 10^2$ s) afterglow implies an emitter of size $\sim 10^{12}$ cm expanding at mildly-relativistic velocity, e.g., $\Gamma \lesssim 4$. This is clearly in contrast with the “collapsar-fireball” scenario in which there is an ultrarelativistic emitter (the jet) with $\Gamma \sim 10^2\text{--}10^3$ extending from the prompt emission all the way to the afterglow.

Therefore, it seems most unlikely that the GRB and the SN can originate from the same single-star progenitor. Following this order of ideas, it was introduced for the explanation of the spatial and temporal coincidence of the two phenomena the concept of *induced gravitational collapse* (IGC) [41,42]. Two scenarios for the GRB-SN connection have been addressed: Ruffini et al. [41] considered that the GRB was the trigger of the SN. However, for this scenario to happen it was shown that the companion star had to be in a very fine-tuned phase of its stellar evolution [41]. Ruffini et al. [42] proposed an alternative scenario in a compact binary: the explosion of a Ib/c SN triggering an accretion process onto a NS companion. The NS, reaching the critical mass value, gravitationally collapses leading to the formation of a BH. The formation of the BH consequently leads to the emission of the GRB. Much more about this binary scenario has been discovered since its initial proposal; its theoretical studies and the search for its observational verification have led to the formulation of a much rich phenomenology which will be the main subject of this article.

Therefore, both short and long GRBs appear to be produced by binary systems, well in line with the expectation that most massive stars belong to binary systems (see, e.g., [43,44], and references therein). The increasing amount and quality of the multiwavelength data of GRBs have revealed the richness of the GRB phenomenon which, in a few seconds, spans different regimes from X-ray precursors to the Gamma-rays of the prompt emission, to the optical and X-rays of the early and late afterglow, to the optical emission of the associated SNe and, last but not least, the presence or absence of high-energy GeV emission. This, in addition to the multiyear effort of reaching a comprehensive theoretical interpretation of such regimes, have lead to the conclusion that GRBs separate into subclasses, each with specific energy release, spectra, duration, among other properties and, indeed, all with binary progenitors [45–49].

1.2. GRB Subclasses

Up to 2017 we had introduced seven GRB subclasses summarized in Table 1. In addition, we have recently introduced in [50,51] the possibility of a further GRB subclass produced by WD-WD mergers. We now give a brief description of all the GRB subclasses identified. In [49] we have renominated the GRB subclasses introduced in [45] and in [50,51], and inserted them into two groups: binary-driven hypernovae (BdHNe) and compact-object binary mergers. Below we report both the old and the new names to facilitate the reader when consulting our works prior to [49].

- X-ray flashes (XRFs).** These systems have CO_{core} -NS binary progenitors in which the NS companion does not reach the critical mass for gravitational collapse [52,53]. In the SN explosion, the binary might or might not be disrupted depending on the mass loss and/or the kick imparted [54]. Thus XRFs lead either to two NSs ejected by the disruption, or to binaries composed of a newly-formed $\sim 1.4\text{--}1.5 M_{\odot}$ NS (hereafter ν NS) born at the center of the SN, and a massive NS (MNS) which accreted matter from the SN ejecta. Some observational properties are: Gamma-ray isotropic energy $E_{\text{iso}} \lesssim 10^{52}$ erg, rest-frame spectral peak energy $E_{p,i} \lesssim 200$ keV and a local observed rate of $\rho_{\text{XRF}} = 100^{+45}_{-34} \text{ Gpc}^{-3} \text{ yr}^{-1}$ [45]. We refer the reader to Table 1 and [45,47] for further details on this class. In [49], this class has been divided into BdHN type II, the sources with $10^{50} \lesssim E_{\text{iso}} \lesssim 10^{52}$ erg, and BdHN type III, the sources with $10^{48} \lesssim E_{\text{iso}} \lesssim 10^{50}$ erg.

- ii. **Binary-driven hypernovae (BdHNe).** Originate in compact CO_{core}-NS binaries where the accretion onto the NS becomes high enough to bring it to the point of gravitational collapse, hence forming a BH. We showed that most of these binaries survive to the SN explosion owing to the short orbital periods ($P \sim 5$ min) for which the mass loss cannot be considered as instantaneous, allowing the binary to keep bound even if more than half of the total binary mass is lost [55]. Therefore, BdHNe produce ν NS-BH binaries. Some observational properties are: $E_{\text{iso}} \gtrsim 10^{52}$ erg, $E_{p,i} \gtrsim 200$ keV and a local observed rate of $\rho_{\text{BdHN}} = 0.77^{+0.09}_{-0.08} \text{ Gpc}^{-3} \text{ yr}^{-1}$ [45]. We refer the reader to Table 1 and [45,47] for further details on this class. In [49] this class has been renominated as BdHN type I.
- iii. **BH-SN.** These systems originate in CO_{core} (or Helium or Wolf-Rayet star)-BH binaries, hence the hypercritical accretion of the SN explosion of the CO_{core} occurs onto a BH previously formed in the evolution path of the binary. They might be the late evolutionary stages of X-ray binaries such as Cyg X-1 [56,57], or microquasars [58]. Alternatively, they can form following the evolutionary scenario XI in [59]. If the binary survives to the SN explosion BH-SNe produce ν NS-BH, or BH-BH binaries when the central remnant of the SN explosion collapses directly to a BH (see, although, [38,39]). Some observational properties are: $E_{\text{iso}} \gtrsim 10^{54}$ erg, $E_{p,i} \gtrsim 2$ MeV and an upper limit to their rate is $\rho_{\text{BH-SN}} \lesssim \rho_{\text{BdHN}} = 0.77^{+0.09}_{-0.08} \text{ Gpc}^{-3} \text{ yr}^{-1}$, namely the estimated observed rate of BdHNe type I which by definition covers systems with the above E_{iso} and $E_{p,i}$ range [45]. We refer the reader to Table 1 and [45,47] for further details on this class. In [49] this class has been renominated as BdHN type IV.

Table 1. Summary of the Gamma-ray bursts (GRB) subclasses. This table is an extended version of the one presented in [49] with the addition of a column showing the local density rate, and it also updates the one in [45,47]. We unify here all the GRB subclasses under two general names, BdHNe and BMs. Two new GRB subclasses are introduced; BdHN Type III and BM Type IV. In addition to the subclass name in “Class” column and “Type” column, as well as the previous names in “Previous Alias” column, we report the number of GRBs with known redshift identified in each subclass updated by the end of 2016 in “number” column (the value in a bracket indicates the lower limit). We recall as well the “in-state” representing the progenitors and the “out-state” representing the outcomes, as well as the the peak energy of the prompt emission, $E_{p,i}$, the isotropic Gamma-ray energy, E_{iso} defined in the 1 keV to 10 MeV energy range, the isotropic emission of ultra-high energy photons, $E_{\text{iso,Gev}}$, defined in the 0.1–100 GeV energy range, and the local observed rate ρ_{GRB} [45]. We adopt as definition of kilonova a phenomenon more energetic than a nova (about 1000 times). A kilonova can be an infrared-optical counterpart of a NS-NS merger. In that case the transient is powered by the energy release from the decay of r-process heavy nuclei processed in the merger ejecta [60–63]. FB-KN stands for fallback-powered kilonova [50,51]: a WD-WD merger can emit an infrared-optical transient, peaking at ~ 5 day post-merger, with the ejecta powered by accretion of fallback matter onto the newborn WD formed in the merger. The density rate of the GRB subclasses BdHN III (HN) and BM IV (FB-KN) have not yet been estimated.

Class	Type	Previous Alias	Number	In-State	Out-State	$E_{p,i}$ (MeV)	E_{iso} (erg)	$E_{\text{iso,Gev}}$ (erg)	ρ_{GRB} ($\text{Gpc}^{-3} \text{ yr}^{-1}$)
Binary-driven hypernova (BdHN)	I	BdHN	329	CO _{core} -NS	ν NS-BH	$\sim 0.2-2$	$\sim 10^{52}-10^{54}$	$\gtrsim 10^{52}$	$0.77^{+0.09}_{-0.08}$
	II	XRF	(30)	CO _{core} -NS	ν NS-NS	$\sim 0.01-0.2$	$\sim 10^{50}-10^{52}$	–	100^{+45}_{-34}
	III	HN	(19)	CO _{core} -NS	ν NS-NS	~ 0.01	$\sim 10^{48}-10^{50}$	–	–
	IV	BH-SN	5	CO _{core} -BH	ν NS-BH	$\gtrsim 2$	$> 10^{54}$	$\gtrsim 10^{53}$	$\lesssim 0.77^{+0.09}_{-0.08}$
Binary Merger (BM)	I	S-GRF	18	NS-NS	MNS	$\sim 0.2-2$	$\sim 10^{49}-10^{52}$	–	$3.6^{+1.4}_{-1.0}$
	II	S-GRB	6	NS-NS	BH	$\sim 2-8$	$\sim 10^{52}-10^{53}$	$\gtrsim 10^{52}$	$(1.9^{+1.8}_{-1.1}) \times 10^{-3}$
	III	GRF	(1)	NS-WD	MNS	$\sim 0.2-2$	$\sim 10^{49}-10^{52}$	–	$1.02^{+0.71}_{-0.46}$
	IV	FB-KN	(1)	WD-WD	NS/MWD	< 0.2	$< 10^{51}$	–	–
	V	U-GRB	(0)	NS-BH	BH	$\gtrsim 2$	$> 10^{52}$	–	$\approx 0.77^{+0.09}_{-0.08}$

We proceed with the short bursts which are amply thought to originate from compact-object binary mergers (BMs). First, we discuss the traditionally proposed BMs namely NS-NS and/or NS-BH mergers [6–9,24,64–66]. These BMs can be separated into three subclasses [45,55,67]:

- iv. **Short Gamma-ray flashes (S-GRFs).** They are produced by NS-NS mergers leading to a MNS, namely when the merged core does not reach the critical mass of a NS. Some observational properties are: $E_{\text{iso}} \lesssim 10^{52}$ erg, $E_{p,i} \lesssim 2$ MeV and a local observed rate of $\rho_{\text{S-GRF}} = 3.6_{-1.0}^{+1.4} \text{ Gpc}^{-3} \text{ yr}^{-1}$ [45]. We refer the reader to Table 1 and [45,47] for further details on this class. In [49] this class has been renominated as BM type I.
- v. **Authentic short GRBs (S-GRBs).** They are produced by NS-NS mergers leading to a BH, namely when the merged core reaches the critical mass of a NS, hence it forms a BH as a central remnant [67–69]. Some observational properties are: $E_{\text{iso}} \gtrsim 10^{52}$ erg, $E_{p,i} \gtrsim 2$ MeV and a local observed rate of $\rho_{\text{S-GRB}} = (1.9_{-1.1}^{+1.8}) \times 10^{-3} \text{ Gpc}^{-3} \text{ yr}^{-1}$ [45]. We refer the reader to Table 1 and [45,47] for further details on this class. In [49] this class has been renominated as BM type II.
- vi. **Ultra-short GRBs (U-GRBs).** This is a theoretical GRB subclass subjected for observational verification. U-GRBs are expected to be produced by ν NS-BH mergers whose binary progenitors can be the outcome of BdHNe type I (see II above) or of BdHNe type IV (BH-SN; see III above). The following observational properties are expected: $E_{\text{iso}} \gtrsim 10^{52}$ erg, $E_{p,i} \gtrsim 2$ MeV and a local observed rate similar to the one of BdHNe type I since we have shown that most of them are expected to remain bound [55], i.e., $\rho_{\text{U-GRB}} \approx \rho_{\text{BdHN}} = 0.77_{-0.08}^{+0.09} \text{ Gpc}^{-3} \text{ yr}^{-1}$ [45]. We refer the reader to Table 1 and [45,47] for further details on this class. In [49] this class has been renominated as BM type V.

Besides the existence of the above three subclasses of long bursts and three subclasses of short bursts in which the presence of NSs plays a fundamental role, there are two subclasses of bursts in which there is at least a WD component.

- vii. **Gamma-ray flashes (GRFs).** These sources show an extended and softer emission, i.e., they have hybrid properties between long and short bursts and have no associated SNe [70]. It has been proposed that they are produced by NS-WD mergers [45]. These binaries are expected to be very numerous [71] and a variety of evolutionary scenarios for their formation have been proposed [72–75]. GRFs form a MNS and not a BH [45]. Some observational properties are: $10^{51} \lesssim E_{\text{iso}} \lesssim 10^{52}$ erg, $0.2 \lesssim E_{p,i} \lesssim 2$ MeV and a local observed rate of $\rho_{\text{GRF}} = 1.02_{-0.46}^{+0.71} \text{ Gpc}^{-3} \text{ yr}^{-1}$ [45]. It is worth noting that this rate is low with respect to the one expected from the current number of known NS-WD in the Galaxy [71]. From the GRB observations only one NS-WD merger has been identified (GRB 060614 [76]). This implies that most NS-WD mergers are probably under the threshold of current X and Gamma-ray instruments. We refer the reader to Table 1 and [45,47] for further details on this class. In [49] this class has been renominated as BM type III.
- viii. **Fallback kilonovae (FB-KNe).** This is a recently introduced GRB subclass having as progenitors WD-WD mergers [50,51]. The WD-WD mergers of interest are those that do not produce type Ia SNe but that lead to a massive ($M \sim 1 M_{\odot}$), fast rotating ($P \sim 1\text{--}10$ s), highly-magnetized ($B \sim 10^9\text{--}10^{10}$ G) WD. Some observational properties are: $E_{\text{iso}} \lesssim 10^{51}$ erg, $E_{p,i} \lesssim 2$ MeV and a local observed rate $\rho_{\text{FB-KN}} = (3.7\text{--}6.7) \times 10^5 \text{ Gpc}^{-3} \text{ yr}^{-1}$ [50,51,77,78]. The coined name FB-KN is due to the fact that they are expected to produce an infrared-optical transient by the cooling of the ejecta expelled in the dynamical phase of the merger and heated up by fallback accretion onto the newly-formed massive WD.

The density rates for all GRB subclasses have been estimated assuming no beaming [45,47,50,51]. The GRB density rates have been analyzed in [45] following the method suggested in [79].

1.3. The Specific Case of BdHNe

We review in this article the specific case of BdHNe type I and II. As we have mentioned, the progenitor system is an exploding CO_{core} as a type Ic SN in presence of a NS companion [45,49]. Figure 1 shows a comprehensive summary of the binary path leading to this variety of compact

binaries that are progenitors of the above subclasses of long GRBs and that, at the same time, have an intimate connection with the short GRBs.

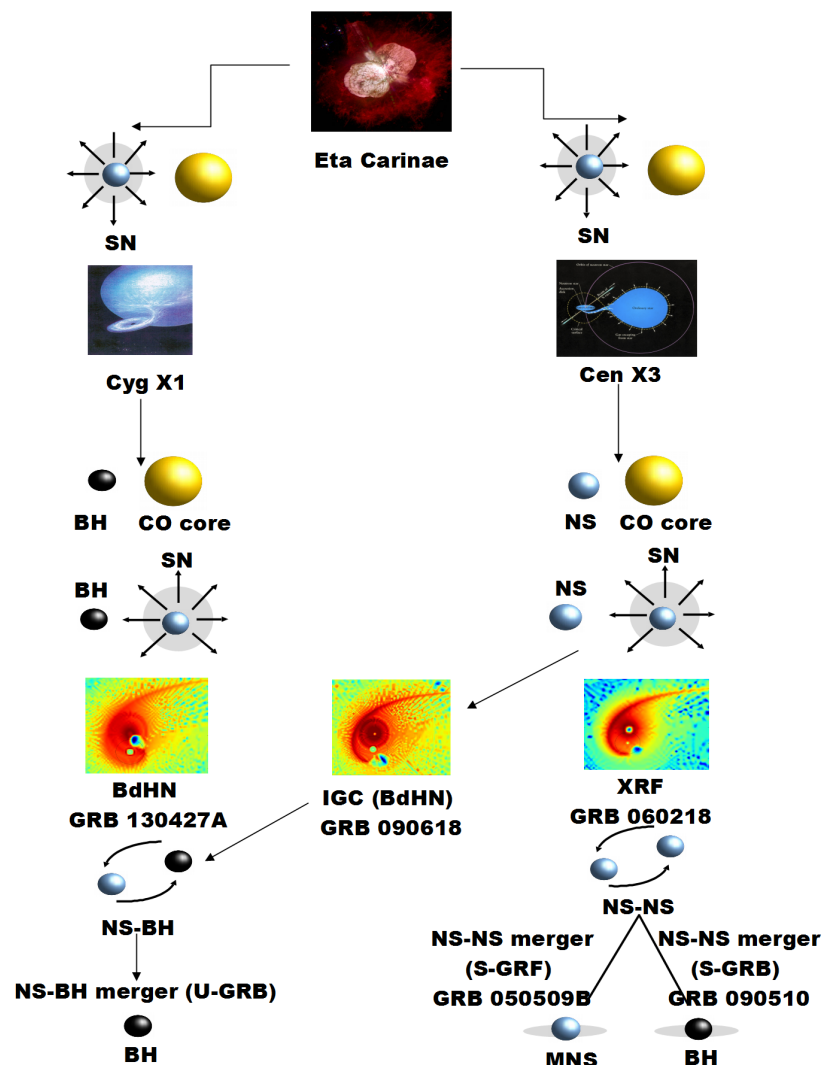


Figure 1. Taken from Figure 1 in [80]. Binary evolutionary paths leading to BdHNe I (previously named BdHNe) and II (previously named XRFs) and whose out-states, in due time, evolve into progenitors of short GRBs. The massive binary has to survive two core-collapse SN events. The first event forms a NS (right-side path) or BH (left-side path). The massive companion continues its evolution until it forms a CO_{core}. This simplified evolution diagram which does not show intermediate stages such as common-envelope phases (see e.g., [53,55], and references therein). At this stage the binary is a CO_{core}-NS (right-side path) or a CO_{core}-BH (left-side path). Then, it occurs the second SN event which forms what we call the ν NS at its center. We focus in this article to review the theoretical and observational aspects of interaction of this SN event with the NS companion (BdHNe I and II). We do not treat here the case of a SN exploding in an already formed BH companion (BdHNe IV). At this point the system can form a ν NS-BH/NS (BdHN I/II) binary (right-side path), or a ν NS-BH (BdHN IV) in the (left-side path). The emission of gravitational waves will make this compact-object binaries to merge, becoming progenitors of short GRBs [55]. We recall to the reader that S-GRBs and S-GRFs stand for, respectively, authentic short GRBs and short Gamma-ray flashes, the two subclasses of short bursts from NS-NS mergers, the former produced when the merger leads to a more massive NS and the latter when a BH is formed [45].

We emphasize on the theoretical framework concerning the CO_{core}-NS binaries which have been extensively studied by our group in a series of publications [52,53,55,81–83]. The CO_{core} explodes as

SN producing an accretion process onto the NS. For sufficiently compact binaries, e.g., orbital periods of the order of few minutes, the accretion is highly super-Eddington (hypercritical) leading to the possibility of the IGC of the NS once it reaches the critical mass, and forms a BH (see Figure 2).

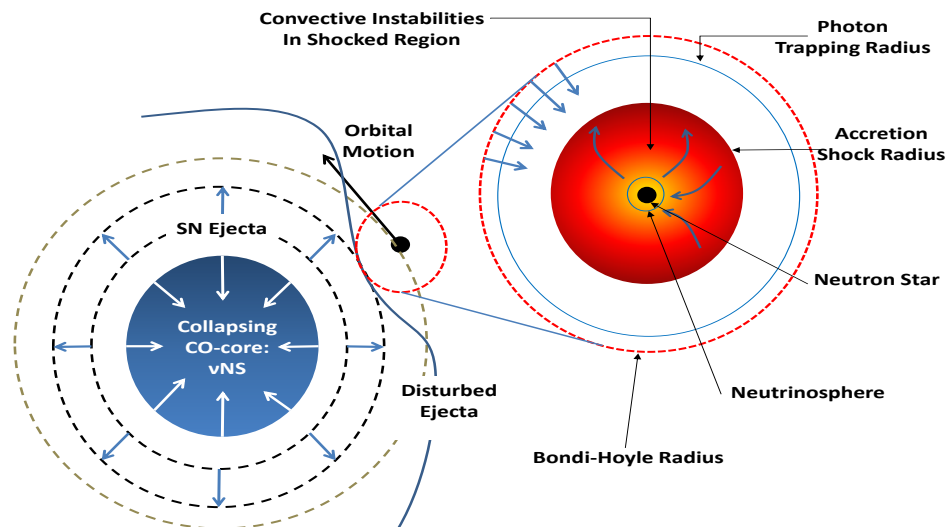


Figure 2. Scheme of the induced gravitational collapse (IGC) scenario (taken from Figure 1 in [83]). The CO_{core} undergoes supernova (SN) explosion, the neutron star (NS) accretes part of the SN ejecta and then reaches the critical mass for gravitational collapse to a black hole (BH), with consequent emission of a GRB. The SN ejecta reach the NS Bondi-Hoyle radius and fall toward the NS surface. The material shocks and decelerates while it piles over the NS surface. At the neutrino emission zone, neutrinos take away most of the gravitational energy gained by the matter infall. The neutrinos are emitted above the NS surface that allow the material to reduce its entropy to be finally incorporated to the NS. For further details and numerical simulations of the above process see [52,53,83].

If the binary is not disrupted by the explosion, BdHNe produces new binaries composed of a new NS (νNS) formed at the center of the SN, and a more massive NS or a BH companion (see Figure 1).

In the case of BH formation, the rotation of the BH together with the presence of the magnetic field inherited from the NS and the surrounding matter conform to what we have called the *inner engine* of the high-energy emission [84–87]. The electromagnetic field of the engine is mathematically described by the Wald solution [88]. The above ingredients induce an electric field around the BH which under the BdHN conditions is initially overcritical, creating electron-positron (e^+e^-) pair plasma which self-accelerates to ultrarelativistic velocities and whose transparency explains to the GRB prompt emission in Gamma-rays. The electric field is also able to accelerate protons which along the rotation axis lead to ultra high-energy cosmic rays (UHECRs) of up to 10^{21} eV. In the other directions the acceleration process lead to proton-synchrotron radiation which explains the GeV emission [84,85]. The interaction/feedback of the GRB into the SN makes it become the hypernova (HN) [89,90] observed in the optical, powered by nickel decay, a few days after the GRB trigger. The SN shock breakout and the hypercritical accretion can be observed as X-ray precursors [52]. The e^+e^- feedback onto the SN ejecta also produces gamma- and X-ray flares observed in the early afterglow [40]. The synchrotron emission by relativistic electrons from the νNS in the expanding magnetized HN ejecta and the νNS pulsar emission explain the early and late X-ray afterglow [91].

The article is organized as follows. In Section 2 we summarized following a chronological order the (1D, 2D and 3D) numerical simulations of BdHNe up to the year 2016, mentioning their salient features. A detailed explanation of the main ingredients of the calculations (equations of motion, accretion modeling, NS evolution equations, critical mass, accretion-zone hydrodynamics, neutrino emission and accretion energy release) can be found in Section 3. The most recent 3D smoothed-particle-hydrodynamics (SPH) numerical simulations of 2018 are presented in Section 4.

Section 5 is devoted to the consequences on these simulations on the analysis and interpretation of the GRB multiwavelength data. In Section 6 we present an analysis of the binary gravitational binding of BdHNe progenitors, so it is shown that most BdHNe type I are expected to be NS-BH binaries. The cosmological evolutionary scenario leading to the formation of BdHN, their occurrence rate and connection with short GRBs is presented in Section 7.

We show in Table 2 a summary of acronyms used in this work.

Table 2. Acronyms used in this work in alphabetical order.

Extended Wording	Acronym
Binary-driven hypernova	BdHN
Black hole	BH
Carbon-oxygen core	CO _{core}
Gamma-ray burst	GRB
Gamma-ray flash	GRF
Induced gravitational collapse	IGC
Massive neutron star	MNS
Neutron star	NS
New neutron star created in the SN explosion	ν NS
Short Gamma-ray burst	S-GRB
Short Gamma-ray flash	S-GRF
Supernova	SN
Ultrashort Gamma-ray burst	U-GRB
Ultra high-energy cosmic ray	UHECR
White dwarf	WD
X-ray flash	XRF

2. A Chronological Summary of the IGC Simulations: 2012–2016

2.1. First Analytic Estimates

The IGC scenario was formulated in 2012 [81] presenting a comprehensive astrophysical picture supporting this idea as well as a possible evolutionary scenario leading to the progenitor CO_{core}-NS binaries. It was also there presented an analytic formula for the accretion rate onto the NS companion on the basis of the following simplified assumptions: (1) a uniform density profile of the pre-SN CO_{core}; (2) the ejecta was evolved following an homologous expansion; (3) the mass of the NS (assumed to be initially $1.4 M_{\odot}$) and the CO_{core} (in the range $4\text{--}8 M_{\odot}$) were assumed nearly constant. So, it was shown that the accretion rate onto the NS is highly super-Eddington, namely it is hypercritical, reaching values of up to $0.1 M_{\odot} \text{ s}^{-1}$ for compact binaries with orbital periods of the order of a few minutes. This estimate implied that the hypercritical accretion could induce the gravitational collapse of the NS which, in a few seconds, would reach the critical mass with consequence formation of a BH. A first test of this IGC first model in real data was soon presented in the case of GRB 090618 [82].

2.2. First Numerical Simulations: 1D Approximation

The first numerical simulations were implemented in 2014 in [83] via a 1D code including (see Figure 3): (1) the modeling of the SN via the 1D core-collapse SN code of Los Alamos [92]; (2) the microphysics experienced by the inflow within the accretion region including the neutrino (ν) emission and hydrodynamics processes such as shock formation; (3) with the above it was followed by the evolution of the material reaching the Bondi-Hoyle capture region and the subsequent in-fall up to the NS surface. Hypercritical accretion rates in the range $10^{-3}\text{--}10^{-1} M_{\odot} \text{ s}^{-1}$ were inferred, confirming the first analytic estimates and the IGC of the NS companion for binary component masses similar to the previous ones and for orbital periods of the order of 5 min.

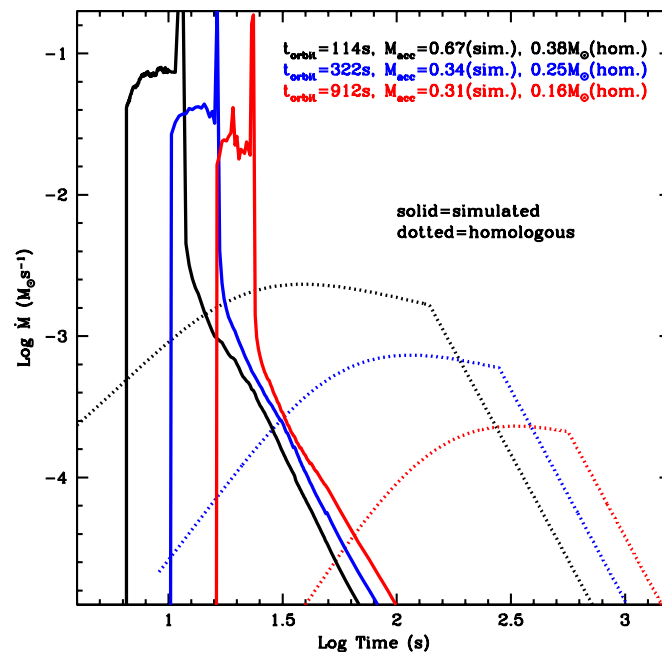


Figure 3. Hypercritical accretion rate onto the NS companion for selected separation distances. The CO_{core} is obtained with a progenitor star of zero-age main-sequence (ZAMS) mass of $20 M_{\odot}$, calculated in [83]. The numerical calculation leads to a sharper accretion profile with respect to the one obtained assuming homologous expansion of the SN ejecta. Taken from Figure 3 in [83].

The above simulations were relevant in determining that the fate of the system is mainly determined by the binary period (P); the SN ejecta velocity (v_{ej}) and the NS initial mass. P and v_{ej} enter explicitly in the Bondi-Hoyle accretion rate formula through the capture radius expression, and implicitly via the ejecta density since they influence the decompression state of the SN material at the NS position.

2.3. 2D Simulations including Angular Momentum Transfer

Soon after, in 2015, we implemented in [53] a series of improvements to the above calculations by relaxing some of the aforementioned assumptions (see Figure 4). We adopted for the ejecta a density profile following a power-law with the radial distance and evolved it with an homologous expansion. The angular momentum transport, not included in the previous estimates, was included. With this addition it was possible to estimate the spin-up of the NS companion by the transfer of angular momentum from the in-falling matter which was shown to circularize around the NS before being accreted. General relativistic effects were also introduced, when calculating the evolution of the structure parameters (mass, radius, spin, etc) of the accreting NS, in the NS gravitational binding energy, and in the angular momentum transfer by the circularized particles being accreted from the innermost circular orbit.

One of the most important results of [53] was that, taking into account that the longer the orbital P the lower the accretion rate, it was there computed the maximum orbital period (P_{max}) for which the NS reaches the critical mass for gravitational collapse, so for BH formation. The dependence of P_{max} on the initial mass of the NS was also there explored. The orbital period P_{max} was then presented as the separatrix of two families of long GRBs associated with these binaries: at the time we called them *Family-1*, the systems in which the NS does not reach the critical mass, and *Family-2* the ones in which it reaches the critical mass and forms a BH. It can be seen that the *Family-1* and *Family-2* long GRBs evolve subsequently into the concepts of *XRFs* and *BdHNe*, respectively.

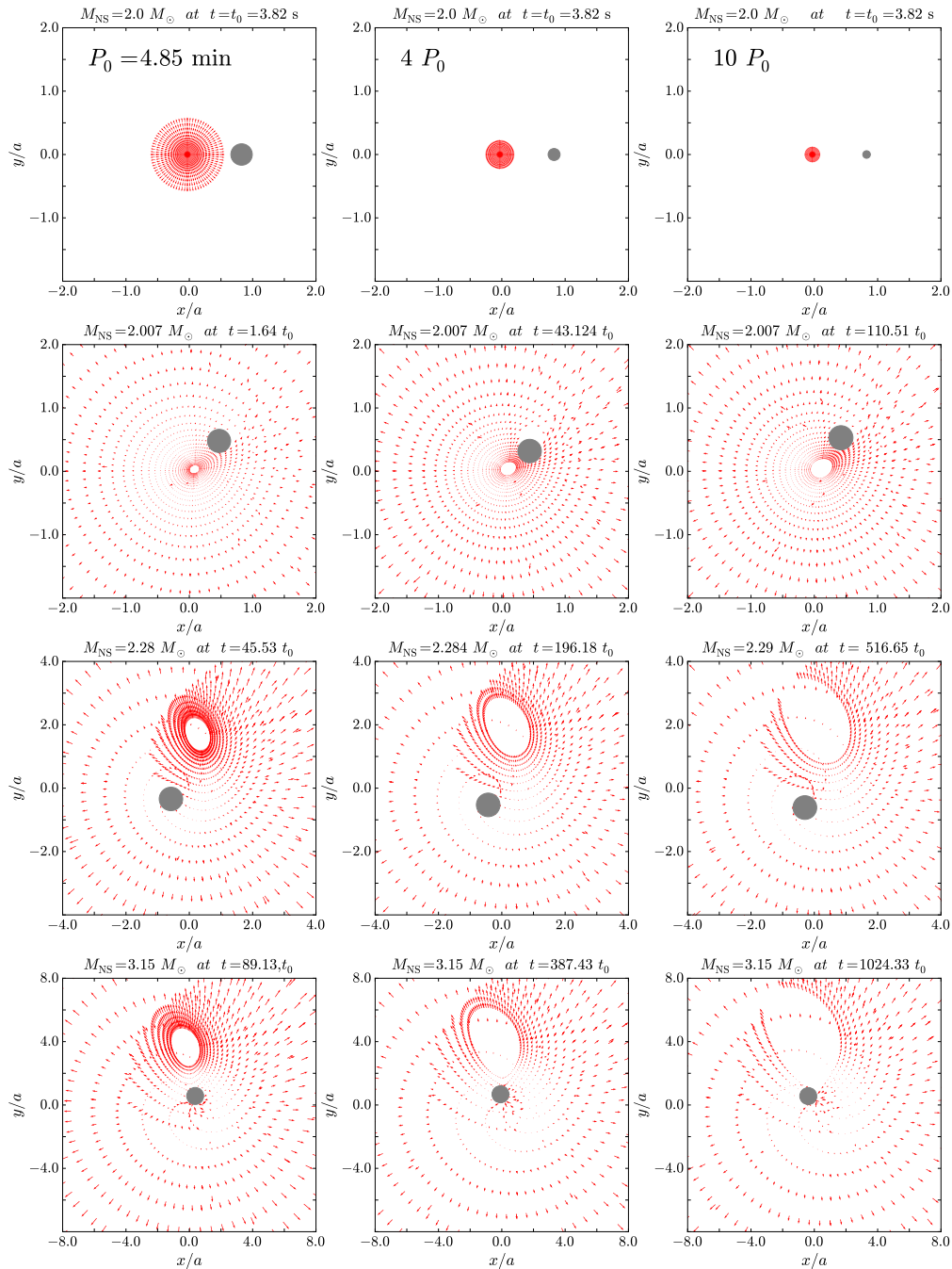


Figure 4. Numerical simulations of the SN ejecta velocity field (red arrows) at selected times of the accretion process onto the NS (taken from Figure 3 in [53]). In these snapshots we have adopted the CO_{core} obtained from a $M_{ZAMS} = 30 M_{\odot}$ progenitor; an ejecta outermost layer velocity $v_{0\text{star}} = 2 \times 10^9 \text{ cm s}^{-1}$, an initial NS mass, $M_{\text{NS}}(t = t_0) = 2.0 M_{\odot}$. The minimum orbital period to have no Roche-lobe overflow is $P_0 = 4.85 \text{ min}$. In the left, central and right columns of snapshots we show the results for binary periods $P = P_0, 4P_0$, and $10P_0$, respectively. The Bondi-Hoyle surface, the filled gray circle, increases as the evolution continues mainly due to the increase of the NS mass (the decrease of the lower panels is only apparent due to the enlargement of the x-y scales). The x-y positions refer to the center-of-mass reference frame. The last image in each column corresponds to the instant when the NS reaches the critical mass value. For the initial conditions of these simulations, the NS ends its evolution at the mass-shedding limit with a maximum value of the angular momentum $J = 6.14 \times 10^{49} \text{ g cm}^2 \text{ s}^{-1}$ and a corresponding critical mass of $3.15 M_{\odot}$.

2.4. First 3D Simulations

A great step toward the most recent simulations was achieved in 2016 in [52] where an SPH-like simulation was implemented in which the SN ejecta was emulated by “point-like” particles. The mass and number of the particles populating each layer were assigned, for self-consistency, according to the power-law density profile. The initial velocity of the particles of each layer was set, in agreement with the chosen power-law density profile, following a radial velocity distribution; i.e., $v \propto r$.

The evolution of the SN particles was followed by Newtonian equations of motion in the gravitational field of the NS companion, also taking into account the orbital motion which was included under the assumption that the NS performs a circular orbit around the CO_{core} center that acts as the common center-of-mass, namely assuming that the mass of the pre-SN core is much larger than the NS mass.

The accretion rate onto the NS was computed, as in [53], using the Bondi-Hoyle accretion formula and, every particle reaching the Bondi-Hoyle surface, was removed from the system. The maximum orbital period P_{\max} in which the NS collapses by accretion could be further explored including the dependence on the mass of the pre-SN CO_{core}, in addition to the dependence on the NS mass.

A detailed study of the hydrodynamics and the neutrino emission in the accretion region on top the NS surface was performed. Concerning the neutrino emission, several ν and antineutrino ($\bar{\nu}$) production processes were considered and showed that electron-positron annihilation ($e^+e^- \rightarrow \nu\bar{\nu}$) overcomes by orders of magnitude any other mechanism of neutrino emission in the range of accretion rates 10^{-8} – $10^{-2} M_{\odot} \text{ s}^{-1}$, relevant for XRFs and BdHNe. The neutrino luminosity can reach values of up to $10^{52} \text{ erg s}^{-1}$ and the neutrino mean energy of 20 MeV for the above upper value of the accretion rate. For the reader interested in the neutrino emission, we refer to [93] for a detailed analysis of the neutrino production in XRFs and BdHNe including flavor oscillations experienced by the neutrinos before abandoning the system.

Concerning the hydrodynamics, the evolution of the temperature and density of outflows occurring during the accretion process owing to convective instabilities was estimated. It was there shown the interesting result that the temperature of this outflow and its evolution can explain the early (i.e., precursors) X-ray emission that has been observed in some BdHNe and in XRFs, exemplified there analyzing the early X-ray emission observed in GRB 090618, a BdHN I, and in GRB 060218, a BdHN II (an XRF).

A most important result of these simulations was the possibility of having a first glance of the morphology acquired by the SN ejecta: the matter density, initially spherically symmetric, becomes highly asymmetric due to the accretion process and the action of the gravitational field of the NS companion (see Figure 5).

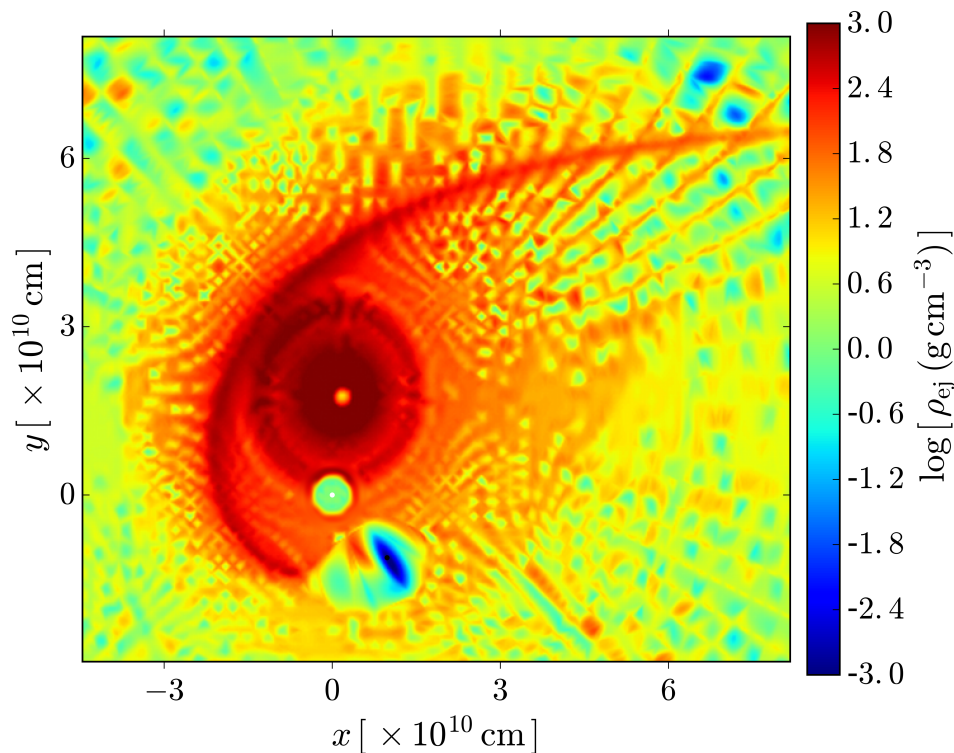


Figure 5. Snapshot of the SN ejecta density in the orbital plane of the CO_{core}-NS binary. Numerical simulation taken from Figure 6 in [52]. The plot corresponds to the instant when the NS reaches the critical mass and forms the BH (black dot), approximately 250 s from the SN explosion. The ν NS is represented by the white dot. The binary parameters are: the initial mass of the NS companion is $2.0 M_{\odot}$; the CO_{core} leading to an ejecta mass of $7.94 M_{\odot}$, and the orbital period is $P \approx 5$ min, namely a binary separation $a \approx 1.5 \times 10^{10}$ cm.

3. The Hypercritical Accretion Process

We now give details of the accretion process within the IGC scenario following [52,53,55,83]. There are two main physical conditions for which hypercritical (i.e., highly super-Eddington) accretion onto the NS occurs in XRFs and BdHNe. The first is that the photons are trapped within the inflowing material and the second is that the shocked atmosphere on top of the NS becomes sufficiently hot ($T \sim 10^{10}$ K) and dense ($\rho \gtrsim 10^6$ g cm⁻³) to produce a very efficient neutrino-antineutrino ($\nu\bar{\nu}$) cooling emission. In this way the neutrinos become mainly responsible for releasing the energy gained by accretion, allowing hypercritical accretion to continue.

3.1. Accretion Rate and NS Evolution

The first numerical simulations of the IGC were performed in [83], including: (1) realistic SN explosions of the CO_{core}; (2) the hydrodynamics within the accretion region; (3) the simulated evolution of the SN ejecta up to their accretion onto the NS. Becerra et al. [53] then estimated the amount of angular momentum carried by the SN ejecta and how much is transferred to the NS companion by accretion. They showed that the SN ejecta can circularize for a short time and form a disc-like structure surrounding the NS before being accreted. The evolution of the NS central density and rotation angular velocity (the NS is spun up by accretion) was computed from full numerical solutions of the axisymmetric Einstein equations. The unstable limits of the NS are set by the mass-shedding (or Keplerian) limit and the critical point of gravitational collapse given by the secular axisymmetric instability, (see, e.g., [53] for details).

The accretion rate of the SN ejecta onto the NS is given by:

$$\dot{M}_B(t) = \pi \rho_{\text{ej}} R_{\text{cap}}^2 \sqrt{v_{\text{rel}}^2 + c_{\text{s,ej}}^2}, \quad R_{\text{cap}}(t) = \frac{2GM_{\text{NS}}(t)}{v_{\text{rel}}^2 + c_{\text{s,ej}}^2}, \quad (1)$$

where G is the gravitational constant, ρ_{ej} and $c_{\text{s,ej}}$ are the density and sound speed of the ejecta, R_{cap} and M_{NS} are the NS gravitational capture radius (Bondi-Hoyle radius) and gravitational mass, and v_{rel} the ejecta velocity relative to the NS: $\vec{v}_{\text{rel}} = \vec{v}_{\text{orb}} - \vec{v}_{\text{ej}}$; $|\vec{v}_{\text{orb}}| = \sqrt{G(M_{\text{core}} + M_{\text{NS}})/a}$, and \vec{v}_{ej} is the velocity of the supernova ejecta (see Figure 2).

Numerical simulations of the SN explosions suggest the adopted homologous expansion of the SN, i.e., $v_{\text{ej}}(r, t) = nr/t$, where r is the position of each layer from the SN center and n is the expansion parameter. The density evolves as

$$\rho_{\text{ej}}(r, t) = \rho_{\text{ej}}^0(r/R_{\text{star}}(t), t_0) \frac{M_{\text{env}}(t)}{M_{\text{env}}(0)} \left(\frac{R_{\text{star}}(0)}{R_{\text{star}}(t)} \right)^3, \quad (2)$$

where $M_{\text{env}}(t)$ the mass of the CO_{core} envelope, $R_{\text{star}}(t)$ is the radius of the outermost layer, and ρ_{ej}^0 is the pre-SN CO_{core} density profile; $\rho_{\text{ej}}(r, t_0) = \rho_{\text{core}}(R_{\text{core}}/r)^m$, where ρ_{core} , R_{core} and m are the profile parameters obtained from numerical simulations. Typical parameters of the CO_{core} mass are (3.5–9.5) M_{\odot} corresponding to (15–30) M_{\odot} zero-age-main-sequence (ZAMS) progenitors (see [53,83] for details). The binary period is limited from below by the request of having no Roche lobe overflow by the CO_{core} before the SN explosion [83]. For instance, for a CO_{core} of 9.5 M_{\odot} forming a binary system with a 2 M_{\odot} NS, the minimum orbital period allowed by this condition is $P_{\text{min}} \approx 5$ min. For these typical binary and pre-SN parameters, Equation (1) gives accretion rates 10^{-4} – $10^{-2} M_{\odot} \text{ s}^{-1}$.

We adopt an initially non-rotating NS companion so its exterior spacetime at time $t = 0$ is described by the Schwarzschild metric. The SN ejecta approach the NS with specific angular momentum, $l_{\text{acc}} = \dot{L}_{\text{cap}}/\dot{M}_B$, circularizing at a radius $r_{\text{circ}} \geq r_{\text{lco}}$ if $l_{\text{acc}} \geq l_{\text{lso}}$ with r_{lco} the radius of the last circular orbit (LCO). For a non-rotating NS $r_{\text{lco}} = 6GM_{\text{NS}}/c^2$ and $l_{\text{lco}} = 2\sqrt{3}GM_{\text{NS}}/c$. For typical parameters, $r_{\text{circ}}/r_{\text{lco}} \sim 10$ – 10^3 .

The accretion onto the NS proceeds from the radius r_{in} . The NS mass and angular angular momentum evolve as [53,94]:

$$\dot{M}_{\text{NS}} = \left(\frac{\partial M_{\text{NS}}}{\partial M_b} \right)_{J_{\text{NS}}} \dot{M}_b + \left(\frac{\partial M_{\text{NS}}}{\partial J_{\text{NS}}} \right)_{M_b} \dot{J}_{\text{NS}}, \quad \dot{J}_{\text{NS}} = \xi l(r_{\text{in}}) \dot{M}_B, \quad (3)$$

where M_b is the NS baryonic mass, $l(r_{\text{in}})$ is the specific angular momentum of the accreted material at r_{in} , which corresponds to the angular momentum of the LCO, and $\xi \leq 1$ is a parameter that measures the efficiency of angular momentum transfer. In this picture we have $\dot{M}_b = \dot{M}_B$.

For the integration of Equations (1) and (3) we have to supply the values of the two partial derivatives in Equation (3). They are obtained from the relation of the NS gravitational mass, M_{NS} , with M_b and J_{NS} , namely from the knowledge of the NS binding energy. For this we use the general relativistic calculations of rotating NSs presented in [95]. They show that, independent on the nuclear EOS, the following analytical formula represents the numerical results with sufficient accuracy (error < 2%):

$$\frac{M_b}{M_{\odot}} = \frac{M_{\text{NS}}}{M_{\odot}} + \frac{13}{200} \left(\frac{M_{\text{NS}}}{M_{\odot}} \right)^2 \left(1 - \frac{1}{137} j_{\text{NS}}^{1.7} \right), \quad (4)$$

where $j_{\text{NS}} \equiv cJ_{\text{NS}}/(GM_{\odot}^2)$.

In the accretion process, the NS gains angular momentum and therefore spins up. To evaluate the amount of angular momentum transferred to the NS at any time we include the dependence of the

LCO specific angular momentum as a function of M_{NS} and J_{NS} . For corotating orbits, the following relation is valid for the NL3, TM1 and GM1 EOS [53,94]:

$$l_{\text{lco}} = \frac{GM_{\text{NS}}}{c} \left[2\sqrt{3} - 0.37 \left(\frac{j_{\text{NS}}}{M_{\text{NS}}/M_{\odot}} \right)^{0.85} \right]. \quad (5)$$

The NS continues the accretion until it reaches an instability limit or up to when all the SN ejecta overcomes the NS Bondi-Hoyle region. We take into account the two main instability limits for rotating NSs: the mass-shedding or Keplerian limit and the secular axisymmetric instability limit. The latter defines critical NS mass. For the aforementioned nuclear EOS, the critical mass can be approximately written as [95]:

$$M_{\text{NS}}^{\text{crit}} = M_{\text{NS}}^{J=0} (1 + k j_{\text{NS}}^p), \quad (6)$$

where k and p are EOS-dependent parameters (see Table 3). These formulas fit the numerical results with a maximum error of 0.45%.

Table 3. Critical NS mass in the non-rotating case and constants k and p needed to compute the NS critical mass in the non-rotating case given by Equation (6). The values are for the NL3, GM1 and TM1 EOS.

EOS	$M_{\text{crit}}^{J=0} (M_{\odot})$	p	k
NL3	2.81	1.68	0.006
GM1	2.39	1.69	0.011
TM1	2.20	1.61	0.017

Additional details and improvements of the hypercritical accretion process leading to XRFs and BdHNe were presented in [52]. Specifically:

1. The density profile included finite size/thickness effects and additional CO_{core} progenitors, leading to different SN ejecta masses being considered.
2. In [53] the maximum orbital period, P_{max} , over which the accretion onto NS companion is not sufficient to bring it to the critical mass, was inferred. Thus, binaries with $P > P_{\text{max}}$ lead to XRFs while the ones with $P \lesssim P_{\text{max}}$ lead to BdHNe. Becerra et al. [52] extended the determination of P_{max} for all the possible initial values of the NS mass. They also examined the outcomes for different values of the angular momentum transfer efficiency parameter.
3. The expected luminosity during the process of hypercritical accretion for a wide range of binary periods covering both XRFs and BdHNe was estimated.
4. It was shown that the presence of the NS companion originates asymmetries in the SN ejecta (see, e.g., Figure 6 in [52]). The signatures of such asymmetries in the X-ray emission was there shown in the specific example of XRF 060218.

3.2. Hydrodynamics in the Accretion Region

The accretion rate onto the NS can be as high as $\sim 10^{-2} - 10^{-1} M_{\odot} \text{ s}^{-1}$. For such accretion rates:

1. The magnetic pressure is much smaller than the random pressure of the infalling material, therefore the magnetic-field effects on the accretion process are negligible [81,96].
2. The photons are trapped within the infalling matter, hence the Eddington limit does not apply and hypercritical accretion occurs. The trapping radius is defined as [97]: $r_{\text{trapping}} = \min\{\dot{M}_B \kappa / (4\pi c), R_{\text{cap}}\}$, where κ is the opacity. [83] estimated a Rosseland mean opacity of $\approx 5 \times 10^3 \text{ cm}^2 \text{ g}^{-1}$ for the CO_{cores} . This, together with our typical accretion rates, lead to $\dot{M}_B \kappa / (4\pi c) \sim 10^{13} - 10^{19} \text{ cm}$. This radius is much bigger than the Bondi-Hoyle radius.

- The above condition, and the temperature-density values reached on top of the NS surface, lead to an efficient neutrino cooling which radiates away the gain of gravitational energy of the infalling material [81,83,96,98,99].

The accretion shock moves outward as the material piles onto the NS. Since the post-shock entropy is inversely proportional to the shock radius position, the NS atmosphere is unstable with respect to Rayleigh-Taylor convection at the beginning of the accretion process. Such instabilities might drive high-velocity outflows from the accreting NS [100,101]. The entropy at the base of the atmosphere is [96]:

$$S_{\text{bubble}} \approx 16 \left(\frac{1.4 M_{\odot}}{M_{\text{NS}}} \right)^{-7/8} \left(\frac{M_{\odot} \text{ s}^{-1}}{\dot{M}_{\text{B}}} \right)^{1/4} \left(\frac{10^6 \text{ cm}}{r} \right)^{3/8} k_{\text{B}} / \text{nucleon}, \quad (7)$$

where k_{B} is the Boltzmann constant. The material expands and cools down adiabatically, i.e., $T^3/\rho = \text{constant}$. In the case of a spherically symmetric expansion, $\rho \propto 1/r^3$ and $k_{\text{B}} T_{\text{bubble}} = 195 S_{\text{bubble}}^{-1} (10^6 \text{ cm}/r) \text{ MeV}$. In the more likely case that the material expand laterally we have [101]: $\rho \propto 1/r^2$, i.e., $T_{\text{bubble}} = T_0(S_{\text{bubble}}) (r_0/r)^{2/3}$, where $T_0(S_{\text{bubble}})$ is obtained from the above equation at $r = r_0 \approx R_{\text{NS}}$. This implies a bolometric blackbody flux at the source from the rising bubbles:

$$F_{\text{bubble}} \approx 2 \times 10^{40} \left(\frac{M_{\text{NS}}}{1.4 M_{\odot}} \right)^{-7/2} \left(\frac{\dot{M}_{\text{B}}}{M_{\odot} \text{ s}^{-1}} \right) \left(\frac{R_{\text{NS}}}{10^6 \text{ cm}} \right)^{3/2} \left(\frac{r_0}{r} \right)^{8/3} \text{ erg s}^{-1} \text{ cm}^{-2}. \quad (8)$$

The above thermal emission has been shown [83] to be a plausible explanation of the early X-ray (precursor) emission observed in some GRBs. The X-ray precursor observed in GRB 090618 [35,82] is explained adopting an accretion rate of $10^{-2} M_{\odot} \text{ s}^{-1}$, the bubble temperature drops from 50 keV to 15 keV while expanding from $r \approx 10^9 \text{ cm}$ to $6 \times 10^9 \text{ cm}$ (see Figure 6). More recently, the X-ray precursor has been observed in GRB 180728A and it is well explained by a bubble of $\sim 7 \text{ keV}$ at $\sim 10^{10} \text{ cm}$ and an accretion rate of $10^{-3} M_{\odot} \text{ s}^{-1}$ (see [49] for details).

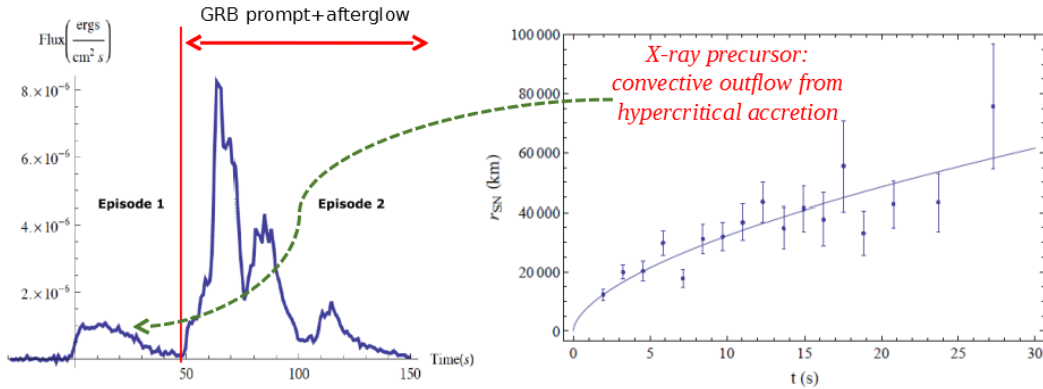


Figure 6. (a) Fermi-GBM (NaI 8–440 keV) light-curve of GRB 090618 (adapted from Figure 1 in [35]). (b) Expanding radius of the thermal blackbody emission observed in the “Episode 1” of GRB 090618 (adapted from Figure 2 in [35]). The interpretation of such an X-ray precursor as being due to the emission of the convective bubbles during the process of hypercritical accretion onto the NS was proposed for the first time in [83].

3.3. Neutrino Emission and Effective Accretion Rate

For the accretion rate conditions characteristic of our models at peak $\sim 10^{-4} - 10^{-2} M_{\odot} \text{ s}^{-1}$, pair annihilation dominates the neutrino emission and electron neutrinos remove the bulk of the energy [52]. The e^+e^- pairs producing the neutrinos are thermalized at the matter temperature. This temperature is approximately given by:

$$T_{\text{acc}} \approx \left(\frac{3P_{\text{shock}}}{4\sigma/c} \right)^{1/4} = \left(\frac{7 \dot{M}_{\text{acc}} v_{\text{acc}} c}{8 4\pi R_{\text{NS}}^2 \sigma} \right)^{1/4}, \quad (9)$$

where P_{shock} is the pressure of the shock developed on the accretion zone above the NS surface, \dot{M}_{acc} is the accretion rate, v_{acc} is the velocity of the infalling material, σ is the Stefan-Boltzmann constant and c the speed of light. It can be checked that, for the accretion rates of interest, the system develops temperatures and densities $T \gtrsim 10^{10}$ K and $\rho \gtrsim 10^6$ g cm $^{-3}$; respectively (see Figure 7).

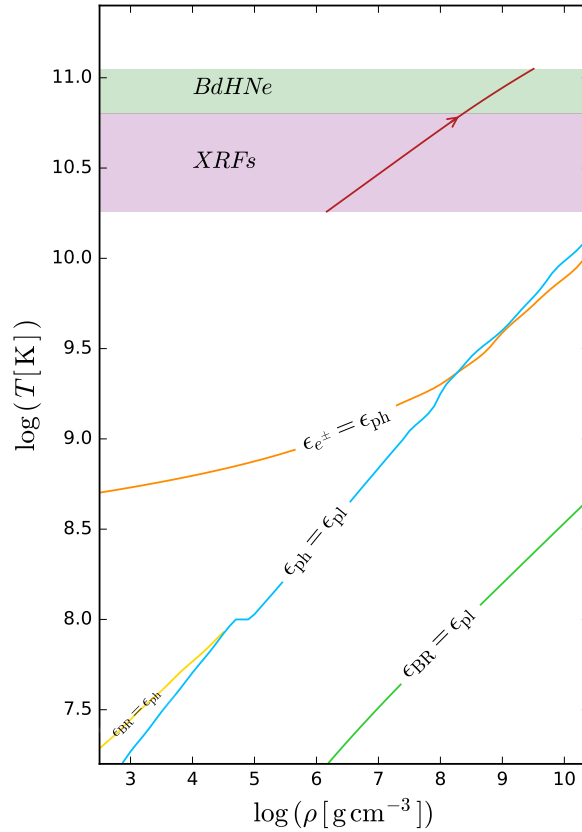


Figure 7. Temperature-density reached by the accreting atmosphere (taken from Figure 16 in [52]). The contours indicate where the emissivity of the different neutrinos processes becomes quantitatively equal to each other. We considered the following processes: pair annihilation (ϵ_{e^\pm}), photo-neutrino emission (ϵ_γ), plasmon decay (ϵ_{pl}) and Bremsstrahlung emission (ϵ_{BR}). The solid red curve spans $T - rho$ values corresponding to accretion rates from 10^{-8} to $10^{-1} M_\odot \text{ s}^{-1}$ from the lower to the upper end. For any accretion rate of interest, the electron-positron pair annihilation dominates the neutrino emission.

Under these conditions of density and temperature the neutrino emissivity of the e^+e^- annihilation process can be estimated by the simple formula [102]:

$$\epsilon_{e^-e^+} \approx 8.69 \times 10^{30} \left(\frac{k_B T}{1 \text{ MeV}} \right)^9 \text{ MeV cm}^{-3} \text{ s}^{-1}, \quad (10)$$

where k_B is the Boltzmann constant.

The accretion zone is characterized by a temperature gradient with a typical scale height $\Delta r_{\text{ER}} = T/\nabla T \approx 0.7 R_{\text{NS}}$. Owing to the aforementioned strong dependence of the neutrino emission on temperature, most of the neutrinos are emitted from a spherical shell around the NS of thickness

$$\Delta r_\nu = \frac{\epsilon_{e^-e^+}}{\nabla \epsilon_{e^-e^+}} = \frac{\Delta r_{\text{ER}}}{9} \approx 0.08 R_{\text{NS}}. \tag{11}$$

Equations (9) and (10) imply the neutrino emissivity satisfies $\epsilon_{e^-e^+} \propto \dot{M}_{\text{acc}}^{9/4}$ as we had anticipated. These conditions lead to the neutrinos to be efficient in balancing the gravitational potential energy gain, allowing the hypercritical accretion rates. The effective accretion onto the NS can be estimated as:

$$\dot{M}_{\text{eff}} \approx \Delta M_\nu \frac{L_\nu}{E_g}, \tag{12}$$

where ΔM_ν , L_ν are, respectively, the mass and neutrino luminosity in the emission region, and $E_g = (1/2)GM_{\text{NS}}\Delta M_\nu / (R_\nu + \Delta r_\nu)$ is half the gravitational potential energy gained by the material falling from infinity to the $R_{\text{NS}} + \Delta r_\nu$. The neutrino luminosity is

$$L_\nu \approx 4\pi R_{\text{NS}}^2 \Delta r_\nu \epsilon_{e^-e^+}, \tag{13}$$

with $\epsilon_{e^-e^+}$ being the neutrino emissivity in Equation (10). For $M_{\text{NS}} = 2 M_\odot$ and temperatures 1–10 MeV, the Equations (12) and (13) result $\dot{M}_{\text{eff}} \approx 10^{-10} - 10^{-1} M_\odot \text{ s}^{-1}$ and $L_\nu \approx 10^{48} - 10^{57} \text{ MeV s}^{-1}$.

Therefore, the neutrino emission can reach luminosities of up to $10^{57} \text{ MeV s}^{-1}$, mean neutrino energies 20–30 MeV, and neutrino densities 10^{31} cm^{-3} . Along their path from the vicinity of the NS surface outward, such neutrinos experience flavor transformations dictated by the neutrino to electron density ratio. We have determined in [93] the neutrino and electron on the accretion zone and use them to compute the neutrino flavor evolution. For normal and inverted neutrino-mass hierarchies and within the two-flavor formalism ($\nu_e \nu_\chi$), we estimated the final electronic and non-electronic neutrino content after two oscillation processes: (1) neutrino collective effects due to neutrino self-interactions where the neutrino density dominates and, (2) the Mikheyev-Smirnov-Wolfenstein (MSW) effect, where the electron density dominates. We find that the final neutrino content is composed by ~55% (~62%) of electronic neutrinos, i.e., $\nu_e + \bar{\nu}_e$, for the normal (inverted) neutrino-mass hierarchy (see Figure 8). This is a first step toward the characterization of a novel source of astrophysical MeV-neutrinos in addition to core-collapse SNe. We refer the reader to [93] for additional details of the flavor-oscillations as well as the final neutrino spectra after such a process.

3.4. Accretion Luminosity

The energy release in a time-interval dt , when an amount of mass dM_b with angular momentum $l\dot{M}_b$ is accreted, is [52]:

$$L_{\text{acc}} = (\dot{M}_b - \dot{M}_{\text{NS}})c^2 = \dot{M}_b c^2 \left[1 - \left(\frac{\partial M_{\text{NS}}}{\partial J_{\text{NS}}} \right)_{M_b} l - \left(\frac{\partial M_{\text{NS}}}{\partial M_b} \right)_{J_{\text{NS}}} \right]. \tag{14}$$

This is the amount of gravitational energy gained by the matter by infalling to the NS surface that is not spent in NS gravitational binding energy. The total energy release in the time interval from t to $t + dt$,

$$\Delta E_{\text{acc}} \equiv \int L_{\text{acc}} dt, \tag{15}$$

is given by the NS binding energy difference between its initial and final state. The typical luminosity is $L_{\text{acc}} \approx \Delta E_{\text{acc}} / \Delta t_{\text{acc}}$, where Δt_{acc} is the duration of the accretion process.

The value of Δt_{acc} is approximately given by the flow time of the slowest layers of the SN ejecta to the NS companion position. If we denote the velocity of these layers by v_{inner} , we have $\Delta t_{\text{acc}} \sim a/v_{\text{inner}}$,

where a is the binary separation. For $a \sim 10^{11}$ cm and $v_{\text{inner}} \sim 10^8$ cm s $^{-1}$, $\Delta t_{\text{acc}} \sim 10^3$ s. For shorter separations, e.g., $a \sim 10^{10}$ cm ($P \sim 5$ min), $\Delta t_{\text{acc}} \sim 10^2$ s. For a binary with $P = 5$ min, the NS accretes $\approx 1 M_{\odot}$ in $\Delta t_{\text{acc}} \approx 100$ s. From Equation (4) one obtains that the binding energy difference of a $2 M_{\odot}$ and a $3 M_{\odot}$ NS, is $\Delta E_{\text{acc}} \approx 13/200(3^2 - 2^2) M_{\odot} c^2 \approx 0.32 M_{\odot} c^2$. This leads to $L_{\text{acc}} \approx 3 \times 10^{-3} M_{\odot} c^2 \approx 0.1 \dot{M}_b c^2$. The accretion power can be as high as $L_{\text{acc}} \sim 0.1 \dot{M}_b c^2 \sim 10^{47} - 10^{51}$ erg s $^{-1}$ for accretion rates in the range $\dot{M}_b \sim 10^{-6} - 10^{-2} M_{\odot} \text{ s}^{-1}$.

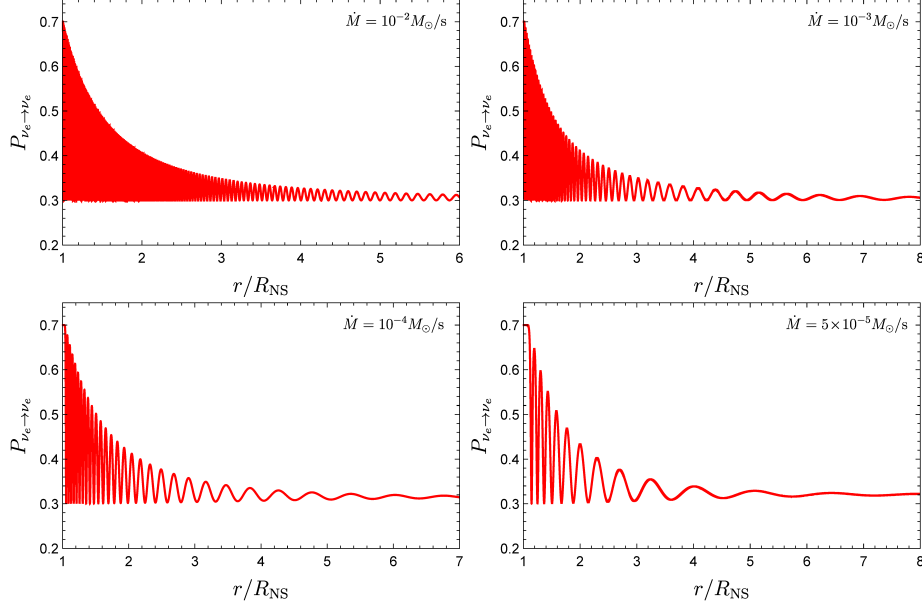


Figure 8. Neutrino flavor evolution in the case of the neutrino-mass inverted hierarchy (taken from Figure 4 in [93]). The electron-neutrino survival probability is shown as a function of the radial distance from the NS surface. The curves for the electron antineutrino overlap the ones for electron-neutrinos.

4. New 3D SPH Simulations

We have recently presented in [90] new, 3D hydrodynamic simulations of the IGC scenario by adapting the SPH code developed at Los Alamos, *SNSPH* [103], which has been tested and applied in a variety of astrophysical situations [104–107].

The time $t = 0$ of the simulation is set as the time at which the SN shock breaks out the CO_{core} external radius. We calculate the accretion rate both onto the NS companion and onto the νNS (via fallback), and calculate the evolution of other binary parameters such as the orbital separation, eccentricity, etc. Figure 9 shows an example of simulation for a binary system composed of a CO_{core} of mass $\approx 6.85 M_{\odot}$, the end stage of a ZAMS progenitor star of $M_{\text{zams}} = 25 M_{\odot}$, and a $2 M_{\odot}$ NS companion. The initial orbital period is ≈ 5 min.

The accretion rate onto both stars was estimated from the flux of SPH particles falling, per unit time, into the Bondi-Hoyle accretion region of the NS (see Figure 10). It is confirmed that the accretion onto the NS companion occurs from a disk-like structure formed by the particles that circularize before being accreted; see vortices in the upper panel of Figure 9 and the disk structure is clearly seen in the lower panel.

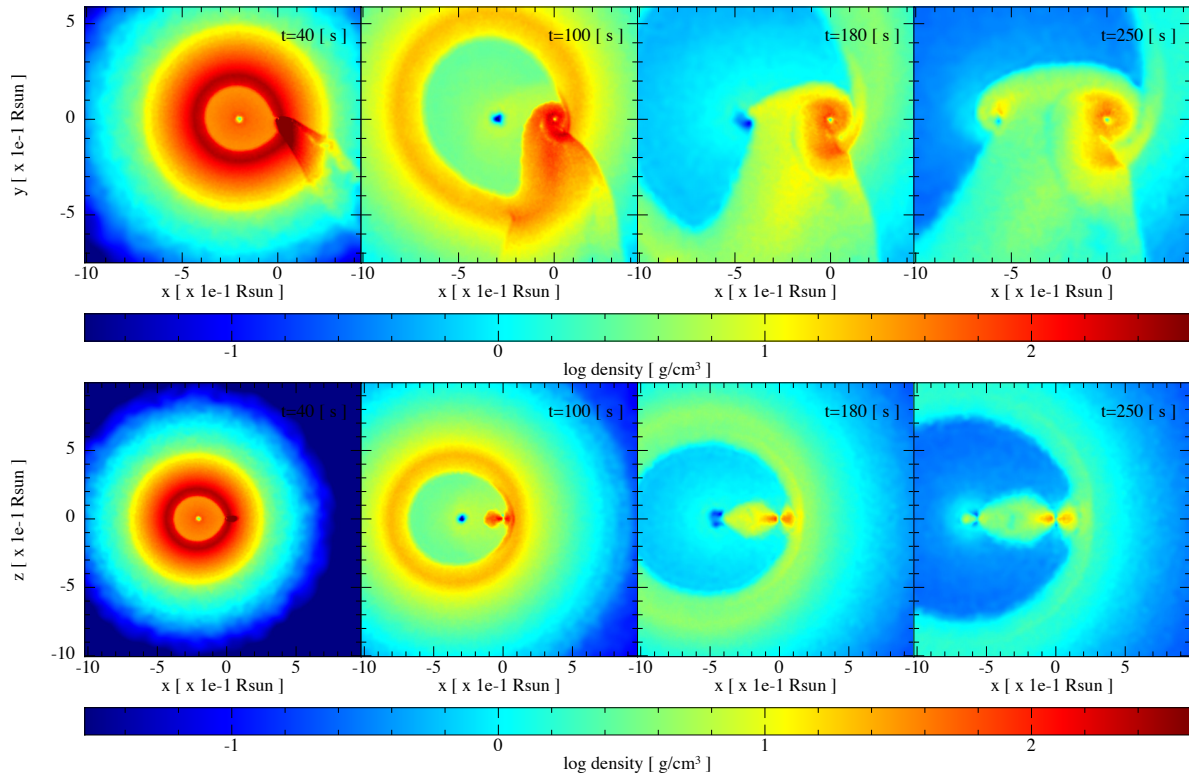


Figure 9. Snapshots of the 3D SPH simulations of the IGC scenario (taken from Figure 2 in [90]). The initial binary system is formed by a CO_{core} of mass $\approx 6.85 M_{\odot}$, from a ZAMS progenitor star of $25 M_{\odot}$, and a $2 M_{\odot}$ NS with an initial orbital period of approximately 5 min. The upper panel shows the mass density on the equatorial (orbital) plane, at different times of the simulation. The time $t = 0$ is set in our simulations at the moment of the SN shock breakout. The lower panel shows the plane orthogonal to the orbital one. The reference system has been rotated and translated for the x -axis to be along the line joining the ν NS and the NS centers, and its origin is at the NS position.

Several binary parameters were explored thanks to the new code. We performed simulations changing the CO_{core} mass, the NS companion mass, the orbital period, the SN explosion energy (so the SN kinetic energy or velocity). We also explored intrinsically asymmetric SN explosion. We checked if the ν NS and/or the NS companion reach the mass-shedding (Keplerian) limit or the secular axisymmetric instability, i.e., the critical mass. The NS can also become just a more massive, fast rotating, stable NS when the accretion is moderate. All this was done for various NS nuclear equations of state (NL3, TM1 and GM1).

We followed the orbital evolution up to the instant when most of the ejecta has abandoned the system to determine if the system remains bound or becomes unbound by the explosion. We thus assessed the CO_{core} -NS parameters leading to the formation of ν NS-NS (from XRFs) or ν NS-BH (from BdHNe) binaries. The first proof that BdHNe remain bound leading to ν NS-BH binaries was presented in [55] (see next section).

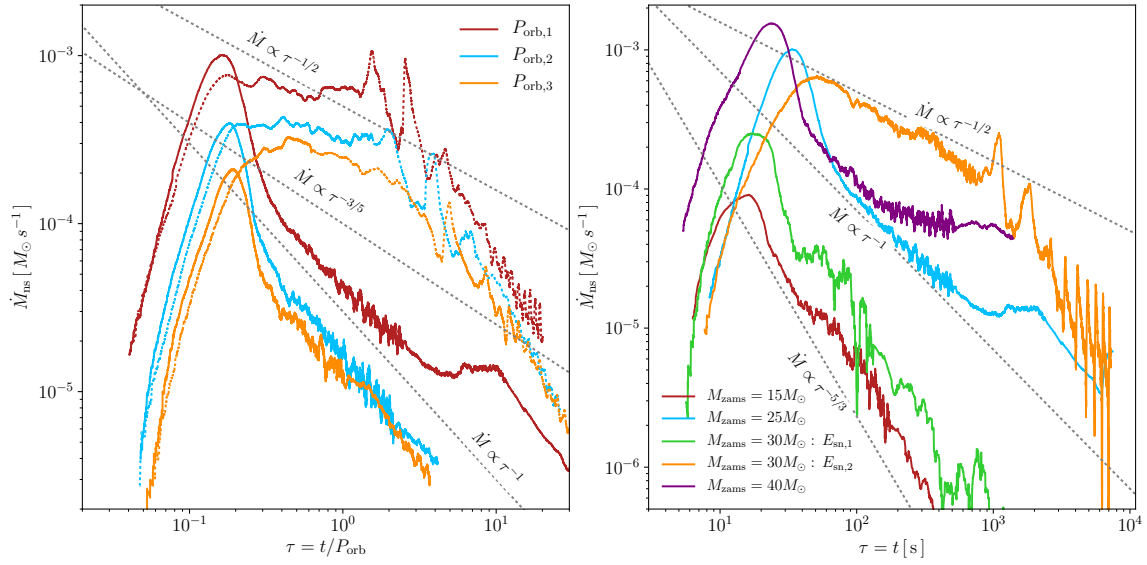


Figure 10. (a) Mass-accretion rate onto the NS companion in the IGC scenario (taken from Figure 9 in [90]). Different colors correspond to different initial orbital periods: $P_{\text{orb},1} = 4.8$ min (red line), $P_{\text{orb},2} = 8.1$ min (blue line), $P_{\text{orb},3} = 11.8$ min (orange line). The other parameters that characterize the initial binary system are the same as in Figure 9. The solid lines correspond to a SN energy of 1.57×10^{51} erg, while the dotted ones correspond to a lower SN energy of 6.5×10^{50} erg. It can be seen that the mass-accretion rate scales with the binary orbital period. (b) Mass-accretion rate on the NS companion for all the CO_{core} progenitors (see Table 1 and Figure 13 in [90]). The NS companion has an initial mass of $2 M_{\odot}$ and the orbital period is close to the minimum period that the system can have in order that there is no Roche-lobe overflow before the collapse of the CO_{core}: 6.5 min, 4.8 min, 6.0 min and 4.4 min for the $M_{\text{zams}} = 15 M_{\odot}$, $25 M_{\odot}$, $30 M_{\odot}$ and $40 M_{\odot}$ progenitors, respectively.

5. Consequences on GRB Data Analysis and Interpretation

In a few seconds a BdHN shows different physical processes that lead to a specific sequence of observables at different times and at different wavelengths. Starting with the at-times-observed X-ray precursors, to the Gamma-ray prompt emission, to the GeV emission, to the early and late X-ray afterglow in which, respectively, are observed flares and a distinct power-law luminosity.

5.1. X-ray Precursor

X-ray precursors can comprise the presence of both the SN shock breakout as well as the hypercritical accretion onto the NS companion until it reaches the critical mass. These processes have been identified in [49,52,82,83].

The conversion of the SN shockwave kinetic energy (see [108] for details on the SN physics) into electromagnetic energy imply that about 10^{50} erg can be emitted.

Once it reached the NS companion, the ejecta induced a hypercritical accretion onto the NS at a rate $\sim 10^{-3} M_{\odot} \text{ s}^{-1}$ for an assumed orbital separation of few 10^{10} cm. As we have recalled (see Figure 6 in Section 3), the accretion process triggers the expansion of thermal convective bubbles on top of the NS owing to the Rayleigh-Taylor instability [49,52,82,83].

It is of special interest to refer the reader to the results presented in [49] on GRB 180728A, a BdHN II. It has been identified in the precursor of this GRB, for the first time, the presence of both the emergence of the SN shockwave as well as the hypercritical accretion process. From this the binary parameters have been extracted and further confirmed by the analysis of the prompt and the afterglow emission.

5.2. GRB Prompt Emission

A BdHN I leaves as a remnant a ν NS-BH binary surrounded by the asymmetric SN ejecta (see Figure 5 and [52,90]). The asymmetric ejecta includes a “cavity” of $\sim 10^{11}$ cm of very low-density matter around the newborn BH. The hydrodynamics inside such a low-density cavity have been recently studied by numerical simulations in [87].

The asymmetric character acquired by the SN ejecta implies that the e^+e^- plasma, expanding from the BH site in all directions with equal initial conditions, experiences a different dynamics along different directions. The reason for this is that the e^+e^- plasma engulfs different amounts of baryonic mass (see Figure 11). This leads to observable signatures as a function of the viewing angle.

The newborn Kerr BH, surrounded by ejecta and immersed in a test magnetic field (likely the one left by the magnetized, collapsed NS), represents what we have called the *inner engine* of the high-energy emission [84–87]. The rotating BH, of mass M and angular momentum J , in the presence of the magnetic field B_0 , induces an electromagnetic field described by the Wald solution [88].

The induced electric field at the BH horizon $r_+ = M(1 + \sqrt{1 - a^2})$ is [84,85]

$$E_{r_+} \approx \frac{1}{2} \alpha B_0 = 6.5 \times 10^{15} \cdot \alpha \left(\frac{B_0}{B_c} \right) \frac{\text{V}}{\text{cm}}, \quad (16)$$

where $\alpha = J/M^2$ is the dimensionless angular momentum of the BH and $B_c = m_e^2 c^3 / (e\hbar) \approx 4.4 \times 10^{13}$ G. This field acquires values over the critical one, $E_c = m_e^2 c^3 / (e\hbar)$ if the following conditions are verified:

$$\alpha(B_0/B_c) \geq 2, \quad B_0/B_c \geq 2, \quad (17)$$

where the second condition comes from the constraint that a rotating BH must satisfy: $\alpha \leq 1$. The above huge value of the electric field (16) guarantees the production of the e^+e^- pair plasma around the newborn BH via the quantum electrodynamics (QED) process of vacuum polarization [109].

In the direction pointing from the CO_{core} to the accreting NS outwards and lying on the orbital plane, the aforementioned cavity represents a region of low baryonic contamination [86,87]. The e^+e^- plasma can then self-accelerate to Lorentz factors $\Gamma \sim 10^2\text{--}10^3$ reaching transparency and impacting on the CBM filaments as described in [37,110,111]. At transparency, MeV-photons are emitted which are observed in the ultrarelativistic prompt emission. This picture has been successfully applied and verified on plenty of GRBs, e.g., GRBs 050904, 080319B, 090227, 090618 and 101023 [35,69,112,113].

5.3. Early X-ray Afterglow: Flares

It was recently addressed in [40] the role of X-ray flares as a powerful tool to differentiate the BdHN model from the “collapsar-fireball” model [114].

First, it is known that the GRB prompt emission shows Gamma-ray spikes occurring at $10^{15}\text{--}10^{17}$ cm from the source and have Lorentz factor $\Gamma \sim 10^2\text{--}10^3$.

Second, the thermal emission observed in the X-ray flares of the early (rest-frame time $t \sim 10^2$ s) afterglow of BdHNe, implies occurrence radii $\sim 10^{12}$ cm expanding at mildly-relativistic velocity, e.g., $\Gamma \lesssim 4$ [40] (see below). The latter observational fact evidences that the X-ray afterglow is powered by a mildly-relativistic emitter. These model-independent observations contrast with the assumption of an ultrarelativistic expansion starting from the GRB prompt emission and extending to the afterglow. Such a “traditional” approach to GRBs has been adopted in a vast number of articles over decades as it is summarized in review articles (see, e.g., [20–25]).

In the other directions, the GRB e^+e^- plasma impacts the SN ejecta at approximately 10^{10} cm, evolves carrying a large amount of baryons reaching transparency at radii 10^{12} cm with a mildly $\Gamma \lesssim 4$. The theoretical description and the consequent numerical simulation have been addressed in [40].

Such a mildly-relativistic photospheric emission is experimentally demonstrated by the thermal radiation observed in the early X-ray afterglow and in the X-ray flares [115,116]. For instance, in the early hundreds of seconds, GRB 090618 is found to have a velocity of $\beta \sim 0.8$ [117,118], GRB 081008 has

a velocity $\beta \sim 0.9$ [40], and GRB 130427A has a velocity of $\beta \sim 0.9$ as well [91,119,120]. We emphasize that the mildly-relativistic photo-sphere velocity is derived from the data in a model-independent way, summarising from [40]:

$$\frac{\beta^5}{4[\ln(1+\beta) - (1-\beta)\beta]^2} \left(\frac{1+\beta}{1-\beta}\right)^{1/2} = \frac{D_L(z)}{1+z} \frac{1}{t_2 - t_1} \left(\sqrt{\frac{F_{\text{bb,obs}}(t_2)}{\sigma T_{\text{obs}}^4(t_2)}} - \sqrt{\frac{F_{\text{bb,obs}}(t_1)}{\sigma T_{\text{obs}}^4(t_1)}} \right), \quad (18)$$

The left-hand side is a function of velocity β , the right-hand side is only from observables, $D_L(z)$ is the luminosity distance and z the cosmological redshift. From the observed thermal flux $F_{\text{bb,obs}}$ and temperature T_{obs} in two times t_1 and t_2 , the velocity β is obtained. This model-independent equation has been derived in a fully relativistic way so it remains valid in the Newtonian non-relativistic regime.

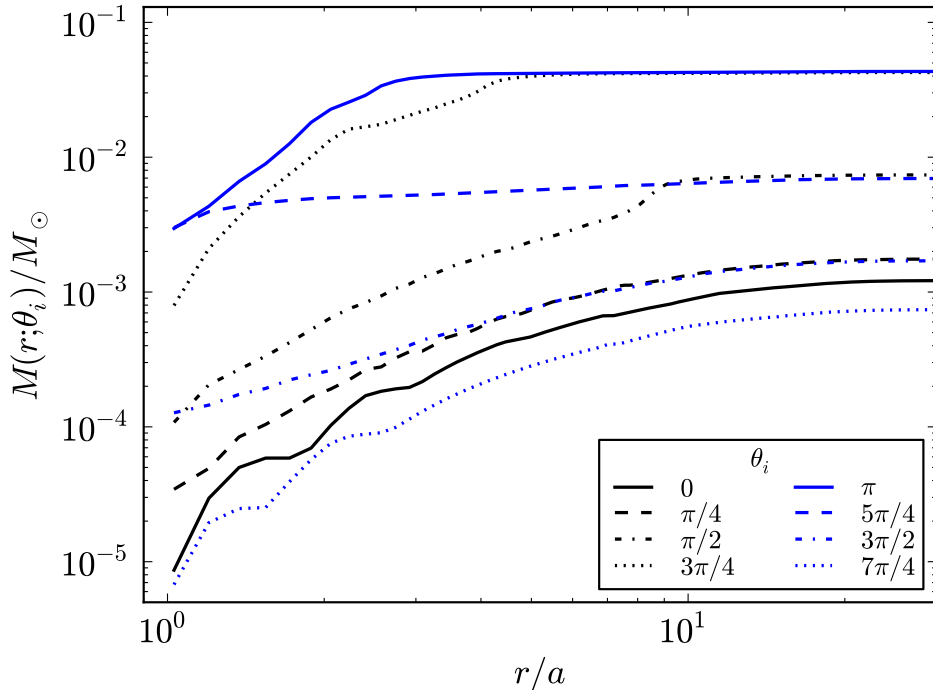


Figure 11. Cumulative radial mass profiles of the SN ejecta enclosed within a cone of 5° of semi-aperture angle with vertex at the BH position (taken from Figure 35 in [40]). These profiles have been extracted from the simulations at the time of BH formation. The binary parameters are: the initial mass of the NS companion is $2.0 M_\odot$; the CO_{core} leading to an ejecta mass of $7.94 M_\odot$, and the orbital period is $P \approx 5$ min, namely a binary separation $a \approx 1.5 \times 10^{10}$ cm.

An additional, and very important prediction of this scenario, is that the injection of energy and momentum from the GRB plasma into the ejecta transforms the SN into an HN (see [89] for the specific case of GRB 151027A).

5.4. Late X-ray Afterglow

We have shown in Ruffini *et al.* [91] that the synchrotron emission by relativistic electrons from the νNS , injected into the expanding magnetized HN ejecta, together with the νNS pulsar emission that extracts its rotational energy, power the X-ray afterglow. This includes the early part and the late power-law behavior. An exceptional by-product of this analysis is that it gives a glimpse on the νNS magnetic field strength and structure (dipole+quadrupole).

Based on the above model [91], GRB 130427A (a BdHN I) and GRB 180728A (a BdHN II) have been analyzed in [49]. The explanation of the afterglow data of GRB 130427A led to an initial 1 ms rotation period for the νNS . For GRB 180728A, a slower spin of 2.5 ms was there obtained. A simple analysis

showed how this result is in agreement with the BdHN I and II nature of these GRBs. First, we recall that compact binary systems have likely synchronized components with the orbital period. Second, we can infer the orbital period from the analysis of the X-ray precursor and the prompt emission (see [49] for the procedure). Then, we can infer the CO_{core} rotation period too. Finally, assuming angular momentum conservation in the core-collapse SN process, we can estimate the rotation period of the νNS formed at the SN center. This method led to a binary separation remarkably in agreement with the one inferred from the precursor and the prompt emission, demonstrating the self-consistency of this scenario [49].

5.5. High-Energy GeV Emission

We turn back again to the already introduced *inner engine*. The joint action of rotation and magnetic field induces an electric potential [84,85]

$$\Delta\phi = - \int_{\infty}^{r_+} E dr = E_{r_+} r_+ = 9.7 \times 10^{20} \cdot \alpha \left(\frac{B_0}{B_c} \right) \left(\frac{M}{M_{\odot}} \right) (1 + \sqrt{1 - \alpha^2}) \frac{V}{e}, \quad (19)$$

capable to accelerate protons to ultrarelativistic velocities and energies up to $\epsilon_p = e\Delta\phi \approx 10^{21}$ eV.

Along the rotation axis, there are no radiation losses and so the *inner engine* leads to UHECRs. In the off-polar directions, the protons radiate synchrotron photons, e.g., at GeV and TeV energies.

In [84] it has been estimated that the available electrostatic energy to accelerate protons is

$$\mathcal{E} = \frac{1}{2} E_{r_+}^2 r_+^3 \approx 7.5 \times 10^{41} \cdot \alpha^2 \left(\frac{B_0}{B_c} \right)^2 \left(\frac{M}{M_{\odot}} \right)^3 (1 + \sqrt{1 - \alpha^2})^3 \text{ erg}, \quad (20)$$

so the number of protons that the *inner engine* can accelerate is

$$N_p = \frac{\mathcal{E}}{\epsilon_p} \approx 4.8 \times 10^{32} \alpha \left(\frac{B_0}{B_c} \right) \left(\frac{M}{M_{\odot}} \right)^2 (1 + \sqrt{1 - \alpha^2})^2. \quad (21)$$

The timescale of the first elementary process is dictated by the acceleration time, i.e.,:

$$\Delta t_{\text{el}} = \frac{\Delta\phi}{E_{r_+} c} = \frac{r_+}{c} \approx 4.9 \times 10^{-6} \left(\frac{M}{M_{\odot}} \right) (1 + \sqrt{1 - \alpha^2}) \text{ s}. \quad (22)$$

so the emission power of the *inner engine* is approximately:

$$\frac{d\mathcal{E}}{dt} \approx \frac{\mathcal{E}}{\Delta t_{\text{el}}} = 1.5 \times 10^{47} \cdot \alpha^2 \left(\frac{B_0}{B_c} \right)^2 \left(\frac{M}{M_{\odot}} \right)^2 (1 + \sqrt{1 - \alpha^2})^2 \text{ erg} \cdot \text{s}^{-1}. \quad (23)$$

The timescale of the subsequent processes depends crucially on the time required to rebuild the electric field. It has been shown that this condition implies an essential role of the density profile of the ionic matter surrounding the BH and its evolution with time [85,86].

For a BH mass of the order of the NS critical mass, say $M \sim 3 M_{\odot}$, a BH spin parameter $\alpha \sim 0.3$, and a strength of the magnetic field $B_0 \sim 10^{14}$ G, the above numbers are in agreement with the observed GeV emission data. See, for instance, in [85] and [86], respectively, the details of the analysis of GRB 130427A and GRB 190114C. We refer to [84,85] for details on the synchrotron emission of the accelerated protons in the above magnetic field.

5.6. Additional Considerations

The strong dependence of P_{max} on the initial mass of the NS companion opens the interesting possibility of producing XRFs and BdHNe from binaries with similar short (e.g., $P \sim$ few minutes)

orbital periods and CO_{core} properties: while a system with a massive (e.g., $\gtrsim 2 M_{\odot}$) NS companion would lead to a BdHN, a system with a lighter (e.g., $\lesssim 1.4 M_{\odot}$) NS companion would lead to an XRF. This predicts systems with a similar initial SN, leading to a similar νNS , but with different GRB prompt and afterglow emission. Given that the GRB energetics are different, the final SN kinetic energy should also be different being that it is larger for the BdHNe. This has been clearly shown by specific examples in [49].

There are also additional novel features unveiled by the new 3D SPH simulations which can be observable in GRB light-curves and spectra, e.g.,:

- (1) the hypercritical accretion occurs not only on the NS companion but also on the νNS and with a comparable rate.
- (2) This implies that BdHNe might be also be able to form, in special cases, BH-BH binaries. Since the system remains bound the binary will quickly merge by emitting gravitational waves. Clearly, no electromagnetic emission is expected from these mergers. However, the typically large cosmological distances of BdHNe would make it extremely difficult to detect their gravitational waves e.g., by LIGO/Virgo.
- (3) Relatively weak SN explosions produce a long-lived hypercritical accretion process leading and enhance, at late times, the accretion onto the νNS . The revival of the accretion process at late times is a unique feature of our binary and does not occur for single SNe, namely in the absence of the NS companion. This feature increases the probability of detection of weak SNe by X-ray detectors via the accretion phase in an XRF/BdHN.
- (4) For asymmetric SN explosions the accretion rate shows a quasi-periodic behavior that might be detected by X-rays instruments, possibly allowing a test of the binary nature and the identification of the orbital period of the progenitor.

6. Post-Explosion Orbits and Formation of NS-BH Binaries

The SN explosion leaves as a central remnant a νNS and the induced gravitational collapse of the NS companion leads to BH formation. Therefore, BdHNe potentially leads to νNS -BH binaries, providing the binary keeps bound. This question was analyzed via numerical simulations in [55].

Typical binaries become unbound during an SN explosion because of mass loss and the momentum imparted (kick) to the νNS by the explosion. A classical astrophysical result shows that, assuming the explosion as instantaneous (sudden mass loss approximation), disruption occurs if half of the binary mass is lost. For this reason the fraction of massive binaries that can produce double compact-object binaries is usually found to be very low (e.g., ~ 0.001 –1%) [54,59,121].

Assuming instantaneous mass loss, the post-explosion semi-major axis is [122]:

$$\frac{a}{a_0} = \frac{M_0 - \Delta M}{M_0 - 2a_0\Delta M/r'} \quad (24)$$

where a_0 and a are the initial and final semi-major axes respectively, M_0 is the (initial) binary mass, ΔM is the change of mass (in this case the amount of mass loss), and r is the orbital separation before the explosion. For circular orbits, the system is unbound if it loses half of its mass. For the very tight BdHNe, however, additional effects have to be taken into account to determine the fate of the binary.

The shock front in an SN moves at roughly 10^4 km s^{-1} , but the denser, lower-velocity ejecta, can move at velocities as low as 10^2 – 10^3 km s^{-1} [83]. This implies that the SN ejecta overcomes an NS companion in a time 10–1000 s. For wide binaries this time is a small fraction of the orbital period and the “instantaneous” mass-loss assumption is perfectly valid. BdHNe have instead orbital periods as short as 100–1000 s, hence the instantaneous mass-loss approximation breaks down.

We recall the specific examples studied in [55]: close binaries in an initial circular orbit of radius $7 \times 10^9 \text{ cm}$, CO_{core} radii of $(1\text{--}4) \times 10^9 \text{ cm}$ with a $2.0 M_{\odot}$ NS companion. The CO_{core} leaves a central $1.5 M_{\odot}$ NS, ejecting the rest of the core. The NS leads to a BH with a mass equal to the NS critical

mass. For these parameters it was there obtained that even if 70% of the mass is lost the binary remains bound, providing the explosion time is of the order of the orbital period ($P = 180$ s) with semi-major axes of less than 10^{11} cm (see Figure 12).

The tight ν NS-BH binaries produced by BdHNe will, in due time, merge owing to the emission of gravitational waves. For the above typical parameters the merger time is of the order of 10^4 year, or even less (see Figure 12). We expect little baryonic contamination around such merger site since this region has been cleaned-up by the BdHN. These conditions lead to a new family of sources which we have called ultrashort GRBs, U-GRBs.

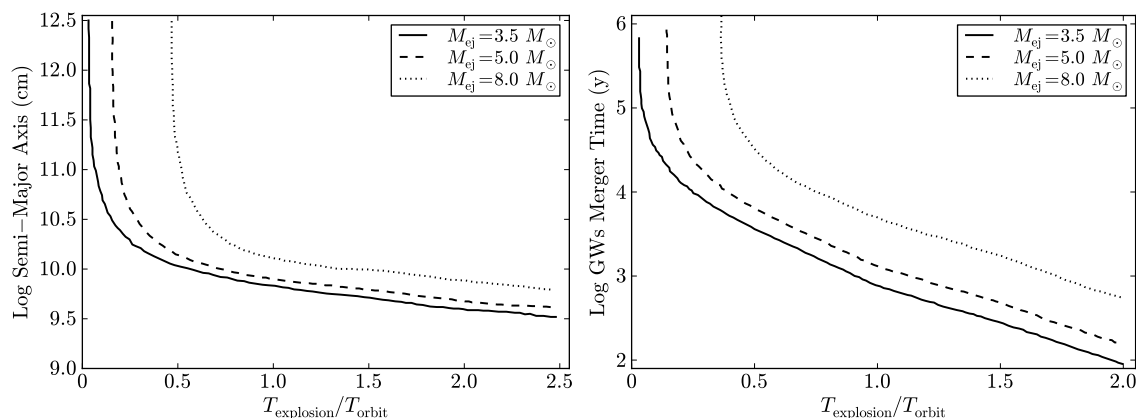


Figure 12. (a) Semi-major axis versus explosion time for three different mass ejecta scenarios: $3.5 M_{\odot}$ (solid), $5.0 M_{\odot}$ (dotted), $8.0 M_{\odot}$ (dashed), including mass accretion and momentum effects (taken from Figure 2 in [55]). Including these effects, all systems with explosion times above 0.7 times the orbital time are bound and the final separations are on par with the initial separations. (b) Merger time due to gravitational wave emission as a function of explosion time for the same three binaries of the left panel (taken from Figure 3 in [55]). Note that systems with explosion times 0.1–0.6 T_{orbit} have merger times less than roughly 10^4 y. For most of our systems, the explosion time is above this limit and we expect most of these systems to merge quickly.

7. BdHN Formation, Occurrence Rate and Connection with Short GRBs

7.1. An Evolutionary Scenario

The X-ray binary and SN communities have introduced a new evolutionary scenario for the formation of compact-object binaries (NS-NS or NS-BH). After the collapse of the primary star forming a NS, the binary undergoes mass-transfer episodes finally leading to the ejection of both the hydrogen and helium shells of the secondary star. These processes lead naturally to a binary composed of a CO_{core} and an NS companion (see Figure 1). In the X-ray binary and SN communities these systems are called “ultra-stripped” binaries [123]. These systems are expected to comprise 0.1–1% of the total SNe [124].

The existence of ultra-stripped binaries supports our scenario from the stellar evolution side. In the above studies most of the binaries have orbital periods in the range 3×10^3 – 3×10^5 s which are longer with respect to the short periods expected in the BdHN scenario. Clearly, XRF and BdHN progenitors should be only a small subset that result from the binaries with initial orbital separation and component masses leading to CO_{core} -NS binaries with short orbital periods, e.g., 100–1000 s for the occurrence of BdHNe. This requires fine-tuning both of the CO_{core} mass and the binary orbit. From an astrophysical point of view the IGC scenario is characterized by the BH formation induced by the hypercritical accretion onto the NS companion and the associated GRB emission. Indeed, GRBs are a rare phenomenon and the number of systems approaching the conditions for their occurrence must be low (see [55] for details).

7.2. Occurrence Rate

If we assume that XRFs and BdHNe can be final stages of ultra-stripped binaries, then the percentage of the ultra-stripped population leading to these long GRBs must be very small. The observed occurrence rate of XRFs and BdHNe has been estimated to be $\sim 100 \text{ Gpc}^{-3} \text{ yr}^{-1}$ and $\sim 1 \text{ Gpc}^{-3} \text{ yr}^{-1}$, respectively [45], namely the 0.5% and 0.005% of the Ibc SNe rate, $2 \times 10^4 \text{ Gpc}^{-3} \text{ yr}^{-1}$ [125]. It has been estimated that (0.1–1%) of the SN Ibc could originate from ultra-stripped binaries [124], which would lead to an approximate density rate of (20–200) $\text{Gpc}^{-3} \text{ yr}^{-1}$. This would imply that a small fraction ($\lesssim 5\%$) of the ultra-stripped population would be needed to explain the BdHNe while, roughly speaking, almost the whole population would be needed to explain the XRFs (see Table 1). These numbers, while waiting for a confirmation by further population synthesis analyses, would suggest that most SNe originated from ultra-stripped binaries should be accompanied by an XRF. It is interesting that the above estimates are consistent with traditional estimates that only ~ 0.001 –1% of massive binaries lead to double compact-object binaries [54,59,121].

7.3. Connection with Short GRBs

It is then clear that XRFs and BdHNe lead to ν NS-NS and ν NS-BH binaries. In due time, the emission of gravitational waves shrink their orbit leading to mergers potentially detectable as short GRBs. This implies a connection between the rate of long and short GRBs. It is clear from the derived rates (see Table 1 and [45,47]) that the short GRB population is dominated by the low-luminosity class of short Gamma-ray flashes (S-GRFs), double NS mergers that do not lead to BH formation. It can be seen that it is sufficient $\lesssim 4\%$ of XRFs to explain the S-GRFs population, which would be consistent with the fact that many XRF progenitor binaries will get disrupted by the SN explosion. Therefore, by now, the observed rates of the GRB subclasses are consistent with the interesting possibility of a connection between the progenitors of the long and the ones of the short GRBs.

8. Conclusions

It is by now clear that short and long Gamma-ray bursts subclassify into eight different families and have as progenitors binary systems of a variety of flavors (see Table 1). We have focused in this work on the specific class of BdHNe of two types: type I and type II BdHNe, what in our old classification [45] we called BdHNe and XRFs, respectively.

We have devoted this article mostly to the theoretical aspects of the *induced gravitational collapse scenario* and its evolution into BdHN as a complete model of long GRBs. We have also discussed, although briefly, the observable features of the model and how they compare with the observational data, providing to the reader the appropriate references for deepening this important aspect.

BdHNe I and II have as a common progenitor a CO_{core} -NS binary. The CO_{core} explodes as type Ic SN, forming at its center a new NS, which we denote ν NS, and produces onto the NS companion a hypercritical accretion process accompanied by an intense neutrino emission. The intensity of the accretion process and the neutrino emission depends mainly on the binary period, being more intense for tighter binaries. The NS companion in such an accretion process can reach or not the critical mass for gravitational collapse, i.e., to form a BH. The former binaries leading to a BH by accretion are the BdHNe I, while the ones in which the NS companion becomes just a more massive NS, are the BdHNe II (the old XRFs) (see Table 1).

We have reviewed the results of the numerical simulations performed of the above physical process starting from the 1D ones all the way to the latest 3D SPH ones. The simulation of this binary process has opened our eyes to a new reality: long GRBs are much richer and more complex systems than every one of us thought before, with the 3D morphology of the SN ejecta, that becomes asymmetric by the accretion process, playing a fundamental role in the GRB analysis.

We have recalled the relevance of each of the following processes in a BdHN:

- (1) the SN explosion;

- (2) the hypercritical accretion onto the NS companion;
- (3) the NS collapse with consequent BH formation;
- (4) the initiation of the *inner engine*;
- (5) the e^+e^- plasma production;
- (6) the e^+e^- plasma feedback onto the SN which converts the SN into a HN;
- (7) the formation of the cavity around the newborn BH;
- (8) the transparency of the e^+e^- plasma along different directions;
- (9) the HN emission powered by the ν NS;
- (10) the action of the *inner engine* in accelerating protons leading to UHECRs and to the high-energy emission.

The aforementioned involved physical processes in a BdHN have specific signatures observable (and indeed observed) in the long GRB multiwavelength lightcurves and spectra. We have recalled for each process its energetics, spectrum, and associated Lorentz factor: from the mildly-relativistic X-ray precursor, to the ultrarelativistic prompt Gamma-ray emission, to the mildly-relativistic X-ray flares of the early afterglow, to the mildly-relativistic late afterglow and to the high-energy GeV emission.

All of the above is clearly in contrast with a simple GRB model attempting to explain the entire GRB process with the kinetic energy of an ultrarelativistic jet extending through all of the above GRB phases, as in the traditional collapsar-fireball model.

If the binaries keep bound during the explosion, BdHNe I lead to ν NS-BH binaries and BdHNe II lead to ν NS-NS binaries. In due time, via gravitational wave emission, such binaries merge producing short GRBs. This unveiled clear interconnection between long and short GRBs and their occurrence rates needs to be accounted for in the cosmological evolution of binaries within population synthesis models for the formation of compact-object binaries.

We have taken the opportunity to include a brief summary of very recent developments published during the peer-review process of this article. These results cover the explanation of the observed GeV emission in BdHNe [84–87]. One of the most relevant aspects of this topic is that it requests the solution of one of the fundamental problems in relativistic astrophysics: how to extract the rotational energy from a BH. This implies the role of a magnetic field around the newborn BH and the presence of surrounding matter as predicted in a BdHN. We have called this part of the system the *inner engine* of the high-energy emission. The BH rotation and surrounding magnetic field, for appropriate values induces an electric field via the Wald's mechanism [88]. Such an electric field is of paramount importance in accelerating surrounding protons to ultrarelativistic velocities leading to the high-energy emission via proton-synchrotron radiation. The details of this exciting new topic are beyond the scope of the present article but we encourage the reader to go through the above references for complementary details.

Funding: This research received no external funding.

Conflicts of Interest: The authors declare no conflict of interest.

References

1. Mazets, E.P.; Golenetskii, S.V.; Ilinskii, V.N.; Panov, V.N.; Aptekar, R.L.; Gurian, I.A.; Proskura, M.P.; Sokolov, I.A.; Sokolova, Z.I.; Kharitonova, T.V. Catalog of cosmic Gamma-ray bursts from the KONUS experiment data. I. *Astrophys. Space Sci.* **1981**, *80*, 3–83. [[CrossRef](#)]
2. Klebesadel, R.W. The durations of Gamma-ray bursts. In *Gamma-ray Bursts—Observations, Analyses and Theories*; Ho, C., Epstein, R.I., Fenimore, E.E., Eds.; Cambridge University Press: Cambridge, UK, 1992; pp. 161–168.
3. Dezalay, J.P.; Barat, C.; Talon, R.; Syunyaev, R.; Terekhov, O.; Kuznetsov, A. Short cosmic events—A subset of classical GRBs? In *American Institute of Physics Conference Series*; Paciesas, W.S., Fishman, G.J., Eds.; American Institute of Physics: College Park, MD, USA, 1992; Volume 265, pp. 304–309.

4. Kouveliotou, C.; Meegan, C.A.; Fishman, G.J.; Bhat, N.P.; Briggs, M.S.; Koshut, T.M.; Paciesas, W.S.; Pendleton, G.N. Identification of two classes of Gamma-ray bursts. *Astrophys. J. Lett.* **1993**, *413*, L101–L104. [[CrossRef](#)]
5. Tavani, M. Euclidean versus Non-Euclidean Gamma-ray Bursts. *Astrophys. J. Lett.* **1998**, *497*, L21–L24. [[CrossRef](#)]
6. Goodman, J. Are Gamma-ray bursts optically thick? *Astrophys. J. Lett.* **1986**, *308*, L47. [[CrossRef](#)]
7. Paczynski, B. Gamma-ray bursters at cosmological distances. *Astrophys. J. Lett.* **1986**, *308*, L43. [[CrossRef](#)]
8. Eichler, D.; Livio, M.; Piran, T.; Schramm, D.N. Nucleosynthesis, neutrino bursts and Gamma-rays from coalescing neutron stars. *Nature* **1989**, *340*, 126–128. [[CrossRef](#)]
9. Narayan, R.; Piran, T.; Shemi, A. Neutron star and black hole binaries in the Galaxy. *Astrophys. J. Lett.* **1991**, *379*, L17–L20. [[CrossRef](#)]
10. Pian, E.; Amati, L.; Antonelli, L.A.; Butler, R.C.; Costa, E.; Cusumano, G.; Danziger, J.; Feroci, M.; Fiore, F.; Frontera, F.; et al. BEPOSAX Observations of GRB 980425: Detection of the Prompt Event and Monitoring of the Error Box. *Astrophys. J. Lett.* **2000**, *536*, 778–787. [[CrossRef](#)]
11. Galama, T.J.; Vreeswijk, P.M.; van Paradijs, J.; Kouveliotou, C.; Augusteijn, T.; Bönhardt, H.; Brewer, J.P.; Doublier, V.; Gonzalez, J.F.; Leibundgut, B.; et al. An unusual supernova in the error box of the γ -ray burst of 25 April 1998. *Nature* **1998**, *395*, 670–672. [[CrossRef](#)]
12. Della Valle, M. Supernovae and Gamma-ray Bursts: A Decade of Observations. *Int. J. Mod. Phys. D* **2011**, *20*, 1745–1754. [[CrossRef](#)]
13. Cano, Z.; Wang, S.Q.; Dai, Z.G.; Wu, X.F. The Observer’s Guide to the Gamma-ray Burst Supernova Connection. *Adv. Astron.* **2017**, *2017*, 8929054. [[CrossRef](#)]
14. Woosley, S.E.; Bloom, J.S. The Supernova Gamma-ray Burst Connection. *Annu. Rev. Astron. Astrophys.* **2006**, *44*, 507–556. [[CrossRef](#)]
15. Blandford, R.D.; McKee, C.F. Fluid dynamics of relativistic blast waves. *Phys. Fluids* **1976**, *19*, 1130–1138. [[CrossRef](#)]
16. Shemi, A.; Piran, T. The appearance of cosmic fireballs. *Astrophys. J. Lett.* **1990**, *365*, L55–L58. [[CrossRef](#)]
17. Meszaros, P.; Laguna, P.; Rees, M.J. Gasdynamics of relativistically expanding Gamma-ray burst sources—Kinematics, energetics, magnetic fields, and efficiency. *Astrophys. J. Lett.* **1993**, *415*, 181–190. [[CrossRef](#)]
18. Piran, T.; Shemi, A.; Narayan, R. Hydrodynamics of Relativistic Fireballs. *MNRAS* **1993**, *263*, 861. [[CrossRef](#)]
19. Mao, S.; Yi, I. Relativistic beaming and Gamma-ray bursts. *Astrophys. J. Lett.* **1994**, *424*, L131–L134. [[CrossRef](#)]
20. Piran, T. Gamma-ray bursts and the fireball model. *Phys. Rep.* **1999**, *314*, 575–667. [[CrossRef](#)]
21. Piran, T. The physics of Gamma-ray bursts. *Rev. Mod. Phys.* **2004**, *76*, 1143–1210. [[CrossRef](#)]
22. Mészáros, P. Theories of Gamma-ray Bursts. *Annu. Rev. Astron. Astrophys.* **2002**, *40*, 137. [[CrossRef](#)]
23. Mészáros, P. Gamma-ray bursts. *Rep. Prog. Phys.* **2006**, *69*, 2259–2321. [[CrossRef](#)]
24. Berger, E. Short-Duration Gamma-ray Bursts. *Annu. Rev. Astron. Astrophys.* **2014**, *52*, 43–105. [[CrossRef](#)]
25. Kumar, P.; Zhang, B. The physics of Gamma-ray bursts and relativistic jets. *Phys. Rep.* **2015**, *561*, 1–109. [[CrossRef](#)]
26. Smith, N.; Li, W.; Silverman, J.M.; Ganeshalingam, M.; Filippenko, A.V. Luminous blue variable eruptions and related transients: Diversity of progenitors and outburst properties. *MNRAS* **2011**, *415*, 773–810. [[CrossRef](#)]
27. Nomoto, K.; Hashimoto, M. Presupernova evolution of massive stars. *Phys. Rep.* **1988**, *163*, 13–36. [[CrossRef](#)]
28. Iwamoto, K.; Nomoto, K.; Höflich, P.; Yamaoka, H.; Kumagai, S.; Shigeyama, T. Theoretical light curves for the type IC supernova SN 1994I. *Astrophys. J. Lett.* **1994**, *437*, L115–L118. [[CrossRef](#)]
29. Fryer, C.L.; Mazzali, P.A.; Prochaska, J.; Cappellaro, E.; Panaitescu, A.; Berger, E.; van Putten, M.; van den Heuvel, E.P.J.; Young, P.; Hungerford, A.; et al. Constraints on Type Ib/c Supernovae and Gamma-ray Burst Progenitors. *Publ. Astron. Soc. Pac.* **2007**, *119*, 1211–1232. [[CrossRef](#)]
30. Yoon, S.C.; Woosley, S.E.; Langer, N. Type Ib/c Supernovae in Binary Systems. I. Evolution and Properties of the Progenitor Stars. *Astrophys. J. Lett.* **2010**, *725*, 940–954. [[CrossRef](#)]
31. Frail, D.A.; Kulkarni, S.R.; Sari, R.; Djorgovski, S.G.; Bloom, J.S.; Galama, T.J.; Reichart, D.E.; Berger, E.; Harrison, F.A.; Price, P.A.; et al. Beaming in Gamma-ray Bursts: Evidence for a Standard Energy Reservoir. *Astrophys. J. Lett.* **2001**, *562*, L55–L58. [[CrossRef](#)]

32. Covino, S.; Malesani, D.; Tagliaferri, G.; Vergani, S.D.; Chincarini, G.; Kann, D.A.; Moretti, A.; Stella, L.; Misticci Collaboration. Achromatic breaks for Swift GRBs: Any evidence? *Nuovo C. Ser.* **2006**, *121*, 1171–1176.
33. Sato, G.; Yamazaki, R.; Ioka, K.; Sakamoto, T.; Takahashi, T.; Nakazawa, K.; Nakamura, T.; Toma, K.; Hullinger, D.; Tashiro, M.; et al. Swift Discovery of Gamma-ray Bursts without a Jet Break Feature in Their X-ray Afterglows. *Astrophys. J. Lett.* **2007**, *657*, 359–366. [[CrossRef](#)]
34. Burrows, D.; Garmire, G.; Ricker, G.; Bautz, M.; Nousek, J.; Grupe, D.; Racusin, J. Chandra Searches for Late-Time Jet Breaks in GRB X-ray Afterglows. In *Chandra's First Decade of Discovery*; Wolk, S., Fruscione, A., Swartz, D., Eds.; Chandra X-ray Center: Cambridge, MA, USA, 2009.
35. Izzo, L.; Ruffini, R.; Penacchioni, A.V.; Bianco, C.L.; Caito, L.; Chakrabarti, S.K.; Rueda, J.A.; Nandi, A.; Patricelli, B. A double component in GRB 090618: A proto-black hole and a genuinely long Gamma-ray burst. *A&A* **2012**, *543*, A10.
36. Ruffini, R. Fundamental Physics from Black Holes, Neutron Stars and Gamma-ray Bursts. *Int. J. Mod. Phys. D* **2011**, *20*, 1797–1872. [[CrossRef](#)]
37. Ruffini, R.; Salmonson, J.D.; Wilson, J.R.; Xue, S.S. On the pair-electromagnetic pulse from an electromagnetic black hole surrounded by a baryonic remnant. *A&A* **2000**, *359*, 855–864.
38. Smartt, S.J. Observational Constraints on the Progenitors of Core-Collapse Supernovae: The Case for Missing High-Mass Stars. *PASA* **2015**, *32*, e016. [[CrossRef](#)]
39. Smartt, S.J. Progenitors of Core-Collapse Supernovae. *Annu. Rev. Astron. Astrophys.* **2009**, *47*, 63–106. [[CrossRef](#)]
40. Ruffini, R.; Wang, Y.; Aimuratov, Y.; Barres de Almeida, U.; Becerra, L.; Bianco, C.L.; Chen, Y.C.; Karlica, M.; Kovacevic, M.; Li, L.; et al. Early X-ray Flares in GRBs. *Astrophys. J. Lett.* **2018**, *852*, 53. [[CrossRef](#)]
41. Ruffini, R.; Bianco, C.L.; Frascchetti, F.; Xue, S.S.; Chardonnet, P. On a Possible Gamma-ray Burst-Supernova Time Sequence. *Astrophys. J. Lett.* **2001**, *555*, L117–L120. [[CrossRef](#)]
42. Ruffini, R.; Bernardini, M.G.; Bianco, C.L.; Caito, L.; Chardonnet, P.; Cherubini, C.; Dainotti, M.G.; Frascchetti, F.; Geralico, A.; Guida, R.; et al. On Gamma-ray Bursts. In *The Eleventh Marcel Grossmann Meeting On Recent Developments in Theoretical and Experimental General Relativity, Gravitation and Relativistic Field Theories*; Kleinert, H., Jantzen, R.T., Ruffini, R., Eds.; World Scientific Publishing Co. Pte Ltd.: Hackensack, NJ, USA, 2008; pp. 368–505.
43. Sana, H.; de Mink, S.E.; de Koter, A.; Langer, N.; Evans, C.J.; Gieles, M.; Gosset, E.; Izzard, R.G.; Le Bouquin, J.B.; Schneider, F.R.N. Binary Interaction Dominates the Evolution of Massive Stars. *Science* **2012**, *337*, 444. [[CrossRef](#)]
44. Smith, N. Mass Loss: Its Effect on the Evolution and Fate of High-Mass Stars. *Annu. Rev. Astron. Astrophys.* **2014**, *52*, 487–528. [[CrossRef](#)]
45. Ruffini, R.; Rueda, J.A.; Muccino, M.; Aimuratov, Y.; Becerra, L.M.; Bianco, C.L.; Kovacevic, M.; Moradi, R.; Oliveira, F.G.; Pisani, G.B.; et al. On the Classification of GRBs and Their Occurrence Rates. *Astrophys. J. Lett.* **2016**, *832*, 136. [[CrossRef](#)]
46. Rueda, J.A.; Aimuratov, Y.; de Almeida, U.B.; Becerra, L.; Bianco, C.L.; Cherubini, C.; Filippi, S.; Karlica, M.; Kovacevic, M.; Fuksman, J.D.M.; et al. The binary systems associated with short and long Gamma-ray bursts and their detectability. *Int. J. Mod. Phys. D* **2017**, *26*, 1730016. [[CrossRef](#)]
47. Ruffini, R.; Rodriguez, J.; Muccino, M.; Rueda, J.A.; Aimuratov, Y.; Barres de Almeida, U.; Becerra, L.; Bianco, C.L.; Cherubini, C.; Filippi, S.; et al. On the Rate and on the Gravitational Wave Emission of Short and Long GRBs. *Astrophys. J. Lett.* **2018**, *859*, 30. [[CrossRef](#)]
48. Ruffini, R.; Moradi, R.; Wang, Y.; Aimuratov, Y.; Amiri, M.; Becerra, L.; Bianco, C.L.; Chen, Y.C.; Eslam Panah, B.; Mathews, G.J.; et al. On the universal GeV emission in binary-driven hypernovae and their inferred morphological structure. *arXiv* **2018**, arXiv:1803.05476.
49. Wang, Y.; Rueda, J.A.; Ruffini, R.; Becerra, L.; Bianco, C.; Becerra, L.; Li, L.; Karlica, M. Two Predictions of Supernova: GRB 130427A/SN 2013cq and GRB 180728A/SN 2018fip. *Astrophys. J. Lett.* **2019**, *874*, 39. [[CrossRef](#)]
50. Rueda, J.A.; Ruffini, R.; Wang, Y.; Aimuratov, Y.; Barres de Almeida, U.; Bianco, C.L.; Chen, Y.C.; Lobato, R.V.; Maia, C.; Primorac, D.; et al. GRB 170817A-GW170817-AT 2017gfo and the observations of NS-NS, NS-WD and WD-WD mergers. *J. Cosmol. Astropart. Phys.* **2018**, *2018*, 006. [[CrossRef](#)]

51. Rueda, J.A.; Ruffini, R.; Wang, Y.; Bianco, C.L.; Blanco-Iglesias, J.M.; Karlica, M.; Lorén-Aguilar, P.; Moradi, R.; Sahakyan, N. Electromagnetic emission of white dwarf binary mergers. *J. Cosmol. Astropart. Phys.* **2019**, *2019*, 044. [[CrossRef](#)]
52. Becerra, L.; Bianco, C.L.; Fryer, C.L.; Rueda, J.A.; Ruffini, R. On the Induced Gravitational Collapse Scenario of Gamma-ray Bursts Associated with Supernovae. *Astrophys. J. Lett.* **2016**, *833*, 107. [[CrossRef](#)]
53. Becerra, L.; Cipolletta, F.; Fryer, C.L.; Rueda, J.A.; Ruffini, R. Angular Momentum Role in the Hypercritical Accretion of Binary-driven Hypernovae. *Astrophys. J. Lett.* **2015**, *812*, 100. [[CrossRef](#)]
54. Postnov, K.A.; Yungelson, L.R. The Evolution of Compact Binary Star Systems. *Living Rev. Relativ.* **2014**, *17*, 3. [[CrossRef](#)]
55. Fryer, C.L.; Oliveira, F.G.; Rueda, J.A.; Ruffini, R. Neutron-Star-Black-Hole Binaries Produced by Binary-Driven Hypernovae. *Phys. Rev. Lett.* **2015**, *115*, 231102. [[CrossRef](#)]
56. Giacconi, R.; Ruffini, R. (Eds.) *Physics and Astrophysics of Neutron Stars and Black Holes*; North Holland Publishing Co.: Amsterdam, The Netherlands, 1978.
57. Belczynski, K.; Bulik, T.; Bailyn, C. The Fate of Cyg X-1: An Empirical Lower Limit on Black-hole-Neutron-star Merger Rate. *Astrophys. J. Lett.* **2011**, *742*, L2. [[CrossRef](#)]
58. Mirabel, I.F.; Rodríguez, L.F. Microquasars in our Galaxy. *Nature* **1998**, *392*, 673–676. [[CrossRef](#)]
59. Fryer, C.L.; Woosley, S.E.; Hartmann, D.H. Formation Rates of Black Hole Accretion Disk Gamma-ray Bursts. *Astrophys. J. Lett.* **1999**, *526*, 152–177. [[CrossRef](#)]
60. Li, L.X.; Paczyński, B. Transient Events from Neutron Star Mergers. *Astrophys. J. Lett.* **1998**, *507*, L59–L62. [[CrossRef](#)]
61. Metzger, B.D.; Martínez-Pinedo, G.; Darbha, S.; Quataert, E.; Arcones, A.; Kasen, D.; Thomas, R.; Nugent, P.; Panov, I.V.; Zinner, N.T. Electromagnetic counterparts of compact object mergers powered by the radioactive decay of r-process nuclei. *MNRAS* **2010**, *406*, 2650–2662. [[CrossRef](#)]
62. Tanvir, N.R.; Levan, A.J.; Fruchter, A.S.; Hjorth, J.; Hounsell, R.A.; Wiersema, K.; Tunnicliffe, R.L. A ‘kilonova’ associated with the short-duration γ -ray burst GRB 130603B. *Nature* **2013**, *500*, 547–549. [[CrossRef](#)]
63. Berger, E.; Fong, W.; Chornock, R. An r-process Kilonova Associated with the Short-hard GRB 130603B. *Astrophys. J. Lett.* **2013**, *774*, L23. [[CrossRef](#)]
64. Meszaros, P.; Rees, M.J. Poynting Jets from Black Holes and Cosmological Gamma-ray Bursts. *Astrophys. J. Lett.* **1997**, *482*, L29. [[CrossRef](#)]
65. Rosswog, S.; Ramirez-Ruiz, E.; Davies, M.B. High-resolution calculations of merging neutron stars—III. Gamma-ray bursts. *MNRAS* **2003**, *345*, 1077–1090. [[CrossRef](#)]
66. Lee, W.H.; Ramirez-Ruiz, E.; Page, D. Opaque or Transparent? A Link between Neutrino Optical Depths and the Characteristic Duration of Short Gamma-ray Bursts. *Astrophys. J. Lett.* **2004**, *608*, L5–L8. [[CrossRef](#)]
67. Ruffini, R.; Muccino, M.; Kovacevic, M.; Oliveira, F.G.; Rueda, J.A.; Bianco, C.L.; Enderli, M.; Penacchioni, A.V.; Pisani, G.B.; Wang, Y.; et al. GRB 140619B: A short GRB from a binary neutron star merger leading to black hole formation. *Astrophys. J. Lett.* **2015**, *808*, 190. [[CrossRef](#)]
68. Ruffini, R.; Muccino, M.; Aimuratov, Y.; Bianco, C.L.; Cherubini, C.; Enderli, M.; Kovacevic, M.; Moradi, R.; Penacchioni, A.V.; Pisani, G.B.; et al. GRB 090510: A Genuine Short GRB from a Binary Neutron Star Coalescing into a Kerr-Newman Black Hole. *Astrophys. J. Lett.* **2016**, *831*, 178. [[CrossRef](#)]
69. Muccino, M.; Ruffini, R.; Bianco, C.L.; Izzo, L.; Penacchioni, A.V. GRB 090227B: The Missing Link between the Genuine Short and Long Gamma-ray Bursts. *Astrophys. J. Lett.* **2013**, *763*, 125. [[CrossRef](#)]
70. Della Valle, M.; Chincarini, G.; Panagia, N.; Tagliaferri, G.; Malesani, D.; Testa, V.; Fugazza, D.; Campana, S.; Covino, S.; Mangano, V.; et al. An enigmatic long-lasting γ -ray burst not accompanied by a bright supernova. *Nature* **2006**, *444*, 1050. [[CrossRef](#)]
71. Cadelano, M.; Pallanca, C.; Ferraro, F.R.; Salaris, M.; Dalessandro, E.; Lanzoni, B.; Freire, P.C.C. Optical Identification of He White Dwarfs Orbiting Four Millisecond Pulsars in the Globular Cluster 47 Tucanae. *Astrophys. J. Lett.* **2015**, *812*, 63. [[CrossRef](#)]
72. Bildsten, L.; Cutler, C. Tidal interactions of inspiraling compact binaries. *Astrophys. J. Lett.* **1992**, *400*, 175–180. [[CrossRef](#)]
73. Fryer, C.L.; Woosley, S.E.; Herant, M.; Davies, M.B. Merging White Dwarf/Black Hole Binaries and Gamma-ray Bursts. *Astrophys. J. Lett.* **1999**, *520*, 650–660. [[CrossRef](#)]

74. Tauris, T.M.; van den Heuvel, E.P.J.; Savonije, G.J. Formation of Millisecond Pulsars with Heavy White Dwarf Companions: Extreme Mass Transfer on Subthermal Timescales. *Astrophys. J. Lett.* **2000**, *530*, L93–L96. [[CrossRef](#)]
75. Lazarus, P.; Tauris, T.M.; Knispel, B.; Freire, P.C.C.; Deneva, J.S.; Kaspi, V.M.; Allen, B.; Bogdanov, S.; Chatterjee, S.; Stairs, I.H.; et al. Timing of a young mildly recycled pulsar with a massive white dwarf companion. *MNRAS* **2014**, *437*, 1485–1494. [[CrossRef](#)]
76. Caito, L.; Bernardini, M.G.; Bianco, C.L.; Dainotti, M.G.; Guida, R.; Ruffini, R. GRB060614: A “fake” short GRB from a merging binary system. *A&A* **2009**, *498*, 501–507.
77. Maoz, D.; Hallakoun, N. The binary fraction, separation distribution, and merger rate of white dwarfs from SPY. *MNRAS* **2017**, *467*, 1414–1425. [[CrossRef](#)]
78. Maoz, D.; Hallakoun, N.; Badenes, C. The separation distribution and merger rate of double white dwarfs: Improved constraints. *MNRAS* **2018**, *476*, 2584–2590. [[CrossRef](#)]
79. Sun, H.; Zhang, B.; Li, Z. Extragalactic High-energy Transients: Event Rate Densities and Luminosity Functions. *Astrophys. J. Lett.* **2015**, *812*, 33. [[CrossRef](#)]
80. Rueda, J.A.; Ruffini, R.; Becerra, L.M.; Fryer, C.L. Simulating the induced gravitational collapse scenario of long Gamma-ray bursts. *Int. J. Mod. Phys. A* **2018**, *33*, 1844031. [[CrossRef](#)]
81. Rueda, J.A.; Ruffini, R. On the Induced Gravitational Collapse of a Neutron Star to a Black Hole by a Type Ib/c Supernova. *Astrophys. J. Lett.* **2012**, *758*, L7. [[CrossRef](#)]
82. Izzo, L.; Rueda, J.A.; Ruffini, R. GRB 090618: A candidate for a neutron star gravitational collapse onto a black hole induced by a type Ib/c supernova. *A&A* **2012**, *548*, L5.
83. Fryer, C.L.; Rueda, J.A.; Ruffini, R. Hypercritical Accretion, Induced Gravitational Collapse, and Binary-Driven Hypernovae. *Astrophys. J. Lett.* **2014**, *793*, L36. [[CrossRef](#)]
84. Ruffini, R.; Rueda, J.A.; Becerra, L.; Bianco, C.L.; Chen, Y.C.; Cherubini, C.; Filippi, S.; Karlica, M.; Melon Fuksman, J.D.; Moradi, R.; et al. The inner engine of GeV-radiation-emitting Gamma-ray bursts. *arXiv* **2018**, arXiv:1811.01839.
85. Ruffini, R.; Moradi, R.; Rueda, J.A.; Becerra, L.; Bianco, C.L.; Cherubini, C.; Filippi, S.; Chen, Y.C.; Karlica, M.; Sahakyan, N.; et al. On the GeV emission of the type I BdHN GRB 130427A. *arXiv* **2018**, arXiv:1812.00354.
86. Ruffini, R.; Li, L.; Moradi, R.; Rueda, J.A.; Wang, Y.; Xue, S.S.; Bianco, C.L.; Campion, S.; Melon Fuksman, J.D.; Cherubini, C.; et al. Self-similarity and power-laws in GRB 190114C. *arXiv* **2019**, arXiv:1904.04162.
87. Ruffini, R.; Melon Fuksman, J.D.; Vereshchagin, G.V. On the role of a cavity in the hypernova ejecta of GRB190114C. *arXiv* **2019**, arXiv:1904.03163.
88. Wald, R.M. Black hole in a uniform magnetic field. *Phys. Rev. D* **1974**, *10*, 1680–1685. [[CrossRef](#)]
89. Ruffini, R.; Becerra, L.; Bianco, C.L.; Chen, Y.C.; Karlica, M.; Kovačević, M.; Melon Fuksman, J.D.; Moradi, R.; Muccino, M.; Pisani, G.B.; et al. On the Ultra-relativistic Prompt Emission, the Hard and Soft X-Ray Flares, and the Extended Thermal Emission in GRB 151027A. *Astrophys. J. Lett.* **2018**, *869*, 151. [[CrossRef](#)]
90. Becerra, L.; Ellinger, C.L.; Fryer, C.L.; Rueda, J.A.; Ruffini, R. SPH Simulations of the Induced Gravitational Collapse Scenario of Long Gamma-ray Bursts Associated with Supernovae. *Astrophys. J. Lett.* **2019**, *871*, 14. [[CrossRef](#)]
91. Ruffini, R.; Karlica, M.; Sahakyan, N.; Rueda, J.A.; Wang, Y.; Mathews, G.J.; Bianco, C.L.; Muccino, M. A GRB Afterglow Model Consistent with Hypernova Observations. *Astrophys. J. Lett.* **2018**, *869*, 101. [[CrossRef](#)]
92. Fryer, C.; Benz, W.; Herant, M.; Colgate, S.A. What Can the Accretion-induced Collapse of White Dwarfs Really Explain? *Astrophys. J. Lett.* **1999**, *516*, 892–899. [[CrossRef](#)]
93. Becerra, L.; Guzzo, M.M.; Rossi-Torres, F.; Rueda, J.A.; Ruffini, R.; Uribe, J.D. Neutrino Oscillations within the Induced Gravitational Collapse Paradigm of Long Gamma-ray Bursts. *Astrophys. J. Lett.* **2018**, *852*, 120. [[CrossRef](#)]
94. Cipolletta, F.; Cherubini, C.; Filippi, S.; Rueda, J.A.; Ruffini, R. Last stable orbit around rapidly rotating neutron stars. *PRD* **2017**, *96*, 024046. [[CrossRef](#)]
95. Cipolletta, F.; Cherubini, C.; Filippi, S.; Rueda, J.A.; Ruffini, R. Fast rotating neutron stars with realistic nuclear matter equation of state. *Phys. Rev. D* **2015**, *92*, 023007. [[CrossRef](#)]
96. Fryer, C.L.; Benz, W.; Herant, M. The Dynamics and Outcomes of Rapid Infall onto Neutron Stars. *Astrophys. J. Lett.* **1996**, *460*, 801. [[CrossRef](#)]
97. Chevalier, R.A. Neutron star accretion in a supernova. *Astrophys. J. Lett.* **1989**, *346*, 847–859. [[CrossRef](#)]

98. Zel'dovich, Y.B.; Ivanova, L.N.; Nadezhin, D.K. Nonstationary Hydrodynamical Accretion onto a Neutron Star. *Sov. Astron.* **1972**, *16*, 209.
99. Ruffini, R.; Wilson, J. Possibility of Neutrino Emission from Matter Accreting into a Neutron Star. *Phys. Rev. Lett.* **1973**, *31*, 1362–1364. [[CrossRef](#)]
100. Fryer, C.L.; Herwig, F.; Hungerford, A.; Timmes, F.X. Supernova Fallback: A Possible Site for the r-Process. *Astrophys. J. Lett.* **2006**, *646*, L131–L134. [[CrossRef](#)]
101. Fryer, C.L. Neutrinos from Fallback onto Newly Formed Neutron Stars. *Astrophys. J. Lett.* **2009**, *699*, 409–420. [[CrossRef](#)]
102. Yakovlev, D.G.; Kaminker, A.D.; Gnedin, O.Y.; Haensel, P. Neutrino emission from neutron stars. *Phys. Rep.* **2001**, *354*, 1–155. [[CrossRef](#)]
103. Fryer, C.L.; Rockefeller, G.; Warren, M.S. SNSPH: A Parallel Three-dimensional Smoothed Particle Radiation Hydrodynamics Code. *Astrophys. J. Lett.* **2006**, *643*, 292–305. [[CrossRef](#)]
104. Fryer, C.L.; Warren, M.S. Modeling Core-Collapse Supernovae in Three Dimensions. *Astrophys. J. Lett.* **2002**, *574*, L65–L68. [[CrossRef](#)]
105. Young, P.A.; Fryer, C.L.; Hungerford, A.; Arnett, D.; Rockefeller, G.; Timmes, F.X.; Voit, B.; Meakin, C.; Eriksen, K.A. Constraints on the Progenitor of Cassiopeia A. *Astrophys. J. Lett.* **2006**, *640*, 891–900. [[CrossRef](#)]
106. Diehl, S.; Fryer, C.; Herwig, F. The Formation of Hydrogen Deficient Stars through Common Envelope Evolution. Hydrogen-Deficient Stars. In *Astronomical Society of the Pacific Conference Series*; Werner, A., Rauch, T., Eds.; Astronomical Society of the Pacific: San Francisco, CA, USA, 2008; Volume 391, p. 221.
107. Batta, A.; Ramirez-Ruiz, E.; Fryer, C. The Formation of Rapidly Rotating Black Holes in High-mass X-ray Binaries. *Astrophys. J. Lett.* **2017**, *846*, L15. [[CrossRef](#)]
108. Arnett, D. *Supernovae and Nucleosynthesis: An Investigation of the History of Matter from the Big Bang to the Present*; Princeton University Press: Princeton, NJ, USA, 1996.
109. Ruffini, R.; Vereshchagin, G.; Xue, S. Electron-positron pairs in physics and astrophysics: From heavy nuclei to black holes. *Phys. Rep.* **2010**, *487*, 1–140. [[CrossRef](#)]
110. Preparata, G.; Ruffini, R.; Xue, S.S. The dyadosphere of black holes and Gamma-ray bursts. *A&A* **1998**, *338*, L87–L90.
111. Ruffini, R.; Salmonson, J.D.; Wilson, J.R.; Xue, S.S. On evolution of the pair-electromagnetic pulse of a charged black hole. *Astron. Astrophys. Suppl.* **1999**, *138*, 511–512. [[CrossRef](#)]
112. Penacchioni, A.V.; Ruffini, R.; Izzo, L.; Muccino, M.; Bianco, C.L.; Caito, L.; Patricelli, B.; Amati, L. Evidence for a proto-black hole and a double astrophysical component in GRB 101023. *A&A* **2012**, *538*, A58.
113. Patricelli, B.; Bernardini, M.G.; Bianco, C.L.; Caito, L.; de Barros, G.; Izzo, L.; Ruffini, R.; Vereshchagin, G.V. Analysis of GRB 080319B and GRB 050904 within the Fireshell Model: Evidence for a Broader Spectral Energy Distribution. *Astrophys. J. Lett.* **2012**, *756*, 16. [[CrossRef](#)]
114. Woosley, S.E. Gamma-ray bursts from stellar mass accretion disks around black holes. *Astrophys. J. Lett.* **1993**, *405*, 273–277. [[CrossRef](#)]
115. Starling, R.L.C.; Page, K.L.; Pe'Er, A.; Beardmore, A.P.; Osborne, J.P. A search for thermal X-ray signatures in Gamma-ray bursts - I. Swift bursts with optical supernovae. *MNRAS* **2012**, *427*, 2950–2964. [[CrossRef](#)]
116. Wang, Y.; Aimuratov, Y.; Moradi, R.; Peresano, M.; Ruffini, R.; Shakeri, S. Revisiting the statistics of X-ray flares in Gamma-ray bursts. *Mem. Soc. Astron. Ital.* **2018**, *89*, 293.
117. Ruffini, R.; Muccino, M.; Bianco, C.L.; Enderli, M.; Izzo, L.; Kovacevic, M.; Penacchioni, A.V.; Pisani, G.B.; Rueda, J.A.; Wang, Y. On binary-driven hypernovae and their nested late X-ray emission. *A&A* **2014**, *565*, L10.
118. Page, K.L.; Starling, R.L.C.; Fitzpatrick, G.; Pandey, S.B.; Osborne, J.P.; Schady, P.; McBreen, S.; Campana, S.; Ukwatta, T.N.; Pagani, C.; et al. GRB 090618: Detection of thermal X-ray emission from a bright Gamma-ray burst. *MNRAS* **2011**, *416*, 2078–2089. [[CrossRef](#)]
119. Ruffini, R.; Wang, Y.; Enderli, M.; Muccino, M.; Kovacevic, M.; Bianco, C.L.; Penacchioni, A.V.; Pisani, G.B.; Rueda, J.A. GRB 130427A and SN 2013cq: A Multi-wavelength Analysis of An Induced Gravitational Collapse Event. *Astrophys. J. Lett.* **2015**, *798*, 10. [[CrossRef](#)]
120. Wang, Y.; Ruffini, R.; Kovacevic, M.; Bianco, C.L.; Enderli, M.; Muccino, M.; Penacchioni, A.V.; Pisani, G.B.; Rueda, J.A. Predicting supernova associated to Gamma-ray burst 130427a. *Astron. Rep.* **2015**, *59*, 667–671. [[CrossRef](#)]

121. Dominik, M.; Belczynski, K.; Fryer, C.; Holz, D.E.; Berti, E.; Bulik, T.; Mandel, I.; O’Shaughnessy, R. Double Compact Objects. I. The Significance of the Common Envelope on Merger Rates. *Astrophys. J. Lett.* **2012**, *759*, 52. [[CrossRef](#)]
122. Hills, J.G. The effects of sudden mass loss and a random kick velocity produced in a supernova explosion on the dynamics of a binary star of arbitrary orbital eccentricity—Applications to X-ray binaries and to the binary pulsars. *Astrophys. J. Lett.* **1983**, *267*, 322–333. [[CrossRef](#)]
123. Tauris, T.M.; Langer, N.; Podsiadlowski, P. Ultra-stripped supernovae: Progenitors and fate. *MNRAS* **2015**, *451*, 2123–2144. [[CrossRef](#)]
124. Tauris, T.M.; Langer, N.; Moriya, T.J.; Podsiadlowski, P.; Yoon, S.C.; Blinnikov, S.I. Ultra-stripped Type Ic Supernovae from Close Binary Evolution. *Astrophys. J. Lett.* **2013**, *778*, L23. [[CrossRef](#)]
125. Guetta, D.; Della Valle, M. On the Rates of Gamma-ray Bursts and Type Ib/c Supernovae. *Astrophys. J. Lett.* **2007**, *657*, L73–L76. [[CrossRef](#)]



© 2019 by the authors. Licensee MDPI, Basel, Switzerland. This article is an open access article distributed under the terms and conditions of the Creative Commons Attribution (CC BY) license (<http://creativecommons.org/licenses/by/4.0/>).



On the Role of a Cavity in the Hypernova Ejecta of GRB 190114C

R. Ruffini^{1,2,3}, J. D. Melon Fuksman^{1,2}, and G. V. Vereshchagin^{1,4,5}

¹ICRANet, P.zza della Repubblica 10, I-65122 Pescara, Italy; ruffini@icra.it, dmelonf@gmail.com, veresh@icra.it

²ICRA and Dipartimento di Fisica, Sapienza Università di Roma, P.le Aldo Moro 5, I-00185 Rome, Italy

³INAF, Viale del Parco Mellini 84, I-00136 Rome, Italy

⁴INAF—Istituto di Astrofisica e Planetologia Spaziali, Via del Fosso del Cavaliere, 100, I-00133 Rome, Italy

⁵ICRANet-Minsk, B.I. Stepanov Institute of Physics, National Academy of Sciences of Belarus, 220072 Nezalezhnasci Av. 68-2, Minsk, Belarus

Received 2019 April 8; revised 2019 August 11; accepted 2019 August 15; published 2019 October 3

Abstract

Within the binary-driven hypernova I (BdHN I) scenario, the gamma-ray burst GRB190114C originates in a binary system composed of a massive carbon–oxygen core (CO_{core}), and a binary neutron star (NS) companion. As the CO_{core} undergoes a supernova explosion with the creation of a new neutron star (νNS), hypercritical accretion occurs on the companion binary neutron star until it exceeds the critical mass for gravitational collapse. The formation of a black hole (BH) captures 10^{57} baryons by enclosing them within its horizon, and thus a cavity of approximately 10^{11} cm is formed around it with initial density 10^{-7} g cm⁻³. A further depletion of baryons in the cavity originates from the expansion of the electron-positron-photon ($e^+e^-\gamma$) plasma formed at the collapse, reaching a density of 10^{-14} g cm⁻³ by the end of the interaction. It is demonstrated here using an analytical model complemented by a hydrodynamical numerical simulation that part of the $e^+e^-\gamma$ plasma is reflected off the walls of the cavity. The consequent outflow and its observed properties are shown to coincide with the featureless emission occurring in a time interval of duration t_{rf} , measured in the rest frame of the source, between 11 and 20 s of the GBM observation. Moreover, similar features of the GRB light curve were previously observed in GRB 090926A and GRB 130427A, all belonging to the BdHN I class. This interpretation supports the general conceptual framework presented in R. Ruffini et al. and guarantees that a low baryon density is reached in the cavity, a necessary condition for the operation of the “inner engine” of the GRB presented in an accompanying article.

Key words: binaries: general – black hole physics – gamma-ray burst: general – gamma-ray burst: individual (GRB 190114C) – stars: neutron – supernovae: general

1. Introduction

Soon after the publication of the cosmological redshift value $z = 0.42$ for GRB190114C (Selsing et al. 2019) and the early GBM data obtained by the *Fermi*-LAT (Kocevski et al. 2019), R. Ruffini et al. (2019, in preparation) have identified this gamma-ray burst (GRB) as a possible candidate for a binary-driven hypernova of type I (BdHN1). Subsequently, the division of the GBM data into three distinct episodes (R. Ruffini et al. 2019, in preparation) has allowed further identification of some of the properties of BdHN1-type GRBs. In Episode 1, evidence was identified for the shock breakout of a supernova giving rise to the entire GRB evolution, see the accompanying article (L. Li et al. 2019b, in preparation). BdHNs have as progenitors a carbon–oxygen core (CO_{core}) which undergoes a supernova event, thus giving birth to a new neutron star (νNS) in the presence of a tight binary neutron star (NS) companion. This NS increases its mass by hypercritical accretion until it reaches the critical mass and a black hole (BH) is formed. In this process, a cavity is carved out of the SN ejecta (Becerra et al. 2016), see Figure 1. Episode 2, observed by the N1, N3, and N4 GBM detectors, includes the dominant ultrarelativistic prompt emission (UPE) phase, and also includes, following the BH formation, the onset of the GeV radiation at a time $t_{\text{rf}} = 1.9$ s, measured in the rest frame of the source. Episode 3, which is discussed in this article, addresses the interaction process between the $e^+e^-\gamma$ plasma and the cavity. Part of the $e^+e^-\gamma$ plasma is directed toward the observer and emits the UPE after becoming transparent; another part is reflected by the high density walls of the cavity. Following both the emission of the UPE and the emission from the cavity considered here, a final density of 10^{-14} g cm⁻³ is reached. This successive series of

events leading to a decreasing value of the baryon density is essential to guarantee the further emission of high energy photons, e.g., TeV radiation, and ultrarelativistic cosmic rays (R. Ruffini et al. 2019, in preparation).

The article is structured as follows. In Section 2 we discuss the main features of the light curve of GRB190114C in the context of this scenario, while in Section 3 we provide an analytic model for the interaction between the electron-positron-photon ($e^+e^-\gamma$) plasma and the baryonic matter in the cavity. In Section 4 we show a hydrodynamical simulation of such a process. In Section 5 we discuss the observed properties of several additional GRBs with a similar structure in their light curves, which supports this scenario. In Section 6 we summarize our conclusions.

2. GRB190114C and the Cavity

At 20:57:02.63 UT on 2019 January 14, GRB 190114C triggered *Fermi*-GBM, having $T_{90} = 116$ s. The isotropic *Fermi*-LAT energy is determined as $E_{\text{iso}} = 1.31 \pm 0.19 \times 10^{53}$ erg in the energy band of 100 MeV–100 GeV (Wang et al. 2019). The light curve of GRB190114C is shown in Figure 2, where two major spikes can be distinguished: the first structured spike corresponds to the SN breakout and UPE emission (Episodes 1 and 2) and lasts about 11 s in the rest frame of the source, while the second one (Episode 3) starts after 11 s and lasts for another 9 s. The total energy in the first spike is 95% of E_{iso} , while the energy in the second one is 5%.

Numerical simulations of the interaction between the SN ejecta and the NS (Becerra et al. 2016) show that just prior to the BH formation the accreting NS is surrounded by an

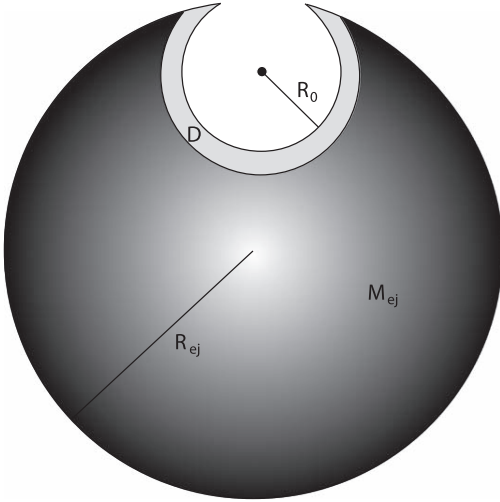


Figure 1. Schematic representation of the cavity in the SN ejecta surrounding the newly formed BH in the BdHN scenario.

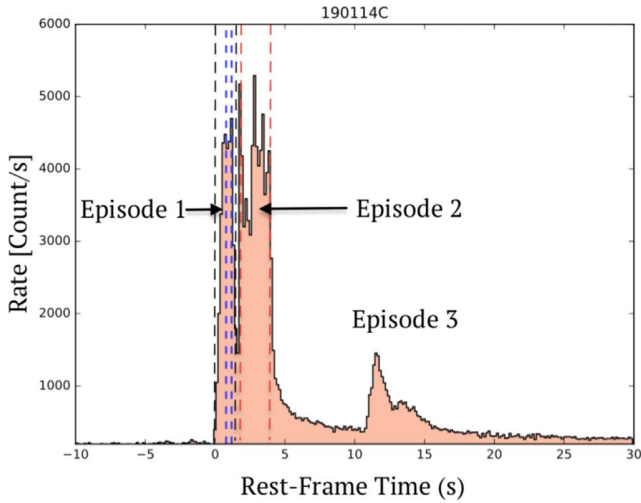


Figure 2. Light curve of GRB190114c in the rest frame of the source contains the precursor up to 1.9 s (Episode 1), then UPE emission up to 3.9 s (Episode 2), then the residual emission following the UPE from 3.9 s up to 11 s. The emission from the cavity (Episode 3) occurs at 11 s and continues up to 20 s. The energy of Episode 3 is about 5% of the energy in Episode 2.

almost spherical cavity with matter density much lower than the SN ejecta (see Figure 6 in that paper). These simulations use the smoothed-particle hydrodynamics (SPH) approach, a mesh-free method allowing one to follow the large-scale evolution of matter strongly coupled to radiation (Passy et al. 2012; Motl et al. 2017; Becerra et al. 2019). The cavity has an opening which permits the $e^+e^-\gamma$ plasma formed around the BH to escape toward the distant observer and emit the UPE, see Figure 1. Assuming that the $e^+e^-\gamma$ plasma explodes isotropically, it will also impact the SN ejecta after propagating in the cavity.

Here we consider the effect of the interaction of the $e^+e^-\gamma$ plasma with the SN ejecta surrounding the cavity, and demonstrate that such an interaction indeed results in a second spike of GRB emission. This follows the first main UPE spike produced by the $e^+e^-\gamma$ plasma which escapes the cavity without interacting with the SN ejecta. The second spike is weaker and delayed with respect to the first one.

Considering the light curve of GRB190114C shown in Figure 2, we argue that the second spike starting at 11 s and ending at 20 s can be explained by such an interaction. Even though the appearance of a cavity is predicted by the mentioned SPH simulations, we recall that it can also be caused by the expansion of the plasma itself, since the creation of such a lower-density region is a generic feature of strong explosions in a medium (see, e.g., van Putten 1994). Consequently, this model is applicable even in absence of an initial cavity.

3. Interaction of GRB with the SN Ejecta near the Cavity

Once the $e^+e^-\gamma$ plasma is created near the BH, it reaches complete thermal equilibrium within a very short time, about 10^{-12} s (Aksenov et al. 2008, 2007). Since the baryon density inside the cavity is very small, the plasma produces a blast wave, which expands with acceleration while transforming its internal energy into kinetic energy (Ruffini et al. 2000). Such an accelerated plasma then impacts the walls of the cavity, which has a radius R_0 (see Figure 1). When the impact occurs, a strong shock wave forms and propagates inside the SN ejecta surrounding the cavity with deceleration until it stalls at a radius R . In this way, the kinetic energy of the $e^+e^-\gamma$ plasma is deposited as internal energy.

One can determine the thickness of the region $D = R - R_0$ of SN ejecta where this energy is deposited. Assuming that the density of the SN ejecta is uniform, it can be estimated as

$$\rho = \frac{3M_{\text{ej}}}{4\pi R_{\text{ej}}^3}, \quad (1)$$

where M_{ej} is the total mass of the ejecta and R_{ej} is its size at the moment when the plasma impacts the walls of the cavity. The interaction between the $e^+e^-\gamma$ plasma and the SN ejecta can be considered to be an inelastic collision. When the $e^+e^-\gamma$ plasma pulse with total energy E impacts the ejecta, its energy is transformed into kinetic energy of the ejecta and internal energy. Assuming that the interaction is adiabatic (e.g., no energy is lost in radiation during the interaction), energy–momentum conservation reads

$$E + Mc^2 = (Mc^2 + W)\Gamma, \quad (2)$$

$$\frac{E}{c} = \left(M + \frac{W}{c^2}\right)\Gamma v, \quad (3)$$

where $\Gamma = [1 - (v/c)^2]^{-1/2}$ is the Lorentz factor of the part of ejecta where the energy is deposited, v is its velocity, W is the internal energy deposited during the interaction, and M is the mass of the ejecta affected by the interaction (swept up by the shock wave).

We now introduce the new variables

$$B = \frac{Mc^2}{E}, \quad \omega = \frac{W}{Mc^2}, \quad u = \Gamma \frac{v}{c} \quad (4)$$

and rewrite the energy–momentum conservation relations as

$$B^{-1} = (\omega + 1)\sqrt{u^2 + 1} - 1, \quad (5)$$

$$B^{-1} = (\omega + 1)u. \quad (6)$$

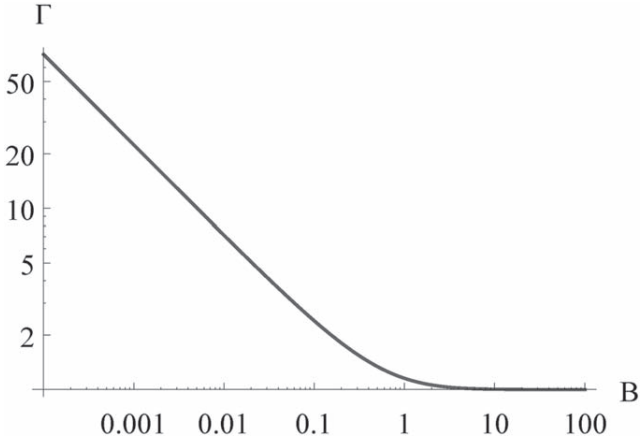


Figure 3. Lorentz factor Γ of the shock wave generated by the impact of the $e^+e^-\gamma$ pulse onto the walls of the cavity as a function of the engulfed mass, parameterized by $B = Mc^2/E$.

The solution to this system is (Ruffini et al. 2017)

$$u = \left(B \sqrt{1 + \frac{2}{B}} \right)^{-1}, \quad \frac{W}{E} = \omega B = \frac{1}{u} - B. \quad (7)$$

Recalling that $\Gamma = \sqrt{1 + u^2}$, we show $\Gamma(B)$ in Figure 3, from which it is clear that the shock wave stalls when

$$E = Mc^2. \quad (8)$$

From this figure it is evident that practically all the energy of the $e^+e^-\gamma$ plasma is deposited as internal energy W in the region when the mass-energy of the ejecta is equal to the total energy E .

The thickness of this region can be evaluated as follows. We indicate by M the mass engulfed by the shock wave

$$M = \frac{4\pi}{3} \rho D^3. \quad (9)$$

Inserting (8) into (9) allows us to express the thickness as

$$D = \left(\frac{E}{M_{\text{ej}} c^2} \right)^{1/3} R_{\text{ej}}. \quad (10)$$

For typical parameters

$$D \simeq 2 \times 10^{11} \left(\frac{E_0}{10^{53} \text{erg}} \right)^{1/3} \left(\frac{M_{\text{ej}}}{10 M_{\odot}} \right)^{-1/3} \frac{R_{\text{ej}}}{10^{12} \text{cm}}. \quad (11)$$

The average temperature in this shocked SN ejecta region can be estimated to be

$$\begin{aligned} T &= \left(\frac{3W}{4\pi a R^2 D} \right)^{1/4} \\ &\simeq 12 \left(\frac{W}{10^{53} \text{erg}} \right)^{1/4} \left(\frac{D}{2 \times 10^{11} \text{cm}} \right)^{-3/4} \text{keV}. \end{aligned} \quad (12)$$

where a is the radiation constant.

After the impact of the $e^+e^-\gamma$ plasma onto the SN ejecta, a reflection wave is generated, which propagates backward into the cavity. Since the internal energy of the shocked SN ejecta is comparable to its rest mass, the speed of the reflection wave is close to the speed of light. This reflection wave fills the cavity

with baryons and radiation. After the reflection wave has passed, the cavity expands. Since the cavity is transparent to radiation, thermal radiation escapes, and produces the second spike in the emission, analogous to the UPE emission, but observed later and weaker in intensity. In the next section we present the results of numerical simulations which support this claim. As the problem under consideration requires the resolution of shock waves on small scales, instead of using the SPH simulations we adopt a different framework based on shock-capturing relativistic hydrodynamics (RHD; for a discussion of the difference between relativistic SPH and RHD see, e.g., Vereshchagin & Aksenov 2017).

4. Numerical Simulations

With the goal to have a deeper insight into the interaction between the $e^+e^-\gamma$ plasma and the SN ejecta, we have run 2D axially symmetric RHD simulations using the publicly available PLUTO code.⁶ For this approach to be valid, we assume local thermal equilibrium between photons and material particles during the time of the simulation.

The consequent equation of state of the resulting $e^+e^-\gamma$ -baryon plasma is studied in Ruffini et al. (2018). In our simulations, we have verified that applying such an equation of state is equivalent to assuming a constant polytropic index $\gamma_p = 4/3$ in all regions occupied by the plasma and $\gamma_p = 5/3$ in all unshocked regions. We impose this by applying the so-called TM equation of state as described in Mignone & McKinney (2007).

We assume that a $e^+e^-\gamma$ plasma with the total energy $E_0 = 10^{53}$ erg forms in the center of a spherical cavity, having a radius $R_{\text{cav}} = 2 \times 10^{11}$ cm, and average density $\rho_{\text{cav}} = 1.9 \times 10^{-7}$ g cm⁻³. The center of the cavity is located at a distance 1.4×10^{11} cm from the edge of the SN ejecta, so that the latter has an opening, as portrayed in Figure 1. At this moment the SN ejecta, expanding homologously, has a radius $R_{\text{ej}} = 10^{12}$ cm.

Since the baryon load in the cavity is small, $B \simeq 10^{-4}$, the blast wave created by the $e^+e^-\gamma$ plasma reaches a bulk Lorentz factor of a few tenths before it impacts the walls of the cavity at $t_{\text{imp}} = 7.3$ s (see Figure 4). The baryons inside the cavity are swept up by the expanding plasma, reducing baryon density in the cavity to $\rho_w \simeq 10^{-14}$ g cm⁻³. The impact of the $e^+e^-\gamma$ plasma on the walls of the cavity produces a shock wave that propagates inside the SN ejecta.

After the impact, in agreement with Equation (12), the walls of the cavity are very hot, and their internal energy is radiated inside the cavity. The latter is transparent to radiation, and thus allows free transport of photons through the opening. Inside the walls of the cavity, the radiation drags baryons with it, creating a reflection wave. This wave propagates relativistically backwards into the cavity, leaving a residual density $\rho_r \simeq 10^{-13}$ g cm⁻³ within it, so the total mass of baryons in the cavity becomes about $M_r \simeq 10^{20}$ g. The reflection wave eventually reaches the origin at $t_r = 13.5$ s. The total energy in the cavity at this point is $E_r = 8.3 \times 10^{51}$ erg, which is only 8.5% of the initial energy E_0 . A large fraction of this energy is emitted toward the observer through the opening, and these estimates agree with the energy in the second spike in the light curve in Figure 2.

⁶ Software: PLUTO (Mignone et al. 2012).

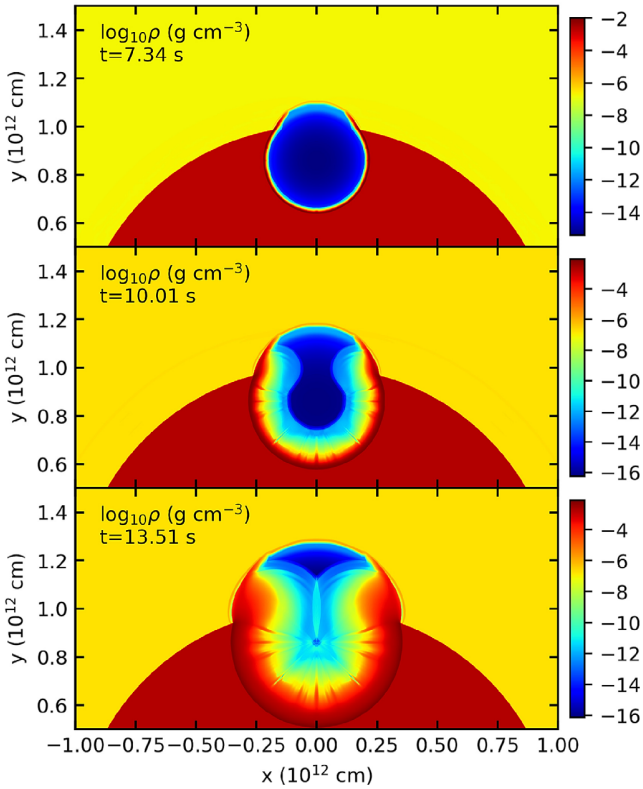


Figure 4. Spatial distribution of matter density at different instants of time: the time of impact of the $e^+e^- \gamma$ plasma onto the cavity walls $t_{\text{imp}} = 7.3$ s (top), the propagation of the reflection wave $t_{\text{imp}} = 10$ s (middle); the reflection wave reaching the origin $t_r = 13.5$ s (bottom).

The timescale of emission can be estimated by using the diffusion time formula (Ruffini et al. 2017)

$$\Delta t = 3\tau \frac{l}{c}, \quad (13)$$

where l is the thickness of the opaque region and τ is its optical depth. Since the density in the cavity wall has a very sharp gradient, while the temperature is nearly uniform, to estimate the duration of the time signal we take the half-thickness of the cavity $l = D/2 \simeq 2.5 \times 10^{10}$ cm, and the average density $\rho \simeq 10^{-9}$ g cm $^{-3}$, which gives $\Delta t \simeq 8$ s, in good agreement with the observed duration 9 s of the second spike. We also show the distributions of the Lorentz factor, matter density, and comoving temperature at $t = 11$ s in Figure 5. At this point one can clearly see that matter is outflowing from the cavity in the vertical direction, while the oblique shocks propagating from the sides of the cavity opening move toward the vertical axis. The cavity is optically thin and radiation continuously escapes from it to a distant observer.

Naively one expects the spectrum of radiation to be a multicolor blackbody with a peak energy near 30 keV. However, our simulations show that matter in the cavity is moving relativistically toward the observer, reaching a bulk Lorentz factor $\gamma \simeq 3$ (see Figure 6). Due to the nonnegligible optical depth, the radiation generated by the walls of the cavity will experience inverse Compton scattering on this relativistically moving matter, Doppler-shifting the peak energy toward higher values. Therefore, we expect the observed spectrum to be similar to a Comptonized blackbody (Aksenov et al. 2013)

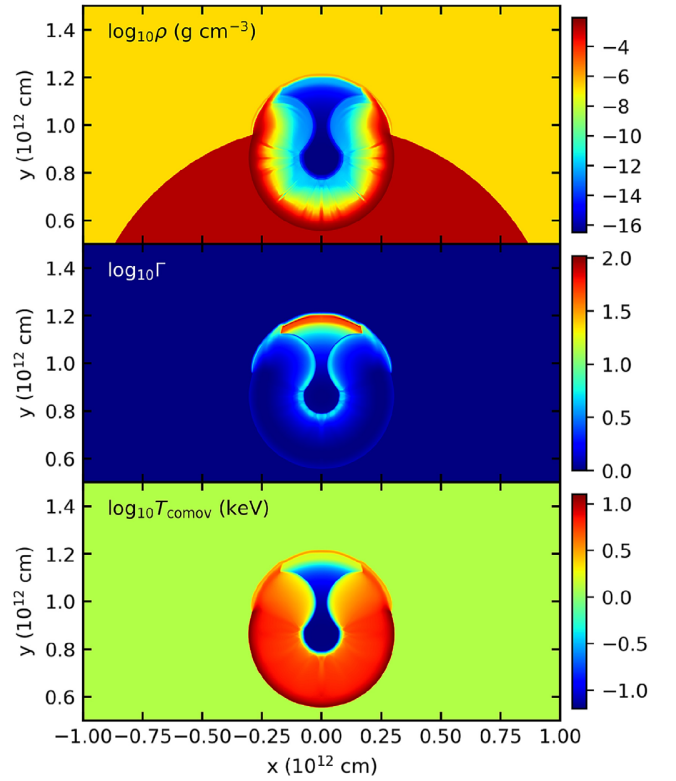


Figure 5. Spatial distributions of matter density (top), Lorentz factor (middle), and comoving temperature (bottom) at $t = 11$ s, showing the mildly relativistic reflection wave propagating backward in the cavity, as well as the ultrarelativistic $e^+e^- \gamma$ plasma wave propagating outside the cavity. The shock wave is visible inside the ejecta.

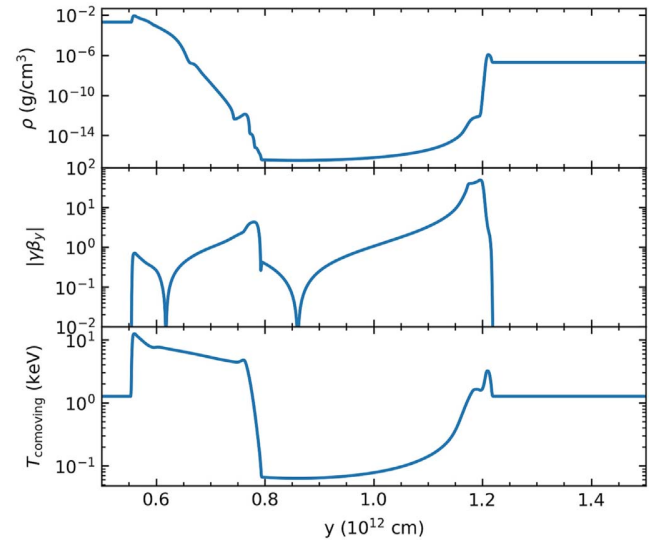


Figure 6. Spatial distributions along the axis of symmetry of matter density (top), Lorentz factor (middle), and comoving temperature (bottom) at $t = 11$ s. The reflection wave with the maximum Lorentz factor of about 4 is clearly visible in the left part of the figure. To the right from the reflection wave the baryons are evacuated by the $e^+e^- \gamma$ plasma, which has accelerated to the bulk Lorentz factor of about 60.

peaked at $E_p \sim 3\gamma^2 kT \simeq 200\text{--}300$ keV. This qualitatively agrees with the observed spectrum of the second spike of GRB190114C. The time-integrated spectrum has a very soft power-law index $\alpha = -1.6$ and a peak energy $E_p = 252$ keV.

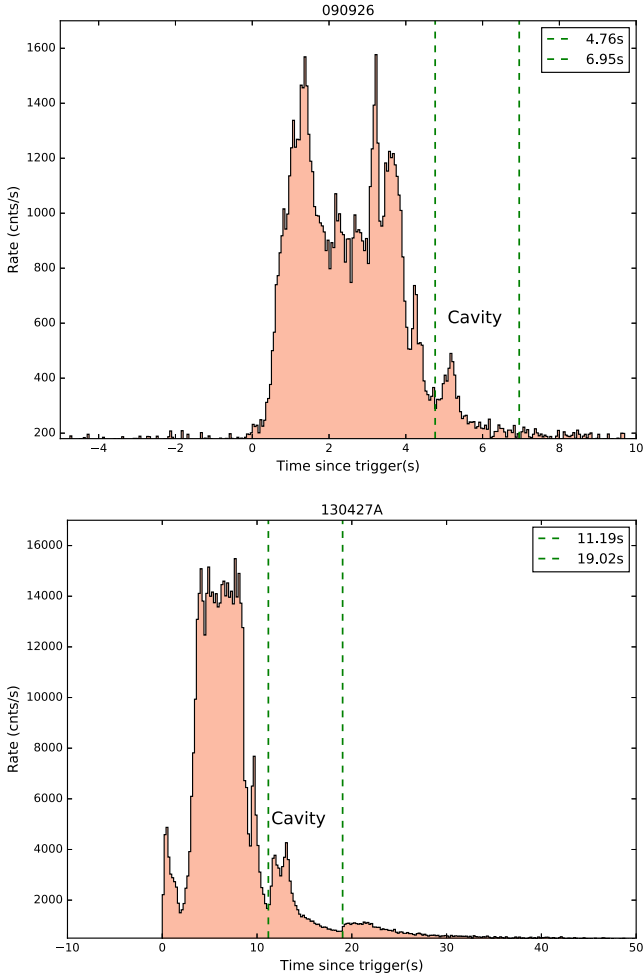


Figure 7. Light curves of GRB 090926A (upper panel) and GRB 130427A (lower panel), in the source rest frame. The structure of the light curves as well as the spectral analysis allows us to identify Episode 3 in these GRBs, for details, see L. Li et al. (2019a, in preparation). Data from Fermi GBM satellite.

The time-resolved spectrum shows spectral evolution toward softening of the spectrum, in agreement with the cooling of the expanding walls of the cavity.

5. Additional Cases with Episode 3

A similar light-curve structure, i.e., with an Episode 3 well separated from the UPE emission, has been identified in several GRBs. In particular, that is the case of GRB 090926A and GRB 130427A. All of these sources belong to the BdHN I class, as they all have an isotropic energy above 10^{52} erg: for GRB 090926A $E_{\text{iso}} = 1.89 \times 10^{54}$ erg, while for GRB 130427A $E_{\text{iso}} = 1.06 \times 10^{54}$ erg. Furthermore, all of them have a featureless emission occurring with a delay with respect to the main emission of Episode 2 of $t_{\text{rf}} \simeq 5$ sec for GRB 090926A $t_{\text{rf}} \simeq 11$ sec for GRB 130427A, see Figure 7. The spectra of Episode 3 in both cases are well fitted by the cutoff power-law model. For details about the light curve and spectra of these GRBs see L. Li et al. (2019a, in preparation). These observations support the interpretation of these three GRB light curves within the BdHN model, and are consistent with the occurrence of reflection waves with properties similar to the one presented above.

We recall that the systems analyzed in this article have as progenitors a binary system composed of CO_{core} undergoing SN explosion, and consequently hypercritically accreting into a companion NS. As shown above, three of these systems have been clearly identified in GRBs 090926A, 130427A, and 190114C, see Figures 2 and 7 and (L. Li et al. 2019a, in preparation).

One of the most interesting aspects of the evolution of these binary systems is that they evolve in a succession of GRB emissions. It is so that the system treated in this article describing long GRBs, with a progenitor composed of a CO core and NS may produce as an outcome a binary system composed of an NS and BH, which evolve after $\sim 10^4$ yr in a new merging, giving origin to a short GRB (Fryer et al. 2015).

Such NS–BH systems were indeed among the first to be considered as progenitors of short GRBs in the pioneering works of Paczynski (1991) and van Putten (1999). van Putten (1999) considered the possibility of toroidal magnetic field structure and cavities in such a system. This work was further developed in great detail in van Putten & Levinson (2003). This field has received a revival thanks to numerical simulations of the toroidal magnetic field created in the NS–BH and NS–NS merging Rezzolla et al. (2011), Nathanael et al. (2017), and references therein. It is interesting that such systems should be quite common (Fryer et al. 2015). They may be related to the problem of fast radio bursts and ultra-short GRBs. It is clear that the cavity considered in SN accretion on an NS leading to formation of BH, and the cavity originating from the NS–BH merging address different physical problems.

6. Conclusions

We have presented an interpretation of the light curve of GRB190114C as the result of BH formation in the BdHN scenario. In this scenario a massive CO_{core} , which forms a binary system with an NS, explodes as a supernova. The NS undergoes gravitational collapse due to hypercritical accretion, creating in the process a low-density cavity in the SN ejecta. In this picture the first spike (UPE) originates from an $e^+e^-\gamma$ plasma formed around the black hole, while the second spike originates from the reflection wave produced by the impact of the plasma on the walls of the cavity. Our 2D RHD simulations support such a picture and match the energetics and timing characteristics of the signal. Spectral characteristics and their time evolution are in qualitative agreement with the observations. Similar features of GRB light curves have been recently observed in GRB 090926A and GRB 130427A, all belonging to the BdHN 1 class. This is consistent with a rather generic occurrence of reflection waves such as the one described in this work.

We thank Carlo Luciano Bianco and She-Sheng Xue for useful discussions and Dr. Li Liang for supplying Figures 2 and 7. We are also grateful to the referee for important remarks which allowed us to focus more clearly on our key results.

References

- Aksenov, A. G., Ruffini, R., & Vereshchagin, G. V. 2007, *PhRvL*, **99**, 125003
- Aksenov, A. G., Ruffini, R., & Vereshchagin, G. V. 2008, in *AIP Conf. Ser.* 966, *Relativistic Astrophysics*, ed. C. L. Bianco & S.-S. Xue (Melville, NY: AIP), 191
- Aksenov, A. G., Ruffini, R., & Vereshchagin, G. V. 2013, *MNRAS*, **436**, L54

- Becerra, L., Bianco, C. L., Fryer, C. L., Rueda, J. A., & Ruffini, R. 2016, *ApJ*, **833**, 107
- Becerra, L., Ellinger, C. L., Fryer, C. L., Rueda, J. A., & Ruffini, R. 2019, *ApJ*, **871**, 14
- Fryer, C. L., Oliveira, F. G., Rueda, J. A., & Ruffini, R. 2015, *PhRvL*, **115**, 231102
- Kocevski, D., Omodei, N., Axelsson, M., et al. 2019, GCN, **23709**, 1
- Mignone, A., & McKinney, J. C. 2007, *MNRAS*, **378**, 1118
- Mignone, A., Zanni, C., Tzeferacos, P., et al. 2012, *ApJS*, **198**, 7
- Motl, P. M., Frank, J., Staff, J., et al. 2017, *ApJS*, **229**, 27
- Nathanail, A., Most, E. R., & Rezzolla, L. 2017, *MNRAS*, **469**, L31
- Paczynski, B. 1991, *AcA*, **41**, 257
- Passy, J.-C., De Marco, O., Fryer, C. L., et al. 2012, *ApJ*, **744**, 52
- Rezzolla, L., Giacomazzo, B., Baiotti, L., et al. 2011, *ApJL*, **732**, L6
- Ruffini, R., Salmonson, J. D., Wilson, J. R., & Xue, S.-S. 2000, *A&A*, **359**, 855
- Ruffini, R., Vereshchagin, G. V., & Wang, Y. 2017, *A&A*, **600**, A131
- Ruffini, R., Wang, Y., Aimuratov, Y., et al. 2018, *ApJ*, **852**, 53
- Selsing, J., Fynbo, J. P. U., Heintz, K. E., Watson, D., & Dyrbye, N. 2019, GCN, **23695**, 1
- van Putten, M. H. P. M. 1994, *IJBC*, **4**, 57
- van Putten, M. H. P. M. 1999, *Sci*, **284**, 115
- van Putten, M. H. P. M., & Levinson, A. 2003, *ApJ*, **584**, 937
- Vereshchagin, G. V., & Aksenov, A. G. 2017, *Relativistic Kinetic Theory* (Cambridge: Cambridge Univ. Press)
- Wang, Y., Li, L., Moradi, R., & Ruffini, R. 2019, arXiv:1901.07505v1



On the GeV Emission of the Type I BdHN GRB 130427A

R. Ruffini^{1,2,3,4,5}, R. Moradi^{1,2}, J. A. Rueda^{1,2,4,6}, L. Becerra⁷, C. L. Bianco^{1,2,6}, C. Cherubini^{2,8}, S. Filippi^{2,8}, Y. C. Chen^{1,2},
M. Karlica^{1,2,3}, N. Sahakyan^{2,9}, Y. Wang^{1,2}, and S. S. Xue^{1,2}

¹ ICRA, Dipartimento di Fisica, Sapienza Università di Roma, P.le Aldo Moro 5, I-00185 Rome, Italy; rahim.moradi@icranet.org, jorge.rueda@icra.it

² ICRA Net, P.zza della Repubblica 10, I-65122 Pescara, Italy

³ Université de Nice Sophia Antipolis, CEDEX 2, Grand Château Parc Valrose, Nice, France

⁴ ICRA Net-Rio, Centro Brasileiro de Pesquisas Físicas, Rua Dr. Xavier Sigaud 150, 22290-180 Rio de Janeiro, Brazil

⁵ INAF, Viale del Parco Mellini 84, I-00136 Rome, Italy

⁶ INAF, Istituto di Astrofisica e Planetologia Spaziali, Via Fosso del Cavaliere 100, I-00133 Rome, Italy

⁷ Escuela de Física, Universidad Industrial de Santander, A.A.678, Bucaramanga, 680002, Colombia

⁸ ICRA and Department of Engineering, University Campus Bio-Medico of Rome, Via Alvaro del Portillo 21, I-00128 Rome, Italy

⁹ ICRA Net-Armenia, Marshall Baghramian Avenue 24a, Yerevan 0019, Armenia

Received 2018 December 6; revised 2019 August 23; accepted 2019 October 9; published 2019 November 22

Abstract

We propose that the inner engine of a type I binary-driven hypernova (BdHN) is composed of Kerr black hole (BH) in a non-stationary state, embedded in a uniform magnetic field B_0 aligned with the BH rotation axis and surrounded by an ionized plasma of extremely low density of $10^{-14} \text{ g cm}^{-3}$. Using GRB 130427A as a prototype, we show that this inner engine acts in a sequence of elementary impulses. Electrons accelerate to ultrarelativistic energy near the BH horizon, propagating along the polar axis, $\theta = 0$, where they can reach energies of $\sim 10^{18} \text{ eV}$, partially contributing to ultrahigh-energy cosmic rays. When propagating with $\theta \neq 0$ through the magnetic field B_0 , they produce GeV and TeV radiation through synchrotron emission. The mass of BH, $M = 2.31M_\odot$, its spin, $\alpha = 0.47$, and the value of magnetic field $B_0 = 3.48 \times 10^{10} \text{ G}$, are determined self-consistently to fulfill the energetic and the transparency requirement. The repetition time of each elementary impulse of energy $\mathcal{E} \sim 10^{37} \text{ erg}$ is $\sim 10^{-14} \text{ s}$ at the beginning of the process, then slowly increases with time evolution. In principle, this “inner engine” can operate in a gamma-ray burst (GRB) for thousands of years. By scaling the BH mass and the magnetic field, the same inner engine can describe active galactic nuclei.

Key words: black hole physics – binaries: general – gamma-ray burst: general – stars: neutron – supernovae: general

1. Introduction

Nine subclasses of gamma-ray bursts (GRBs) with binary progenitors have been recently introduced in Ruffini et al. (2016a, 2018c), Rueda et al. (2018), and Wang et al. (2019). One of the best prototypes of the long GRBs emitting 0.1–100 GeV radiation is GRB 130427A (Ruffini et al. 2015). GRB 130427A belongs to a special subclass of GRBs originating from a tight binary system with an orbital period of ~ 5 minutes, and is composed of a carbon-oxygen core (CO_{core}) undergoing a supernova (SN) event in presence of a neutron star (NS) companion. The SN, as usual, gives rise to a new NS (νNS). For binary periods $\lesssim 5$ minutes, the hypercritical accretion of the SN ejecta onto the companion NS leads it to exceed the critical mass for gravitational collapse and form a Kerr black hole (BH). We call these systems binary-driven hypernovae of type I (BdHNe I) with $E_{\text{iso}} > 10^{52} \text{ erg}$, as opposed to BdHNe II with binary periods $\gtrsim 5$ minutes and $E_{\text{iso}} < 10^{52} \text{ erg}$ when the NS critical mass is not exceeded (Wang et al. 2019). Figure 1 shows the ejecta density distribution of a BdHN I on the binary equatorial plane (left panel) and in a plane orthogonal to it (right panel) at the moment of gravitational collapse of the NS companion, namely at the moment of BH formation. These plots are the result of three-dimensional, numerical smoothed-particle-hydrodynamic (SPH) simulations of BdHNe recently described in Becerra et al. (2019).

In the specific case of GRB 130427A, this BdHN I is seen from “the top,” with the viewing angle in a plane orthogonal to the plane of the orbit of the binary progenitor. This allows us to follow all the details of the high-energy activities around the

BH. These include (a) the first appearance of the supernova (the *SN-rise*); (b) the observation of the ultrarelativistic prompt emission (UPE) following the BH formation (Ruffini et al. 2019a); (c) the feedback of the SN ejecta accreting onto the νNS leading to the X-ray afterglow (Ruffini et al. 2018b); and (d) the ultrahigh-energy process extracting the rotational energy of the BH, reducing its mass and spin, and generating the GeV and TeV radiation are presented in this article.

Soon after the BH formation, approximately 10^{57} baryons, which include the ones composing the NS companion, are enclosed in the BH horizon beyond any possible measurable effect apart from the total mass and spin of the BH.

A cavity of approximately 10^{11} cm is formed around the BH with a finite density of $10^{-6} \text{ g cm}^{-3}$; see Becerra et al. (2018, 2019). The evolution of such a cavity following the GRB explosion and its overtones inside the cavity has been addressed in Ruffini et al. (2019b), finally reaching a density of $10^{-13} \text{ g cm}^{-3}$ inside the cavity.

The Kerr BH formation occurs in such a cavity in presence of an external uniform magnetic field aligned with the BH rotation axis, which we estimate to be $B_0 \sim 10^{10} \text{ G}$. For quantitative estimates, we consider it as mathematically described by a non-stationary Papapetrou solution (Wald 1974; Rueda et al. 2019).

As we will quantify later in this article, a sufficient amount of low-density ionized matter will be needed in the cavity to feed this inner engine.

In this article, we assume that the magnetic field and the BH spin are parallel. In that case, the induced electric field given by

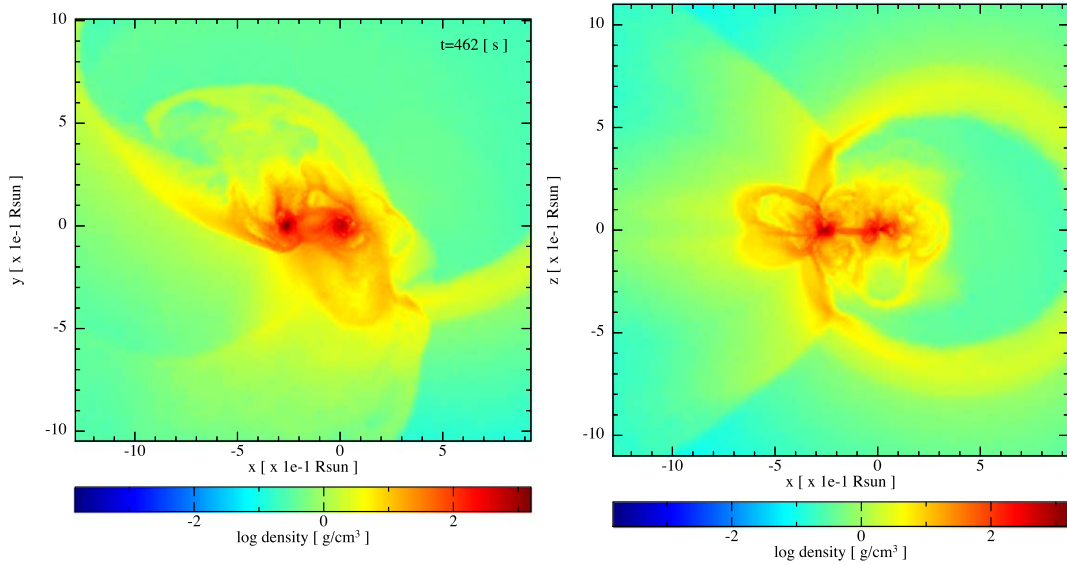


Figure 1. Selected SPH simulation from Becerra et al. (2019) of the exploding CO_{core} as SN in the presence of a companion NS: Model “25m1p07e” with $P_{\text{orb}} \approx 5$ minutes. The CO_{core} is taken from the $25 M_{\odot}$ zero-age main-sequence (ZAMS) progenitor, so it has a mass $M_{\text{CO}} = 6.85 M_{\odot}$. The mass of the NS companion is $M_{\text{NS}} = 2 M_{\odot}$. The plots show the surface density on the equatorial binary plane (left panel) and on a plane orthogonal to it (right panel) at the time in which the NS companion reaches the critical mass and collapses to a BH, $t = 462$ s from the SN shock breakout ($t = 0$ of our simulation). The coordinate system has been rotated and translated in such a way that the NS companion is at the origin and the νNS is along the $-x$ axis.

the Wald solution is such that electrons (protons) along and near the rotation axis in the surrounding ionized circumburst medium are repelled (attracted) by the BH. The behavior is vice versa in the antiparallel case. As pointed out by Gibbons et al. (2013), the stability of Wald-like solutions is guaranteed only if the uniform field is confined to a radius smaller than the Melvin radius,

$$R_M \sim 2/B_0, \quad (1)$$

which imposes an upper limit for this geometry of about 10^{15} cm in our present case.¹⁰ In this article, we show that the particle acceleration occurs near the BH horizon within distance of approximately 10^5 cm, much smaller than R_M .

We recall the definition of the critical electric and magnetic fields, E_c and B_c , i.e.,

$$E_c = \frac{m_e^2 c^3}{e \hbar}, \quad B_c = \frac{m_e^2 c^2}{e \hbar} = 4.4 \times 10^{13} \text{ G} \quad (2)$$

where m_e and e are the electron mass and charge, respectively.

Particular attention is devoted to identify the regimes in which the electric and magnetic fields are undercritical or overcritical and, correspondingly, study the pair creation process and the associated absorption or transparency conditions for the GeV emission. In this article we focus on the undercritical regime in GRB 130427A.

Our main goal is to develop an “inner engine” model consistent with the transparency condition of the GeV and high-energy emissions from GRB 130427A. The model makes use of

- (1) the rotational energy of the BH as its energy source;
- (2) the acceleration and radiation processes of ultrarelativistic electrons near the horizon of the BH and in presence of

- the uniform magnetic field B_0 , determined by using the electrodynamic properties of the Wald solution; and
- (3) the determination of the highly anisotropic GeV, TeV, and UHECR emission by the synchrotron radiation, as a function of the injection angle of the ultrarelativistic electrons in the Wald solution.

As a byproduct, we show that

- (1) the high-energy emission of GRB 130427A, far from being emitted continuously, actually occurs in a repetitive sequence of discrete, quantized, elementary impulsive events (or “quanta” for short);
- (2) each quantum carries an energy of the order of 10^{37} erg; and
- (3) each quantum is repetitively emitted with a repetition time $\sim 10^{-14}$ s.

The three fundamental parameters of the model, i.e., the Kerr BH mass, M , spin parameter, $\alpha = cJ/(GM^2)$, where J is the BH angular momentum, and the magnetic field B_0 , are determined as follows:

- (1) The magnetic field B_0 is obtained by imposing the transparency condition of the GeV luminosity, as well as the coincidence between the theoretical predicted repetition time of the “quanta” and the timescale of first impulsive event.
- (2) The BH mass M and spin parameter α , as well as their temporal evolution, are determined by obtaining the GeV luminosity via the extractable energy of the BH.
- (3) In each one of these elementary impulsive events, we can estimate the depletion of the rotational energy of the Kerr BH; consequently, we can estimate that the high-energy emission process can indeed last for thousands of years.

The article is organized as follows. In Section 2 we recall the count rate and light curves of Fermi-GBM and *Fermi*-LAT for GRB 130427A. In Section 3 the basic equations for determining

¹⁰ The conversion factor from CGS to geometric units for the magnetic field is $\sqrt{G}/c^2 \approx 2.86 \times 10^{-25}$, where G and c are the gravitational constant and speed of light in CGS units, respectively. Therefore, a magnetic field on the order of 10^{10} G in geometric units is $\approx 2 \times 10^{-25} \times 10^{10} \approx 2 \times 10^{-15}$ cm⁻¹, which leads to the Melvin radius of $R = 2/B_0 \approx 10^{15}$ cm.

the extraction of rotational energy from a Kerr BH to explain the GeV energetic are expressed in terms of the BH mass and spin. In Section 4 the electrodynamics of the “inner engine” is presented. In Section 5 the basic equations governing the synchrotron radiation in the magnetic field B_0 , the first elementary event and the limit on the magnetic field to ground the transparency of the GeV radiation, are established. In Section 6 we determine the mass and spin of the BH to fulfill the GeV energy, and we address the decrease of the mass and spin of the BH as a function of the extracted rotational energy. In Section 7 the synchrotron radiation power and the need of a low-density ionized plasma in order to explain the number of needed electrons to feed the system is presented. In Section 8 the sequence of quanta and their repetition times are indicated. We also outline the mounting evidence that this system, developed here for the Wald solution applied for GRB 130427A, may well be extended to the much more massive BHs of $10^9 M_\odot$ in AGN such as M87.

2. Count Rate and Light Curves of Fermi-GBM and Fermi-LAT

As detailed in Levan et al. (2013), von Kienlin (2013), Xu et al. (2013), Flores et al. (2013), and Ruffini et al. (2015), GRB 130427A records a well-observed fluence in the optical, X-ray, gamma-ray, and GeV bands; see Figure 2.

The Fermi-GBM count rate of GRB 130427A with isotropic energy $E_{\text{iso}} = (9.2 \pm 1.3) \times 10^{53}$ erg and $z = 0.34$ is shown in Figure 2(a). Clearly identified are (a) the supernova raise (SN-rai; Liang et al. 2019) (b) the UPE phase following the BH formation (c) the emission of the cavity mentioned in the introduction, details in Liang et al. (2019). During the UPE phase, the event count rate of n9 and n10 of Fermi-GBM surpasses $\sim 8 \times 10^4$ counts per second in the prompt radiation between rest-frame times $T_0 + 3.4$ s and $T_0 + 8.6$ s. The GRB is affected by pile-up, which significantly deforms the spectrum; for details, see Ackermann et al. (2014) and Ruffini et al. (2015).

We therefore impose as the starting point of our analysis, the value $t_{\text{rf}} = 16$ s, with t_{rf} being the rest-frame time, and cover all of the successive Fermi-GBM and Fermi-LAT data; see Figure 7(a).

In Figure 2(b) we give the luminosity of Fermi-LAT (red) and Fermi-GBM (blue); for details, see Ruffini et al. (2015) and Ajello et al. (2019). From the observations in Figure 2(b), at the onset of the GeV emission, the magnetic field B_0 and the corresponding electric field are largely overcritical, $E > E_c$ (Ruffini et al. 2019a). In these conditions, a plasma consisting of a vast number of e^+e^- pairs is produced by the vacuum polarization process. Such a plasma self-accelerates and emits at transparency region the MeV radiation; see, e.g., the vast literature quoted in Ruffini et al. (1999, 2000, 2007, 2010).

The vacuum polarization process creates the optically thick condition by which the GeV radiation is drastically reduced until the end of the UPE phase is reached (Ruffini et al. 2019a).

It was already shown in Damour & Ruffini (1975) that the feedback of such a vacuum polarization process can reduce the original overcritical magnetic field down to $\sim 10^{11}$ G.

One of the new issues raised by the data in Figure 2(b) (shown in more detail in Figure 2(c)), is precisely the conversion of the GeV photons into the MeV photons for $t_{\text{rf}} < 16$ s. The conversion mechanism likely involves the Breit–Wheeler (Breit & Wheeler 1934) photon–photon pair creation $\gamma + \gamma \rightarrow e^+ + e^-$ (for details, see Ruffini et al. 2010, 2016b),

because for GeV photons, their energy is larger than the threshold energy for pair production. Such a process is indeed responsible for absorption of GeV emission in some GRBs (see, e.g., Ackermann et al. 2011). This process leads to significant production of optically thick e^+e^- plasma and thermalization of high-energy photons at MeV energy. As the luminosity of photons in the MeV energy range decreases approaching $t_{\text{rf}} = 16$ s, its number density decreases and consequently the opacity decreases as well. This implies less absorption of GeV photons: indeed, the flux of GeV photons increases.

Based on our recent work about the hard and soft X-ray flares (Ruffini et al. 2018a), the flare in the MeV band around $t_{\text{rf}} = 100$ s observed in Figure 2(b) clearly occurs in the accreting hypernova ejecta that is well outside the conical GeV emission region. This feature is therefore not associated with the GeV emission mechanism treated in this article, and as it occurs outside the cone of the GeV emission, these GeV and MeV radiations are not interacting.

In view of the pile-up effect of GBM data indicated in Figure 2(a) and the absence of accurate data at $t_{\text{rf}} < 16$ s, we will not approach the study of the overcritical field in GRB 130427A in this article.

We address instead the observation after $t_{\text{rf}} = 16$ s, see Figure 2, where the condition of transparency of the GeV radiation is reached. We determine the self-consistent set of parameters that allow the transparency condition to be implemented and the mass and the spin of the BH will be in this context uniquely determined (see Section 5).

3. Determination of the Mass and Spin of the BH

In this section we identify the rotational energy of a Kerr BH as the energy source powering the GeV emission at $t > t_{\text{rf}} = 16$ s; consequently, the mass and spin of the BH have to be determined.

The luminosity of Fermi-LAT (0.1–100 GeV), together with a power law best fit to the GeV luminosity of this GRB after $t > t_{\text{rf}} = 16$ s are shown in Figure 3.

After $t > t_{\text{rf}} = 16$ s, $E_{\text{GeV}} = (1.2 \pm 0.01) \times 10^{53}$ erg, and the GeV luminosity is best fitted by

$$L = A \left(\frac{t}{1\text{s}} \right)^{-\eta} \text{ erg s}^{-1}, \quad (3)$$

with a slope of $\eta = 1.2 \pm 0.04$ and an amplitude of $A = (5.125 \pm 0.2) \times 10^{52}$; data and energy are retrieved from the second Fermi-LAT catalog (Ajello et al. 2019).

We now verify that the energetics of the GeV radiation can be explained by the extractable rotational energy of the Kerr BH, i.e.,

$$E_{\text{GeV}} = E_{\text{extr}} = (1.2 \pm 0.01) \times 10^{53} \text{ erg}. \quad (4)$$

From the mass–energy formula of the Kerr BH (Christodoulou 1970; Christodoulou & Ruffini 1971; Hawking 1971; see also Misner et al. 1973), we have

$$M^2 = \frac{c^2 J^2}{4G^2 M_{\text{irr}}^2} + M_{\text{irr}}^2, \quad (5a)$$

$$S = 16 \pi G^2 M_{\text{irr}}^2 / c^4, \quad (5b)$$

where J , M , M_{irr} , and S are the angular momentum, mass, irreducible mass, and horizon surface area of the Kerr BH, from

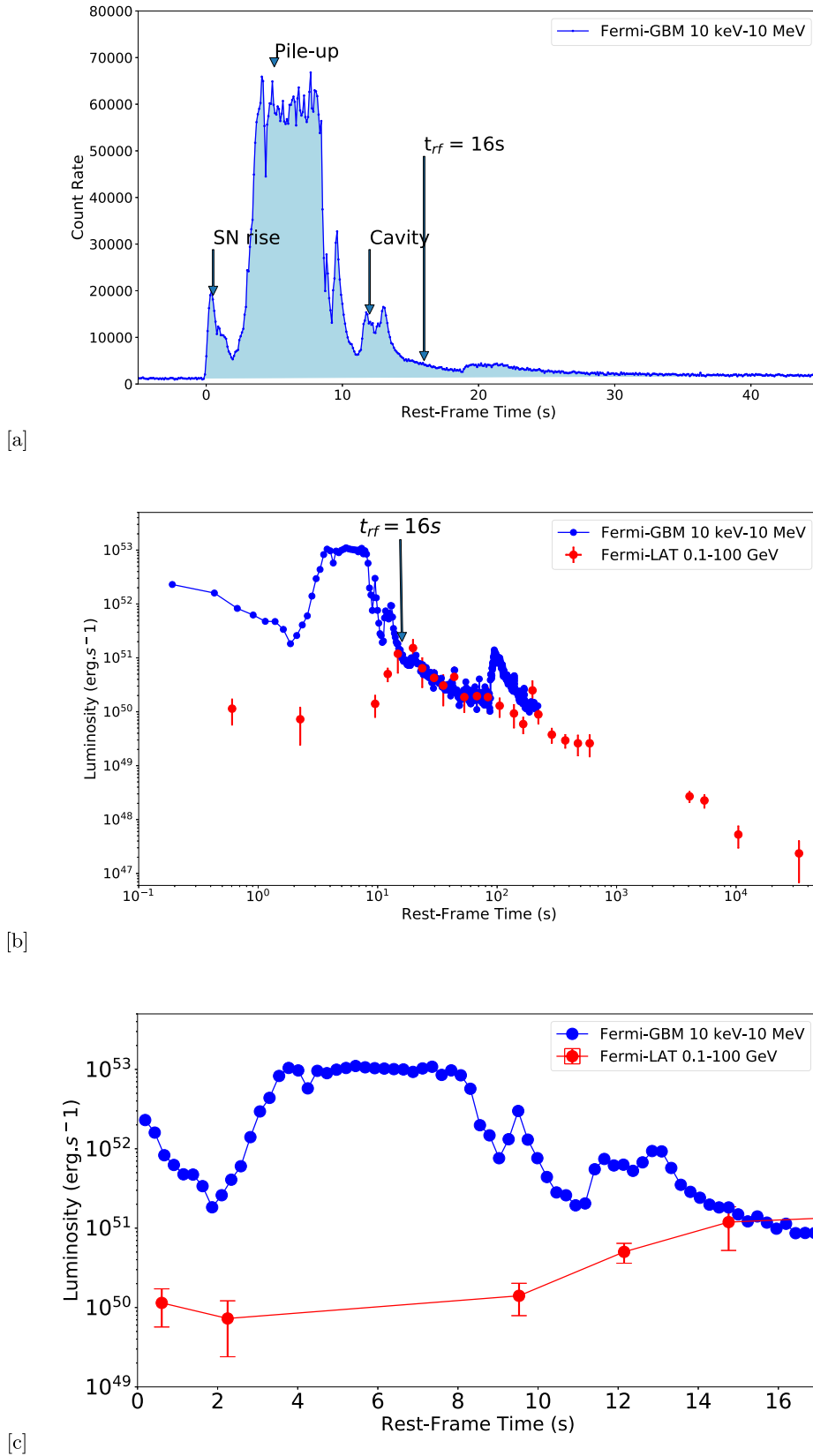


Figure 2. (a) The Fermi-GBM count rate of GRB 130427A. In the rest-frame time interval $[T_0 + 3.4 \text{ s}, T_0 + 8.6 \text{ s}]$, the GRB is affected by pile-up. (b) The luminosity of GRB 130427A in the Fermi energy range. (c) The anticorrelation between the flux (luminosity) received by Fermi-GBM and *Fermi*-LAT in the time interval [1 s, 16 s], indicates that the primary photons in the GeV energy range are converted to the MeV photons due to the high opacity; for details, see Ruffini et al. (2015).

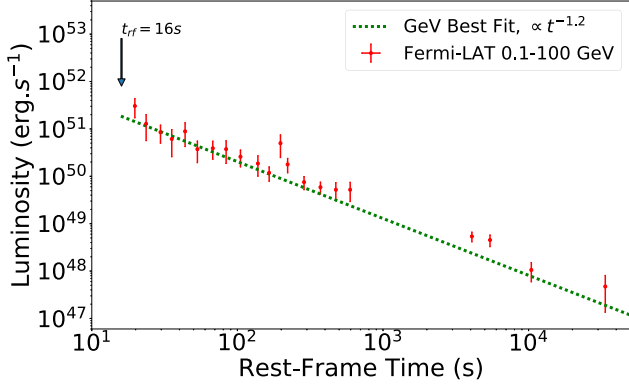


Figure 3. Rest-frame 0.1–100 GeV luminosity light curve of GRB 130427A obtained from *Fermi*-LAT, respectively. The green line shows the best fit for power-law behavior of the luminosity with slope of 1.2 ± 0.04 and amplitude of $5.125 \times 10^{52} \text{ erg s}^{-1}$.

which we obtain consequently the extractable energy:

$$E_{\text{extr}} = Mc^2 - M_{\text{irr}}c^2 = \left(1 - \sqrt{\frac{1 + \sqrt{1 - \alpha^2}}{2}}\right) Mc^2, \quad (6)$$

where $\alpha = ca/(GM) = cJ/(GM^2)$ is the dimensionless angular momentum parameter, being $a = J/M$ the angular momentum per unit mass.

As we have two unknowns, M and α , and only one equation for one observable (Equation (4)), we need to provide a closure equation to the system to determining the two BH parameters.

In Section 5 we show how the transparency condition and the demand of the synchrotron radiation timescale to be equal to the timescale of the first impulsive event, inferred from the theory of “inner engine,” gives the additional constraint to determine the mass and spin of the Kerr BH in this GRB.

4. On the Electrodynamics of the “Inner Engine”

We turn now to the electro-dynamical mechanism which extracts the rotational energy in the inner engine.

We focus on a Wald solution within a cone of opening angle $\pi/3$ about the magnetic field direction; see Figure 4. In Figure 4 we consider the case of magnetic field “parallel,” Figure 4(a) (antiparallel, Figure 4(b)) to the Kerr BH rotation axis, in which the electrons (protons) are accelerated away in the polar direction.

In this article we shall address the case of magnetic field parallel to the Kerr BH rotation axis, in which the electrons are accelerated away in the polar direction; see Figure 4(a).

We address only the leading in the angular and radial dependence of the field in the equation of motion. The electromagnetic field of the inner engine, in the first-order, slow rotation approximation and at second-order, small angle approximation, reads

$$E_{\hat{r}} \approx \frac{aB_0}{r} \left[\left(1 + \frac{GM}{c^2 r}\right) \theta^2 - \frac{2GM}{c^2 r} \right], \quad (7)$$

$$E_{\hat{\theta}} \approx \frac{aB_0}{r} \left(1 - \frac{2GM}{c^2 r}\right)^{1/2} \theta, \quad (8)$$

$$B_{\hat{r}} \approx B_0 \left(1 - \frac{\theta^2}{2}\right), \quad (9)$$

$$B_{\hat{\theta}} \approx -B_0 \left(1 - \frac{2GM}{c^2 r}\right)^{1/2} \theta. \quad (10)$$

Up to linear order in θ , the radial component of the electric field can be approximated by the expression

$$E_r \approx -\frac{1}{2} \alpha B_0 c \frac{r_+^2}{r^2}. \quad (11)$$

At the BH horizon, $r_+ = (1 + \sqrt{1 - \alpha^2})GM/c^2$, the above electromagnetic field becomes

$$E_{\hat{r}} \approx -\frac{1}{2} \alpha B_0 c \left(1 - \frac{3}{2} \theta^2\right), \quad (12)$$

$$E_{\hat{\theta}} \approx 0, \quad (13)$$

$$B_{\hat{r}} \approx B_0 \left(1 - \frac{\theta^2}{2}\right), \quad (14)$$

$$B_{\hat{\theta}} \approx 0. \quad (15)$$

It can be seen from the full numerical solution, keeping all orders in the angular momentum (shown in Figure 4), that this approximation is valid up to $\theta_{\pm} = \pi/3$ and for the arbitrary value of α and within such limits our small angle approximation gives accurate qualitative and quantitative results.

We show how in the presence of a fully ionized low-density plasma, the GRB inner engine accelerates electrons up to ultrarelativistic energies in the abovementioned cavity. We assume that the emission process occurs near the BH and within magnetic field lines constant in time and uniform in space. The equations of motion for the electrons injected for selected angles θ are given below and specific examples in the Section 5.

When emitted in the polar direction $\theta = 0$, the inner engine can give rise to UHECRs. For $\theta \neq 0$, we integrate the equations of motion and evaluate the synchrotron emission keeping the leading terms.

5. Synchrotron Emission from the Wald Solution and the First Elementary Impulsive Event

The relativistic expression for the Lorentz force is

$$\frac{dp^\mu}{d\tau} = \frac{e}{c} F^{\mu\nu} u_\nu, \quad p^\mu = mu^\mu, \quad u^\mu = \frac{dx^\mu}{d\tau}, \quad (16)$$

where τ is the proper time, p^μ is the four-momentum, u^μ is the four-velocity, x^μ are the coordinates, $F^{\mu\nu}$ is the electromagnetic field tensor, m is the particle mass, e is the elementary charge, and c is the speed of light. This expression can be rewritten in the laboratory frame using vector notation as

$$mc \frac{d(\gamma \mathbf{v})}{dt} = e(\mathbf{E} + \mathbf{v} \times \mathbf{B}). \quad (17)$$

Assuming the one-dimensional motion along the radial directions, the dynamics of the electrons in the electromagnetic field (12)–(15), for $\gamma \gg 1$, is determined by the equation (see, e.g., de Jager et al. 1996)

$$m_e c^2 \frac{d\gamma}{dt} = e \frac{1}{2} \alpha B_0 c^2 - \frac{2}{3} e^4 \frac{B_0^2 \sin^2 \langle \theta \rangle}{m_e^2 c^3} \gamma^2 c^2, \quad (18)$$

where γ is the electron Lorentz factor, $\langle \theta \rangle$ is the injection angle between the direction of electron motion and the magnetic field, and m_e is the electron mass. This equation is here

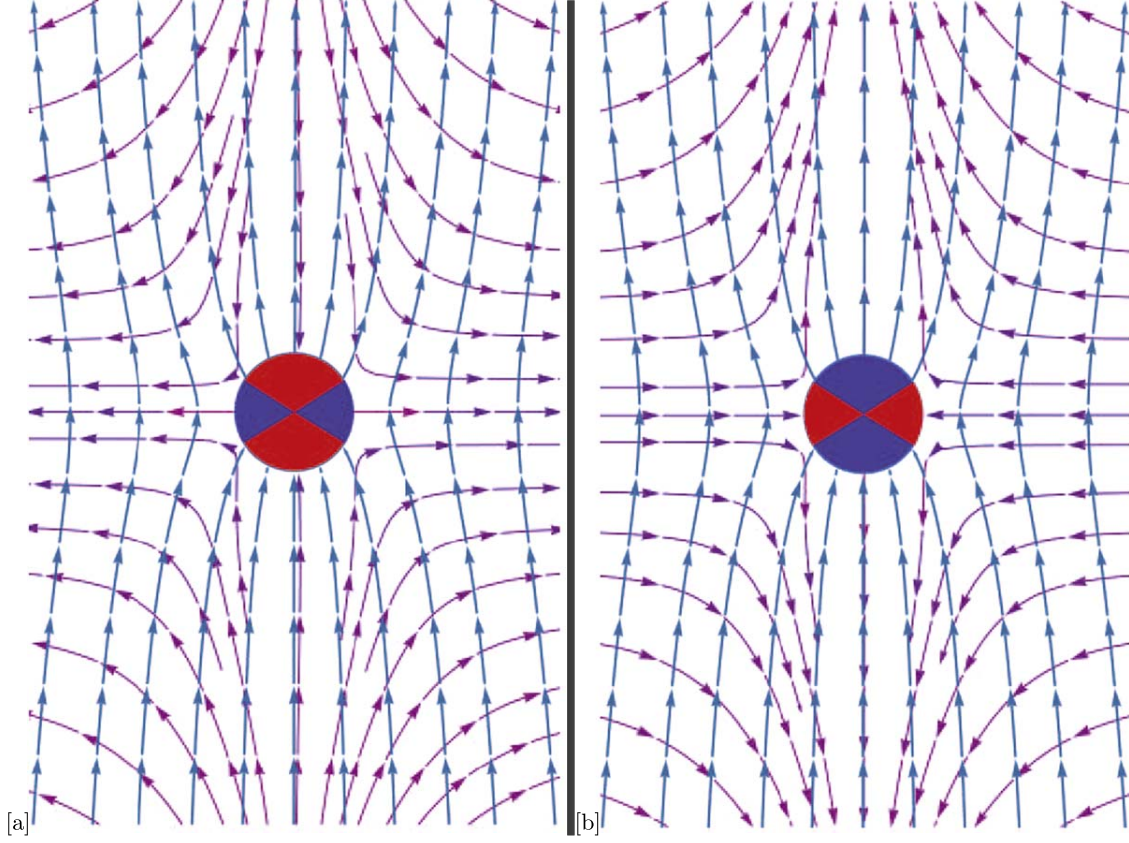


Figure 4. Electromagnetic field lines of the Wald solution. The blue lines show the magnetic field lines, and the violet show the electric field lines. (a) Magnetic field is “parallel” to the spin of the Kerr BH, so therefore parallel to the rotation axis. On the polar axis up to $\theta \sim \pi/3$, electric field lines are inwardly directed; therefore, electrons are accelerated away from the BH. For $\theta > \pi/3$, electric field lines are outwardly directed, and consequently protons are accelerated away from the BH. (b) Magnetic field is antiparallel to the Kerr BH rotation axis. On the polar axis up to $\theta \sim \pi/3$, electric field lines are outwardly directed; therefore, protons will be accelerated away from the BH. For $\theta > \pi/3$, electric field lines are inwardly directed, and consequently electrons will be accelerated away from the BH.

integrated for electrons assumed to be injected near the horizon, for the selected value of the injection angle $\langle\theta\rangle$, with an initial Lorentz factor of $\gamma = 1$ at $t = 0$.

Equation (18) is valid for every injection angle θ . The angle dependence in the electric field in Equation (18) is neglected, because the second term of the right-hand side of Equation (18), namely the synchrotron radiation term, is largely dominant for the parameters of interest in this work.

Assuming all parameters are constant, the approximate solution in the limit $\gamma \gg 1$ is

$$\gamma = \gamma_{\max} \tanh \left[\frac{2}{3} \frac{e^2}{\hbar c} \left(\frac{B_0 \sin \langle\theta\rangle}{B_c} \right)^2 \gamma_{\max} \frac{t}{\hbar/m_e c^2} \right], \quad (19)$$

which has the following asymptotic value:

$$\gamma = \begin{cases} \frac{1}{2} \frac{B_0}{B_c} \alpha \frac{t}{\hbar/m_e c^2}, & t \ll t_c, \\ \gamma_{\max}, & t \gg t_c, \end{cases} \quad (20)$$

where

$$\gamma_{\max} = \frac{1}{2} \left(\frac{3}{\hbar c} \alpha \frac{B_c}{B_0 \sin^2 \langle\theta\rangle} \right)^{1/2} \quad (21)$$

and the critical time is

$$t_c = \frac{\hbar}{m_e c^2} \frac{3}{\sin \langle\theta\rangle} \left[\frac{e^2}{\hbar c} \left(\frac{B_0}{B_c} \right)^3 \alpha \right]^{-1/2}. \quad (22)$$

The maximum peak photon energy of the synchrotron spectrum is obtained by using the maximum Lorentz factor of the radiating electrons, which is given by the equilibrium between energy gain and energy loss in Equation (18). Consequently, the following maximum energy of the electron-synchrotron photons is found:

$$\begin{aligned} \epsilon_{\max, \gamma} &= \frac{3e\hbar}{2m_e c} B_0 \sin \langle\theta\rangle \gamma_{\max}^2 = \frac{9}{8} \frac{m_e c^2}{e^2/\hbar c} \frac{\alpha}{\sin \langle\theta\rangle} \\ &\approx \frac{80}{\sin \langle\theta\rangle} \alpha \text{ MeV}. \end{aligned} \quad (23)$$

The maximum energy is independent of the magnetic field strength, which for different angles leads to different energy bands for the photons; see Figure 8. From this upper limit, some inferences on the TeV emission are in preparation, awaiting the publication of the TeV data. Here, we return to the GeV emission and to its energy originating from the BH rotational energy.

A vast amount of literature exists on the propagation of ultrahigh-energy protons/electrons in a magnetic field with $\theta = \pi/2$ (see e.g., Erber 1966 and references therein). Very

little has been published for computations for small injection angles, $\theta \approx 0$ (an important exception being Harding 1991), which we also address here.

The maximum electric potential difference associated with the electric field is obtained by bringing an electron from the BH horizon to infinity along the symmetry/rotation ($\theta = 0$) axis:

$$\begin{aligned} \Delta\phi &= \frac{\epsilon_e}{e} = \int_{r_+}^{\infty} E dr = E_{r_+} r_+ \\ &= 9.7 \times 10^{20} \cdot \xi \beta \mu (1 + \sqrt{1 - \xi^2}) \frac{eV}{e}, \end{aligned} \quad (24)$$

where we have introduced $\beta \equiv B_0/B_c$ and $\mu \equiv M/M_\odot$, and E_{r_+} is the electric field evaluated at the horizon (see Equation (12)),

$$E_{r_+} = \frac{1}{2} \alpha B_0 c. \quad (25)$$

This potential can accelerate electrons along the symmetry axis up to a maximum Lorentz factor and energy given by

$$\epsilon_{e,\max} = e \Delta\phi = \gamma m_e c^2. \quad (26)$$

For $\theta = 0$, there is no energy loss due to synchrotron radiation, hence the total electrostatic energy goes into electron acceleration. The time of acceleration for $\theta = 0$ can be obtained from Equation (18) when the synchrotron loss term in the right-hand side is zero, i.e.,

$$m_e c^2 \frac{d\gamma}{dt} = e \frac{1}{2} \alpha B_0 c^2 = e E_{r_+} c, \quad (27)$$

therefore,

$$t(\theta = 0) = \frac{m_e c^2 \gamma}{e E_{r_+} c} = \frac{E_{r_+} r_+}{E_{r_+} c} = \frac{r_+}{c}, \quad (28)$$

where we have used Equations (24) and (26).

5.1. Timescale of the First Impulsive Event

The electrostatic energy available is

$$\mathcal{E} = \frac{1}{2} E_{r_+}^2 r_+^3 = 7.5 \times 10^{41} \cdot \alpha^2 \beta^2 \mu^3 (1 + \sqrt{1 - \alpha^2})^3 \text{ erg}, \quad (29)$$

where we have used Equation (25).

Therefore, the timescale of the first impulsive event obtained from the GeV luminosity at $t_{\text{tr}} = 16$ s, denoted as $\mathcal{E}_1 \equiv \mathcal{E}_{t_{\text{tr}}=16 \text{ s}}$, is

$$\tau_1 = \frac{\mathcal{E}_{t_{\text{tr}}=16 \text{ s}}}{L_{\text{GeV}}(t_{\text{tr}} = 16 \text{ s})}, \quad (30)$$

which reads

$$\tau_1 = 4.08 \times 10^{-10} \alpha^2 \beta^2 \mu^3 (1 + \sqrt{1 - \alpha^2})^3 \text{ s}, \quad (31)$$

where we have used Equation (3) we turn now to a crucial relation between α and β .

5.2. Transparency of GeV Photons

The hypercritical accretion onto the NS and its subsequent collapse forming the BH, depletes the BdHN by $\approx 10^{57}$ baryons, creating a cavity of $\approx 10^{11}$ cm of radius in the hypernova ejecta around the BH site (see Becerra et al. 2016, 2019). The density

inside the cavity at BH formation is about $10^{-6} \text{ g cm}^{-3}$ (Becerra et al. 2016, 2019), and is further decreased to about $10^{-13} \text{ g cm}^{-3}$ by the GRB explosion (Ruffini et al. 2019b). The low density of this cavity guarantees a condition of low baryon density necessary for the transparency and therefore for the observation of the MeV emission in the UPE, as well as the higher-energy band emission discussed in the present work (see Ruffini et al. 2019a, 2019b for details). However, this condition for transparency, while necessary, is not sufficient.

There is a most stringent condition imposed by the interaction of the synchrotron photons with the field B_0 .

Synchrotron photons of energy ϵ_γ may produce e^+e^- pairs in external magnetic field. The inverse of the attenuation coefficient (Daugherty & Harding 1983),

$$\bar{R} \sim 0.23 \frac{e^2}{\hbar c} \left(\frac{\hbar}{m_e c^2} \right)^{-1} \beta \sin \langle \theta \rangle \exp \left(- \frac{4/3}{\frac{\epsilon_\gamma}{2m_e c^2} \beta \sin \langle \theta \rangle} \right). \quad (32)$$

Imposing the following transparency condition for 0.1 GeV photons, $\bar{R}^{-1} \geq 10^{16} \text{ cm}$, we obtain

$$\beta \leq 3.67 \times 10^{-4} \alpha^{-1}, \quad (33)$$

where we have replaced Equation (23) with (32) to express the dependence of \bar{R} on the pitch angle in terms of the peak photon energy and the spin parameter (see Figure 6).

We shall use this equation in next section to obtain mass and spin of BH in GRB 130427A.

6. Mass and Spin of BH

As there are three unknown parameters, namely M , α , and β , and only two equations, namely Equation (4) via (6), and Equation (33), an additional equation is needed to determine the three parameters of the inner engine.

For this purpose, we request the additional constraint that the timescale of the synchrotron radiation, obtained from Equation (22), be equal to the radiation timescale obtained from Equation (30), at the time $t_{\text{tr}} = 16$ s, i.e., the following three equations must be solved simultaneously:

$$E_{\text{GeV}} = E_{\text{extr}}(\mu, \alpha), \quad (34)$$

$$\beta = 3.67 \times 10^{-4} \alpha^{-1}, \quad (35)$$

$$t_c(\langle \theta \rangle, \alpha, \beta) = \tau_{\text{ob},1}(\mu, \alpha, \beta, L_{\text{GeV}}). \quad (36)$$

We can solve this system of equations as follows. First, from Equation (34), we can isolate μ as a function of E_{GeV} and α :

$$\mu = \left(1 - \sqrt{\frac{1 + \sqrt{1 - \alpha^2}}{2}} \right)^{-1} \frac{E_{\text{GeV}}}{M_\odot c^2}. \quad (37)$$

Then, by replacing Equation (37) with (36), we obtain an expression for β as a function of the observables E_{GeV} and L_{GeV} , and α :

$$\begin{aligned} \beta &= \beta(\epsilon_\gamma, E_{\text{GeV}}, L_{\text{GeV}}, \alpha) \\ &= \frac{1}{\alpha} \left(\frac{64}{9} \sqrt{3} \frac{e^2}{\hbar c} \frac{\epsilon_\gamma}{B_c^2 r_+(\mu, \alpha)^3 e B_c c^2} \right)^{2/7}, \end{aligned} \quad (38)$$

where we have replaced Equation (23) into (22) to express t_c as a function of the peak photon energy ϵ_γ instead of the pitch

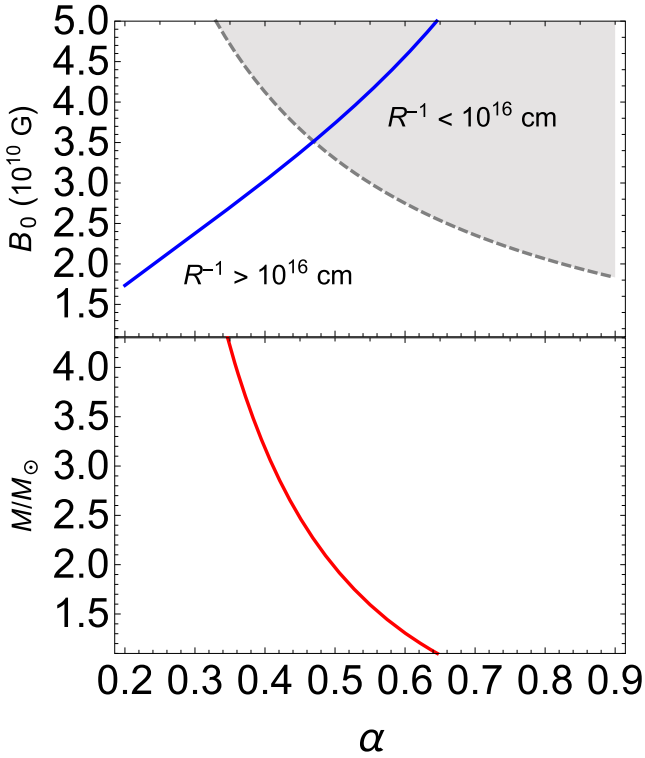


Figure 5. Upper panel: self-consistent family of solutions of the magnetic field B_0 as a function of the BH spin parameter α (blue curve), Equation (38), for given values of $E_{\text{GeV}} = 1.2 \times 10^{53}$ erg, $L_{\text{GeV}} = 1.84 \times 10^{51}$ erg s $^{-1}$, and $\epsilon_\gamma = 0.1$ GeV. Inside the gray shaded region 0.1 GeV photons have $\bar{R}^{-1} < 10^{16}$ cm, while in the white one they fulfill the condition of transparency $\bar{R}^{-1} \geq 10^{16}$ cm, namely Equation (33). The crossing between the blue curve and the border of the gray region gives us the upper limit of the magnetic field $B_0 \approx 3.5 \times 10^{10}$ G and the spin parameter $\alpha = 0.47$, to have transparency of the GeV photons. Lower panel: self-consistent solution of the BH mass as a function of the BH spin parameter α (red curve). To the maximum spin parameter for transparency, it corresponds a lower limit to the BH mass, $M = 2.31 M_\odot$.

angle, and r_+ is the BH horizon, which is a function of μ and α , but via Equation (37), becomes a function of E_{GeV} and α .

Therefore, given the energy E_{GeV} (integrated for times $t_{\text{rf}} \geq 16$ s) and luminosity L_{GeV} (at $t_{\text{rf}} = 16$ s), Equation (38) gives the self-consistent family of solutions of the magnetic field β as a function of the BH spin parameter α . In Figure 5 (blue curve in the upper panel) we show such a family of self-consistent solutions in the case of $E_{\text{GeV}} = 1.2 \times 10^{53}$ erg (see Equation (4)), $L_{\text{GeV}} = 1.84 \times 10^{51}$ erg s $^{-1}$ given by Equation (3), and photon energy $\epsilon_\gamma = 0.1$ GeV.

From Equation (33), we know β as a function of α , for which the condition of transparency is satisfied. Therefore, by equating Equations (38) and (33), we obtain, as can be seen from Figure 5, a maximum spin parameter, α , to fulfill the transparency condition for 0.1 GeV photons. Correspondingly, there is the maximum magnetic field value that can be obtained by substituting the upper value of α either into Equation (38) or (33). Then, the maximum α is used in Equation (37) to obtain the corresponding lower limit for the BH mass. For the above numbers, the upper magnetic field value to have transparency is $\beta = 7.8 \times 10^{-4}$, i.e., $B_0 \approx 3.5 \times 10^{10}$ G. The maximum spin and a minimum BH mass are, respectively, $\alpha \approx 0.47$ and $M = 2.31 M_\odot$. For the above spin value, we obtain from

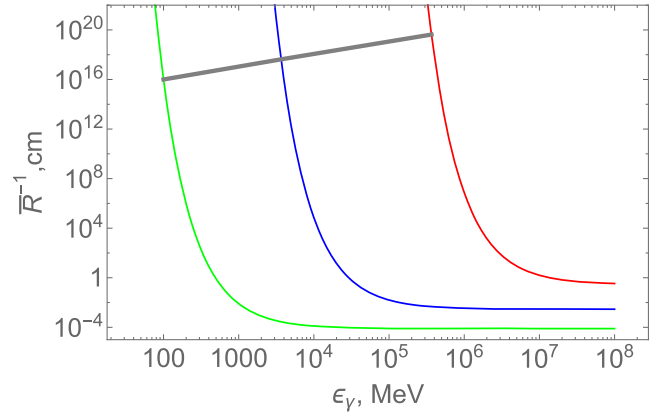


Figure 6. Inverse of the attenuation coefficient for pair production in magnetic field (Equation (32)) computed for $\beta = B_0/B_c = 7.84 \times 10^{-4}$, and selected $\langle \theta \rangle$ of $\pi/8$ (green), 10^{-2} (blue) and 10^{-4} (red). The peak of the synchrotron spectrum, given by Equation (23) and shown by the gray line, is in the transparent region.

Equation (23) the pitch angle to emit 0.1 GeV photons, $\theta \approx \pi/8$. The corresponding BH irreducible mass is $M_{\text{irr}} = 2.24 M_\odot$, which is close to critical mass of the NS for some specific nuclear equation of state, in particular to the TM1 one (see Cipolletta et al. 2017). These parameters will be used in next subsection as the initial values of mass and spin parameters to find the spin-down of the BH.

The inverse of the attenuation coefficient from Equation (32) computed for $\beta = 7.84 \times 10^{-4}$ and different $\langle \theta \rangle$ is presented in Figure 6. The peak of the synchrotron spectrum (Equation (23)) shown by the gray line in Figure 6 is located in the transparent region. We can see from the figure that synchrotron photons, when produced in the 0.1 GeV to 1 TeV energy band, do not produce pairs if magnetic field is below $B_0 < 3.5 \times 10^{10}$ G. Therefore, this region is transparent for such photons.

6.1. The Decrease of the Mass and Spin of the BH as a Function of the Extracted Rotational Energy

From the luminosity expressed in the rest-frame of the sources, and from the initial values of the spin and of the mass of the BH, we can now derive the slowing down of the BH due to the energy loss in the GeV emission. The time derivative of Equation (6) gives the luminosity

$$L = -\frac{dE_{\text{extr}}}{dt} = -\frac{dM}{dt}. \quad (39)$$

Because M_{irr} is constant for each BH during the energy-emission process, and using our relation for luminosity from Equation (3), we obtain the relation of the loss of mass–energy of the BH by integrating Equation (39):

$$M = M_0 + 5At^{-0.2} - 5At_0^{-0.2}, \quad (40)$$

where M_0 is the initial BH mass at, $t_0 = 16$ s, and $A = (5.125 \pm 0.2) \times 10^{52}$. From the mass–energy formula of the BH we have

$$J = 2M_{\text{irr}} \sqrt{M^2 - M_{\text{irr}}^2}, \quad (41)$$

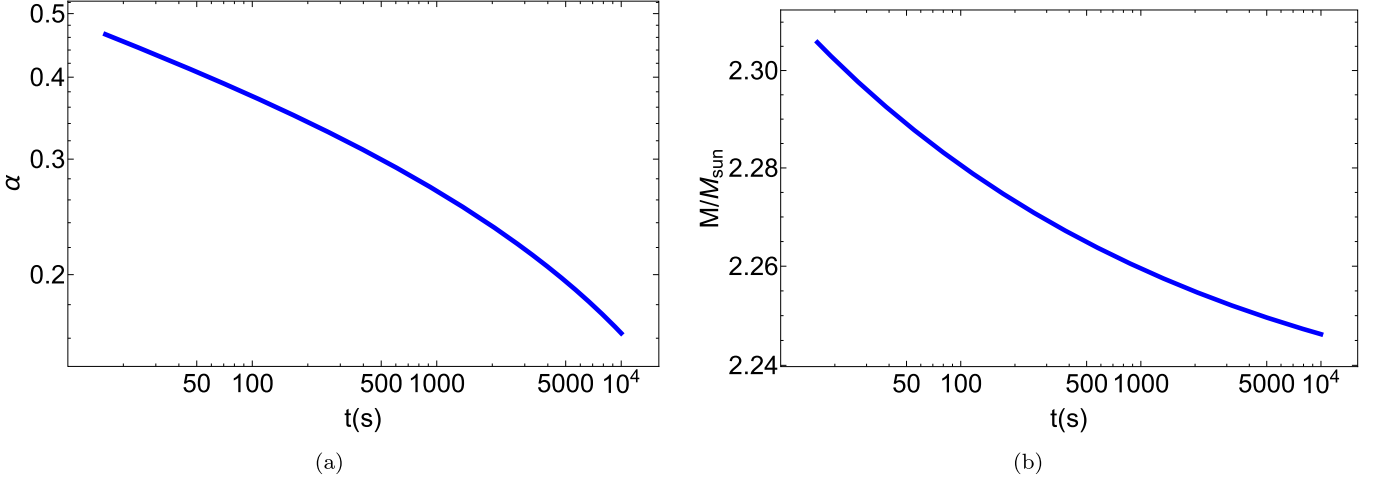


Figure 7. (a) and (b) The decrease of the BH spin and Mass, as a function of rest-frame time for GRB 130427A. The values of spin and mass at the moment which prompt is finished, which has been assumed to occur at the rest-frame time of $t_{\text{rf}} = 16$ s, are: $\alpha = 0.47$ and $M(\alpha) = 2.31M_{\odot}$.

therefore,

$$a = \frac{J}{M} = 2M_{\text{irr}} \sqrt{1 - \frac{M_{\text{irr}}^2}{(M_0 + 5At^{-0.2} - 5At_0^{-0.2})^2}}. \quad (42)$$

The values of mass and spin parameters at $t_0 = t_{\text{rf}} = 16$ s; see Figure 3 are $M_0 = 2.31M_{\odot}$ and $\alpha = 0.47$, and the irreducible mass is $M_{\text{irr}} = 2.24M_{\odot}$. The behavior of $\alpha = J/M^2$ and M with time are shown in Figure 7. Both α and M decrease with time, which shows the decrease of rotational energy of the BH due to the energy loss in GeV radiation; see Figure 7. It is important to recall that, since we are here inferring the BH energy budget using only the GeV emission data after the UPE phase, the above BH mass and spin have to be considered as lower limits.

7. Synchrotron Radiation Power and the Need of a Low Density Ionized Plasma

Having obtained the values of spin, $\alpha = 0.47$, mass $M = 2.31M_{\odot}$, and magnetic field, $B_0/B_c = 7.8 \times 10^{-4}$, we integrate the equation of motion given by Equation (18) to obtain the radiation in the GeV and TeV bands corresponding to selected values of θ .

As an example, we show the results for the electron propagation and radiation for selected angles, i.e., $\theta = \pi/8$, $\theta = 1 \times 10^{-2}$, $\theta = 1 \times 10^{-4}$ with respect to the direction of the magnetic field. According to Equation (23), these angles are related to ~ 0.1 GeV, ~ 4 GeV and ~ 0.4 TeV energy of photons, respectively, which covers the lower limit of *Fermi-LAT* instrument until the lower limit of *MAGIC* telescope; see Figure 8(a). The numerical solution of Equation (18), along with analytic solutions, are represented in Figure 8(a). The electron-synchrotron luminosity from the right-hand side of Equation (18) is

$$\dot{E}_{\text{sync}} = \frac{2}{3} e^4 \frac{B_0^2 \sin^2 \langle \theta \rangle}{m_e^2 c^3} \gamma^2. \quad (43)$$

In Figure 8(c), we present the total power of the synchrotron emission by a single electron as a function of time for selected injected angles θ . The power increases with time, and then at $t > t_c$ approaches a constant value, which does not depend on

the angle

$$\dot{E}_{\text{sync}, \gamma_{\text{max}}} = \frac{1}{2} \frac{(m_e c^2)^2 B_0}{\hbar B_c} \alpha = 1.16 \times 10^{11} \text{ erg s}^{-1}. \quad (44)$$

In Figure 8(d) we show the peak energy of the synchrotron photons given by Equation (23) as a function of the electron injection angle and the magnetic field.

The total energy emitted by an electron in synchrotron radiation, computed by integrating the synchrotron power with time, gives

$$E_{\text{sync}} = \begin{cases} \frac{1}{18} \frac{e^2}{\hbar c} \left(\frac{B_0}{B_c} \right)^4 \alpha^2 \left(\frac{t}{\hbar/m_e c^2} \right)^3 \sin^2 \langle \theta \rangle m_e c^2, & t < t_c, \\ \frac{1}{2} \alpha \frac{B_0}{B_c} \frac{t}{\hbar/m_e c^2} m_e c^2, & t > t_c, \end{cases} \quad (45)$$

where, from Equation (22), the critical time for $\alpha = 0.47$, $B_0/B_c = 7.8 \times 10^{-4}$ is

$$t_c \simeq \frac{5.9 \times 10^{-15}}{\sin \langle \theta \rangle} \text{ s}. \quad (46)$$

The synchrotron timescale, obtained from Equation (46), has values between 1.6×10^{-14} s and 2×10^{-5} s; see Figure 8(a). According to Equation (45), the total energy available for the synchrotron radiation of one electron is a function of synchrotron timescale; see Figure 8(b). Each timescale corresponds to the time which takes for one electron to radiate by synchrotron mechanism its acceleration energy $\epsilon_e = \gamma_{\text{max}} m_e c^2$, where γ_{max} is given by Equation (21). For $\theta = \pi/8$, which is related to the lower limit of *Fermi-LAT* energy bandwidth, namely 0.1 GeV, $t_c = 1.6 \times 10^{-14}$ s, corresponds to $\epsilon_e = 1.02 \times 10^9$ eV. Therefore,

$$t_{c, \text{GeV}} = 1.6 \times 10^{-14} \text{ s}. \quad (47)$$

For the available electromagnetic energy budget, the system can accelerate a total number of electrons with the above energy:

$$N_e = \mathcal{E}_1 / \epsilon_e \approx 6.6 \times 10^{39}, \quad (48)$$

where $\mathcal{E}_1 \approx 10^{37}$ erg is electrostatic energy available, the blackholic quantum (Rueda & Ruffini 2019), for the first impulsive event obtained from Equation (29).

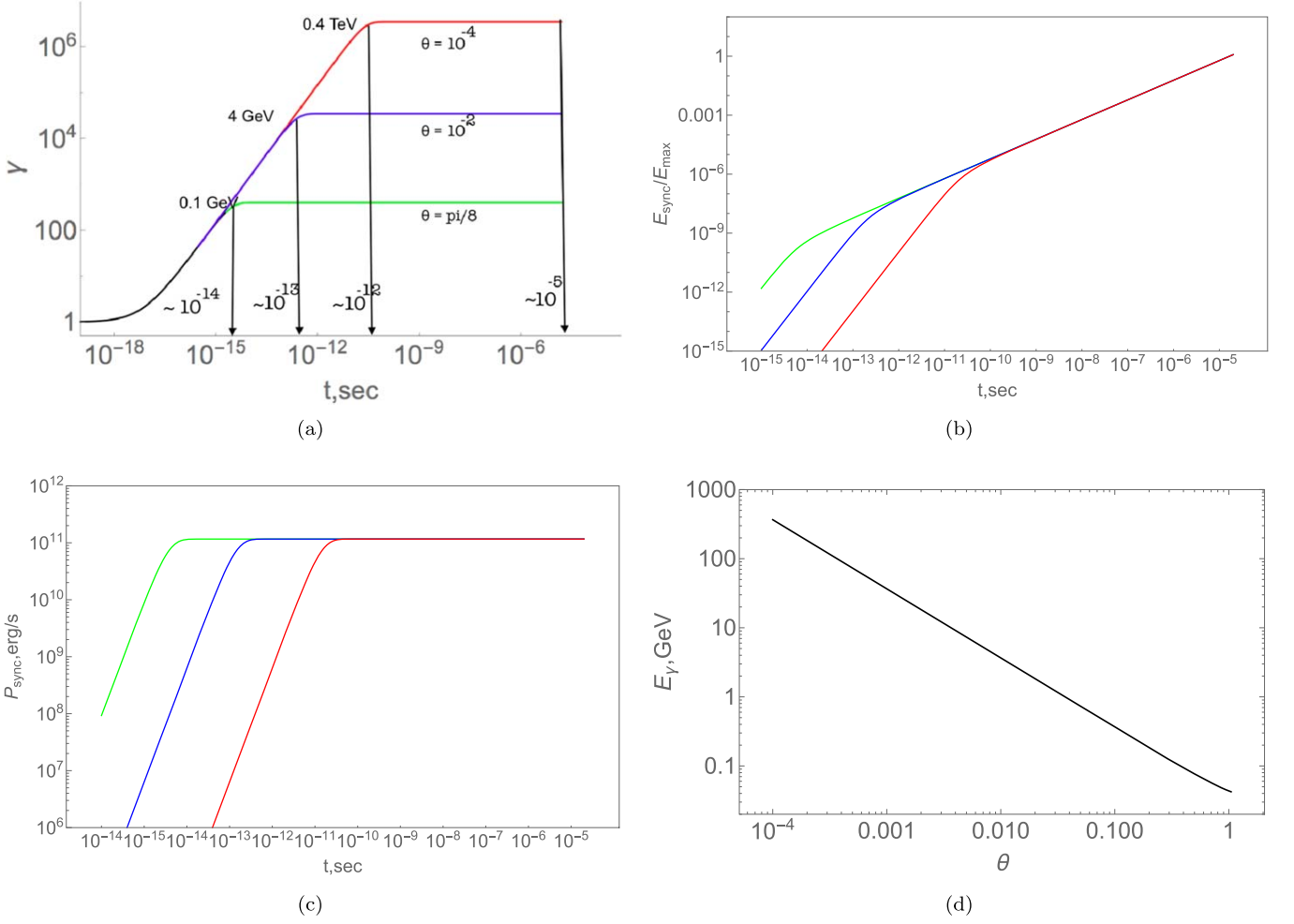


Figure 8. (a) The electron Lorentz gamma factor obtained from solutions of Equation (18) as functions of time: numerical (black), and analytic for selected angles: $\theta = \pi/8$ (green), $\theta = 1 \times 10^{-2}$ (blue), $\theta = 1 \times 10^{-4}$ (red) which according to Equation (23), they are related to ~ 0.1 GeV, ~ 4 GeV and ~ 0.4 TeV energy of synchrotron photons, respectively. Parameters assumed: $a/M = 0.47$, $B_0/B_c = 7.8 \times 10^{-4}$. The arrow indicates the time when the energy emitted in synchrotron radiation equals $\epsilon_{\text{max},\gamma} = 10^{18}$ eV, which is $t = r_+/c \sim 2 \times 10^{-5}$ s. (b) Total energy emitted in synchrotron radiation from Equation (45) as a function of time for selected angles given in Figure 8(a). (c) Power of synchrotron emission by a single electron as a function of time for selected angles given in Figure 8(a). (d) Peak energy of synchrotron photons as a function of the angle between the electron velocity and the magnetic field.

In principle, as the timescale increases, the total available electron will decrease; we will return to this subject in Section 8, when we study the evolution of the time of sequence of elementary impulses.

Using Equation (23), the maximum energy $\epsilon_e \sim 1.6 \times 10^{18}$ eV is reached at the critical angle $\langle \theta \rangle \approx 2.2 \times 10^{-11}$. This gives an absolute lower limit on the $\langle \theta \rangle$ value for emitting synchrotron radiation. For $\langle \theta \rangle$ smaller than this critical angle, only UHECRs are emitted. See Figures 8(a) and 9.

The timescale of the process is in general set by the density of particles around the BH, which is provided by the structure of the cavity and SN ejecta; see Section 5.

We have already shown that during each such elementary process the BH experiences a very small fractional change of angular momentum:

$$\begin{aligned} |\Delta J|/J &\approx (|\dot{J}|/J)\tau_{\text{ob}} \approx 10^{-16}, \\ |\Delta M|/M &\approx (|\dot{M}|/M)\tau_{\text{ob}} \approx 10^{-16}. \end{aligned} \quad (49)$$

The electromagnetic energy of the first impulsive event given above is a small fraction of total extractable rotational

energy of the Kerr BH; see Equation (4):

$$\frac{\mathcal{E}_1}{E_{\text{ext}}} \approx 10^{-16}. \quad (50)$$

This clearly indicates that the rotational energy extraction from Kerr BH

- (1) occurs in “discrete quantized steps”;
- (2) is temporally separated by 10^{-14} – 10^{-10} s; and
- (3) that the luminosity of the GeV emission in GRB 130427A is not describable by a continuous function as traditionally assumed: it occurs in a “discrete sequence of elementary quantized events” (Rueda & Ruffini 2019).

There are two main conclusions which can be inferred from the theory of synchrotron radiation implemented in this section.

1. Synchrotron radiation is not emitted isotropically and is angle dependent: the smaller the angle, the higher the synchrotron photon energy (see Equation (23) and Figure 9).

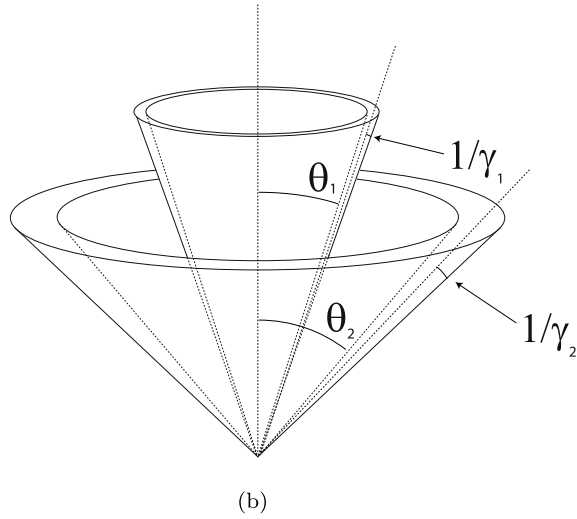
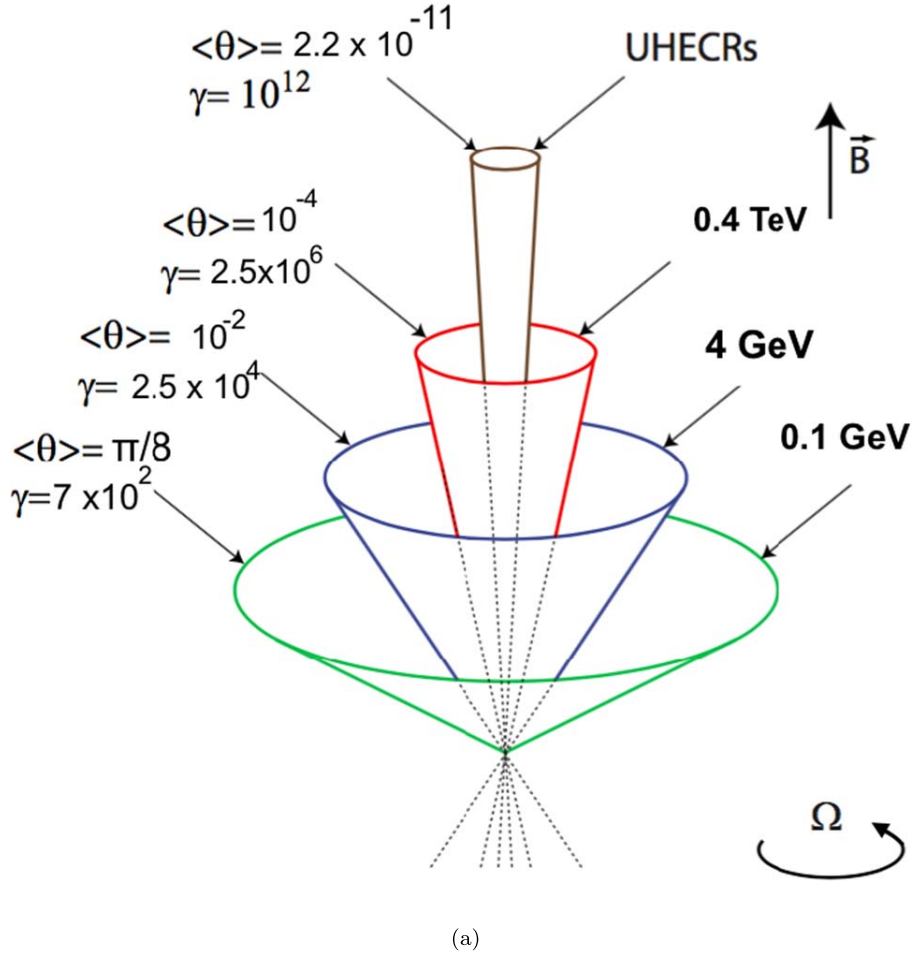


Figure 9. (Not to scale) (a) Having the values of spin and magnetic field, $a/M = 0.47$, $B_0/B_c = 7.8 \times 10^{-4}$, from Equation (23) for selected injection angles, we obtain the radiation in the different bands, 0.1 GeV to 0.4 TeV. Using Equation (23), the maximum energy $\epsilon_e \sim 1.6 \times 10^{18}$ eV is reached at the critical angle $\langle\theta\rangle = 2.2 \times 10^{-11}$. This angle is an absolute lower limit for emitting synchrotron radiation, therefore for $\langle\theta\rangle < 2.9 \times 10^{-11}$, electrons are accelerated to give rise to UHECRs. In this figure, the magnetic field is “parallel” to the Kerr BH rotation axis and electrons are accelerated outward and electrons captured by the horizon. (b) Synchrotron emission from electrons with pitch angle, θ . Radiation is concentrated in a cone of angle of $1/\gamma$.

2. The energy emitted in synchrotron radiation before reaching its asymptotic value is a function of injection angle θ ; see the first line of Equation (45) and Figure 8(b).

To compare and contrast the results based on this essential theoretical treatment with observation, we need to determine (1) the number of electrons for each selected injection angle θ

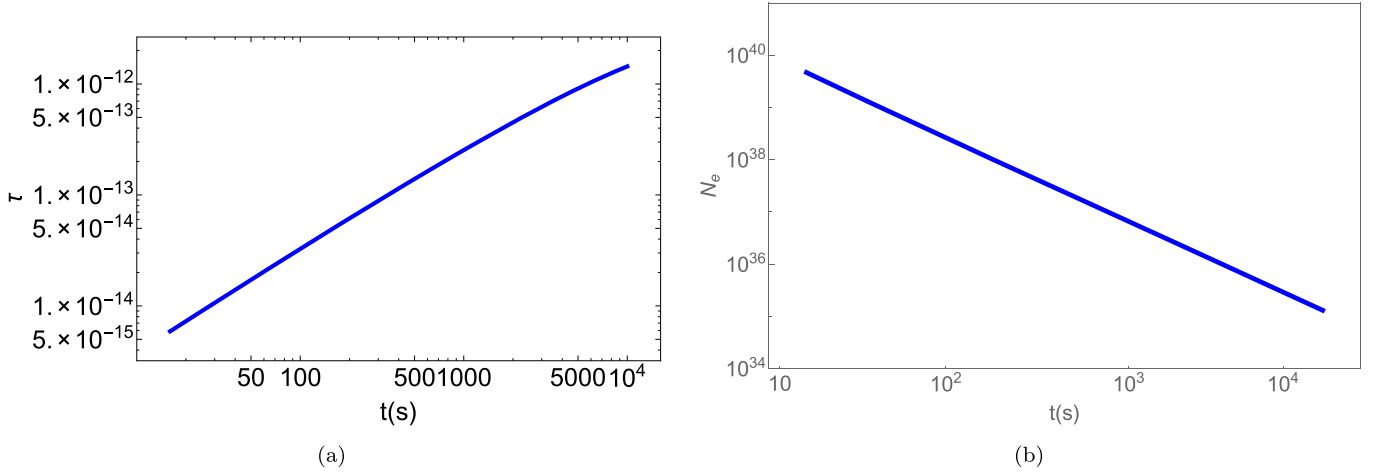


Figure 10. (a) The value of $\tau_{\text{ob}}(t) = E_{r_+}^2 r_+^3 / (2L_{\text{GeV}})$ calculated from the GeV luminosity data obtained from *Fermi*-LAT together with the values of E_{r_+} and r_+ obtained in each impulsive event. This timescale increases linearly with the time t (in s) as $\tau_{\text{ob}} \approx 3 \times 10^{-16} t^1$. (b) The number of electrons available in each impulse to fulfill the observed properties of the inner engine of GRB 130427A.

and (2) to verify that the radiated synchrotron energy is compatible with the electrostatic energy for each electron. (3) Taking into due account the role of the beaming angle which we have here derived; see Figure 9 and extending the number of parameters by allowing the anisotropic distribution of electrons.

8. The Repetition Time of Sequence of the Discrete Elementary Impulsive Events

Finally, we study the sequence of iterative impulsive events in which the system starts over with a new value of the electric field set by the new values of the BH angular momentum and mass, $J = J_0 - \Delta J$ and $M = M_0 - \Delta M$, keeping the magnetic field value constant B_0 .

We infer from the luminosity the evolution of the timescale $\tau(t)$ of the repetition time of the impulsive events by requiring it to explain the GeV emission, i.e.,

$$L_{\text{GeV}} = \frac{\mathcal{E}}{\tau(t)}, \quad (51)$$

where \mathcal{E} is electrostatic energy available for each impulsive event. Therefore, we obtain for the timescale

$$\tau(t) = \frac{1}{2} \frac{E_{r_+}^2 r_+^3}{L_{\text{GeV}}}, \quad (52)$$

where E_{r_+} is the electric field evaluated at the horizon determined from the new values of J and M for each elementary impulsive event consisted with Equation (49). Figure 10(a) shows that τ_{ob} is a increasing power-law function of time, i.e.,

$$\tau_{\text{ob}} \propto \frac{\alpha^2}{L_{\text{GeV}}} \propto t. \quad (53)$$

We identify the timescale τ_{ob} with the repetition time of each impulsive event. The efficiency of the system diminishes with time, as shown by the increasing value of τ_{ob} (see Figure 10(a)). This can be understood by the evolution of the density of particles near the BH decreasing in time owing to the expansion of the SN remnant, making the iterative process

become less efficient. As we have mentioned, in the immediate vicinity of the BH a cavity is created of approximate radius 10^{11} cm and with very low density on the order of $10^{-13} \text{ g cm}^{-3}$ (Ruffini et al. 2019b). This implies an approximate number of $\sim 10^{47}$ electrons inside the cavity. Then, the electrons of the cavity can power the iterative process only for a short time of 1–100 s. We notice that at the beginning of the gamma-ray emission, the required number of electrons per unit time for the explanation of the prompt and the GeV emission can be as large as $10^{46} - 10^{54} \text{ s}^{-1}$. This confirms that this iterative process has to be sustained by the electrons of the remnant, at $r \gtrsim 10^{11}$ cm, which are brought from there into the region of low density and then into the BH. The synchrotron timescale, obtained from Equation (46), has values between 1.6×10^{-14} s and 2×10^{-5} s; see Figure 8(a). According to Equation (45) and Figure 8(b), the total energy available for the synchrotron radiation of one electron is a function of synchrotron timescale.

Therefore, when $t_c = 1.6 \times 10^{-14}$ s the total energy available for each electron is $\epsilon_e = 1.02 \times 10^9$ eV, which leads to the total number of electrons from Equation (48), $N_e = \mathcal{E}_1 / \epsilon_e \approx 6.6 \times 10^{39}$ and when $t_c = 2 \times 10^{-5}$ s, the total energy available for each electron is $\epsilon_{e,\text{max}} = 1.65 \times 10^{18}$ eV and the total number of electrons is $N_e = \mathcal{E} / \epsilon_{e,f} \approx 4 \times 10^{30}$, which can be seen in Figure 10(b).

It is worth mentioning that since the TeV synchrotron photons, in this picture, will start to be produced at $t_c \sim 10^{-11}$ s; see Figure 8(a). Therefore, according to Equation (53), the onset of TeV photons for GRB 130427A should be around 10^5 s (see Figure 10). This is clearly a zero-order approximation since, considering the effect of angle-dependent distribution of electrons, this time could be shorter (J. A. Rueda 2019, in preparation). In any case, the feedback from the observations is needed in order to improve the model.

9. Conclusions

In this paper, we confirm that the high-energy GeV radiation observed by *Fermi*-LAT originate from the rotational energy of a Kerr BH of mass $M = 2.31M_\odot$ and a spin parameter of $\alpha = 0.47$ immersed in an homogeneous magnetic field of $B_0 \sim 3.48 \times 10^{10}$ G and an ionized plasma of a very low

density, $10^{-14} \text{ g cm}^{-3}$ (Ruffini et al. 2019b). The radiation occurs following the formation of the BH, via synchrotron radiation emitted by ultrarelativistic electrons accelerating and radiating in the framework of the Wald solution in the sequence of elementary impulses.

In the traditional approach, see e.g., Zhang (2018), there is a blast wave originating in the prompt radiation phase and propagating in a ultrarelativistic jet into the ISM medium emitting synchrotron radiation following the approach of Sari et al. (1999). There, the kinetic energy of the blast wave is used as the energy source. This process of emission occurs at large distances typically of 10^{15} – 10^{16} cm and is traditionally used to explain the GeV emission observed by *Fermi*-LAT, as well as the X-ray afterglow emission observed by *SWIFT* and the radio emission observed by radio interferometers like the Westerbork Synthesis Radio Telescope (WSRT).

In our approach, the model is only a function of three parameters: the mass, M , and spin, α , of the Kerr BH, and the background magnetic test field, which have been self-consistently derived in this article. They fulfill all the energetic and transparency requirements. The acceleration and synchrotron radiation process occurs within 10^5 cm from the horizon. The photon energy emitted by the synchrotron radiation process is a very strong function of the injection angle of the ultrarelativistic electrons with respect to the polar axis. The outcome is an emission over a large angle, up to $\theta = \pi/3$: GeV at angle $\theta = \pi/8$ and TeV at $\theta = 10^{-4}$ all the way up to UHECR at angle $\theta < 10^{-11}$. The particles accelerated by the electromagnetic field of the Wald solution gyrate into the magnetic field, B_0 . The highly anisotropic distribution in the energy and in the spectra is a specific consequence of the current model.

A byproduct of our model has been to evidence for the first time that the high-energy emission of GRB 130427A is not emitted continuously, but in a repetitive sequence of discrete and quantized “elementary impulsive events,” each of energy 10^{37} erg and with a repetition time of $\sim 10^{-14}$ s and slowly increasing with time. This implies a very long time of extraction of the BH rotational energy via this electromagnetic process each utilizing a fraction of $\sim 10^{-16}$ of the mass-rotational energy of the BH. This result was truly unexpected, and it appears to be a general property both of GRBs and of much more massive Kerr BHs in active galactic nuclei. The results obtained in this paper lead to the concept of a “Blackholic Quantum” affecting our fundamental knowledge of physics and astrophysics (Rueda & Ruffini 2019).

It is appropriate here to recall that within BdHN model the GeV and TeV emission observed by *Fermi*-LAT and MAGIC detectors, originating from the Kerr BH, have a separate origin from the X-ray and radio observation of the afterglow. As recently demonstrated in five BdHN, GRB 130427A, GRB 160509A, GRB 160625B, GRB 180728A, and GRB 190114C (Rueda et al. 2019), the afterglow emission occurs due to the accretion process of the hypernova ejecta on the ν NS spinning with a few millisecond period and the associated synchrotron emission.

We thank the referee for the detailed reports and precise questions, which motivated a more precise formulation of our

paper. We are grateful to Prof. G. V. Vereshchagin and to S. Campion for discussions in formulating the synchrotron radiation considerations and the related figures in the revised version. M.K. is supported by the Erasmus Mundus Joint Doctorate Program grant No. 2014–0707 from EACEA of the European Commission. N.S. acknowledges the support of the RA MES State Committee of Science, in the framework of the research project No. 18T-1C335.

ORCID iDs

J. A. Rueda  <https://orcid.org/0000-0002-3455-3063>
N. Sahakyan  <https://orcid.org/0000-0003-2011-2731>

References

- Ackermann, M., Ajello, M., Asano, K., et al. 2011, *ApJ*, 729, 114
 Ackermann, M., Ajello, M., Asano, K., et al. 2014, *Sci*, 343, 42
 Ajello, M., Arimoto, M., Axelsson, M., et al. 2019, *ApJ*, 878, 52
 Becerra, L., Bianco, C. L., Fryer, C. L., Rueda, J. A., & Ruffini, R. 2016, *ApJ*, 833, 107
 Becerra, L., Ellinger, C. L., Fryer, C. L., Rueda, J. A., & Ruffini, R. 2019, *ApJ*, 871, 14
 Becerra, L., Guzzo, M. M., Rossi-Torres, F., et al. 2018, *ApJ*, 852, 120
 Breit, G., & Wheeler, J. A. 1934, *PhRv*, 46, 1087
 Christodoulou, D. 1970, *PhRvL*, 25, 1596
 Christodoulou, D., & Ruffini, R. 1971, *PhRvD*, 4, 3552
 Cipolletta, F., Cherubini, C., Filippi, S., Rueda, J. A., & Ruffini, R. 2017, *PhRvD*, 96, 024046
 Damour, T., & Ruffini, R. 1975, *PhRvL*, 35, 463
 Daugherty, J. K., & Harding, A. K. 1983, *ApJ*, 273, 761
 de Jager, O. C., Harding, A. K., Michelson, P. F., et al. 1996, *ApJ*, 457, 253
 Erber, T. 1966, *RvMP*, 38, 626
 Flores, H., Covino, S., Xu, D., et al. 2013, *GCN*, 14491
 Gibbons, G. W., Mujtaba, A. H., & Pope, C. N. 2013, *CQGra*, 30, 125008
 Harding, A. K. 1991, *Sci*, 251, 1033
 Hawking, S. W. 1971, *PhRvL*, 26, 1344
 Levan, A. J., Cenko, S. B., Perley, D. A., & Tanvir, N. R. 2013, *GCN*, 14455
 Liang, L., Ruffini, R., Rueda, J. A., et al. 2019, arXiv:1910.12615
 Misner, C. W., Thorne, K. S., & Wheeler, J. A. 1973, *Gravitation* (San Francisco, CA: Freeman)
 Rueda, J. A., & Ruffini, R. 2019, arXiv:1907.08066
 Rueda, J. A., Ruffini, R., Karlica, M., Moradi, R., & Wang, Y. 2019, *ApJ*, submitted (arXiv:1905.11339)
 Rueda, J. A., Ruffini, R., Wang, Y., et al. 2018, *JCAP*, 10, 006
 Ruffini, R., Becerra, L., Bianco, C. L., et al. 2018a, *ApJ*, 869, 151
 Ruffini, R., Bernardini, M. G., Bianco, C. L., et al. 2007, in *AIP Conf. Proc.* 910, XIIth Brazilian School of Cosmology and Gravitation, ed. M. Novello & S. E. Perez Bergliaffa (Cambridge: Cambridge Univ. Press), 55
 Ruffini, R., Karlica, M., Sahakyan, N., et al. 2018b, *ApJ*, 869, 101
 Ruffini, R., Li, L., Moradi, R., et al. 2019a, arXiv:1904.04162
 Ruffini, R., Melon Fuksman, J. D., & Vereshchagin, G. V. 2019b, *ApJ*, 883, 191
 Ruffini, R., Rodriguez, J., Muccino, M., et al. 2018c, *ApJ*, 859, 30
 Ruffini, R., Rueda, J. A., Muccino, M., et al. 2016a, *ApJ*, 832, 136
 Ruffini, R., Salmonson, J. D., Wilson, J. R., & Xue, S.-S. 1999, *A&A*, 350, 334
 Ruffini, R., Salmonson, J. D., Wilson, J. R., & Xue, S.-S. 2000, *A&A*, 359, 855
 Ruffini, R., Vereshchagin, G., & Xue, S.-S. 2010, *PhR*, 487, 1
 Ruffini, R., Vereshchagin, G. V., & Xue, S. S. 2016b, *Ap&SS*, 361, 82
 Ruffini, R., Wang, Y., Enderli, M., et al. 2015, *ApJ*, 798, 10
 Sari, R., Piran, T., & Halpern, J. P. 1999, *ApJL*, 519, L17
 von Kienlin, A. 2013, *GCN*, 14473
 Wald, R. M. 1974, *PhRvD*, 10, 1680
 Wang, Y., Rueda, J. A., Ruffini, R., et al. 2019, *ApJ*, 874, 39
 Xu, D., de Ugarte Postigo, A., Schulze, S., et al. 2013, *GCN*, 14478
 Zhang, B. 2018, *The Physics of Gamma-Ray Bursts* (Cambridge: Cambridge Univ. Press)

